

THESIS

IMPROVING THE COLD TEMPERATURE PROPERTIES OF TALLOW-BASED METHYL ESTER
MIXTURES USING FRACTIONATION, BLENDING, AND ADDITIVES

Submitted by

Caleb Elwell

Department of Mechanical Engineering

In partial fulfillment of the requirements

For the Degree of Master of Science

Colorado State University

Fort Collins, Colorado

Fall 2017

Master's Committee:

Advisor: Anthony J. Marchese

T. Gordon Smith
Bret C. Windom

Copyright by Caleb Chris Elwell 2017

All Rights Reserved

ABSTRACT

IMPROVING THE COLD TEMPERATURE PROPERTIES OF TALLOW-BASED METHYL ESTER MIXTURES USING FRACTIONATION, BLENDING, AND ADDITIVES

Beef tallow is a less common feedstock source for biodiesel than soy or canola oil, but it can have economic benefits in comparison to these traditional feedstocks. However, tallow methyl ester (TME) has the major disadvantage of poor cold temperature properties. Cloud point (CP) is a standard industry metric for evaluating the cold temperature performance of biodiesel and is directly related to the thermodynamic properties of the fuel's constituents. TME has a CP of 14.5°C compared with 2.3°C for soy methyl ester (SME) and -8.3°C for canola methyl ester (CME).

In this study, three methods were evaluated to reduce the CP of TME: fractionation, blending with SME and CME, and using polymer additives. TME fractionation (i.e. removal of specific methyl ester constituents) was simulated by creating FAME mixtures to match the FAME profiles of fractionated TME. The fractionation yield was found to be highest at the eutectic point of methyl palmitate (MP) and methyl stearate (MS), which was empirically determined to be at a MP/(MP+MS) ratio of approximately 82%. Since unmodified TME has a MP/(MP+MS) ratio of 59%, initially only MS should be removed to produce a ratio closer to the eutectic point to reduce CP and maximize yield. Graphs relating yield (with 4:1 methyl stearate to methyl oleate carryover) to CP were produced to determine the economic viability of this approach.

To evaluate the effect of blending TME with other methyl esters, SME and CME were blended with TME at blend ratios of 0 to 100%. Both the SME/TME and CME/TME blends exhibited decreased CPs with increasing levels of SME and CME. Although the CP of the SME/TME blends varied linearly with SME content, the CP of the CME/TME blends varied quadratically with CME content.

To evaluate the potential of fuel additives to reduce the CP of TME, 11 different polymer additives were tested. Although all of these additives were specifically marketed to enhance the cold temperature properties of petroleum diesel or biodiesel, only two of the additives had any significant effect on TME CP. The additive formulated by Meat & Livestock Australia (MLA) outperformed Evonik's Viscoplex 10-530. The MLA additive was investigated further and its effect on CP was characterized in pure TME and in CME/TME blends. When mixed in CME/TME blends, the MLA additive had a synergistic effect and produced lower CPs than the addition of mixing MLA in TME and blending CME with TME.

To evaluate the cold temperature properties of TME blended with petroleum diesel, CPs of TME/diesel blends from 0 to 100% were measured. The TME/diesel blends were treated with the MLA additives to determine the effects of the additives under these blend conditions. The MLA additive also had a synergistic effect when mixed in TME/diesel blends.

Finally, all three of the TME CP reduction methods were evaluated in an economic model to determine the conditions under which each method would be economically viable. Each of the CP reduction methods were compared using a common metric based on the cost of reducing the CP of 1 gallon of finished biodiesel by 1°C (i.e. \$/gal/°C). Since the cost of each method is dependent on varying commodity prices, further development of the economic model (which was developed and tested with 2012 prices) to account for stochastic variation in commodity prices is recommended.

ACKNOWLEDGEMENTS

There are numerous people who contributed to this research that I would be remiss if I did not acknowledge. First, I would like to thank Dr. Marchese for his guidance of this research, his understanding in allowing me to leave to work as a wrangler, and his patience in letting me come back after many years to complete this thesis. I would like to sincerely thank Sun West Biofuels, namely Lee Meisel, Chris Hopper and Jace Hopper for their funding and support of this research. Jace had a large part in conducting these tests and was a valuable sounding board for me.

There were a number of people at the EECL and CSU who contributed to this work. Esteban Hincapie walked me through the ICP procedures and calibrations. Marc Baumgardner and Tara Schumacher both taught me transesterification techniques. Greg Wardle from Solix was key to developing my understanding of the gas chromatograph and in troubleshooting it in order to get it running. Jessica Tryner has been very kind to review my thesis and has been the primary person I have gone to for thesis and defense advice.

I appreciate Dr. Smith for his work as a committee member and his distillation modeling which informed the direction of this research. I also am grateful for Dr. Windom for being willing to join the committee near the completion of this thesis.

Finally, I need to acknowledge my wife, Taylor. She has been the one to bear the brunt of the load as I have completed this thesis. Thank you for all of the unrecognized work you have done to make this possible. I am so glad that you are my teammate!

TABLE OF CONTENTS

ABSTRACT	ii
ACKNOWLEDGEMENTS.....	iv
LIST OF TABLES	ix
LIST OF FIGURES	xi
LIST OF EQUATIONS	xvi
Chapter 1 : Introduction	1
1.1 Motivation for Research	1
1.1.1 Environmental Reasons.....	3
1.1.2 Energy Security	5
1.1.3 Biodiesel vs. Renewable diesel	5
1.1.4 Sun West Biodiesel Plant.....	6
1.2 Biodiesel Overview.....	6
1.2.1 Transesterification.....	6
1.2.2 Feedstocks	8
1.2.3 Fatty Acid Methyl Esters.....	9
1.3 Beef Tallow Biodiesel	10
1.3.1 Pretreatment Processes.....	10
1.3.2 Existing Tallow Biodiesel Plants	12
1.4 Fuel Properties.....	12
1.4.1 ASTM D6751 Biodiesel Standard.....	12
1.4.2 Cold Temperature Properties.....	13
1.4.3 Oxidative Stability	16
1.4.4 Cetane Number	17
1.4.5 Iodine Value	18
1.4.6 Tables of TME, SME and CME Fuel Properties	18
1.5 Solutions to TME Cold Temperature Problems	21
1.5.1 Fractionation.....	22
1.5.2 Blending With Other FAMES	24
1.5.3 Additives	24
1.5.4 Forming Different Esters.....	25
1.6 Organization of the Thesis.....	25
Chapter 2 : Experimental Equipment and Methods.....	28
2.1 Cloud Point Test.....	28
2.2 Cold Filter Plugging Point Test.....	29

2.3	Gas Chromatography	30
2.3.1	Gas Chromatography Description.....	30
2.3.2	Gas Chromatography Test Method.....	31
2.3.3	Gas Chromatography Standards.....	33
2.4	Inductively Coupled Plasma with Optical Emission Spectrometer Test	34
2.4.1	ICP-OES Description	35
2.4.2	ICP-OES Test Method	35
2.4.3	ICP-OES Calibration.....	36
2.5	Oxidative Stability Test.....	36
2.5.1	Oxidative Stability Test Description	36
2.5.2	Oxidative Stability Test Method	38
2.5.3	Oxidative Stability Calibration	38
2.6	Flash Point Test.....	39
Chapter 3 : Tallow Methyl Ester Production.....		40
3.1	Tallow Pretreatment Process.....	40
3.1.1	Initial Pretreatment Process.....	40
3.1.2	Modifications to Pretreatment Process.....	42
3.1.3	Optimized Pretreatment Process.....	46
3.2	Transesterification Process	47
3.2.1	Feedstock Titration.....	48
3.2.2	Initial Transesterification Process	48
3.2.3	Modifications to Transesterification Process	49
3.2.4	Optimized Transesterification Process	50
3.2.5	Biodiesel Quality Checks.....	51
Chapter 4 : Distillation Fractionation Cloud Point Reduction.....		55
4.1	Introduction	55
4.2	Distillation Fractionation Computer Simulations.....	56
4.3	Distillation Fractionation Modeling.....	58
4.3.1	Thermodynamic Cloud Point Prediction Models	58
4.3.2	Theoretical Eutectic Point.....	63
4.3.3	Target Cloud Point FAME Profiles	64
4.3.4	Tallow Methyl Ester FAME Profiles	67
4.3.5	Fractionation FAME Profile Simulation.....	67
4.3.6	Methyl Stearate/Methyl Oleate Carryover.....	69
4.4	Empirical Fractionation Data	70
4.4.1	Exploratory Fractionation Cloud Point Tests	70
4.4.2	Eutectic Fractionation Tests Results	72

4.4.3	Expanded Cloud Point Data.....	77
4.4.4	Empirical Eutectic Point.....	79
4.5	Comparison of Fractionation Data with Cloud Point Prediction Models.....	81
4.6	Conclusions.....	85
Chapter 5 :	Blending with FAMEs Cloud Point Reduction.....	86
5.1	Introduction.....	86
5.2	Soy Methyl Ester Blending.....	88
5.3	Canola Methyl Ester Blending.....	89
5.4	Comparison of Blending Data with Cloud Point Prediction Models.....	92
5.5	Conclusion.....	98
Chapter 6 :	Additive Cloud Point Reduction.....	99
6.1	Introduction.....	99
6.2	Evonik Viscoplex 10-530.....	100
6.3	CorsiTech Additives.....	104
6.4	Infineum Additives.....	109
6.5	MLA Additive.....	116
6.5.1	MLA Additive Makeup.....	116
6.5.2	MLA Additive and CME Blending.....	117
6.5.3	MLA Additive Components.....	122
6.6	Conclusion.....	126
Chapter 7 :	Blending with Diesel Fuel.....	128
7.1	Diesel Blended with Tallow Biodiesel.....	128
7.2	MLA Additive in TME/Diesel Blend.....	129
7.3	MLA Additive in TME then Blended with Diesel.....	134
7.4	Conclusion.....	137
Chapter 8 :	Economic Comparison of CP Reduction Methods.....	138
8.1	Economic Motivation to Tallow Research.....	138
8.2	Distillation Fractionation Standardized Cost.....	138
8.3	Crystallization Fractionation Standardized Cost.....	141
8.4	SME Blending Standardized Cost.....	142
8.5	CME Blending Standardized Cost.....	143
8.6	MLA Additive in TME Standardized Cost.....	144
8.7	MLA Additive in CME/TME Blends Standardized Cost.....	145
8.8	Economic Decision Making for Multiple Methods.....	147
Chapter 9 :	Conclusions and Future Work.....	151
9.1	Improved Fuel Production Steps.....	152
9.2	Comparing Cloud Point Reduction Methods.....	152

9.2.1	Fractionation.....	152
9.2.2	Blending.....	153
9.2.3	Additives	154
9.2.4	Combination of Methods	154
9.2.5	Diesel Blends	155
9.3	Economics	155
9.4	Future Work.....	156
	References	159
	Appendix A : Cloud Point Models' Calculated Curves.....	162
	Appendix B : Comparison of TME FAME Profiles.....	164
	Appendix C : FAME Profiles of Fractionation Tests.....	166
	Appendix D : Fractionation Cold Filter Plugging Point Results.....	178
	Appendix E : Comparison of Fractionation Tests with CP Models.....	180
	Appendix F : FAME Profiles of Blending Tests	182
	Appendix G : Blending Cold Filter Plugging Point Results.....	184
	Appendix H : Comparison of Blending Tests with CP Models.....	185
	Appendix I : FAME Profiles of Various Feedstocks.....	187
	Appendix J : Additional Data of MLA in TME/Diesel Blends.....	188
	Appendix K : Comparison of Measured and Literature Cloud Points	191
	List of Abbreviations	192

LIST OF TABLES

Table 1.1 – Table of fatty acid methyl esters commonly found in tallow biodiesel with short hand name, chemical name, chemical formula and a chemical structure representation [22].....	9
Table 1.2 - Table of fuel properties and their requirements to meet ASTM D6751 [26]	13
Table 1.3 – Measured FAME profiles and CPs for TME, SME and CME with FAME MPs [3],[31].....	15
Table 1.4 – Table of TME properties in relation to ASTM D6571 standard [13]	19
Table 1.5 – Table of SME properties in relation to ASTM D6571 standard [13].....	20
Table 1.6 – Table of CME properties in relation to ASTM D6571 standard [13]	21
Table 3.1 - Initial pretreatment steps provided by Sun West Biofuels	41
Table 3.2 – ICP-OES results for initial tallow pretreatment using the Sun West process	42
Table 3.3 – ICP-OES results for second tallow pretreatment using a modified process	42
Table 3.4 – ICP-OES results for third tallow pretreatment using a modified process	44
Table 3.5 - ICP-OES results for fourth tallow pretreatment using a modified process	45
Table 3.6 - ICP-OES results for additional tallow pretreatment steps to reduce P and Si.....	46
Table 3.7 – Optimized pretreatment steps to reduce metals in tallow	47
Table 3.8 – Initial transesterification process	49
Table 3.9 – Optimized transesterification steps to make TME from tallow.....	51
Table 4.1 – Flow rates and FAME profiles in PNNL’s initial distillation model [51]	57
Table 4.2 – Flow rates and FAME profiles in PNNL’s second distillation model [52].....	58
Table 4.3 – Imahara’s molar enthalpy of melting for saturated methyl esters [30]	60
Table 4.4 – Dunn’s results for MP, FP, ΔH_m , and ΔH_{fus} from DSC analyses of pure FAME [29]	61
Table 4.5 – Dunn’s results for heat capacities of pure FAME in liquid and solid phases [29]	61
Table 4.6 – Proposed tests to reach 10°C, 7°C, 2°C, and 0°C CP at the theoretical eutectic ratio with additional tests at +/- 20% MS	66
Table 4.7 – “Model TME Profile” compared with average of other TME profiles	67
Table 4.8 – FAME profiles of Sigma Aldrich FAME mixtures used for fractionation modeling.....	68
Table 4.9 – Initial exploratory CP tests with explanations, calculated CPs, target MP/(MP+MS) ratios and target MP+MS fractions.....	70
Table 4.10 – Proposed CP tests with explanations, calculated CPs, target MP/(MP+MS) ratios and target MP+MS fractions.....	72
Table 4.11 – Additional CP tests with purpose, calculated CPs, target MP/(MP+MS) ratios and target MP+MS fractions.....	73
Table 6.1 – Tested additives designed to improve various cold temperature properties	99
Table 6.2 – Percentage breakdown of MLA additive components.....	124
Table 7.1 – Table of CP and CFPP for TME/Diesel blends	129
Table B.1 – FAME profiles of different TME samples used to make “Standard TME Profile”	164
Table C.1 – CP, CFPP, yields and GC FAME profile results of exploratory fractionation tests.....	166
Table C.2 – CP, CFPP, yields and measured FAME profiles of fractionation test groups 1 and 2	167
Table C.3 – CP, CFPP, yields and measured FAME profiles of fractionation test group 5.....	168
Table C.4 – CP, CFPP, yields and measured FAME profiles of fractionation test groups 6 and 7	169
Table F.1 – CP, CFPP and FAME profiles for SME in TME blending tests	182

Table F.2 – CP, CFPP and FAME profiles from CME blending with TME using CAN-BD-A..... 182
Table F.3 - CP, CFPP and FAME profiles from CME blending with TME using CAN-BD-B..... 183

LIST OF FIGURES

Figure 1.1 – World oil consumption and production in million barrels per day from 1965 to 2012. Consumption (yellow), production (grey). [1].....	1
Figure 1.2 – Average change in NO _x , PM, CO and HC emissions from petroleum diesel to biodiesel in heavy-duty highway engines [5].....	4
Figure 1.3 – Visualization of the transesterification process [15].....	7
Figure 1.4 – Comparison of soybean oil and inedible tallow prices historically [24].....	11
Figure 1.5 – Melting points of individual FAMES commonly found in biodiesel feedstocks.....	15
Figure 2.1 – GC oven temperature method “BD_Method_7” used to measure FAME profiles.....	32
Figure 2.2 – Sample GC readout in Peak Simple showing peaks for each FAME type in TME.....	33
Figure 2.3 – Schematic of Rancimat heating block, sample vial and conductivity measuring vessel [49].....	37
Figure 2.4 – Sample oxidative stability chart with Rancimat 743 showing OSI at 8.97h.....	38
Figure 3.1 – Typical pretreatment process flow chart similar to Sun West method [13].....	40
Figure 3.2 – Comparison of measured CP and CFPP temperatures for TME, SME and CME.....	52
Figure 3.3 – Oxidative stability conductivity graph for JBS-BD-D.....	53
Figure 4.1 – PNNL’s initial CHEMCAD distillation model solving to remove high purity MP. The FAME percentages and flow rates for each stream are detailed in Table 4.1. [51].....	56
Figure 4.2 - PNNL’s second CHEMCAD distillation model to separate MS and MO.	57
Figure 4.3 – Eutectic point of binary MP and MS mixture.....	60
Figure 4.4 – Plot of Dunn’s activity coefficients from the DSC analysis of MP or MS in a MO solvent [29].....	62
Figure 4.5 – CP vs MP/(MP+MS) for the Hildebrand “Ideal” model at varying MP+MS fractions.....	64
Figure 4.6 – Proposed test points in relation to MP/(MP+MS) ratio and percent MP+MS.....	66
Figure 4.7 – Comparison of ideal yield and 4:1 MS/MO carryover yield for fractionation tests.....	69
Figure 4.8 – Comparison of calculated and empirical CPs of the initial exploratory tests.....	71
Figure 4.9 – Calculated and empirical CPs of planned test points from Table 4.10.....	73
Figure 4.10 – Comparison of calculated and empirical CPs of additional tests.....	74
Figure 4.11 – All empirical fractionation CP tests in relation to the MP/(MP+MS) ratio.....	75
Figure 4.12 – All empirical fractionation CPs in relation to MP/(MP+MS) ratio sorted by MP+MS fraction.....	76
Figure 4.13 – Contrast of empirical fractionation test CPs with 4:1 MS/MO carryover yield.....	77
Figure 4.14 – Calculated MP (solid) and MS (dashed) CP curves for MP+MS groups. Brackets show portion of 11% and 33% MP curves where average values were calculated.....	78
Figure 4.15 – Expanded CPs at various MP+MS fractions with empirical CPs (X’s). Diamonds are adjusted using the MP curves and circles are adjusted using the MS curves.....	80
Figure 4.16 – Comparison all empirical CPs (fractionation, and SME and CME blending) of MP/(MP+MS) ratio versus various MP+MS fractions.....	80
Figure 4.17 – Comparison of expanded CPs versus 4:1 carryover yield (points) with calculated CP/carryover yield curves. Expanded cloud points adjusted with the MP curve are diamonds while those adjusted from the MS curve are circles.....	81

Figure 4.18 – Comparison of the empirical CP for each fractionation test with each CP model	82
Figure 4.19 – Average variation of FPDT CP models from empirical fractionation test CPs	83
Figure 4.20 – Maximum variation of FPDT CP models from empirical fractionation test CPs.....	84
Figure 4.21 – Comparison of calculated CP lines and expanded fractionation CPs. Dashed lines are the MP CP and solid lines are the MS CP. Diamonds are CPs adjusted from the MP curves while circles are CPs adjusted from the MS curves.....	85
Figure 5.1 – Comparison of tallow, canola and soy biodiesel FAME profiles	87
Figure 5.2 – CPs and CFPPs for SME blends in TME with best fit equations.....	88
Figure 5.3 – CP variation along MP/(MP+MS) ratio for SME blended in TME.....	89
Figure 5.4 - CPs and CFPPs for CME blends in TME with best fit equations	90
Figure 5.5 – Comparison of SME/TME and CME/TME blend CPs.....	91
Figure 5.6 - CP variation along MP/(MP+MS) ratio for CME blended in TME	92
Figure 5.7 – Variation between empirical CPs and CP models for each SME/TME blend.....	93
Figure 5.8 – Average variation for all SME/TME blend tests for each CP prediction model.....	94
Figure 5.9 – Maximum variation for each CP prediction model for all SME/TME blend tests.....	94
Figure 5.10 – Variation between empirical CPs and CP models for CAN-BD-A/TME blends	95
Figure 5.11 – Variation between empirical CPs and CP models for CAN-BD-B/TME blends	95
Figure 5.12 – Average variation for all CME/TME blend tests for each CP prediction model.....	96
Figure 5.13 – Maximum variation for each CP prediction model for all CME/TME blend tests.....	96
Figure 5.14 –Variation between “Average Calculated CP” and empirical CP for all tests at MP/(MP+MS) fractions	97
Figure 6.1 – Effect of Evonik’s Viscoplex 10-530 dosage on CME/TME blend CPs.....	100
Figure 6.2 – Effect of Evonik’s Viscoplex 10-530 dosage on CME/TME blend CFPPs.....	101
Figure 6.3 – CP reduction by Viscoplex 10-530 from 0% dosage for various CME blends.....	101
Figure 6.4 – CFPP reduction by Viscoplex 10-530 from 0% dosage for various CME blends	102
Figure 6.5 – Additional CP reduction from synergy of CME blend and Viscoplex 10-530	103
Figure 6.6 - Additional CFPP reduction from synergy of CME blends and Viscoplex 10-530	103
Figure 6.7 – CP effect of CorsiTech 4006 additive in 25% CME/TME blend	105
Figure 6.8 – CFPP effect of CorsiTech 4006 additive in 25% CME/TME blend	105
Figure 6.9 – CP effect of CorsiTech 4027 additive in CME/TME blends	106
Figure 6.10 – CFPP effect of CorsiTech 4027 additive in 25% CME/TME blend	106
Figure 6.11 – CP effect of CorsiTech 4028 additive in 25% CME/TME blend.....	107
Figure 6.12 – CFPP effect of CorsiTech 4028 additive in 25% CME/TME blend	107
Figure 6.13 – CP effect of CorsiTech 6144 additive in 25% CME/TME blend.....	108
Figure 6.14 – CFPP effect of CorsiTech 6144 additive in 25% CME/TME blend	108
Figure 6.15 – CP effect of Infineum R408 additive in 25% CME/TME blend	110
Figure 6.16 – CFPP effect of Infineum R408 additive in 25% CME/TME blend.....	110
Figure 6.17 - CP effect of Infineum R440 additive in 25% CME/TME blend	111
Figure 6.18 - CFPP effect of Infineum R440 additive in 25% CME/TME blend.....	111
Figure 6.19 - CP effect of Infineum R511 additive in 25% CME/TME blend	112
Figure 6.20 - CFPP effect of Infineum R511 additive in 25% CME/TME blend.....	112
Figure 6.21 – CP and CFPP effect of Infineum R511 additive in SME	113
Figure 6.22 - CP effect of Infineum R518 additive in 25% CME/TME blend	114

Figure 6.23 - CFPP effect of Infineum R518 additive in 25% CME/TME blend.....	114
Figure 6.24- CP effect of Infineum R536 additive in 25% CME/TME blend	115
Figure 6.25 - CFPP effect of Infineum R536 additive in 25% CME/TME blend.....	115
Figure 6.26 – Chart from MLA report showing CP and CFPP reduction in B20 biodiesel.....	117
Figure 6.27 – CP effect of MLA additive in CME/TME blends	118
Figure 6.28 – CFPP effect of MLA additive in CME/TME blends.....	118
Figure 6.29 – CP reduction by MLA additive from 0% dosage for various CME/TME blends.....	119
Figure 6.30 – CFPP reduction by MLA additive from 0% dosage for various CME/TME blends	120
Figure 6.31 – Additional CP reduction from synergy of CME blend and MLA additive.....	121
Figure 6.32– Additional CFPP reduction from synergy of CME blend and MLA additive	121
Figure 6.33 – Visualization of CME blending and MLA additive CP reduction.....	122
Figure 6.34 – Percentage breakdown of diesel, surfactant and polymer in MLA additive	123
Figure 6.35 – Breakdown of polymer and surfactant constituent percentages	124
Figure 6.36 – CP and CFPP reduction from solid and liquid portions of MLA additive.....	125
Figure 6.37 – Comparison of CP effect of Viscoplex 10-530 and MLA additives in CME blends	126
Figure 7.1 – CP and CFPP for TME/diesel blends with best fit equations.....	128
Figure 7.2 – CP effect of MLA additive mixed with various TME/diesel blends.....	130
Figure 7.3 – CFPP effect of MLA additive mixed with various TME/diesel blends	130
Figure 7.4 – CP reduction from MLA additive mixed with TME/diesel blends	131
Figure 7.5 – CFPP reduction from MLA additive mixed with TME/diesel blends	132
Figure 7.6 – Synergistic effect on CP from diesel blend interaction with MLA additive	133
Figure 7.7 – Synergistic effect on CFPP from diesel blend interaction with MLA additive.....	133
Figure 7.8 – CP reduction from MLA additive mixed with TME then blended with diesel.....	134
Figure 7.9 – CFPP reduction from MLA additive mixed with TME then blended with diesel.....	135
Figure 7.10 – Synergistic effect on CP from MLA additive in TME, then blended with diesel.....	136
Figure 7.11 – Synergistic effect on CFPP from MLA additive in TME, then blended with diesel.....	136
Figure 8.1 – Model for finding fractionation yield from desired CP with best fit equations	140
Figure 8.2 – Correlation between CP and SME/TME blend with best fit equation	142
Figure 8.3 – Correlation between CP and CME/TME blend with best fit equation.....	143
Figure 8.4 – Correlation between CP and MLA additive dosage with best fit equation	144
Figure 8.5 – Correlation between CP and MLA additive dosage at different CME/TME blends.....	146
Figure 8.6 – Correlation between CP and CME/TME blends at different MLA additive dosages.....	147
Figure 8.7 – Example of input interface for economic comparison model	148
Figure 8.8 – Example of standardized cost comparison with blend and additive percentages for economic comparison model.....	148
Figure 8.9 – Example of a results table for economic comparison model showing most cost effective method.....	149
Figure 8.10 – Economic comparison of CP reduction methods with 2012 prices.....	149
Figure 8.11 – Economic comparison of CP reduction methods with 2017 prices.....	150
Figure 9.1 – Biodiesel sorted by monounsaturated, polyunsaturated and saturated methyl esters. Areas satisfying parameter of the European Standard UNE-EN 14214: yellow (right), good cetane number and iodine value; blue (left), good CFPP; green (intersection), biodiesel that satisfied UNE-EN 14214. [18].....	158

Figure A.1 - CP vs MP/(MP+MS) ratio for the “Imahara” model at varying MP+MS fractions	162
Figure A.2 - CP vs MP/(MP+MS) ratio for the “Imahara (Dunn)” model at varying MP+MS fractions	162
Figure A.3 - CP vs MP/(MP+MS) ratio for the “Dunn (Simple)” model at varying MP+MS fractions	163
Figure B.1 – Comparison of FAME profiles of various TME sources	164
Figure B.2 – Comparison of “Model TME Profile” with measured TME profiles	165
Figure C.1 – Estimated and measured FAME Profile for “Test TME”	169
Figure C.2 – Target, expected and measured FAME Profile for “Test 1”	170
Figure C.3 – Target, expected and measured FAME Profile for “Test 2 +MS”	170
Figure C.4 – Target, expected and measured FAME Profile for “Test 2 TEP”	171
Figure C.5 – Target, expected and measured FAME Profile for “Test 2 -MS”	171
Figure C.6 – Target, expected and measured FAME Profile for “Test 5”	172
Figure C.7 – Target, expected and measured FAME Profile for “Test 5 EEPL”	172
Figure C.8 – Target, expected and measured FAME Profile for “Test 5 EEPR”	173
Figure C.9 – Target, expected and measured FAME Profile for “Test 6”	173
Figure C.10 – Target, expected and measured FAME Profile for “Test 6 EEP”	174
Figure C.11 – Target, expected and measured FAME Profile for “Test 6 EEPL”	174
Figure C.12 – Target, expected and measured FAME Profile for “Test 6 EEPR”	175
Figure C.13 – Target, expected and measured FAME Profile for “Test 7 EEP”	175
Figure C.14 – Comparison of FAME Profiles for Test 2 group.....	176
Figure C.15 – Comparison of FAME Profiles for Test 5 group.....	176
Figure C.16 – Comparison of FAME Profiles for Test 6 group.....	177
Figure D.1 –Cold filter plugging point for fractionation tests	178
Figure D.2 – All empirical fractionation CFPPs in relation to MP/(MP+MS) ratio and sorted by MP+MS fraction.....	178
Figure D.3 – All empirical fractionation CFPPs in relation to MP/(MP+MS) ratio	179
Figure E.1 – Comparison of fractionation tests’ empirical, calculated average and “Ideal” CPs.....	180
Figure E.2 – Comparison of fractionation tests’ empirical, calculated average and “Imahara” CPs. 180	
Figure E.3 – Comparison of fractionation empirical, calculated average and “Imahara (Dunn)” CPs	181
Figure E.4 – Comparison of fractionation tests’ empirical, calculated average and “Dunn” CPs.....	181
Figure G.1 – SME blending CFPPs in relation to MP/(MP+MS) ratio	184
Figure G.2 – CME blending CFPPs in relation to MP/(MP+MS) ratio.....	184
Figure H.1 – Comparison of empirical CPs with CP models for each SME/TME blend	185
Figure H.2 – Comparison of empirical CPs with CP models for each CAN-A-BD/TME blend	185
Figure H.3 – Comparison of empirical CPs with CP models for each CAN-B-BD/TME blend	186
Figure I.1 – FAME profiles of a diverse set of biodiesel feedstocks possibilities [13]	187
Figure J.1 – Effect of MLA additive on cloud point of TME/diesel blends	188
Figure J.2 – Effect of MLA additive on cold filter plugging point of TME/diesel blends	188
Figure J.3 – CP reduction with all MLA/TME/Diesel blend data at percent MLA of total	189
Figure J.4 – CFPP reduction with all MLA/TME/Diesel blend data at percent MLA of total	189
Figure J.5 – Detailed view of Figure J.3 at lower dosages	190

Figure J.6 – Detailed view of Figure J.4 at lower dosages	190
Figure K.1 – Plot of measured FAME CPs from CSU, Dunn and Imahara at MP/(MP+MS) ratio	191
Figure K.2 – Plot of measured FAME CPs from CSU, Dunn and Imahara by MP+MS fraction.....	191

LIST OF EQUATIONS

Equation 4.1 - Freezing point depression theory model for independent crystallization [29]	59
Equation 4.2 - Hildebrand equation for ideal freezing point depression solutions [29]	59
Equation 4.3 - Freezing point depression theory model variation by Imahara et al. [29]	59
Equation 8.1 - General equation to find standardized cost of fractionation	140
Equation 8.2 - Standardized cost for SME/TME blending	143
Equation 8.3 - Standardized cost for CME/TME blending.....	144
Equation 8.4 - Equation to find the standardized cost of MLA additive in TME.....	145

Chapter 1: Introduction

1.1 Motivation for Research

Liquid, energy-dense petroleum products are the fuel that literally drives the American economy. Before the availability of liquid petroleum fuels, energy was very hard to mobilize. Solid fuels, like coal and wood are more challenging from a fuel management standpoint and are less energy dense. Until recently, gaseous fuels were problematic because storing enough energy was difficult without extremely high pressures or cryogenic storage. Liquid hydrocarbon fuels avoid both those problems, so through the Industrial Age, petroleum products became the king of fuels. In the heyday of initial discoveries in Pennsylvania, Texas, then the Middle East, fossil-derived petroleum seemed like an unending resource. But as worldwide consumption has increased 55% from 1982 to 2012 (Figure 1.1), the world is beginning to realize that fossil fuels, like all finite resources, will eventually run out [1]. When that will happen is very much up to much debate.

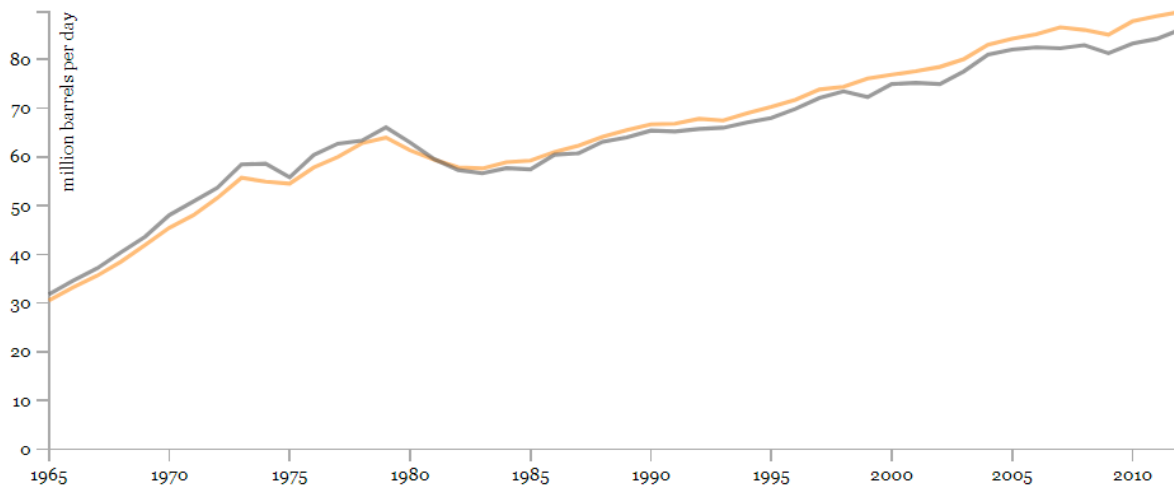


Figure 1.1 – World oil consumption and production in million barrels per day from 1965 to 2012. Consumption (yellow), production (grey). [1]

Unfortunately, the effects of burgeoning demand and diminishing reserves will be felt much earlier than that. The concept of “peak oil” is the point where the rate of oil production reaches its peak and can no longer keep up with rising consumption. While the details of when exactly that will happen are disputed, the issue remains that eventually we will run out of fossil fuels and will need a liquid energy source that can be produced as long as we inhabit this planet.

Our sun is a fusion reactor that constantly emits radiative energy. Within 1.5 hours, the small fraction of its energy that intersects the Earth surpasses the energy consumed by the whole world in 2001 [2]. If we consider the Sun to be our primary energy source, and ultimately our only energy source, we can start to see a host of renewable energy sources here on Earth. We can harness the sun’s energy to directly produce electricity with photovoltaic solar panels, or to heat water with passive solar. We can harness energy from the wind, which is produced from the movement of air warmed by the sun. Even energy from tidal and wave motions are a result of the gravitational pull of the Sun and the Moon. But to return to our original problem - what liquid fuel, energized by the Sun can replace our need for the depleting fossil fuel supply?

Hydrocarbon fuels derive their high energy density from the simple hydrogen to carbon bond. This bond is extremely energetic and exothermic when disassociated. In nature, we can find a host of organisms that contain hydrocarbon chains. In animals we call them fats, and in plants they are called oils. When extracted, fats and oils have similar properties to petroleum products and with some modifications can closely imitate fossil fuel products. Plants derive their energy directly from the Sun through photosynthesis, and herbivores derive their energy from plants. Carnivores eat herbivores to get their energy. Ultimately, any plant or animal derived hydrocarbon chain is fueled by the Sun. The variety of oxygenated hydrocarbon chains in fats and oils are known as fatty acids, often joined together in threes as triglycerides. Biodiesel is the name for plant or animal derived mono-alkyl esters of fatty acids, which closely imitates diesel fuel, and is one solution to replacing finite fossil fuels with renewable, liquid, energy-dense sources.

1.1.1 Environmental Reasons

While the eventual runout of petroleum is a significant issue, another issue of increasing concern is the byproducts of burning hydrocarbons. The byproducts of ideal combustion are always carbon dioxide (CO_2) and water (H_2O). We live in an imperfect world, so combustion is always incomplete to some extent, and can produce other products such as carbon monoxide (CO), unburnt hydrocarbons (HC), particulate matter (PM), nitrogen oxides (NO_x), and sulfur oxides (SO_x), since petroleum diesel fuel often has sulfur present [3].

Fossil fuel emissions have become increasingly worrisome. When internal combustion engines first powered vehicles, the effects of the emissions were inconsequential. But as the population of the U.S. has increased, as well as the standard of living, the average household now has 1.74 cars, or around 258 million vehicles in total [4]. When the emissions of all those cars are combined, the effects are much more noticeable.

Less visibly noticeable, CO_2 is a greenhouse gases (GHG) which traps in more of the sun's energy, contributing to climate effects and rising global temperatures. Additionally, CO , NO_x , SO_x , HC and PM are all harmful emissions that are detrimental to air quality. Using biodiesel in place of petroleum diesel reduces CO and PM by 40% and HC by 70% compared to petroleum diesel, although NO_x does increase 10% with biodiesel (Figure 1.2). While burning biodiesel does release CO_2 , it is important to consider the life cycle of biodiesel compared to petroleum diesel. Petroleum diesel takes carbon that is stored underground and releases it in the air in the form of CO_2 when combusted. Biodiesel is produced either from plants, or from animals that ate plants. Plants intake CO_2 from the air to produce their biomass, so the CO_2 released from the biodiesel is much closer to a closed loop cycle than petroleum diesel.

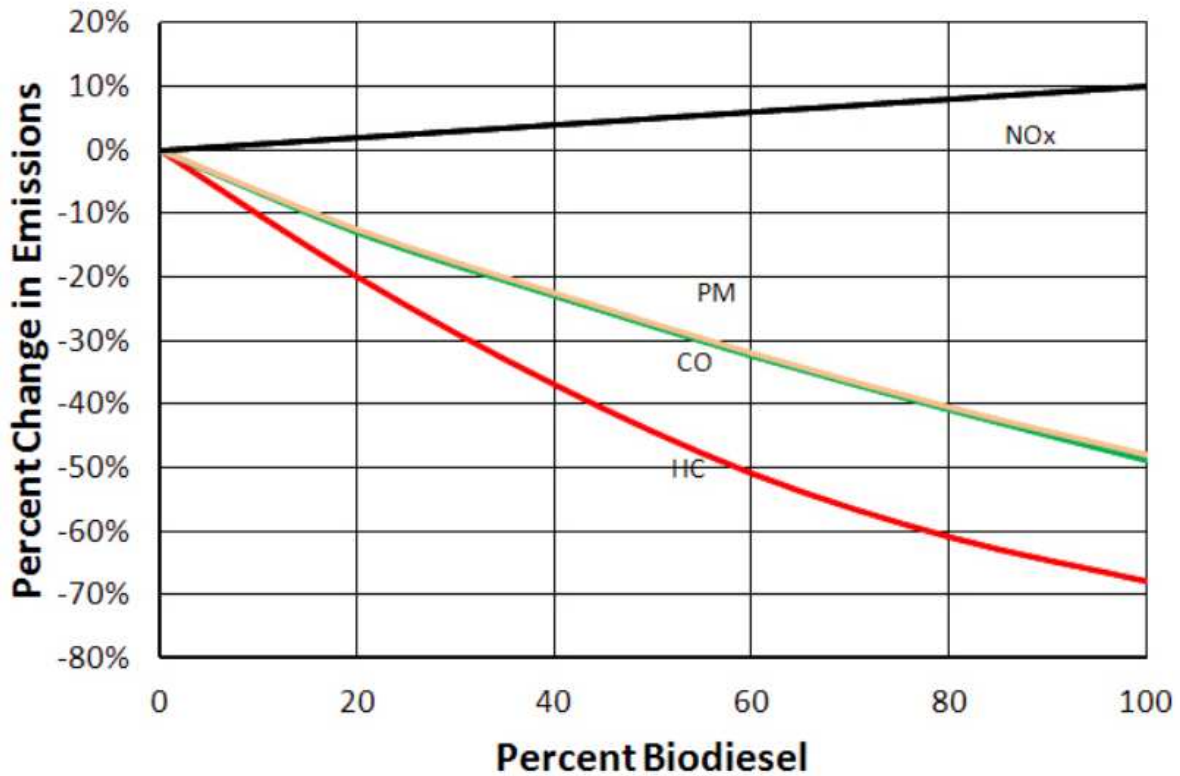


Figure 1.2 – Average change in NOx, PM, CO and HC emissions from petroleum diesel to biodiesel in heavy-duty highway engines [5]

To reduce SOx emissions, the U.S. mandated that all highway diesel fuel contain less than 15 ppm of sulfur by 2014 [6]. As fuel refiners remove sulfur, the lubrication (lubricity) afforded by the fuel decreases as well. Unfortunately, this leads to increased wear and decreased engine life which cause increased emissions. Plant or animal derived biodiesel generally has minimal sulfur content and naturally has greater lubricity than petroleum diesel.

Another benefit biodiesel provides to our environment is that it is biodegradable, unlike petroleum diesel. Countless oil spills have ruined natural habitats and have had significant costs to clean up. If a biodiesel spill were to happen, 80% would naturally biodegrade within 28 days, the biodiesel would be 6 times less toxic than table salt if ingested and 15 times less toxic for fish than petroleum diesel [7], [8].

1.1.2 Energy Security

National security concerns also increase the appeal of biodiesel. A large portion of the world's oil reserves are located in the Middle East. Many of these nations are either hostile to the United States or are suspect allies, that seem to be motivated primarily by financial gain. As demonstrated by the Oil Embargo in the 1970s, access to energy-dense liquid fuels quickly becomes a national security issue. The beauty of biodiesel is that the plants or animals that are used to produce biodiesel can be grown domestically or in friendly nations, greatly increasing control over our energy supply and decreasing the sway unfriendly nations have over us.

1.1.3 Biodiesel vs. Renewable diesel

Another renewable diesel-like fuel that competes with biodiesel to replace petroleum diesel is called "renewable diesel". Renewable diesel is produced from the same feedstock sources as biodiesel but it is refined and processed with hydrogen to create chemically close-to-identical molecules as petroleum diesel, but from renewable sources and with minimal sulfur content. Renewable diesel meets the Standard Specification of Diesel Fuel Oil (ASTM D975), and is therefore a drop-in replacement for petroleum diesel in regards to both cold temperature properties and energy content [9], [10]. This sounds like the perfect renewable fuel, but while it has a lot of advantages there are some significant disadvantages. The refining and hydro-treating process requires a large infrastructure and would have to have enough production to support the expense. In contrast, biodiesel can be produced effectively at small scales. Additionally, the amount of hydrogen required for the process necessitates that the plant has access to a hydrogen pipeline which greatly restricts viable locations in the US to the Gulf Coast of Texas and Louisiana [11].

1.1.4 Sun West Biodiesel Plant

There are a number of cattle slaughterhouses in the Front Range of Colorado. Because of this, the rendered fat from the cattle is an inexpensive, readily available feedstock source in this area. In 2012, when this research was conducted, Sun West Biofuels funded this project as they sought to capitalize on the possibility of using beef tallow as a biodiesel feedstock source. Their goal, if it was economically feasible, was to produce a 60 MGY tallow biodiesel plant in Northern Colorado. At the time, it would have been the first biodiesel plant in Colorado and the largest tallow biodiesel plant in the nation [12]. The major issue that was necessary to research before progressing with this business venture was the cold temperature properties of beef tallow biodiesel. According to REG's "Feedstock Report", beef tallow biodiesel starts to solidify at 16.0°C (60.8°F), well above the temperature at which biodiesels from common feedstocks like soy or canola oil solidify [13]. Without reducing the crystallization temperature, the tallow biodiesel would be worth less and would be unable to compete with soy and canola derived biodiesel.

1.2 Biodiesel Overview

Biodiesel is derived from oils or fats from a variety of organic sources. Biodiesel is the layman's term for mixtures of what is known as fatty acid methyl ester (FAME) or fatty acid ethyl ester (FAEE) depending on whether methanol or ethanol is used in the production process. In this document, biodiesel refers to FAME, unless explicitly stated otherwise, since methanol is much more commonly used at production scale.

1.2.1 Transesterification

Oils and fats are both composed largely of triglycerides; the difference is that oils are liquid at room temperature whereas fats are solid [14]. Oils can be used for fuel as Straight Vegetable Oil

(SVO) but they have much higher viscosities and freezing temperatures than diesel fuel and therefore require modifications in the vehicle fuel delivery system. Converting oils to biodiesel through the transesterification process, illustrated in Figure 1.3, allows the fuel to be run in a largely unmodified vehicle [15].

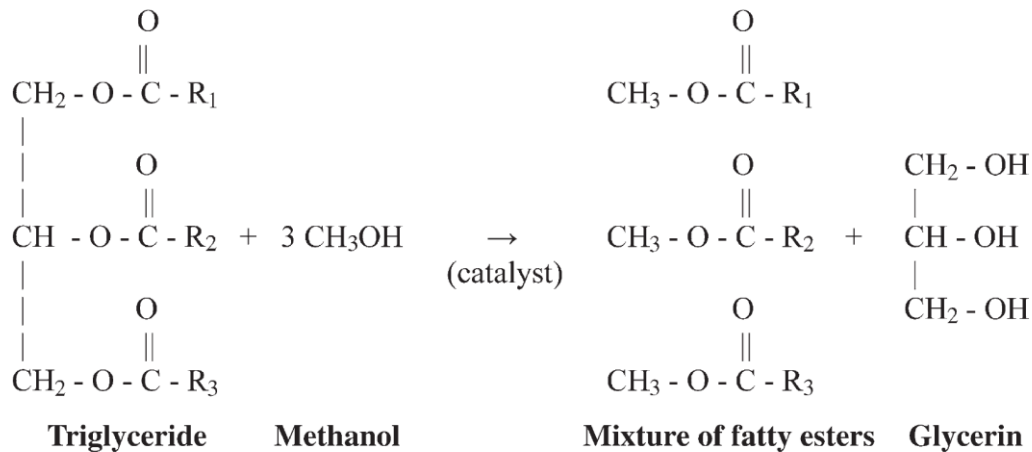


Figure 1.3 - Visualization of the transesterification process [15]

Transesterification converts the fatty acids (FAs) of the triglycerides into fatty acid methyl or ethyl esters (i.e., biodiesel). Aided by heat and a strong base catalyst, like sodium or potassium hydroxide, the FAs are stripped off of the glycerol backbone and react with an alcohol. Ethanol and methanol (MeOH) are the two most common alcohols, but methanol is usually used in production due to its lower cost. The catalyst (often sodium hydroxide) is dissolved in the alcohol (often methanol) to make sodium methoxide, which conjoins the methanol and the FAs into fatty acid methyl esters (FAMES) leaving glycerin and leftover catalyst behind. The glycerin easily separates out and the catalyst can be recycled at plant scale. Once this process is completed, the methyl ester properties are much closer to diesel fuel than the original triglycerides [15], [16].

Transesterification does not alter the fatty acid composition from the original feedstock. This is important since the chain length and number of double bonds determine the characteristics of critical parameters of biodiesel such as oxidative stability, cetane number, and cold flow properties [17], [18].

1.2.2 Feedstocks

Biodiesel can be made from a variety of feedstocks derived from plant or animal sources. In the United States, soybean oil has been the biodiesel feedstock of choice, accounting for 54% of all biodiesel feedstocks in 2012 [19]. Since soy has already been a common crop for U.S. farmers, it has been both less expensive than other feedstocks and available in sufficient quantities to be used as a fuel. The soybean seeds are crushed to extract soybean oil while the rest of the plant is commonly used for animal feed. Soy methyl ester (SME) has a low free fatty acid (FFA) content, contributing to high yields. SME also has more desirable cold temperature properties than tallow methyl ester (TME) [13]. The primary cold temperature metric is cloud point (CP), the temperature at which the fuel begins to crystallize into the solid phase. SME has a reported CP of 0.9°C (33.6°F) compared to a CP of 16.0°C (60.8°F) for TME [13].

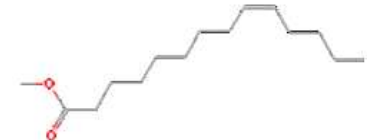
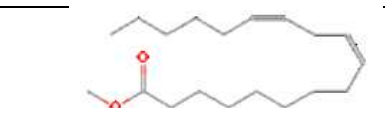
Another common feedstock is oil from the seeds of the canola plant. The canola plant was developed in Canada as a variation of the rapeseed plant and is the premier biodiesel feedstock there [20]. Canola is becoming more common in the US with a 325% increase in production from 2010 to 2014, but it tends to cost more than soy [19]. However, canola methyl ester (CME) has even better cold temperature properties than SME with a reported CP of -3.3°C (26.1°F) [13].

Tallow is another name for the rendered fat from beef cattle. Some physical properties of tallow are less desirable than those of soy or canola. The CP of TME is 16.0°C (60.8°F) which is significantly higher than either SME or CME. The FFA content also tends to be higher as well [13]. However, tallow does have a higher cetane number than soy and canola biodiesel due to its higher saturated FA content [21]. Tallow is not as widely available as either soy or canola but is a viable feedstock in areas with large beef production industries.

1.2.3 Fatty Acid Methyl Esters

All fatty acid methyl esters (FAMES) are not created equal and can vary in both their chain length and the number of double bonds. FAMES are composed of a hydrocarbon chain and an ester end group. The chain length is determined by the number of carbon atoms, not including the carbon atom in the end group. The shorthand notation for differentiating methyl esters based on their hydrocarbon chain length is in the format CXX:Y. The “XX” stands for the number of carbon atoms in the chain length and the “Y” is for the number of double bonds. For instance, methyl palmitate has a chain with sixteen carbon atoms (XX = 16) and no double bonds (Y=0) so it is abbreviated as C16:0. Methyl oleate has eighteen carbon atoms in its chain and one double bond so its shorthand form is C18:1.

Table 1.1 – Table of fatty acid methyl esters commonly found in tallow biodiesel with short hand name, chemical name, chemical formula and a chemical structure representation [22]

Short Hand	Chemical Name	Chemical Formula	Chemical Structure
C14:0	Methyl Myristate	C ₁₅ H ₃₀ O ₂	
C14:1	Methyl Myristoleate	C ₁₅ H ₂₈ O ₂	
C16:0	Methyl Palmitate	C ₁₇ H ₃₄ O ₂	
C16:1	Methyl Palmitoleate	C ₁₇ H ₃₂ O ₂	
C18:0	Methyl Stearate	C ₁₉ H ₃₈ O ₂	
C18:1	Methyl Oleate	C ₁₉ H ₃₆ O ₂	
C18:2	Methyl Linoleate	C ₁₉ H ₃₄ O ₂	
C18:3	Methyl Linolenate	C ₁₉ H ₃₂ O ₂	

In the case of methyl palmitate (C16:0), the molecule is “saturated” with hydrogen atoms and therefore the carbon atoms cannot form double bonds. Any molecule with one double bond (like C18:1) is known as “monounsaturated” and any molecule with more than one double bond (like C18:2) is referred to as “polyunsaturated”. Table 1.1 above lists the shorthand name, the long form chemical name, the chemical formula, and a chemical structure diagram for FAMES commonly found in tallow biodiesel.

1.3 Beef Tallow Biodiesel

Tallow is not a common biodiesel feedstock because its quantity is limited by the amount of beef produced, it is not available throughout the US and it has unfavorable cold temperature properties. In areas where beef production is prominent, like Greeley, CO, tallow can provide a less expensive feedstock than soy or canola oil at quantities large enough to support a full-scale biodiesel plant. The greatest obstacle blocking a large-scale plant from producing tallow biodiesel is the unacceptably high CP temperature of the unmodified TME. A secondary issue that must be addressed, is a pretreatment process is necessary to reduce FFAs to prepare the tallow for transesterification.

1.3.1 Pretreatment Processes

Converting the raw fat from cattle carcasses to purified triglycerides ready for transesterification takes a number of processes. First, at the slaughterhouse, the carcass scraps undergo rendering, which isolates and dehydrates the fat and converts it into a tallow product.

Multiple products can be made from the rendering step including edible tallows and inedible tallows like top white tallow, all beef packer tallow, extra fancy tallow, fancy tallow, bleachable fancy tallow and prime tallow [23]. Edible tallow can be used in human food and pet

food production and has a premium value associated with it. Inedible tallow cannot be used for those purposes, so it is less expensive and is more appealing to be used as a biodiesel feedstock.

Inedible tallow grades with minimal FFA content, like top white and extra fancy tallow, are preferable for producing biodiesel. FFAs lead to reduced yields during transesterification by interfering with the catalyst and forming emulsions that make separation of the oil and water more difficult [13]. To upgrade tallow to the point that it can be converted to biodiesel, a pretreatment step must be incorporated that removes FFAs, gums, metals, and moisture to increase transesterification yields and to meet ASTM fuel standards.

Inedible tallow is not as prolific a feedstock as either soy or canola but is usually less expensive than both of them, which is the driving factor for using tallow as a biodiesel feedstock (Figure 1.4 below) [24]. Since inedible tallow is a byproduct of beef production, it does not have the same dilemma of food vs. fuel as canola and soy do. For the purposes of this paper, “tallow” is referring specifically to “inedible tallow” unless otherwise specified.

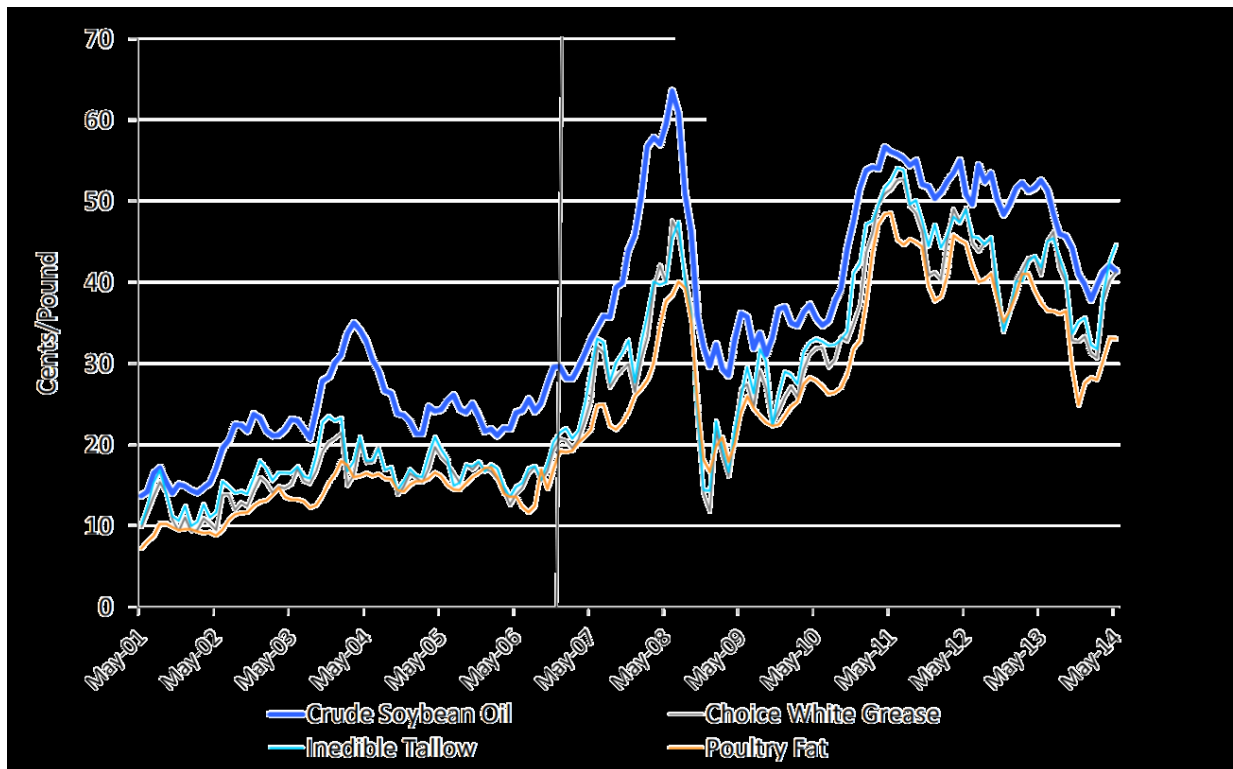


Figure 1.4 - Comparison of soybean oil and inedible tallow prices historically [24]

1.3.2 Existing Tallow Biodiesel Plants

Tallow is a largely untapped inexpensive feedstock waiting for technical solutions to be fully used. In the US it appears that most every plant that uses tallow, uses it as one of many feed stocks. Of those plants that do use tallow, most are located in climates with mild winters like the Gulf Coast or Southern California. According to the Biodiesel Magazine website, the only U.S. biodiesel plant that uses animal tallow (either beef, pork or chicken fat) as a primary feedstock source is Agron Bioenergy in Southern CA [12]. To use TME as a main feedstock in a state that has colder winters like Colorado, further research must be done to improve the cold temperature properties.

1.4 Fuel Properties

Biodiesel is formulated to have fuel properties as similar to petroleum diesel as possible. There are some characteristics where biodiesel tends to underperform petroleum diesel like cold temperature properties, oxidation stability and energy content but biodiesel inherently outperforms petroleum diesel in cetane number and lubricity [25]. Both the chain length and the degree of saturation directly influence a variety of a FAME mixture's physical properties including cloud point, oxidative stability and cetane number.

1.4.1 ASTM D6751 Biodiesel Standard

To be sold in the U.S. as biodiesel, a methyl ester mixture must meet the requirements of ASTM Standard D6751, the "Standard Specification for Biodiesel Fuel Blend Stock (B100) for Middle Distillate Fuels". This standard specifies the limits for metals content, methanol content, glycerin content, oxidative stability, cetane number, and other important fuel properties as seen below in Table 1.2.

Table 1.2 - Table of fuel properties and their requirements to meet ASTM D6751 [26]

Property	Test Method ^A	Grade No. 1-B S15
Sulfur, ^B % mass (ppm), max	D5453	0.0015 (15)
Cold soak filterability, seconds, max	D7501	200
Monoglyceride content, % mass, max	D6584	0.40
Calcium and Magnesium, combined, ppm (µg/g), max	EN 14538	5
Flash point (closed cup), °C, min	D93	93
Alcohol control One of the following shall be met:		
1. Methanol content, mass %, max	EN 14110	0.2
2. Flash point, °C, min	D93	130
Water and sediment, % volume, max	D2709	0.050
Kinematic viscosity, ^D mm ² /s, 40 °C	D445	1.9-6.0
Sulfated ash, % mass, max	D874	0.020
Copper strip corrosion, max	D130	No. 3
Cetane number, min	D613	47
Cloud point, ^E °C	D2500	Report
Carbon residue, ^F % mass, max	D4530	0.050
Acid number, mg KOH/g, max	D664	0.50
Free glycerin, % mass, max	D6584	0.020
Total glycerin, % mass, max	D6584	0.240
Phosphorus content, % mass, max	D4951	0.001
Distillation temperature, Atmospheric equivalent temperature, 90 % recovered, °C, max	D1160	360
Sodium and Potassium, combined, ppm (µg/g), max	EN 14538	5
Oxidation stability, hours, min	EN 15751	3

The relevance of the fuel properties detailed in this research, specifically, cloud point (CP), cold filter plugging point (CFPP), and oxidative stability, as well as the techniques used to measure those properties, are described in detail in the following sections.

1.4.2 Cold Temperature Properties

Regardless of feedstock, biodiesel performs worse in cold weather than petroleum diesel. Cold temperature properties can be tested in a number of ways but all of them seek to determine the change in phase or functionality of biodiesel as the ambient temperature decreases. The original and most common cold temperature property test is the cloud point test. Cloud point (CP) is the temperature at which liquid biodiesel begins to crystalize into the solid phase. The CP has the advantage of describing an actual thermodynamic phenomenon, which makes this metric useful for research [27].

Cold testing biodiesel in vehicles demonstrated that CP was not always indicative of cold temperature problems. Two biodiesels with identical CPs could begin to block the vehicle's fuel filter at different temperatures, sometimes above and sometimes below the fuel's CP, due to variations in crystal structure and size. Because of this inconsistency, the cold filter plugging point (CFPP) test was developed to simulate the clogging of a fuel filter. In the CFPP test, biodiesel is suctioned through a filter with a specific vacuum at decreasing temperatures until the biodiesel no longer flows through the filter. This test was much more accurate at predicting when fuel gelling problems would occur in real life situations compared to the CP test [28].

There are various other cold temperature tests to simulate different situations how the fuel would be used. The cold soak filtration test (CSFT) is used to determine biodiesel performance after liquefying solidified biodiesel. The pour point (PP) is a measure of the temperature when the biodiesel can no longer be poured. The low temperature flow test (LTFT) is a longer CFPP type test allowing more time for the fuel to cold soak. These tests were not conducted since they have limited research applications. CP is more useful for research because it is a thermodynamic event, whereas the other tests are standardized man-made tests that are useful to compare biodiesel performance as it relates to specific usage. Since CFPP, PP, and LTFT have all been shown to correlate linearly with CP, improvements in CP should lead to improvements in other cold temperature properties [28].

CP has been directly correlated with the FAME composition of the biodiesel being tested [29], [30]. The CP of FAMEs improve (i.e. the FAMEs remain in the liquid phase at lower temperatures) as the chain length and the level of saturation decrease. The predominant factor determining CP is whether the FAME is saturated or unsaturated. The two TME molecules with the highest melting points (MP), by far, are the saturated methyl stearate (C18:0; MP=39.1°C) and methyl palmitate (C16:0; MP=30.5°C) FAMEs (See Figure 1.5 below). The effect on a FAME

mixture's CP due to saturation level is much less pronounced between mono and polyunsaturated FAMES than between saturated and monounsaturated FAMES.

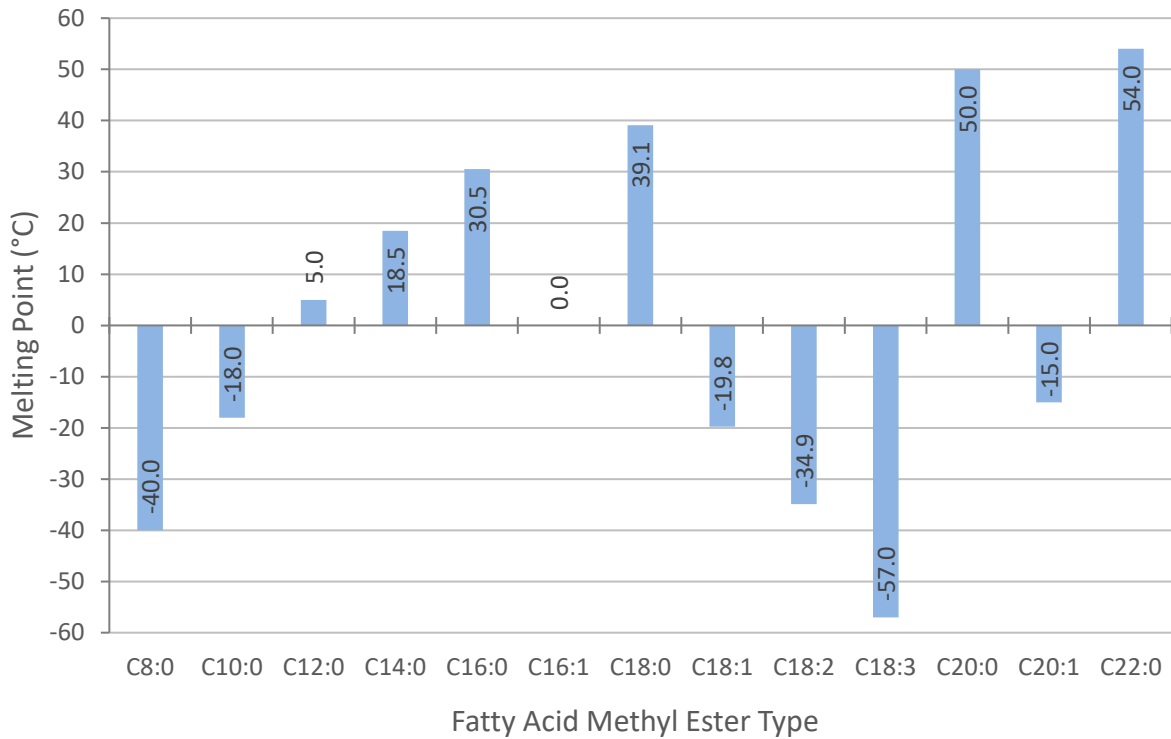


Figure 1.5 – Melting points of individual FAMES commonly found in biodiesel feedstocks

As illustrated in Table 1.3, TME contains a larger percentage of C16:0 and C18:0 than SME or CME, resulting in a much greater CP for TME. SME contains more saturated FAMES than CME, which accounts for the higher CP of SME. Note that even with much more polyunsaturated C18:2 in SME compared to CME, the CP of SME is still higher due to the higher saturated C16:0 and C18:0 content in SME.

Table 1.3 – Measured FAME profiles and CPs for TME, SME and CME with FAME MPs [3],[31]

	CP (°C)	C14:0	C14:1	C16:0	C16:1	C18:0	C18:1	C18:2	C18:3	Other
Tallow Methyl Ester	14.5	4%	1%	25%	3%	21%	40%	2%	0%	4%
Soy Methyl Ester	2.3	0%	0%	10%	0%	4%	23%	54%	8%	0%
Canola Methyl Ester	-8.3	0%	0%	4%	0%	2%	64%	19%	10%	1%
Melting Point (°C)		18.5	-	30.5	0.0	39.1	-19.8	-34.9	-57.0	-

The CP of biodiesel does not have to meet any set temperature to conform to ASTM D6571, it only has to be reported. This means the CP specification only needs to be agreed upon by the supplier and the buyer, which allows flexibility for regional temperature variations. TME could be sold without cold temperature modifications for customers with fuel tank heaters, to suppliers with low TME/diesel blends or in more temperate regions. However, Sun West's target TME CPs were 10°C, 7°C, and 2°C. From a quick primer on how FAME type affects CP, it is clear that reducing the level of saturated FAMES or increasing the level of unsaturated FAMES would favorably affect CP.

1.4.3 Oxidative Stability

Petroleum diesel is superior to biodiesel in that its shelf life is pretty much indefinite. Because biodiesel is an organic, bio-degradable fluid it does have a limited shelf life. When exposed to oxygen, biodiesel undergoes auto-oxidation, degrading the quality of the fuel and creating undesirable byproducts like hydroperoxides, aldehydes, alcohols, shorter chain carboxylic acids, and high molecular weight oligomers which can lead to clogged filters and unwanted deposits. Biodiesels with higher levels of unsaturation (i.e. polyunsaturated FAMES) or lower levels of natural antioxidants are quicker to oxidize [13], [17], [32]. To determine how susceptible different biodiesels are to oxidation, the oxidative stability of fuels can be tested in an instrument that accelerates the oxidation process. This is done by heating a fuel to a standard temperature and flowing air over the sample then through distilled water. The secondary products of oxidation increase the conductivity of the water, and the time it takes the conductivity of the water to reach an inflection point can be used to determine a reproducible oxidative stability index (OSI). The ASTM D6751 standard for biodiesel, requires an oxidative stability time of at least 3 h using the EN 14112 test method. A OSI of 3 h has been shown to correlate to B100 and B20 remaining within specification for four months and for B5 to be acceptable for at least 12 months [17]. According to the REG Feedstock Report, TME typically reaches its inflection point at 1.6 hours, indicating that

additional steps need to be taken to meet the oxidative stability requirement [13]. Since this is a critical fuel property but it is outside of the scope of this paper, it will be measured but not considered further.

1.4.4 Cetane Number

Another critical fuel property, called the cetane number (CN), is a dimensionless number that relates to the ignition delay period of fuels. A higher CN denotes a shorter ignition delay, which is generally desirable, and a lower number indicates a longer ignition delay. All CNs are simply a comparison between the CN of two fuels - one with a very short and one with a very long ignition delay period. The short ignition delay fuel is n-hexadecane ($C_{16}H_{34}$), which was assigned a CN of 100. The long ignition delay fuel is 2,2,4,4,6,8,8-heptamethylnonane (HMN, also $C_{16}H_{34}$), which was assigned the minimum CN of 15. The CN of a specific fuel is determined by the percent of the n-hexadecane mixed in 2,2,4,4,6,8,8-heptamethylnonane that has the same ignition delay period as the test fuel [17]. The ASTM 6751 biodiesel standard requires that the CN must be at least 47. Too high of a CN can lead to incomplete combustion due to too fast an ignition, while too low a CN can lead to misfiring and incomplete combustion as well. Mid-range CNs greater than 47 are best for ideal diesel engine operation and for cold weather startability [17].

Biodiesels with higher concentrations of saturated and longer chained FAMES have higher CNs than those with more unsaturated FAMES and shorter chained CNs. Since TME has a high percentage of saturated FAMES it is common to have cetane numbers between 58 and 65, well above the minimum CN required by the ASTM standard [33]. Given that the CN of tallow is well established and is outside of the scope of this research, it was not measured.

1.4.5 Iodine Value

Iodine Value (IV) is an index measured from biodiesel and is a way of quantifying the level of unsaturation of a FAME mixture. Specifically, the IV relates to the number of double bonds in the solution. Biodiesels with more unsaturated FAMES will have a higher IV than those with more saturated FAMES [17]. IV can be calculated from the FAME profile, with each unsaturated FAME weighted differently. Polyunsaturated and shorter chain FAMES contribute more to the IV [34]. IV could potentially be used to correlate with CP, which is related to FAME saturation, since IV is a metric related the level of saturation.

1.4.6 Tables of TME, SME and CME Fuel Properties

Renewable Energy Group (REG) released a comprehensive report on 34 different biodiesel feedstocks comparing fuel properties such as CP, CFPP, oxidation stability, FFA content, metal content, flash point, moisture, density and viscosity. In addition, they published the fatty acid profiles for each feedstock (see Appendix I) [13]. This report is invaluable for evaluating the feasibility of different feedstocks. Table 1.4, Table 1.5, and Table 1.6 below, come from this report and compare TME, SME and CME fuel properties to the ASTM standards.

Table 1.4 – Table of TME properties in relation to ASTM D6571 standard [13]

		Biodiesel Certificate of Analysis				
Feedstock: Beef Tallow			Product Type: B100			
ASTM D 6751 Analysis of Biodiesel						
Test Parameter	Result	ASTM Limit	Units	Test Method (current revision)		
Cloud point:	16.0 (60.8)	Report	°C (°F)	D 2500		
CFPP ¹ :	14	N/A	°C	D 6371		
Free Glycerin:	0.008	0.020 max.	% Mass	D 6584		
Total Glycerin:	0.076	0.240 max.	% Mass	D 6584		
Monoglycerides ² :	0.223	N/A	% Mass	D 6584		
Diglycerides ³ :	0.063	N/A	% Mass	D 6584		
Triglycerides ⁴ :	0.000	N/A	% Mass	D 6584		
Water & Sediment:	< 0.005	0.050 max.	% Volume	D 2709		
Acid Number:	0.147	0.50 max.	mg KOH/g	D 664, Test Method A		
Visual Inspection:	1	N/A	Haze	D 4176, Procedure 2		
Relative Density at 60 °F:	0.8740	N/A	N/A	D 1298		
Oxidative Stability (110 °C):	1.6	3 min.	hrs	EN 14110		
Flashpoint (closed cup):	>160	93 min.	°C	D 93		
Moisture ⁵ :	0.038	N/A	% Mass	E 203		
Cold Soak Filtration:	76	360	seconds	D 6751 Annex		
Sulfur:	7	15	ppm	D 7039		
Calcium:	<0.1	5 max. Ca+Mg	ppm (ug/g)	EN 14538		
Magnesium:	0.3	5 max. Ca+Mg	ppm (ug/g)	EN 14538		
Phosphorus:	<0.1	0.001 max.	% Mass	D 4951		
Carbon Residue:	0.028	0.050 max.	% Mass	D 524		
Sulfated Ash:	<0.005	0.020 max.	% Mass	D 874		
Kinematic Viscosity at 40 °C:	4.824	1.9-6.0	mm ² /sec.	D 445		
Copper Corrosion (3 hrs at 50 °C):	1a	No. 3 max.	N/A	D 130		

^{1,2,3,4,5} These are not ASTM D 6751 specification requirements.

Table 1.5 – Table of SME properties in relation to ASTM D6571 standard [13]

		Biodiesel Certificate of Analysis				
Feedstock: Soybean			Product Type: B100			
ASTM D 6751 Analysis of Biodiesel						
Test Parameter	Result	ASTM Limit	Units	Test Method (current revision)		
Cloud point:	0.9 (33.62)	Report	°C (°F)	D 2500		
CFPP ¹ :	-4	N/A	°C	D 6371		
Free Glycerin:	0.012	0.020 max.	% Mass	D 6584		
Total Glycerin:	0.149	0.240 max.	% Mass	D 6584		
Monoglycerides ² :	0.473	N/A	% Mass	D 6584		
Diglycerides ³ :	0.088	N/A	% Mass	D 6584		
Triglycerides ⁴ :	0.019	N/A	% Mass	D 6584		
Water & Sediment:	< 0.005	0.050 max.	% Volume	D 2709		
Acid Number:	0.266	0.50 max.	mg KOH/g	D 664, Test Method A		
Visual Inspection:	1	N/A	Haze	D 4176, Procedure 2		
Relative Density at 60 °F:	0.8840	N/A	N/A	D 1298		
Oxidative Stability (110 °C):	2.1	3 min.	hrs	EN 14110		
Flashpoint (closed cup):	>160	93 min.	°C	D 93		
Moisture ⁵ :	0.035	N/A	% Mass	E 203		
Cold Soak Filtration:	67	360	seconds	D 6751 Annex		
Sulfur:	0.8	15	ppm	D 7039		
Calcium:	<0.1	5 max. Ca + Mg	ppm (ug/g)	EN 14538		
Magnesium:	0.3	5 max. Ca + Mg	ppm (ug/g)	EN 14538		
Phosphorus:	<0.1	0.001 max.	% Mass	D 4951		
Carbon Residue:	0.038	0.050 max.	% Mass	D 524		
Sulfated Ash:	<0.005	0.020 max.	% Mass	D 874		
Kinematic Viscosity at 40 °C:	4.039	1.9-6.0	mm ² /sec.	D 445		
Copper Corrosion (3 hrs at 50 °C):	1a	No. 3 max.	N/A	D 130		

^{1,2,3,4,5} These are not ASTM D 6751 specification requirements.

Table 1.6 – Table of CME properties in relation to ASTM D6571 standard [13]

		Biodiesel Certificate of Analysis				
Feedstock: Canola			Product Type: B100			
ASTM D 6751 Analysis of Biodiesel						
Test Parameter	Result	ASTM Limit	Units	Test Method (current revision)		
Cloud point:	-3.3 (26.06)	Report	°C (°F)	D 2500		
CFPP ¹ :	-13	N/A	°C	D 6371		
Free Glycerin:	0.006	0.020 max.	% Mass	D 6584		
Total Glycerin:	0.098	0.240 max.	% Mass	D 6584		
Monoglycerides ² :	0.301	N/A	% Mass	D 6584		
Diglycerides ³ :	0.078	N/A	% Mass	D 6584		
Triglycerides ⁴ :	0.020	N/A	% Mass	D 6584		
Water & Sediment:	< 0.005	0.050 max.	% Volume	D 2709		
Acid Number:	0.010	0.50 max.	mg KOH/g	D 664, Test Method A		
Visual Inspection:	1	N/A	Haze	D 4176, Procedure 2		
Relative Density at 60 °F:	0.8820	N/A	N/A	D 1298		
Oxidative Stability (110 °C):	7.6	3 min.	hrs	EN 14110		
Flashpoint (closed cup):	>160	93 min.	°C	D 93		
Moisture ⁵ :	0.036	N/A	% Mass	E 203		
Cold Soak Filtration:	113	360	seconds	D 6751 Annex		
Sulfur:	1.4	15	ppm	D 7039		
Calcium:	0.4	5 max. Ca+Mg	ppm (ug/g)	EN 14538		
Magnesium:	0.5	5 max. Ca+Mg	ppm (ug/g)	EN 14538		
Phosphorus:	<0.1	0.001 max.	% Mass	D 4951		
Carbon Residue:	0.030	0.050 max.	% Mass	D 524		
Sulfated Ash:	<0.005	0.020 max.	% Mass	D 874		
Kinematic Viscosity at 40 °C:	4.439	1.9-6.0	mm ² /sec.	D 445		
Copper Corrosion (3 hrs at 50 °C):	1a	No. 3 max.	N/A	D 130		

^{1,2,3,4,5} These are not ASTM D 6751 specification requirements.

1.5 Solutions to TME Cold Temperature Problems

The cold temperature properties of TME are the primary issues preventing wider usage of TME and are the crux of this research. Prior research has demonstrated various methods of reducing the CP of methyl ester mixtures, including fractionation, blending with other methyl esters, mixing in polymer additives and creating FAEEs instead of FAMEs [28], [31], [35]–[37].

Saturated FAMES influence the CP of a FAME mixture to a greater extent than unsaturated FAMES since, as shown earlier in Figure 1.5, saturated FAMES have much higher individual melting points. Additionally, research from Dunn, et al., and Imahara, et al., shows that the CP of a FAME mixture can be calculated solely from the saturated FAME content without even considering the specifics of the unsaturated FAME content [29], [30]. One way to lower the CP of a FAME mixture is to reduce the saturated FAME content. Two methods to change that ratio are fractionation and blending TME with FAME mixtures that contain high levels of unsaturated FAMES.

1.5.1 Fractionation

Fractionation describes a family of methods used to separate out specific FAMES to tailor the mixture for optimal properties. Various forms of fractionation, including distillation and crystallization, have been successfully used to modify FAME mixtures to reduce the CP [28], [31], [35].

1.5.1.1 Distillation Fractionation

Distillation fractionation takes advantage of the dissimilar boiling points to separate each type of FAME. Distillation heats the liquid, often under a vacuum, until the FAME with the highest boiling point vaporizes and separates, and continues until each FAME is removed. Once each FAME stream is separated, the final FAME mixture can be tailored to match the desired FAME profile. The purity of each removed stream can vary depending on the proximity of other FAME's boiling points. For instance, methyl stearate (C18:0/MS) and methyl oleate (C18:1/MO) have very close boiling points of 352°C and 349°C, respectively, that causes issues when trying to separate them individually [3]. While distillation fractionation is energy intensive, it can be economically viable in some cases and gives great control over what the final FAME profile looks like [28]. Distillation

fractionation is advantageous to use with biodiesel production because a distillation column is often already required to separate undesirable monoglycerides from the FAMES.

1.5.1.2 Crystallization Fractionation

Crystallization fractionation is similar to distillation fractionation but uses the freezing point of each FAME to cause separation. Crystallization fractionation is also referred to as winterization and has been shown to successfully reduce the CP of SME by reducing the percentage of methyl palmitate (MP) and methyl stearate (MS) [38]. Because the saturated FAMES have the higher melting points, this method separates them prior to other FAMES. To effectively separate high purity FAMES, the mixture must be continuously agitated to have even heat transfer when the solids start to form.

A benefit of using the freezing points to fractionate TME is that MS and MO have very different freezing points of 33.7°C and -40.6°C, so there is not any MS/MO carryover yield loss with crystallization fractionation as there is with distillation fractionation [29]. If the MS does clump with the MP when the FAMES crystallize, a combination of crystallization fractionation and distillation fractionation could be done. The MS/MP mixture could be removed, and that fraction could be distilled through a single tower without having the capital costs, operation costs and carryover costs associated with separating MS and MO.

Economically, while there may not be significant issues with carryover loss, there are still other costs similar to distillation fractionation. There is the upfront cost of purchasing an industrial chiller, the ongoing energy costs to cool 60 MGY of biodiesel, and the yield loss of removing FAMES to reach the desired CP. Only a single chiller would need to be purchased for crystallization fractionation instead of four distillation columns for distillation fractionation (see Section 4.2). From an energy standpoint, while cooling a gallon of biodiesel 1°C takes more energy than heating

it 1°C, the temperature differential is significantly less when cooling to remove MS (CP in TME = 14.5°C) versus heating to remove MS (from a preheated 300°C to 572°C @ 2 psia) [39].

There are two important considerations with either type of fractionation. Since FAMES are being separated and removed, there is a loss in yield, which needs to be factored into the feedstock cost. The second consideration, which offsets the first, is that separated FAMES are not a waste stream. While they may not be a high value stream, they can still be sold for other purposes like soaps, detergents, cosmetics and high CP biodiesel.

1.5.2 Blending With Other FAMES

Another less energy intensive option to reduce the saturated to unsaturated FAME ratio is to blend various biodiesels together. Blending TME with FAME mixtures that contain more unsaturated FAMES can lower the CP temperature. This approach has been shown to be successful in reducing the CP of TME using SME [36]. Blending FAMES requires much less infrastructure, lower capital costs, and lower energy costs compared to fractionation, but the CP reduction potential is limited by the methyl esters that are introduced. Blending also reduces the cost advantage that tallow has over soy and canola.

1.5.3 Additives

A variety of polymer additives are made to reduce the CP and other cold temperature properties of petroleum diesel and soy and canola methyl esters. These additives reduce the CP by delaying the formation of crystalline structures as the FAME cools down which delays the onset of freezing by a few degrees. Smith, et al., review and report on the efficacy of various additives for cold temperature property improvement [35]. An additive already produced for petroleum diesel or other FAMES could produce good results with TME, or perhaps another additive could be

developed just for tallow methyl esters. Additives can be used in conjunction with any other cloud point reduction method(s).

1.5.4 Forming Different Esters

Biodiesel is most commonly formed by reacting fatty acids with methanol (wood alcohol) to create fatty acid methyl esters (FAMES). Alternatively, the fatty acids could be reacted with a more commonly known alcohol, namely ethanol. This reaction produces fatty acid ethyl esters (FAEEs) which have a lower CP and CFPP than a FAME with identical chain length and degree of saturation. Because ethanol is more expensive than methanol, this route is atypical at a production scale.

Foglia, et al., researched the change in fuel properties caused by reacting triglycerides with various alcohols. The CP of TME was reduced by 2°C when methanol was replaced with ethanol. Propyl alcohol reduced the CP by 5°C while butyl alcohol reduced it 8°C [37]. However, the latter two alcohols are even less common and more expensive than ethanol.

1.6 Organization of the Thesis

The goal of the research described in this thesis was to investigate and report on known methods of reducing the CP of FAME mixtures and how they apply specifically to TME. The test equipment and methods used to measure various fuel properties are described in Chapter 2. Cold temperature properties were evaluated for cloud point (CP) and cold filter plugging point (CFPP). Gas chromatography (GC) was used to determine FAME profiles and inductively coupled plasma (ICP) was used to measure the presence of metals. The Rancimat was used to determine the oxidative stability index, and the flash point was also measured to verify the methanol content was within acceptable limits.

The tallow pretreatment procedure used to reduce FFAs and metals prior to transesterification, as well as the transesterification process, are detailed in Chapter 3. Both of

these methods were modified from the original pretreatment and transesterification processes and optimized for tallow. The changes in the pretreatment methods were evaluated by the reduction in metals as measured by the ICP. Changes in transesterification were measured by improvement in yield. The final, detailed instructions for optimal pretreatment and transesterification were then presented.

The use of fractionation to reduce the CP of TME is investigated in Chapter 4. Both distillation fractionation and crystallization fractionation were considered. CP prediction models based on the FAME profile were compared and reveal a major finding, the eutectic point of methyl palmitate (MP) and methyl stearate (MS). The eutectic point was found to be an ideal ratio of MP and MS that minimizes the CP and maximizes fractionation yields.

The CP models were used to estimate the FAME profiles at the theoretical eutectic point (TEP) that would reach CPs of 10°C, 7°C, 2°C, and 0°C. Empirical CP and CFPP tests were conducted on FAME mixtures designed to simulated distillation fractionation. The empirical CP tests were examined in detail and an empirical eutectic point (EEP) was approximated. Furthermore, the issue of methyl oleate (MO) carryover with methyl stearate (MS) in distillation fractionation was detailed and accounted for. The relationship between the fractionation MS/MO carryover yield and CP was related for each of the simulated fractionated TME mixtures. Finally, the effectiveness of the CP prediction models was compared to the fractionation empirical data.

Blending TME with SME and CME is the subject of Chapter 5. Both of these methods were shown to reduce the CP and CFPP. Equations relating CP and blend percentage were presented and can be used for economic considerations. The CP prediction models were also compared to the empirical blending CP data and to the complete empirical CP data set.

The effectiveness of four additive families, and 11 total additives, in reducing the CP and CFPP of TME and CME/TME mixtures was measured and is shown in Chapter 6. The most effective additive, the MLA additive, was examined in detail and was found to have a synergistic effect when

mixed in CME/TME blends. The solid and liquid components of the MLA additive were separated and tested for their individual effectiveness. As with blending, the relationship between additive dosage and CP reduction was established for economic evaluation.

The end usage of TME biodiesel was investigated by measuring the CP and CFPP of TME/diesel blends from B0 to B100 in Chapter 7. Additionally, the synergistic effect of using the MLA additive in diesel blends was discovered.

Chapter 8 brings together all the results from Chapters 4-7 and makes some preliminary economic comparisons. Since the economics of all of these CP reduction methods are largely dependent on commodity prices, hard and fast results cannot be stated. However, the process for comparing these various methods was presented. To facilitate economic evaluation, the cost of each CP reduction method was standardized to the cost of reducing one gallon of finished biodiesel by 1°C (\$/gal/°C).

Overall conclusions are presented in Chapter 9. Using fractionation, blending and additives to reduce cloud point are compared from a technical and economic perspective. Finally, future work is proposed.

Chapter 2: Experimental Equipment and Methods

2.1 Cloud Point Test

Cloud point (CP) is defined as the temperature at which liquid biodiesel begins clouding due to crystals forming larger than $0.5\ \mu\text{m}$ [28]. This is indicative of the fluid crystallizing into the solid phase. CP is addressed in ASTM Standard Test Methods D2500 and D5771. ASTM D2500 is referenced as the primary CP test method in the ASTM D6751 B100 standard and describes a manual test method where the sample is placed in different baths of decreasing temperatures and is visually checked at every 1°C interval for clouding [40]. ASTM D5771 details a CP test method using a cooling bath that automatically steps down in temperature with an automated optical light sensor. In the latter test, the CP temperature is recorded to a 0.1°C resolution. The results from the ASTM D5771 method can be used in lieu of the ASTM D2500 method by rounding the result down to the next integer [41].

The testing apparatus used was a Lawler DR4-14L combination CP and CFPP automated tester. It consists of a coolant circuit that can produce the jacket temperatures required for ASTM D2500 and two independent test heads for CP and CFPP. The CP clear glass sample jar is designed to hold 40mL of biodiesel and mounts onto a head that lowers the sample jar into the cold bath. Attached to the head and immersed in the jar are a temperature probe as well as a fiber optic that emits red light and determines the level of light transmission. The apparatus tests at every 1°C drop and records the temperature to a 0.1°C resolution when crystal formation in the fluid blocks the sensor from “seeing” the light. This device satisfies the ASTM D2500 test method, and almost satisfies the ASTM D5771 test method. It has automated optical CP detection, a stepped cooling bath temperature, and 0.1°C resolution, but because it only tests for CP every 1.0°C it does not meet ASTM D5771 [42].

The machine only tests at every 1.0°C temperature drop but has a resolution of 0.1°C. To take advantage of the 0.1°C temperature resolution, each sample had three tests run. The first test was started at XX.0°C, the second at XX.3°C and the third at XX.7°C, and the highest of these three temperatures was reported as the CP. This was done both to narrow the CP down to within 0.4°C and to run triplicates of each sample.

The following test procedure was used for the CP tests to provide consistency. First the machine was turned on and the cold bath was allowed to reach 0°C. While it cooled, the biodiesel sample was poured into the sample glass up to the 40mL line and warmed to a temperature at least 14°C above the estimated CP before starting the test. In between subsequent tests of the same sample, I raised the head with the vial, then warmed the sample back up by setting the vial back down into a beaker with hot water. After unscrewing the vial and swirling the sample around to dissolve any remaining crystals, I screwed the vial back on the machine head and started the following test. In between tests of different samples I poured out the biodiesel and rinsed the vial out with methanol. I then wiped the vial down with a paper towel and allowed the methanol to evaporate. At the end of the each day I would wash the vial with soap and water, rinse it very well, and allow it to dry completely.

2.2 Cold Filter Plugging Point Test

The CFPP test method, ASTM D6371, tests a 45 mL sample at 1°C intervals by suctioning it through a 45 micron filter with 2 kPa of vacuum and 15 L/h of airflow. The CFPP temperature is considered the temperature at which the vacuum fails to move 20 mL of the sample in 60 s.

The same Lawler DR4-14L machine that tested for CP also performed the CFPP test. This device runs the suction at 1°C intervals until the biodiesel is too viscous to pass between both light sensors before and after a 20mL cavity in the pipet. Between each test, I would raise the head then lower the vial into a beaker filled with hot water to warm the sample, as with the CP test. I would

continue to pull vacuum as the sample warmed, until the sample cycled easily through the filter a number of times. Also like the CP test, I would start tests at XX.0°C, XX.3°C and XX.7°C to narrow down the actual CFPP to within 0.4°C and to run triplicates of the sample. To clean the CFPP test apparatus between samples, I would fill the vial with methanol and run the test procedure to pull the methanol through the filter to clean it out. I would then rinse out the vial and dry it with a paper towel before I began the next test. At the end of each day of testing I cleaned out the CFPP vial and filter apparatus with soap and water, rinsed them very well, and allowed them to dry overnight.

2.3 Gas Chromatography

A gas chromatograph (GC) paired with a flame ionization detector (FID) was used to determine the fatty acid methyl ester (FAME) profile of a sample. A FAME profile is the percentages of each type of FAME compound that make up the whole mixture. Most biodiesel properties, and specifically cold temperature properties, are dependent on the FAME makeup, so determining the FAME profile is vital to any correlation.

2.3.1 Gas Chromatography Description

Gas chromatography is a process used to separate out individual components of a FAME mixture. The sample is injected into a long and very thin capillary tube, called a column, which is inside of a temperature controlled oven. An inert carrier gas, like helium, moves the components as they elute through the column. The inside of the column is coated with a reactive stationary phase designed to interact with FAMES, causing them to elute at varying speeds. By varying the oven temperature profile over time, the separation of each component can be controlled in relation to its boiling point. As the components exit the column, an instrument is needed to determine the concentration of each component. With a FID, the flame combusts the sample in hydrogen gas,

which creates an electrical potential from the ions produced by the combustion of the C-H bonds in organic compounds. This voltage is measure with the FID's electrodes and directly relates to the concentration of each organic compound that has been separated out by the column [43].

2.3.2 Gas Chromatography Test Method

FAME profiles were determined using a SRI 8610C gas chromatograph with a flame ionization detector using a 30m long, Restek MXT-WAX (70655-271), 0.53 mm ID column, made of Siltek treated stainless steel, with a polar stationary phase film thickness of 1.00 μm [44]. SRI's packaged integration software, Peak Simple, was used to control the temperature method, read the FID output, generate the chromatographs and integrate the peak areas.

FAME samples were diluted with hexane between a 1:10 and 1:40 ratio to prevent overloading and clogging the column. This sample to hexane ratio also optimized the FID detector's sensitivity by keeping the TME peaks near the midpoint of the FID's 5000 mV scale.

The FID was setup with its gain on high, with an air flow of 250 mL/min and a hydrogen flow of 25 mL/min. Once gas flow was established, the FID flame was ignited by holding the ignitor switch until a small pop was heard. Since a hydrogen flame is transparent, the flame was checked by verifying that condensation formed on a chrome wrench placed by the exhaust of the detector. Before each test, the oven temperature was increased to 240°C (just below the maximum column temperature of 250°C) for 20 min to clear out any remaining compounds [43], [44]. Then, the oven temperature was manually set to 190°C to stabilize the unit before operation. A temperature method was developed (BD_Method_7) to control the oven temperature profile to separate out methyl esters from C12:0 to C22:0 within 65 minutes while still having adequate separation between close peaks like C18:0 and C18:1.

When preparing samples for injection into the column, 1 μL of air was pulled into a 10 μL syringe followed by 1 μL of sample and another 1 μL of air. The needle of the syringe was inserted

into the septum of the on-column direct injection port and carefully guided into end of the column, then inserted until the base of the syringe contacted the septum. The plunger was firmly depressed and the syringe quickly removed, then the GC oven temperature method (BD_Method_7) was immediately initiated on the computer (Figure 2.1).

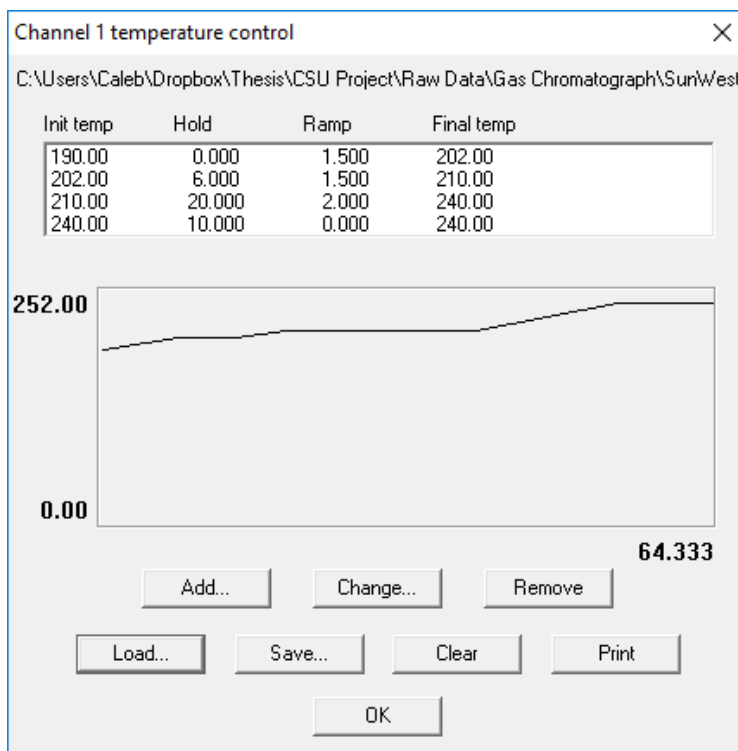


Figure 2.1 - GC oven temperature method “BD_Method_7” used to measure FAME profiles

With the oven already at 190°C, the method ramped the oven temperature by 1.5°C/min for 8 min until 202°C then held it there for 6 min (0:14 elapsed time). The hexane solvent would pass through the column after 2 to 3 mins and cause the FID’s signal to max out above 5000 mV due to its large concentration. C14:0 followed close behind at (0:7.5), then C16:0 and C16:1 at (0:12) and (0:12.75) respectively. At (0:14), the oven temperature increased by 1.5°C/min until the oven reached 210°C (0:19.3) and held it for 20 min (0:39.3). This allowed C18:0 and C18:1 to separate out in distinct peaks at (0:20) and (0:20.75) and C18:2 at (0:23). At (0:39.3), the temperature ramped up by 2°C/min for 15 min until it reached the final temperature of 240°C (0:54.3) and held

there for 10 min (0:64.3) to bake out any leftover material. Before the next test, hexane was injected into the column to help flush out any leftover components.

2.3.3 Gas Chromatography Standards

To determine the retention time of each FAME, the Supelco 37 component FAME standard (47885-U), which contains FAMES from C4-C24 in a 10 mg/mL methylene chloride solution, was run through the GC using the “BD_Method_7” temperature method [45]. Given the published FAME profile percentages of the Supelco 37 FAME standard and their elution order, each peak of the standard could be matched with its FAME chain length and bond level. Then, after running a FAME sample with an unknown composition, the peaks of the sample and the standard could be lined up to determine the FAME type of each peak of the sample (Figure 2.2).

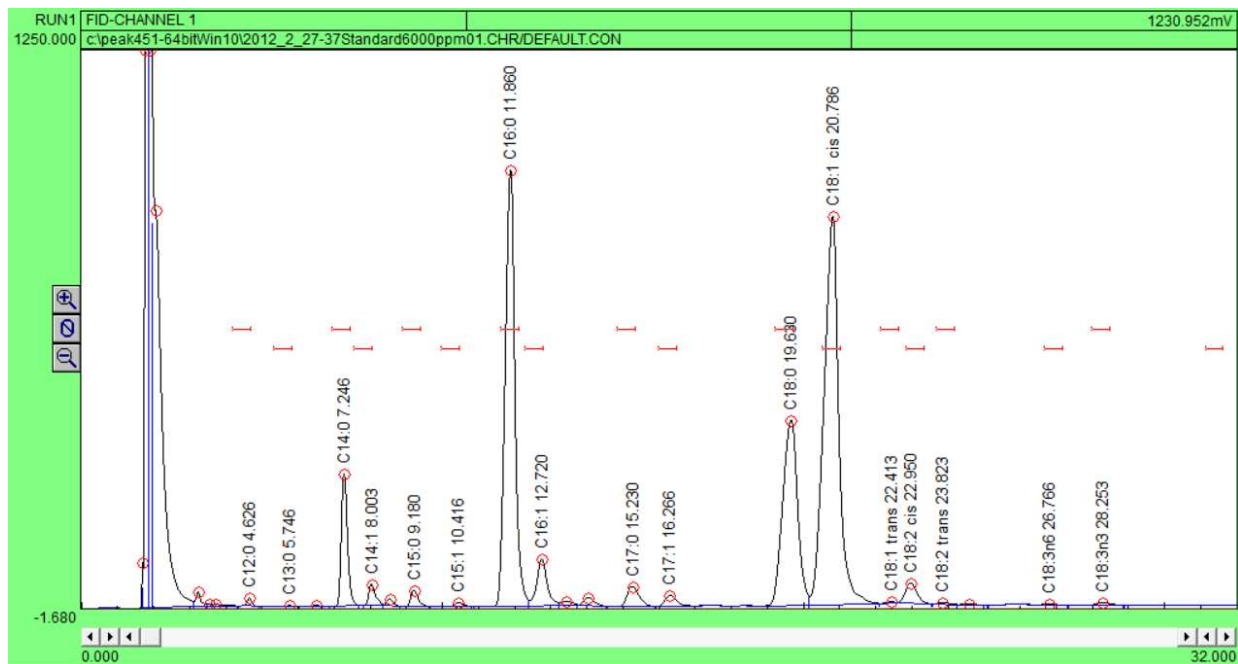


Figure 2.2 – Sample GC readout in Peak Simple showing peaks for each FAME type in TME

Since the peaks were clear with this temperature method and only the FAME profile was needed, the individual FAME percentages were calculated by dividing the area of each peak by the area of all the FAME peaks in the graph. This method of calculating FAME profile does not measure

the percentage of FAMES compared to the entire mixture, since it does not account for non-FAME organic compounds like mono-, di- and triglycerides. If desired, total concentrations of each FAME type could be determined after testing serial dilutions of the 37 FAME standard, by matching peak heights with the standard's known FAME concentrations. Additionally, a foreign FAME like C19:0, which is not present in naturally occurring fatty acids, could be added at a known concentration. This internal standard creates a unique peak that makes the dilution ratio easy to determine.

2.4 Inductively Coupled Plasma with Optical Emission Spectrometer Test

The ASTM D6751 B100 standard regulates various elements that can cause issues with biodiesel in production, storage, combustion or with emissions equipment. To be compatible with the Ultra-Low Sulfur Diesel (ULSD) standard, to prevent engine wear and to decrease emissions of sulfur oxides (SO_x), the maximum sulfur content must be less than 15ppm, which is often naturally the case with biodiesel [6]. Phosphorus is limited to 10ppm, and calcium and magnesium combined must be less than 5ppm, since all three can act as emulsifiers, create sediment, reduce the transesterification yield, and increase engine wear [13], [26]. Sodium and potassium combined are limited to less than 5ppm because they also contribute to premature engine wear.

All of these elements are primarily introduced by the feedstock, so it is necessary to sample both the raw and pretreated feedstock and the finished biodiesel to determine that the ASTM standard is met and that the pretreatment steps are working adequately. To determine the concentrations of these elements at each stage, the raw tallow feedstock and various stages of pretreated tallow were sampled using an inductively coupled plasma optical emission spectrometer (ICP-OES) device in accordance with the ASTM D4951 test method.

2.4.1 ICP-OES Description

The ICP-OES operates on the principle that a plasma flame can be used to break down molecules into ionized atoms that emit electromagnetic radiation associated with each element. The plasma flame is created by flowing argon gas through a powerful magnetic field, which the liquid sample enters as an aerosol after passing through a nebulizer. The emitted electromagnetic radiation (EMR) is diffracted across charge coupled devices (CCDs) that are calibrated with known standards that relate the location on the CCDs with specific elements. The intensity measured by the CCDs at a specific EMR wavelength is directly related to the concentration of that element in the sample [46].

2.4.2 ICP-OES Test Method

The ICP-OES instrument used to conduct these tests was the Spectro GENESIS. The standard operating procedures for the Spectro Genesis ICP-OES are as follows. The first step was to check that the argon pressure was at 120 psi, then the sample introduction system was flushed for 5 or 20 min depending on if the ICP-OES had been running previously or not. The nitrogen used for the optical system flush was set to 58 psi. While the sample introduction system was flushing, the peristaltic pump and tubing were inspected for cracks and the nebulizer and torch were checked for any irregularities or carbon build-up. The blower was turned on, and the plasma sequence began until ignition occurred after 120 s. Once the plasma lit, the power was set to 1450 W, coolant to 14 L/min, auxiliary gas (N₂) to 2.0 L/min and the nebulizer gas (Ar) to 0.70 L/min. The ICP-OES warmed up for 30 minutes, then had blank kerosene flushed through it for another 30 minutes to clean all the lines and to allow the unit to reach equilibrium. Once the unit was stabilized, the standards were run through to calibrate the sensors with known metal concentrations. Finally, the samples were tested and kerosene was flushed through between subsequent tests. The analysis

was carried out using Spectro's Smart Analyzer Vision software which determined the mass percent concentration of each element detected.

2.4.3 ICP-OES Calibration

The calibration method for the ICP-OES is as follows. First, the VHG sulfur standard (SB-100-100-100) at 100 µg/g concentration in B100 was divided up into serial dilutions of 0 ppm (blank), 25 ppm, 50 ppm, 75 ppm and 100 ppm [47]. These serial dilutions were then diluted further at a 1:9 g/g ratio in kerosene to calibrate the ICP-OES for sulfur. VHG's "V23 Wear Metals Standard" (V23-300-100G), which contains 23 other elements, was used to calibrate the ICP-OES for phosphorus, calcium, magnesium, sodium and potassium with concentrations of 300 µg/g per element in a matrix of 75 cSt hydrocarbon oil [48]. Serial dilutions of 0 ppm (blank), 75 ppm, 150 ppm, and 300 ppm were created and subsequently diluted to a 1:9 g/g ratio in kerosene to match the sample dilution. Test samples were diluted to a 1:9 g/g ratio of sample to kerosene to optimize the concentrations to the detector's range.

2.5 Oxidative Stability Test

Oxidative stability is an important property to measure when working with tallow since TME contains 43% unsaturated FAMES, which are vulnerable to oxidation. The oxidative stability index (OSI) is a way to relate how quickly FAMES will degrade in the field in relation to each other FAMES, by testing their oxidation at accelerated rates using elevated temperatures.

2.5.1 Oxidative Stability Test Description

For these test, the Metrohm 743 Rancimat was used (Figure 2.3). The EN 14112 oxidative stability test method is sometimes referred to as the "Rancimat method" since it was developed by Metrohm using their Rancimat instrument as an automatic method [49]. EN 14112 details a test

method that measures the conductivity of distilled water where 10 L/h of filtered and dried air is passed through a 3 g FAME sample. This air then bubbles through distilled water while the sample is maintained at 110°C. As the FAMEs degrade, the conductivity of the distilled water increases. Electrodes in the distilled water measure the change in conductivity, measured in micro-Siemens per centimeter, over time. The reported OSI is based off of the inflection point of the conductivity curve (Figure 2.4) [49].

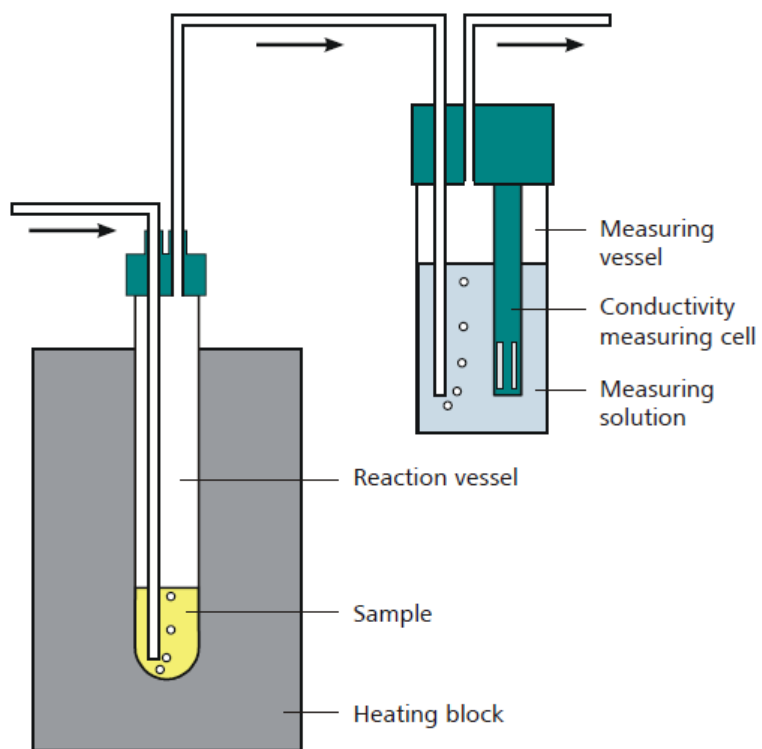


Figure 2.3 - Schematic of Rancimat heating block, sample vial and conductivity measuring vessel [49]

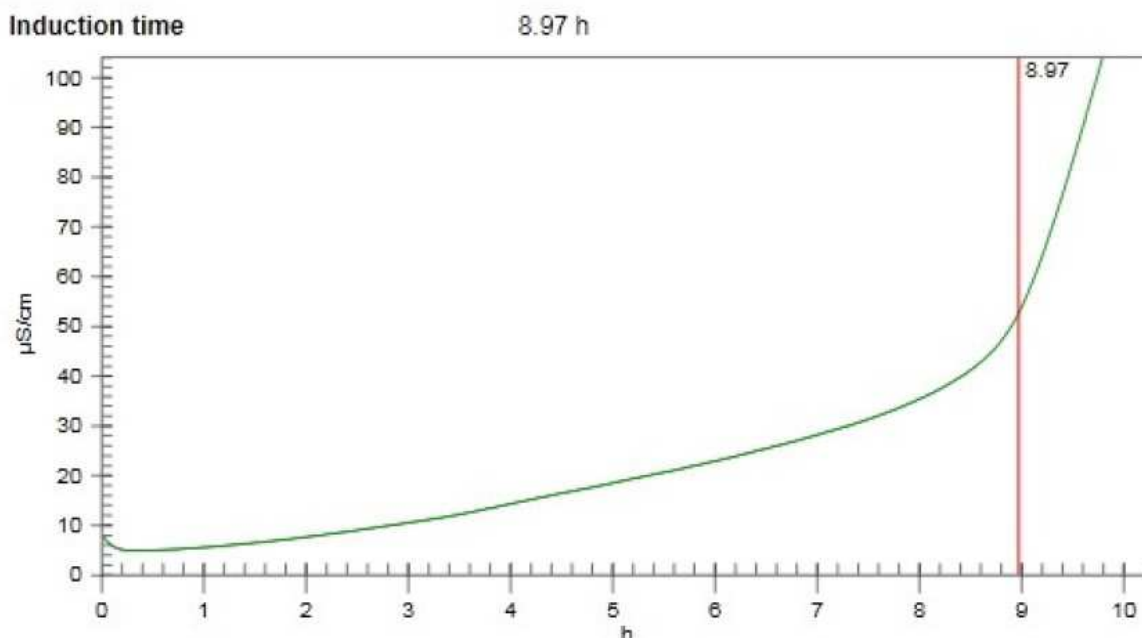


Figure 2.4 – Sample oxidative stability chart with Rancimat 743 showing OSI at 8.97h

2.5.2 Oxidative Stability Test Method

The test procedure was conducted as follows. First, the Metrohm 743 Rancimat was turned on and the heating block was allowed to reach 110°C while the following steps were completed. Cleaned glass vials were tared on a scale and then 3 g of the sample were transferred by pipet into the reaction vial. The conductivity measuring vessel was filled with 60 mL of distilled water. After about 45 minutes, the heating block stabilized at 110°C and the reaction and measuring vessels were placed in the Rancimat and all hoses were connected. Then the EN14112 preprogrammed test method was started until the OSI was found and the test was automatically ended (Figure 2.4).

2.5.3 Oxidative Stability Calibration

The Metrohm 743 Rancimat conductivity electrodes were calibrated using potassium chloride (KCl) solution conductivity standards at 100 and 10,000 uS/cm. The ΔT temperature

calibration for each heating block was performed using the Pt100 temperature probe, silicone oil and followed the method delineated in the Rancimat 743 manual [49].

2.6 Flash Point Test

When biodiesel is transesterified, methanol is used in excess to accelerate the reaction. While the excess methanol is boiled off after the reaction, there is a possibility that some methanol remained, which can increase the biodiesel's flammability and cause storage safety issues. The flash point of a fuel is the temperature at which an ignition source will ignite the vapors of a sample in a controlled setting.

The Pensky-Martens closed cup flash point test method, in ASTM D93 Procedure C for B100, specifies a testing vessel size, heating rate, stir rate and ignition source to measure flash point. ASTM D6751 requires a minimum flash point of 93°C for B100 using this method. The flash points for most pure biodiesels are over 150°C. The flash point of TME has been reported to >160°C, but even minor contamination with methanol, which has a flash point of 12°C, can quickly reduce that below 93°C [13]. The PetroTest PMA 4 used an automatic method, in line with ASTM D93 Procedure C, to determine an effective flash point at 1.0°C intervals from a 70mL sample, accounting for barometric pressure and using electric ignition. The PetroTest PMA 4 was calibrated with an n-Dedecane standard [50].

Chapter 3: Tallow Methyl Ester Production

3.1 Tallow Pretreatment Process

Biodiesel is made from the transesterification of triglycerides into fatty acid methyl esters. To upgrade inedible tallow to the point that it can be transesterified a pretreatment step must first be incorporated that removes gums, moisture, harmful metals, and neutralizes FFAs. During transesterification, both moisture content and high FFA levels can interfere with and degrade the catalyst. Additionally, gums, moisture, some metals, and FFAs can reduce yields by causing emulsions that make separation of the oil and water content more difficult [13]. To meet the ASTM D6751 B100 standard, a pretreatment process like Figure 3.1, is required to ensure that metals concentrations are below their allowable limits.

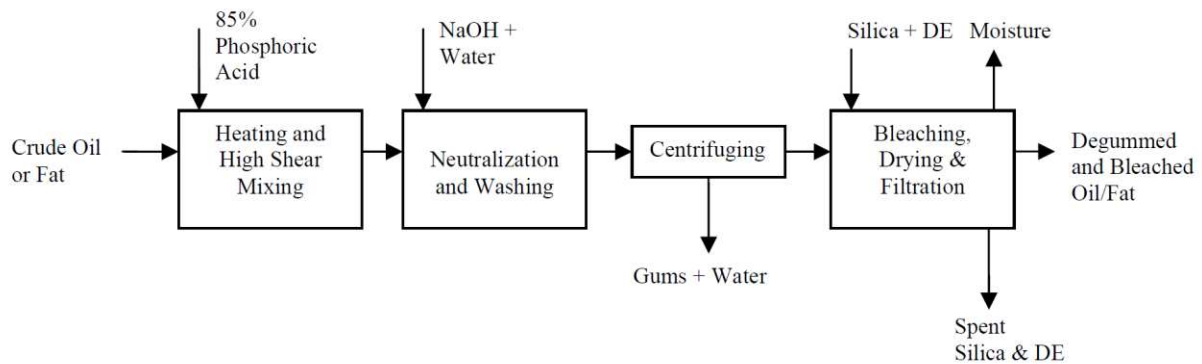


Figure 3.1 – Typical pretreatment process flow chart similar to Sun West method [13]

3.1.1 Initial Pretreatment Process

Initially, the pretreatment was carried out following a process supplied by Sun West that is detailed below in Table 3.1. Sodium hydroxide (NaOH) was used as the caustic in steps 4-7. The centrifuge speed of step 8 was limited to 1000 RPM due to the maximum speed of the available centrifuge, so the time was increased to 15 min.

Table 3.1 - Initial pretreatment steps provided by Sun West Biofuels

Step	Description
1	Test the oil sample for FFA, metals by ICP (including P, Mg and Ca), and moisture. Retain a sample of the original feedstock and label 'C1', 'C2', etc.
2	Heat 500 g of the sample to 70°C in an Erlenmeyer flask. Add a stirring bar and stir at medium speed.
3	Add 0.1% wt/wt of Citric Acid (20% conc.). Maintain 70°C and continue stirring for 10 min.
4	Calculate the amount of caustic required to neutralize the oil based on citric acid added, free fatty acids in the oil including experimental excess (this example assumes 1.5% FFA and caustic excess of 1.25): [(500 g)*(1.5%)*(0.142) + (500 g)*(0.1%)*(0.625)]*(1+25%) = 1.72 g caustic (dry)
5	In a separate beaker, make up a 20% caustic solution.
6	Calculate the amount of dilute caustic solution to add to the oil sample: (1.72 g caustic) / (0.20) = 8.61 g dilute caustic
7	Add the dilute caustic solution calculated in step 6 to the oil sample. Stopper the flask and shake gently for 5-10 seconds. Maintain 70°C and stir for 2 min.
8	Using a lab centrifuge, spin the sample for 3 min. @ 3,000 rpm to separate the gums/soap. This may require multiple batches depending on the size of the centrifuge tubes.
9	Decant the light phase from the centrifuge tubes with a pipette to a clean vacuum flask.
10	Save a portion of the light phase sample marked with 'N1', 'N2', etc. and test for FFA, metals by ICP (including P, Mg and Ca) and moisture.
11	Weigh the remaining light phase and heat the sample to 70°C while stirring at medium speed.
12	Heat the light phase sample to 80°C. Add 1% by weight TriSyl 300B silica and 0.25% diatomaceous earth to the sample and mix for 15 minutes while maintaining temperature.
13	Connect a vacuum pump to the flask and pull as much vacuum as possible. Heat to 95°C and continue stirring for 10 min or until it stops bubbling.
14	Pour the sample over a vacuum filter with 5 or 10 micron filter paper to remove the solids from the oil.
15	Mark the sample 'SB1', 'SB2', etc. Test the finished sample for FFA, metals by ICP (including P, Mg and Ca), and moisture.

The samples were not measured for moisture or FFAs in steps 1, 10, and 15, since the lab was not equipped to test for those properties, but the metals were measured at those steps using an ICP-OES. The feedstock was initially reported to be <1.5% FFAs (1.22%) which gave confidence that the FFA levels were acceptable (Table B.1). The 1.5% FFA value was used as the assumed FFA percentage for the calculations.

Samples of the initial tallow pretreatment process were saved to test in the ICP-OES from the crude tallow in step 1 (JBS-C-01), neutralized tallow from step 10 (JBS-N-01) and completely pretreated tallow from step 15 (JBS-SB-01). These samples were diluted at a 1:9 g/g ratio in kerosene and were run through the ICP-OES twice. The first time, the test was run before the ICP-OES was recalibrated, and the second time the sample ran out before the test was finished. Because of this, the specific concentrations for each element are not very reliable but there is a clear

decrease in all metals from the JBS-C-01 crude sample in Table 3.2. The yield for this first pretreatment batch was only 56%.

Table 3.2 – ICP-OES results for initial tallow pretreatment using the Sun West process

Element	Ca	K	Mg	Na	P	S
Concentration	ppm	ppm	ppm	ppm	ppm	ppm
JCB-C-01 (1/10/12)*	117.242	38.608	6.032	58.551	173.53	30.124
JBS-N-01-1	< -8.930	1.87	0.11	24.045	< -11.371	< -6.220
JBS-N-01-2**	< -11.401	25.564	< 0.012	< -2.202	26.875	< 0.178
JBS-SB-01-1	< -11.137	< -0.669	0.043	< -2.067	< -11.333	< -10.450
JBS-SB-01-2**	< -10.907	1.664	< 0.047	< -1.212	39.814	16.007

* This is a crude tallow sample that was tested on 1/10/12. Added for comparison.

** These are not reliable as we ran out of sample before the test was complete.

3.1.2 Modifications to Pretreatment Process

The second pretreatment process (JBS-XX-02) used 38% excess citric acid with the original 25% excess caustic (NaOH), while adding 69% additional Trisyl 300B and 93% additional diatomaceous earth (DE) than the original recipe. By repeating the process, a number of improvements for the next pretreatment were noted, like doubling the centrifugation of step 8 to further separate phases, increasing the vacuum to speed up filtration, slowly pouring the hot sample on the filter to keep it hot, and using two filters to allow filter change out when the filter beings to clog.

For the second pretreatment, only samples from steps 10 and 15 were taken to test in the ICP-OES. The ICP-OES was calibrated to the V23 and sulfur standards immediately before testing the samples. Because of this the minimum detection limit was lowered for many of the metals besides calcium (Ca). The results for JBS-SB-02 in Table 3.3 show that the process is able to produce pretreated tallow that will be below the metal content levels required by ASTM D6751.

Table 3.3 – ICP-OES results for second tallow pretreatment using a modified process

Element	Ca	K	Mg	Na	P	S
Concentration	ppm	ppm	ppm	ppm	ppm	ppm
JBS-N-02	< -11.014	< -0.620	< -0.236	< -0.315	< -0.447	6.402
JBS-SB-02	< -11.274	< -0.660	< -0.244	< -1.951	< -0.342	14.8

Ca was not detectable at 11.2 ppm but it does not mean that there was 11.2 ppm of Ca. The ICP-OES likely just needed better calibration for Ca. The metals were calibrated at 0 ppm, 75 ppm, 150 ppm, and 300 ppm, which might be causing uncertainty with small concentrations because of the 75 ppm gap between the lowest standard concentrations. Previous tests using the same ICP-OES, with samples from Sun West prepared with this pretreatment process, showed final Ca levels at <1.1 ppm, making this not a concern. If Ca reduction was of more concern, the calibration standards could be formulated at smaller intervals than 75 ppm, or a distinct Ca standard could be used. The yield for this second pretreatment improved to 67%.

Once the second pretreatment gave confidence that the process would reduce metals to acceptable levels, the third pretreatment had samples taken for the ICP-OES at each major step of the process, whenever material was added or taken away. This was to determine what effect each step had on metal removal to optimize the pretreatment process for tallow. Modifications to each of those steps could then be compared to see if they were beneficial or not.

Samples for the ICP-OES were taken of the crude tallow at step 1 like before, and labeled JBS-C-03. After the citric acid was added at step 3, samples were labeled JBS-CA-03, and after the sodium hydroxide was added at step 7, they were labeled JBS-SH-03. The neutralized oil, after water and gums were removed with the first centrifugation, was labeled JBS-N-03A, then a second sample was labeled JBS-N-03B after repeating the centrifuge process in steps 8-10. After the DE and Trisyl 300D silica were added and filtered out at step 15 to bleach and dry the oil, the final pretreated oil was labeled JBS-SB-03 [13].

The third pretreatment used an excess of 75% citric acid over the original recipe, and 75% excess NaOH. Trisyl 300B and DE had 109% and 179% excess, respectively. This pretreatment had the oil centrifuged a second time after step 10 to see if additional separation would occur.

A look at the ICP-OES results from the third pretreatment in Table 3.4, show no real decrease in metals from the crude sample after adding the citric acid at step 3 (JBS-CA-03).

However, the following step of adding the NaOH shows a significant decrease in all metals across the board (JBS-SH-03). Centrifuging out the solids and gums in steps 8-10 further reduced the metals, especially all the sodium introduced from the sodium hydroxide, as well as phosphorus (JBS-N-03A).

Table 3.4 – ICP-OES results for third tallow pretreatment using a modified process

Element	Ca	K	Mg	Na	P	Si	S
Concentration	ppm	ppm	ppm	ppm	ppm	ppm	ppm
JCB-C-03*	126.865	38.472	6.359	58.856	189.861	7.441	30.976
JBS-CA-03	134.662	36.296	4.82	57.878	205.438	6.081	34.098
JBS-SH-03	< -10.802	1.137	< -1.582	106.994	18.969	4.35	16.826
JBS-N-03A	< -13.730	< -1.304	< -1.609	< -2.459	9.33	< -0.810	16.927
JBS-N-03B	< -13.757	< -0.489	< -1.598	< -2.912	9.799	< -0.711	16.751
JBS-SB-03	< -13.079	< 0.487	< -0.795	< -4.007	7.931	286.325	11.314

* This is a crude tallow sample that was tested on 1/10/12. Added to results table for comparison.

While conducting the pretreatment process, the second centrifuging step (JBS-N-03B) was observed to create additional separation. However, the difference in metals between JBS-N-03A and JBS-N-03B is insignificant and do not warrant that additional process. After the citric acid NaOH addition, as well as the centrifugation, the sulfur levels were still too high. With the addition of the Trisyl 300B and DE and their subsequent filtering in steps 12-15, the sulfur levels were successfully brought below the 15ppm limit (JBS-SB-03). However, all the excess silicon from the Trisyl 300B and DE caused the silicon levels to skyrocket and caused the oil to darken. The following pretreatments would have to use less Trisyl 300B and DE to prevent this. For subsequent pretreatments, only samples “N” and “SB” really need to be tested to see what material percentages give optimal results. The yield for this pretreatment dropped to 44%, most likely because of the high excess of Trisyl 300B and DE.

This third pretreatment gave confidence that this pretreatment process was ready to scale up to provide material for transesterification while revealing what process steps could be tinkered with to increase yield or reduce specific metals. Sulfur was below the 15 ppm limit but phosphorus was slightly high at 7 ppm. Phosphorus was well below the 5 ppm limit in previous tests so this is

not a concern for now. Calcium was not detectable at <13.1 ppm which is likely due to the same issues discussed in the previous pretreatment batch.

The fourth pretreatment was the first one at scale (500 g crude tallow) for biodiesel production. The citric acid was reduced to 25% excess and the sodium hydroxide to 50% excess, while the Trisyl 300B and DE were reduced to 50% excess. Even with the reduced Trisyl 300B and DE, the filters were still clogging up, so subsequent tests needed to have the excess Trisyl 300B and DE reduced more. By switching out filter papers as they clogged, the filtering time was greatly decreased. A new centrifuge was used that allowed speeds of 3000 RPM, which greatly increased separation. The solid portion was firm enough that it was not necessary to decant, so the liquid phase could be poured out.

Since this pretreated tallow was produced at larger quantities to use for transesterification, instead of solely for improving the pretreatment process, the naming convention was switched from numbers to letter. Samples for the ICP-OES were named JBS-N-A and JBS-SB-A and the results are presented in Table 3.5 below.

Table 3.5 - ICP-OES results for fourth tallow pretreatment using a modified process

Element	Ca	K	Mg	Na	P	Si	S
Concentration	ppm	ppm	ppm	ppm	ppm	ppm	ppm
JBS-N-A	< -10.056	3.734	< -1.158	4.573	47.727	0.326	17.38
JBS-SB-A	< -12.613	< -0.466	< -1.082	< -3.206	19.297	145.561	14.097

The metal reduction results from this one are good but not great. Sulfur levels are acceptable. However, silicon levels are still very high, and the phosphorus is much higher than the acceptable 7 ppm. Since silicon is added by the Trisyl 300B and DE, even less excess can be used in later pretreatments which also would reduce the filters clogging. The yield after this pretreatment increased to 78%, probably due to the decrease in Trisyl 300B/DE as well as the better separation from the centrifuge.

The third pretreatment with detailed ICP-OES results for each step, showed the two steps that effectively reduced phosphorus were adding NaOH then centrifuging, and adding Trisyl

300B/DE then filtering them out (Table 3.4). To determine which method would be best at reducing the phosphorus to acceptable levels, the finished JBS-SB-A pretreated oil had additional DE added, then was filtered again and tested as JBS-SB-A 2. JBS-SB-A 3 had an additional 25% NaOH added to the JBS-SB-A and then was centrifuged.

Table 3.6 - ICP-OES results for additional tallow pretreatment steps to reduce P and Si

Element	Ca	K	Mg	Na	P	Si	S
Concentration	ppm	ppm	ppm	ppm	ppm	ppm	ppm
JBS-SB-A	< -12.613	< -0.466	< -1.082	< -3.206	19.297	145.561	14.097
JBS-SB-A 2	< -20.261	3.356	4.807	2.11	12.6	99.411	11.375
JBS-SB-A 3	< -11.146	1.591	< -0.334	0.389	0.497	4.446	14.246

According to Table 3.6, adding DE then filtering did decrease both phosphorus and silicon (JBS-SB-A 2), but the additional NaOH and centrifugation drastically reduced them both (JBS-SB-A 3), well below acceptable levels. Future pretreatments would include both of these steps by repeating the NaOH and centrifugation as well as the Trisyl 300D/DE and filtering. Additionally, a final centrifuge step was added after filtration to further clean up the oil and remove excess DE/Trisyl 300B that made it through the filter.

3.1.3 Optimized Pretreatment Process

After these major improvements, ten more pretreatments were carried out (up through “J”) with minor tweaks to improve to a maximum yield of 85%. The finalized pretreatment process used 25% more citric acid than the original recipe, 100% of the original NaOH with an additional 50% NaOH added for the second reaction, and 100% of the suggested Trisyl 300B/DE with 20% more added for an additional step. The final recipe is listed below in Table 3.7.

Table 3.7 – Optimized pretreatment steps to reduce metals in tallow

Step	Description
1	Test the oil sample for metals by ICP (S, P, Ca, Mg, Na, K and Si). Retain a sample of the original feedstock and label 'JBS-C-X'
2	Heat 500 g of the sample to 70°C in an Erlenmeyer flask. Add a stirring bar and stir at medium speed.
3	Add 0.125% wt/wt (25% excess) of Citric Acid (20% conc.). Maintain 70°C and continue stirring for 10 min.
4	Calculate the amount of caustic required to neutralize the oil based on citric acid added, assumed 1.5% FFAs in the oil without experimental excess. $[(500\text{ g}) \cdot (0.015) \cdot (0.142) + (0.6\text{ g}) \cdot (0.625)] = 1.46\text{ g caustic (dry)}$
5	In a separate beaker, make up a 20% caustic solution.
6	Calculate the amount of dilute caustic solution to add to the oil sample: $(1.46\text{ g caustic}) / (0.20) = 7.3\text{ g diluted caustic}$
7	Add the diluted caustic solution calculated in step 6 to the oil sample. Stopper the flask and shake gently for 5-10 seconds. Maintain 70°C and stir for 2 min.
8	Using a lab centrifuge, spin the sample for 5 min. @ 3,000 rpm to separate the gums/soap. This may require multiple batches depending on the size of the centrifuge tubes.
9	Decant the light phase from the centrifuge tubes with a pipette to a clean vacuum flask.
10	Repeat steps 7-8 using an additional 50% of the calculated dilute caustic in step 6. $(7.3\text{ g dilute caustic}) \cdot (0.50) = 3.6\text{ g dilute caustic}$
11	Save a portion of the light phase sample marked with 'JBS-N-X' and test for metals by ICP (S, P, Ca, Mg, Na, K and Si).
12	Weigh the remaining light phase and heat the sample to 70°C while stirring at medium speed.
13	Heat the light phase sample to 80°C. Add 1% TriSyl 300B silica and 0.25% diatomaceous earth by weight to the sample and mix for 15 minutes while maintaining temperature.
14	Connect a vacuum pump to the flask and pull as much vacuum as possible. Heat to 95°C and continue stirring for 10 min or until it stops bubbling.
15	Pour the sample over a vacuum filter with 5 micron filter paper to remove the solids from the oil.
16	Repeat steps 13-15 using an additional 20% of the calculated Trisyl 300 B and diatomaceous earth in step 13.
17	Centrifuge for 5 min. @ 3000 RPM if necessary to remove excess sludge.
18	Mark the pretreated sample 'JBS-SB-X' Test the finished sample for metals by ICP (S, P, Ca, Mg, Na, K and Si).

3.2 Transesterification Process

Biodiesel is converted from the feedstock oil by the process of transesterification, where the oil reacts with methanol and a catalyst to strip fatty acids off of a glycerol backbone and re-forms the fatty acids with ester end groups to make fatty acid methyl esters (FAMES). The main purpose in performing this process is to decrease viscosity and improve cold temperature properties compared to the feedstock triglycerides [14], [15].

3.2.1 Feedstock Titration

Before performing the first transesterification with a specific catalyst and fatty acid feedstock, the oil had to be titrated with the potassium hydroxide (KOH) or sodium hydroxide (NaOH) catalyst to determine how much would be needed to reach a pH of 8.5. To perform the titration, 1 mL of oil was mixed with 10 mL of isopropyl alcohol and the pH was measured to be 5 for tallow. A catalyst mixture with KOH or NaOH was made from 0.1 g of catalyst with 100 mL of deionized (DI) water. 1 mL of this catalyst solution was added to the tallow/alcohol mixture and the pH when mixing either catalysts was 8. An additional 0.5 mL of both catalyst solutions yielded a pH of 8.5 and another 0.5 mL produced a pH of 9. From this it was determined that adding 1.5 mL of the KOH or NaOH solution would give a pH around 8.5. From this titration the necessary catalyst was calculated to be 10.5 mL (1.5 mL + 9 mL) of KOH or NaOH per liter of tallow, or 1.05 g KOH or NaOH per 100 mL of tallow.

3.2.2 Initial Transesterification Process

The initial transesterification process (see Table 3.8 below) was a common recipe used to make biodiesel at the Engines and Energy Conversion Laboratory (EECL). This recipe called for potassium hydroxide (KOH) to be used as the catalyst. Transesterification requires 12.56% v/v of methanol (MeOH)/feedstock oil for a stoichiometric reaction. This recipe uses a 60% excess (20% v/v MeOH/oil), and based off of the titration, KOH was mixed into heated MeOH at a rate of 1.05 g KOH per 100 mL of oil to make potassium hydroxide.

The first reaction had 80% of the potassium methoxide mixed into the feedstock oil and reacted at 55-60°F for 30 min to form fatty acid methyl esters (FAMES) with leftover glycerin and unreacted triglycerides (TGs). This mixture was poured into a separatory funnel and allowed to settle, the glycerin was drained off the bottom, and the FAME/TG mixture was drained into a clean beaker. The remaining 20% of the potassium methoxide was mixed into the FAME/TG mix at 55-

60°C and reacted for another 30 min. Once again the separatory funnel was used to separate the glycerin and FAMES. The FAMES were heated up to 75°C to boil off any remaining MeOH for 5 min then washed with DI water repeatedly until the pH was between 6 and 7. After this, the water was boiled off at 105°C for 5 min.

Table 3.8 – Initial transesterification process

Step	Description
1	Use pretreated oil, and label it
2	Heat 500 g (598mL) of the sample to 55-60°C in a beaker. Add a stirring bar and stir at medium speed.
3	In a separate beaker, make up a potassium methoxide mixture. Measure 60% v/v excess methanol. (598 mL oil*12.56%*1.60)=120mL MeOH Crush potassium hydroxide and weigh out 1.05 g/ml oil. (598mL*1.05g/mL)=6.28g KOH Mix potassium hydroxide with methanol at 55°C until dissolved to make potassium methoxide.
4	Mix 80% of the potassium methoxide mixture into the pretreated oil and react at 55-60°C for 30 min. (120mL)*(80%) = 96mL potassium methoxide
5	Pour the mixture into a separatory funnel to separate the glycerin and methyl esters.
6	Drain the glycerin into one beaker, then drain the methyl esters into another beaker.
7	Mix the remaining 20% of the potassium methoxide mixture into the methyl esters and react at 55-60°C for 30 min. (120mL)*(20%) = 24mL potassium methoxide
8	Pour the mixture into a separatory funnel to separate the glycerin and methyl esters.
9	Drain the glycerin into one beaker, then drain the methyl esters into another beaker.
10	Heat the methyl esters at 75°C for 5 min. to boil off any remaining MeOH.
11	Wash the methyl esters with DI water in a separatory funnel until the pH is between 6-7.
12	Heat the methyl esters to 105°C for 5 min. to boil off any remaining water.
13	Label the finished biodiesel with date and type

3.2.3 Modifications to Transesterification Process

To produce the TME, SME and CME required for cold temperature testing, fourteen transesterifications were conducted, ten with tallow, three with canola and one with soy. The process was continuously tweaked to optimize the reaction to produce a consistent high yield product. The biggest change was the switch from the KOH to NaOH catalyst to more closely mimic the process that would be used in a biodiesel plant. KOH was originally used because it is less likely to form soaps when FFA levels are high, so it was more forgiving. At plant scale, NaOH would likely be the catalyst of choice due to its lower cost. To prevent soap formation in a biodiesel plant, the FFA content would need to be reduced to less than 2.5% with the pretreatment process [16].

The excess MeOH in the transesterification process was varied from 20% to 100%, with too much MeOH excess causing a gelatinous mixture, a film on top and poor yields. The use of the centrifuge for the pretreatment process prompted the idea to test its ability to separate the methyl esters and glycerin in steps 5, 6, 8 and 9. The centrifuge created much cleaner separation compared to the separatory funnel which improved yield and decreased time, so it was implemented into the updated process. As these changes were made, the yield steadily increased from 33% to 82% for TME and up to 80% for SME and 85% for CME.

When optimizing transesterification to increase yield, there were only a handful of variables to adjust. There was some success by changing the MeOH excess and by switching from a separatory funnel to the centrifuge. The temperature of the reaction could not be increased above 60°C because the vaporization temperature of MeOH at standard atmospheric pressure is 66°C and in Colorado with the atmospheric pressure around 12 psia, MeOH boils at 61°C [22]. With a pressurized system, the reaction temperature could be raised which would decrease the time to complete the reaction and potentially improve yield. Another variable that was not modified was the ratio of catalyst in the MeOH, which could be investigated further.

Instead of strong base catalysts like KOH and NaOH, an acid catalyst could be used instead. The advantages to using an acid catalyst are that high FFA feedstocks could have the FFAs converted straight to methyl esters without forming soaps that can reduce yield. The downsides are that the reaction time is much longer with acid catalysts, they are more expensive than common base catalysts and they are harder to recycle which would increase the overall cost further [15].

3.2.4 Optimized Transesterification Process

After modifying different steps of the original transesterification process, the optimal procedure for tallow with our lab setup was determined, and is presented in Table 3.9 below. The major change was switching the catalyst from KOH to NaOH. To make sure the transesterification

was complete the reaction time was increased from 30 min to 45 min. The MeOH excess was reduced from 60% to 20% for tallow and to 30% for canola and soy to increase yield. The sodium methoxide mixture was still split 80/20 into two reactions with glycerin separation after each reaction. Greater glycerin separation was achieved and at a faster rate by using a centrifuge at 3000 RPM for 5 min versus the separatory funnel. The boil-off step to remove any residual MeOH remained unchanged. The water wash was found to reliably reduce the pH to 6-7 after 15 washes. The final water boil-off step remained at the same temperature and time.

Table 3.9 – Optimized transesterification steps to make TME from tallow

Step	Description
1	Use pretreated oil, and label it "JBS-SB-X"
2	Heat 500 g (598mL) of the sample to 55-60°C in a beaker. Add a stirring bar and stir at medium speed.
3	In a separate beaker, make up a sodium methoxide mixture.
	Measure 20% v/v excess methanol. (598 mL oil*12.56%*1.20)=90mL MeOH
	Crush sodium hydroxide and weigh out 1.05 g/ml oil. (598mL*1.05g/mL)=6.28g NaOH
	Mix sodium hydroxide with methanol at 55°C until dissolved to make sodium methoxide (NaMeOH).
4	Mix 80% of the sodium methoxide mixture into the pretreated oil and react at 55-60°C for 45 min. (90mL NaMeOH)*(80%) = 72mL NaMeOH
5	Using a lab centrifuge, spin the sample for 5 min. @ 3,000 rpm to separate the glycerin and methyl esters.
6	Pour the liquid phase methyl esters from the centrifuge tubes into a clean beaker.
7	Mix the remaining 20% of the sodium methoxide mixture into the methyl esters and react at 55-60°C for 45 min. (90mL NaMeOH)*(20%) = 18mL NaMeOH
8	Using a lab centrifuge, spin the sample for 5 min. @ 3,000 rpm to separate the glycerin and methyl esters.
9	Pour the liquid phase methyl esters from the centrifuge tubes into a clean beaker.
10	Heat the methyl esters at 75°C for 5 min. to boil off any remaining MeOH.
11	Wash the methyl esters with DI water in a separatory funnel until the pH is between 6-7. (~15 times) Add water and swirl together to mix well but be gentle to prevent forming emulsions.
12	Heat the methyl esters to 105°C for 5 min. to boil off any remaining water.
13	Place the finished biodiesel in a sealed container with minimum headspace to reduce oxidation and label it with "JBS-BD-X" and the date.

3.2.5 Biodiesel Quality Checks

To make sure the transesterification process was producing quality biodiesel, the TME needed to be tested for a few specific properties. The primary quality metrics the finished TME were tested for were CP, CFPP, oxidative stability, and flash point.

3.2.5.1 Cloud Point and Cold Filter Plugging Point Check

Some of the initial tallow biodiesel (JBS-BD-1) was tested for CP and CFPP. The 14.0°C CP and CFPP gave confidence that the transesterification process was producing biodiesel with cold temperature properties comparable to tallow biodiesel reported in REG’s feedstock report (CP=16.0°C, CFPP=14.0°C) [13]. Five other TME batches throughout this research were tested for CP and three others were tested for CFPP, including one batch made with tallow from a second slaughterhouse. The average CP of those samples was 14.5°C with a minimum of 14.0°C and a maximum of 15.3°C. The samples’ CFPPs had an average temperature of 14.2°C with a minimum of 13.3°C and a maximum of 15.7°C. CP and CFPP were not regularly measured as new biodiesel batches were made unless a questionable batch was produced.

The CP and CFPP of SME and CME were only tested once each as there was only two batches of CME and one batch of SME. The average CP and CFPP for SME were 2.3°C and -5.3°C and for CME the average CP and CFPP were -8.3°C and -9.0°C (Figure 3.2). These are the CP values that will be used for TME, SME and CME going forward.

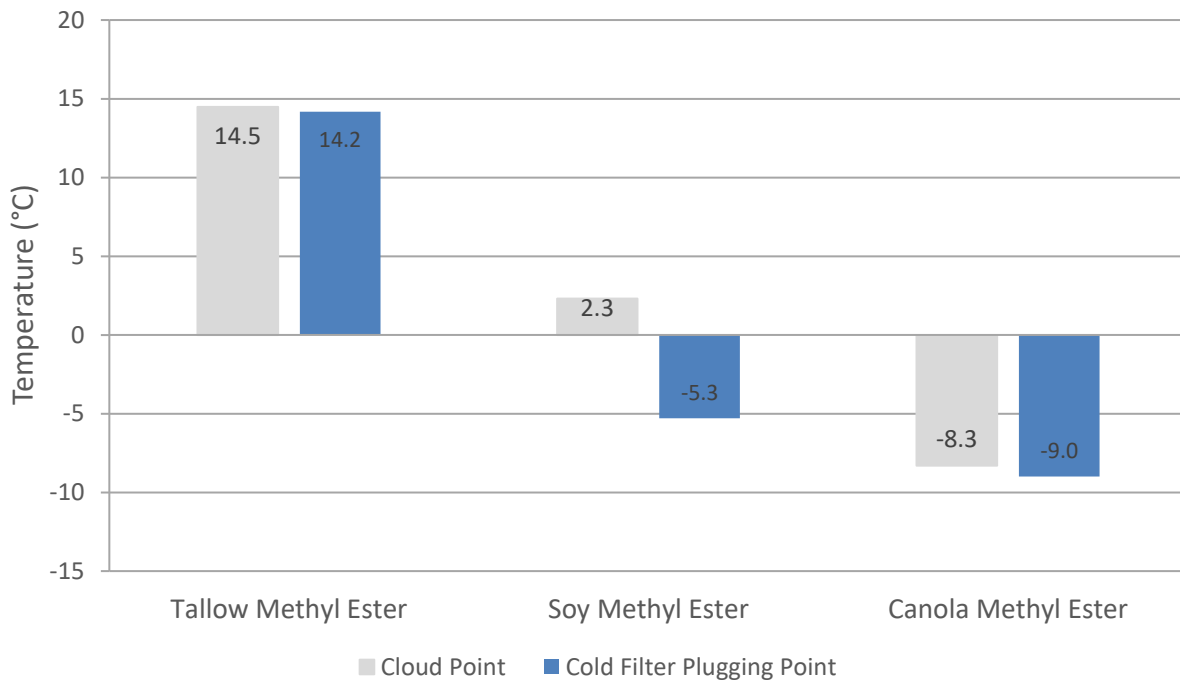


Figure 3.2 – Comparison of measured CP and CFPP temperatures for TME, SME and CME

3.2.5.2 Oxidative Stability Check

Tallow biodiesel samples were tested for oxidative stability to relate our TME with the oxidative stability index (OSI) of TME in literature. According to the REG Feedstock Report, tallow biodiesel typically reaches its inflection point at 1.6 h [12].

After initially getting OSI results at times much shorter than 1.6 h, I found two procedures that were likely causing this issues. I would leaving the reaction vessel in the heating block during the 45 minutes it took to heat up, which was speeding the oxidation process of the sample and providing inaccurate results. Additionally, when the initial samples were tested for oxidative stability, the biodiesel was almost two months old, exposed to air, light and at room temperature.

After this evaluation, I modified my method to the reported method in Section 2.5.2 and only placed the reaction vessel in the heating block right before starting the test, and after the heating block it stabilized to 110°C. The test below was performed on biodiesel (JBS-BD-D) that was made 3 days prior and stored sealed to minimize air contact. This time the OSI was a reasonable 2.66 h shown in Figure 3.3.

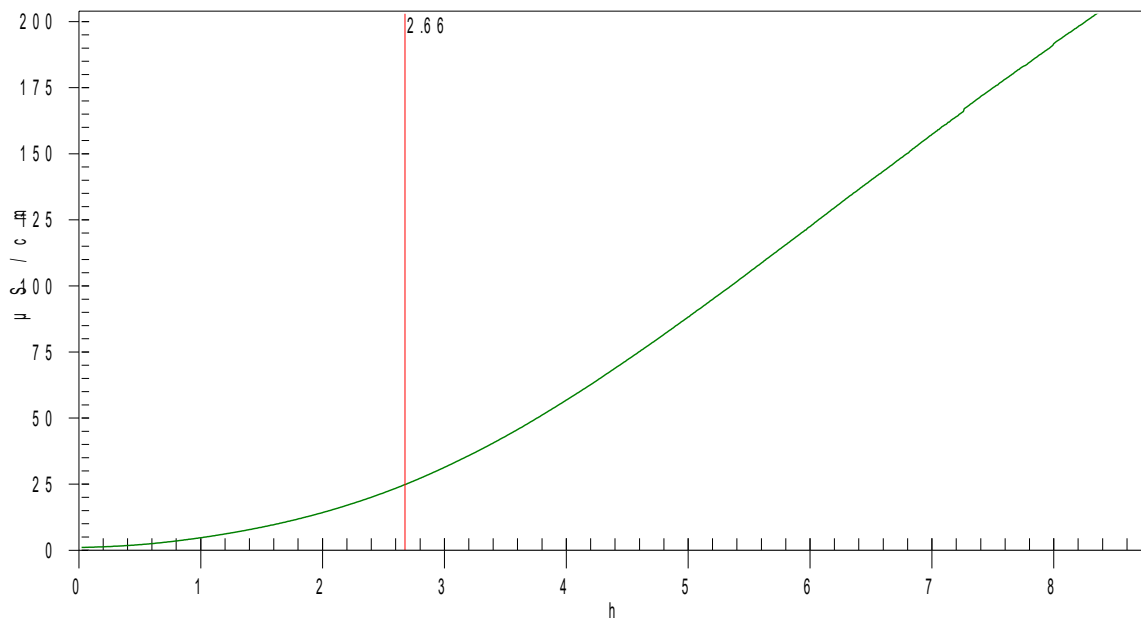


Figure 3.3 – Oxidative stability conductivity graph for JBS-BD-D

This test gave me confidence that the oxidative stability, while not meeting the 3h requirement for ASTM D6751, would have a reasonable induction time if the biodiesel was stored properly (sealed, minimal oxygen contact, out of the light) and used quickly. Given that the REG Feedstock Report lists TME with an OSI of 1.6h, this is a known issue for TME. Since the OSI is not critical to this research, and in light of the availability of antioxidant additives, this was not considered any further.

3.2.5.3 Flash Point Check

The PetroTest PMA 4 measured an “effective flash point” of the TME sample, of approximately 172°C. This is greater than 160°C, the maximum tested temperature and much higher than the 93°C flash point temperature required by the ASTM D6751 B100 Standard [26]. If there was excess methanol remaining, the flash point would have been reduced significantly since MeOH has a flash point of 12°C [13]. The result of the flash point test gave greater confidence that the transesterification process was successfully using or removing all methanol.

Chapter 4: Distillation Fractionation Cloud Point Reduction

4.1 Introduction

Biodiesels made from different feedstocks are all mixtures of fatty acid methyl esters, but have varied chain lengths and amounts of saturated and unsaturated FAMES, that determine most of its unique properties. In a biodiesel, the percentages of each unique type of FAME (chain length and saturation level) is known as its FAME profile. The prevalence of long chain, saturated FAMES (specifically methyl palmitate (C16:0/MP) and methyl stearate (C18:0/MS) gives biodiesel made from tallow a high cloud point (14.5°C). The large amount of unsaturated FAMES in SME and CME cause them to have lower CPs (2.3°C and -8.3°C respectively; see Figure 5.1 for FAME profiles).

Any biodiesel can have most of its important fuel properties changed then, by adjusting the FAME profile. Specifically, the CP of TME can be reduced by removing methyl palmitate (MP) and methyl stearate (MS) in the biodiesel, through the process of fractionation. However, fractionation of MP and MS is not a panacea, because reducing the level of saturated FAMES negatively affects both the oxidative stability and the cetane number of the FAME mixture.

Distillation fractionation is the process of separating individual FAME streams by heating the mixture to each FAME's boiling point and removing the vapor portion. This is usually done under a reduced atmosphere to reduce the boiling temperature, which minimizes the heating energy required and prevents accelerated oxidation. Once each stream is separated, the final FAME mixture can be tailored to match the desired FAME profile by mixing the streams at varying ratios. The purity of each stream can vary depending on the proximity of different FAME's boiling points.

This chapter documents various approaches to determining the feasibility of using distillation fractionation to reduce the CP of TME. First, computer simulations of distilling TME were conducted to determine the high level feasibility of separating individual FAME constituents.

These simulations prompted the need to have target FAME profiles. To determine a target FAME profile, multiple thermodynamic models were employed that could predict the cloud point of a given FAME profile. Given Sun West’s target CPs of 10°C, 7°C, 2°C, and 0°C, the CP prediction models were used to back out the FAME profiles that would produce those CPs, with the lowest yield loss. Due to the lack of access to a distillation column, the fractionated FAME profiles were simulated by mixing together various high purity FAMEs to modify TME to mimic the target FAME profiles. These simulated fractionated TME mixtures were then tested for CP and CFPP.

4.2 Distillation Fractionation Computer Simulations

Sun West Biofuels requested Pacific Northwest National Lab (PNNL) through their Technology Assistance Program to run a distillation simulation to determine the feasibility of using distillation columns to tailor the TME FAME profile (Figure 4.1).

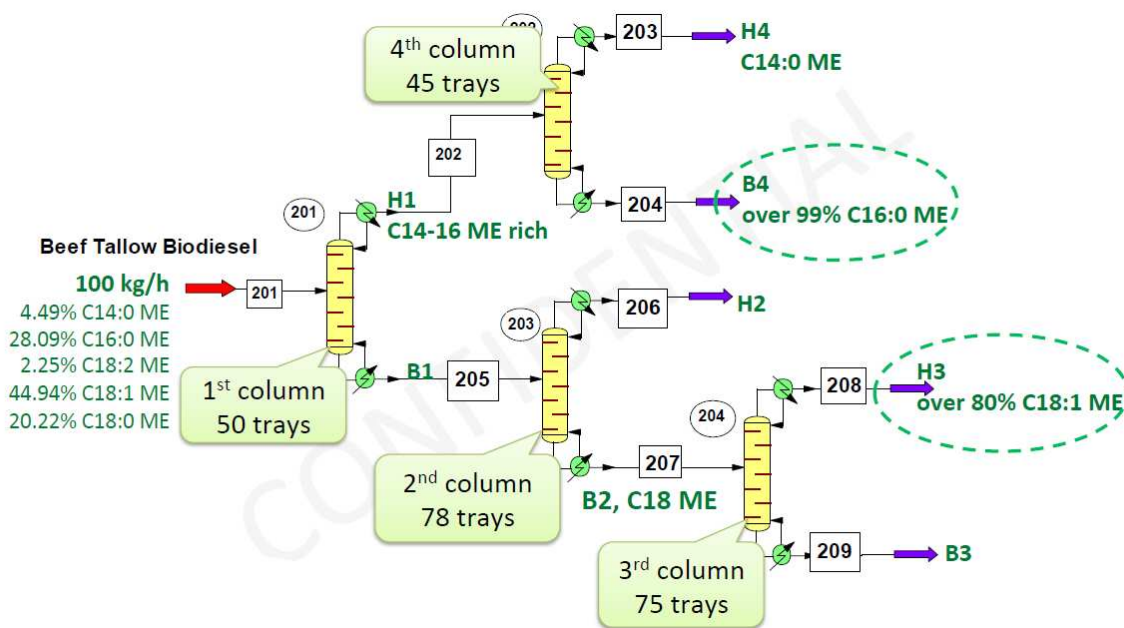


Figure 4.1 – PNNL’s initial CHEMCAD distillation model solving to remove high purity MP. The FAME percentages and flow rates for each stream are detailed in Table 4.1. [51]

Their CHEMCAD simulation initially targeted high purity MP for removal to reduce CP, and high purity methyl oleate (C18:1/MO) as a saleable byproduct. Preliminary CP tests showed that

removing only MP actually increased CP and that MS would have to be removed to lower the CP of TME. A look at the modeled streams in Table 4.1 show that the highest purity MS stream is “B3 (209)” that accounts for 34% of the flow. Using this stream though, would remove MO in addition to MS at a 1.1:1 MS/MO carryover ratio.

Table 4.1 – Flow rates and FAME profiles in PNNL’s initial distillation model [51]

Stream Number	201	202	205	206	207	208	209	203	204
Stream name	Feed	H1	B1	H2	B2	H3	B3	H4	B4
Methyl Myristate (C14:0)	4.5%	14.8%	0.0%	0.0%	0.0%	0.0%	0.0%	94.6%	0.2%
Methyl Palmitate (C16:0)	28.1%	84.5%	3.6%	30.5%	0.0%	0.1%	0.0%	5.5%	99.0%
Methyl Stearate (C18:0)	20.2%	0.0%	29.0%	15.8%	30.7%	6.0%	50.9%	0.0%	0.0%
Methyl Oleate (C18:1)	44.9%	0.4%	64.3%	50.0%	66.2%	88.4%	48.0%	0.0%	0.5%
Methyl Linoleate (C18:2)	2.3%	0.2%	3.1%	3.7%	3.1%	5.5%	1.1%	0.0%	0.2%
Flow Rate (kg/h)	100.0	30.3	69.7	8.1	61.6	27.7	34.0	4.7	25.6

Once it was determined that MS would need to be the primary saturated FAME removed, PNNL reran the model to solve for the highest purity MS separation. The second model (Figure 4.2) simulated taking the “B1 (205)” stream from the first distillation column in Figure 4.1 then distilling it further. That stream contained 69.7% of the flow and had a 1:2 MS/MO carryover ratio.

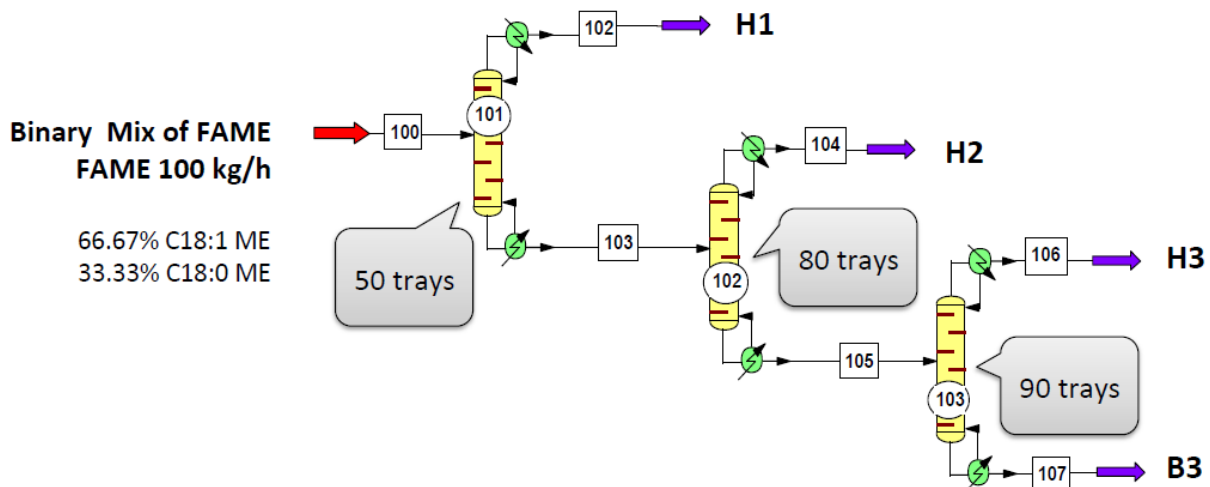


Figure 4.2 - PNNL’s second CHEMCAD distillation model to separate MS and MO. The FAME percentages and flow rates for each stream are detailed in Table 4.2. [52]

Using three additional columns, the maximum MS/MO ratio is from stream “B3 (107)” with a 3.6:1 ratio and 12.4% of the flow of the second model, or 8.6% of the initial flow (Table 4.2). In their conclusion, PNNL states that the MS/MO carryover ratio is likely limited to a 4:1 maximum ratio. That means, for every 3.6 to 4 gal of MS that is removed, an additional gallon of MO is removed. The yield loss cost could be mitigated by finding markets for the MS/MO byproduct.

Table 4.2 – Flow rates and FAME profiles in PNNL’s second distillation model [52]

Stream Number	Feed	H1	B1	H2	B2	H3	B3
Stream name	100	102	103	104	105	106	107
Methyl Stearate (C18:0)	33.3%	29.7%	37.2%	14.1%	41.3%	25.3%	78.4%
Methyl Oleate (C18:1)	66.7%	70.3%	62.8%	85.9%	58.7%	74.7%	21.7%
Flow Rate (kg/h)	100.0	51.4	48.6	7.3	41.2	28.8	12.4

4.3 Distillation Fractionation Modeling

To determine the economic feasibility of fractionating TME to reduce CP, the fractionated TME FAME profiles required to reach target CPs needed to be estimated so yield losses and CPs could be compared. A number of authors have investigated the best theories to model the CP of a FAME mixture. Three models were summarized in Dunn’s “Crystallization Behavior of Fatty Acid Methyl Esters”. All of them posited that since the CP is a thermodynamic phase change event, the freezing-point depression theory (FPDT) could be used to predict CP from the FAME profile [29].

4.3.1 Thermodynamic Cloud Point Prediction Models

The overarching FPDT equation is Equation 4.1 which accounts for independent crystallization of solid precipitates. To determine the overall CP of the mixture, this equation must be solved for each solute species. The maximum individual CP of all the species is the overall CP of the mixture, since a mixture’s CP is dependent on the first crystallization. For tallow the two species that will determine the CP are methyl palmitate (MP) and methyl stearate (MS).

$$\ln(\gamma_i x_i) = -\frac{\Delta H_{fus,i}}{R_g} \left[\frac{MP_i - T_{f,i}}{MP_i(T_{f,i})} \right] - \frac{\Delta C_{p,i}}{R_g} \left[1 - \frac{MP_i}{T_{f,i}} + \ln \left(\frac{MP_i}{T_{f,i}} \right) \right]$$

Equation 4.1 - Freezing point depression theory model for independent crystallization [29]

The variables used for species “i” in the equation above are “ γ_i ” for the activity coefficient, “ x_i ” for the mole fraction, “ $\Delta H_{fus,i}$ ” for the enthalpy of fusion, “ R_g ” for the gas constant, “ MP_i ” for the melting point of the pure solute, “ $T_{f,i}$ ” for the temperature at which the solute begins to crystallize in the solution (i.e. the CP temperature of that FAME), and “ $\Delta C_{p,i}$ ” for the difference in the solid and liquid heat capacities for that constituent.

The first variation of the FPDT model considered was the Hildebrand version for ideal solutions, seen below in Equation 4.2. The major assumptions that differentiate it from Equation 4.1, are that the activity coefficients are considered to be ideal ($\gamma_i=1$) and the change in heat capacity is negligible ($\Delta C_{p,i}=0$).

$$\ln(x_i) = -\frac{\Delta H_{fus,i}}{R_g} \left[\frac{MP_i - T_{f,i}}{MP_i(T_{f,i})} \right]$$

Equation 4.2 - Hildebrand equation for ideal freezing point depression solutions [29]

Imahara et al. used a variation of the FPDT equation above (Equation 4.1), and also assumed that $\gamma_i = 1$ due to low ambient pressures and that ΔC_p was negligible. These assumptions would make the equation identical to the Hildebrand ideal equation (Equation 4.2), but “ ΔH_{fus} ” was replaced with “ $\Delta H_{m,i}$ ”, the enthalpy of melting (

Equation 4.3). The values for the enthalpy of melting of various FAMEs used by Imahara are listed below in Table 4.3 [29].

$$\ln(x_i) = -\frac{\Delta H_{m,i}}{R_g} \left[\frac{MP_i - T_{f,i}}{MP_i(T_{f,i})} \right]$$

Equation 4.3 - Freezing point depression theory model variation by Imahara et al. [29]

Imahara et al., were able to get good correlation between their model and empirical data for up to five FAMEs mixtures with the maximum deviation less than 5°C. Their results also showed

that the overall FAME CP was not dependent on the composition of the unsaturated FAMES in the solvent but solely on the two FAMES (usually saturated) with the highest individual CPs in solution.

Table 4.3 – Imahara’s molar enthalpy of melting for saturated methyl esters [30]

FAME Type	$\Delta H_{m,i}$ (J/mol)
Methyl Myristate (C14:0)	44,480
Methyl Palmitate (C16:0)	55,350
Methyl Stearate (C18:0)	64,430

In addition to that, they demonstrated that there is a mole ratio of where the two saturated FAMES (MP and MS in this case) create a minimum CP for the same mole fraction of MP+MS in the overall FAME mixture [30]. This ratio is called the eutectic ratio and is shown for a mixture of MP and MS in Figure 4.3. The ramifications of this are very important. If the goal is to minimize CP while maximizing the yield, the eutectic point is where this will happen!

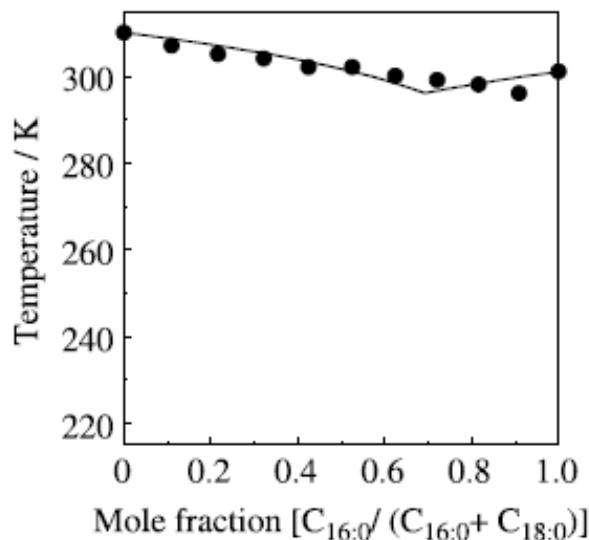


Figure 4.3 – Eutectic point of binary MP and MS mixture. Measured CPs (dots), Calculated CPs (line) [30]

The third variation of the FPDT model, used by Suppes et al., is the full Equation 4.1. It includes the second term to adjust for variation in ΔH_{fus} due to temperature, and accounts for the differential heat capacity between liquid and solid phases for each species. In addition, it incorporates activity coefficients to account for non-ideal behavior [29].

In Dunn's comparison of the three models, he saw that all three of these models relied heavily on the " ΔH_{fus} ", " ΔH_m ", " MP " and " ΔC_p " terms, and that the calculated CPs were sensitive to any variation in these values. To have higher confidence in the predicted CPs, Dunn used differential scanning calorimetry (DSC) to verify these properties with pure FAMES. The " MP ", " ΔH_m ", and " ΔH_{fus} ", values for MP, MS and MO are listed below in Table 4.4. The heat capacities of MP, MS and MO in the solid and liquid phase are listed below in Table 4.5.

Table 4.4 – Dunn's results for MP, FP, ΔH_m , and ΔH_{fus} from DSC analyses of pure FAME [29]

FAME	MP (°C)	P_H (°C)	ΔH_m (kJ/mol)
(a) Heating curves at 5 °C/min			
MeC16	27.79 ± 0.042	29.9 ± 0.31	49.4 ± 0.53
MeC18	37.05 ± 0.050	39.0 ± 0.17	56.5 ± 0.77
MeC18:1	-20.71 ± 0.059	-18.9 ± 0.14	40.9 ± 0.98
FAME	FP (°C)	P_F (°C)	ΔH_{fus} (kJ/mol)
(b) Cooling curves at 5 °C/min			
MeC16	24.4 ± 0.93	23.7 ± 0.80	47 ± 5.0
MeC18	33.7 ± 0.79	32.7 ± 0.58	51 ± 6.5
MeC18:1	-40.6 ± 0.29	-41.1 ± 0.16	28 ± 3.1

DSC, differential scanning calorimetry; *MP*, melting point (melting peak onset) temperature of pure compound; P_H , melting peak minimum temperature (exothermic); ΔH_m , enthalpy of melting; *FP*, freezing point (crystallization peak onset) of pure compound; P_F , freezing peak maximum temperature (exothermic); ΔH_{fus} , enthalpy of fusion. See Table 1 for other abbreviations

Table 4.5 – Dunn's results for heat capacities of pure FAME in liquid and solid phases [29]

FAME	Liquid phase		Solid phase	
	T (°C)	C_p^L (J/mol-K)	T (°C)	C_p^S (J/mol-K)
MeC16	40.00	640 ± 7.1	5.00	535 ± 8.6
MeC18	50.00	634.6 ± 0.86	15.00	539 ± 4.4
MeC18:1	-30.00	410 ± 13	-65.00	320 ± 12

FAME fatty acid methyl esters, *MeC16* methyl palmitate, *MeC18* methyl stearate, *MeC18:1* methyl oleate, T , measurement temperature, C_p^L , C_p^S , heat capacities in the liquid and solid phase

Having precise values for those variables, Dunn was able to calculate the activity coefficients at varying mole percentages of MP and MS using Equation 4.1. He measured the activity coefficient values for molar percentages of MP from 4.4-22.0% and 4.0-20.0% for MS. The activity coefficient values are charted in Figure 4.4 below. Unfortunately, many of the tests simulating TME fractionation in this research were outside of these bounds, making the “Dunn” model not very useful. To solve Equation 4.1 with the full second term, using Dunn’s activity coefficients, requires first solving for y_i given x_i , using Figure 4.4, then iteratively guessing T_f to match the known x_i . It is very handy to use Excel’s Solver function to do this.

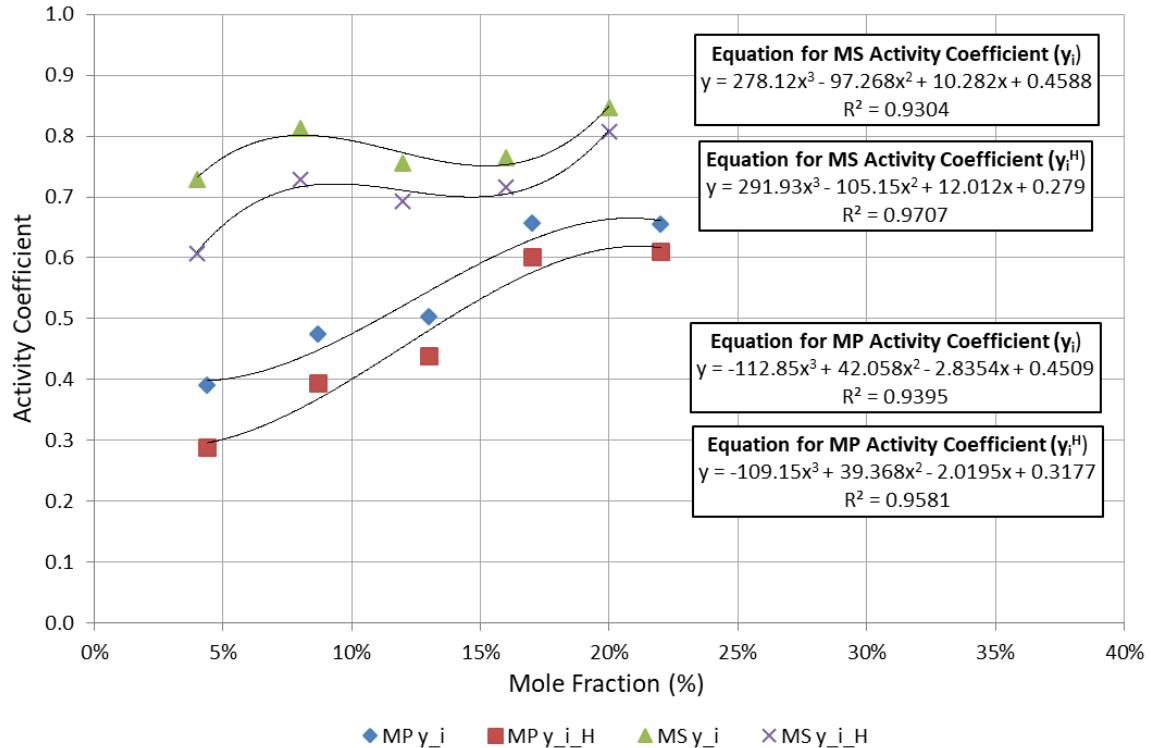


Figure 4.4 – Plot of Dunn’s activity coefficients from the DSC analysis of MP or MS in a MO solvent [29]

In addition to the models described by Dunn, variations of these were also calculated. The full FPDT (Suppes) equation with Dunn activity coefficients and FAME properties was calculated with and without the second (ΔC_p) term and those two models were referred to as “Dunn (Full)”

and “Dunn (Simple)”. The second (ΔC_p) term was found to be negligible ($<0.1^\circ\text{C}$ difference) and removing it allowed a direct calculation without the iterative approach using Excel’s Solver function. The “Imahara” model was run both with Imahara’s and Dunn’s FAME material properties. Those two variations were referred to as “Imahara” and “Imahara (Dunn)”. The Hildebrand “Ideal” equation was calculated using Dunn’s material properties.

4.3.2 Theoretical Eutectic Point

Prior research had suggested that the CP of a FAME was simply related to the percentage of saturated FAMES in the mixture [28]. However, Dunn demonstrated that it was not the percentage of saturated FAMES that determined the CP, but the percentage of the two FAMES with the highest melting points [29]. For many biodiesel feedstocks, and specifically for tallow those two FAMES are MP and MS.

Imahara et al., proposed that for a specific fraction of MP+MS in a FAME mixture, there is a eutectic ratio of MP to MS where the CP is at a minimum. The eutectic ratio is not constant but as the overall percentage of MP and MS increases in the mixture, the eutectic ratio of MP/(MP+MS) shifts slightly lower according to the FPDT models. The eutectic ratios determined by each CP prediction model are similar, but do vary some.

For the Hildebrand “Ideal” model, the eutectic point is at approximately 70% MP/(MP+MS) at a 7% fraction of MP+MS but lowers to around 65% MP/(MP+MS) at 100% MP+MS as shown in Figure 4.5. The other models all have similar CP curve graphs as Figure 4.5 and are presented in Appendix A. The “Imahara” model has a eutectic point at 78% for 7% MP+MS and 72% at 100% MP+MS. The “Imahara (Dunn)” model has a eutectic point at 76% for 7% MP+MS and 68% at 100% MP+MS. The “Dunn (Simple)” model has a eutectic point at 79% for 7% MP+MS and 72% at 35% MP+MS. Modeling CPs for a MP+MS fraction greater than 35% in the “Dunn (Simple)” model is unreliable because the MP and MS percentages are outside of the bounds of measured activity

coefficients. In general, the eutectic ratio varies between 65-79% MP/(MP+MS). On average the ratio at 7% MP+MS is 76% and 69% at 100% MP+MS.

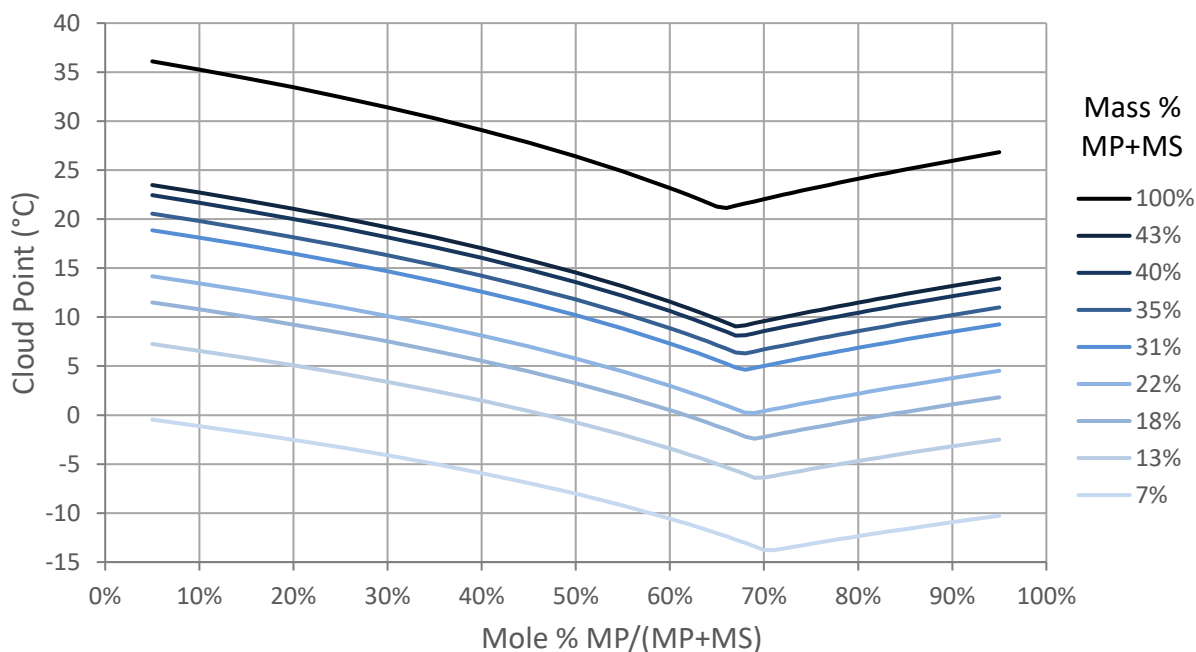


Figure 4.5 – CP vs MP/(MP+MS) for the Hildebrand “Ideal” model at varying MP+MS fractions

4.3.3 Target Cloud Point FAME Profiles

Once the thermodynamic models were determined to reasonably predict the CP from a FAME profile, the next step was to work backwards and determine what FAME profiles would give the CPs we desired. The target CPs chosen by Sun West were 10°C, 7°C, 2°C, and 0°C. The CP models showed that specific CPs could be reached by modifying the total amount of MP and MS, by changing the ratio of MP to MS, or by combining both methods.

To avoid testing an infinite number of points, I decided to limit tests to the theoretical eutectic point (TEP) when possible, to maximize yield and to minimize CP. The TEP was estimated to be at a ratio of 70.9% MP/(MP+MS). In addition to that I added tests with +/- 20% of the eutectic quantity of MS to better empirically identify the precise eutectic ratio. Since TME has a MP/(MP+MS) ratio of 59%, MS must first be removed to bring that ratio closer to the eutectic point.

Once the MP/(MP+MS) ratio is at the eutectic ratio, MP and MS need to be removed at the eutectic ratio in order to maintain the eutectic ratio.

Calculating the FAME profiles that had the highest ideal yield for a specific CP was an involved process. This calculation was done using the Excel Solver function. The FAME species that were accounted for were C14:0, C14:1, C16:0, C16:1, C18:0, C18:1, C18:2, and C18:3, all which are detectable in TME. The input variables were “% MP Removed” and “% MS Removed”. The Solver function would iterate those two inputs, and Excel would calculate the new TME FAME profile by dividing each individual FAME by the new total amount of FAME (with the MP and MS removed). To stay at the TEP, the ratio of MP/(MP+MS) was constrained to 70.9%. Once a FAME profile was determined, the CP of that FAME profile was calculated using the average of the “Imahara” and “Dunn” (with linear activity coefficients) models. The Solver function would alter the input variables (% MP Removed, % MS Removed) until the CP reached the desired temperature. Additionally, the yield was calculated from the yield loss based on the percentage of MP and MS that was removed. The target FAME profile and its yield were recorded and saved as a target test case. To determine the tests cases with +/- 20% MS was as simple as adding or subtracting 20% of the amount of MS from the TEP test and running Solver to determine the MP and MS removal percentages it would take to make that FAME profile.

Table 4.6 below lists the proposed test cases to measure CP when first removing only MS to reach 10°C, then at the TEP at estimated CPs of 7°C, 2°C, and 0°C, and with +/-20% MS to determine the MP/(MP+MS) ratio of the empirical eutectic point (EEP).

The terminology used to name the tests are “TEP” for “theoretical eutectic point”, “+MS” for tests with 20% extra methyl stearate than the TEP and “-MS” for test with 20% less methyl stearate than the TEP. “Test 1” does not have a “-MS” test associated with it because it would be virtually identical to “Test 2 +MS”.

Table 4.6 – Proposed tests to reach 10°C, 7°C, 2°C, and 0°C CP at the theoretical eutectic ratio with additional tests at +/- 20% MS

Test #	Purpose	Calculated Average CP	Target Mole % MP/(MP+MS)	Target Mass % MP + MS	Tested?
Test TME	100% Tallow Methyl Esters	14.5	58.9%	44.3%	Yes
Test 1 +MS	10°C Calculated CP + 20% MS	12.4	61.2%	43.9%	No
Test 1	10°C Calculated CP	10.0	65.8%	40.9%	Yes
Test 2 +MS	7°C CP @ Theoretical EP + 20% MS	9.3	67.0%	40.1%	Yes
Test 2 TEP	7°C CP @ Theoretical EP	7.0	70.9%	37.8%	Yes
Test 2 -MS	7°C CP @ Theoretical EP - 20% MS	7.5	75.3%	35.4%	Yes
Test 3 +MS	Theoretical EP + 20% MS	4.2	67.0%	26.2%	No
Test 3 TEP	2°C CP, Theoretical EP	2.0	70.9%	24.7%	No
Test 3 -MS	Theoretical EP - 20% MS	0.4	75.3%	23.2%	No
Test 4 +MS	Theoretical EP + 20% MS	2.1	67.0%	22.0%	No
Test 4 TEP	0°C CP, Theoretical EP	0.0	70.9%	20.7%	No
Test 4 -MS	Theoretical EP - 20% MS	-2.3	75.3%	19.4%	No

Figure 4.6 below, graphically shows how all of the proposed test points compare with the MP/(MP+MS) ratio on the x-axis and the MP+MS fraction as the y-axis.

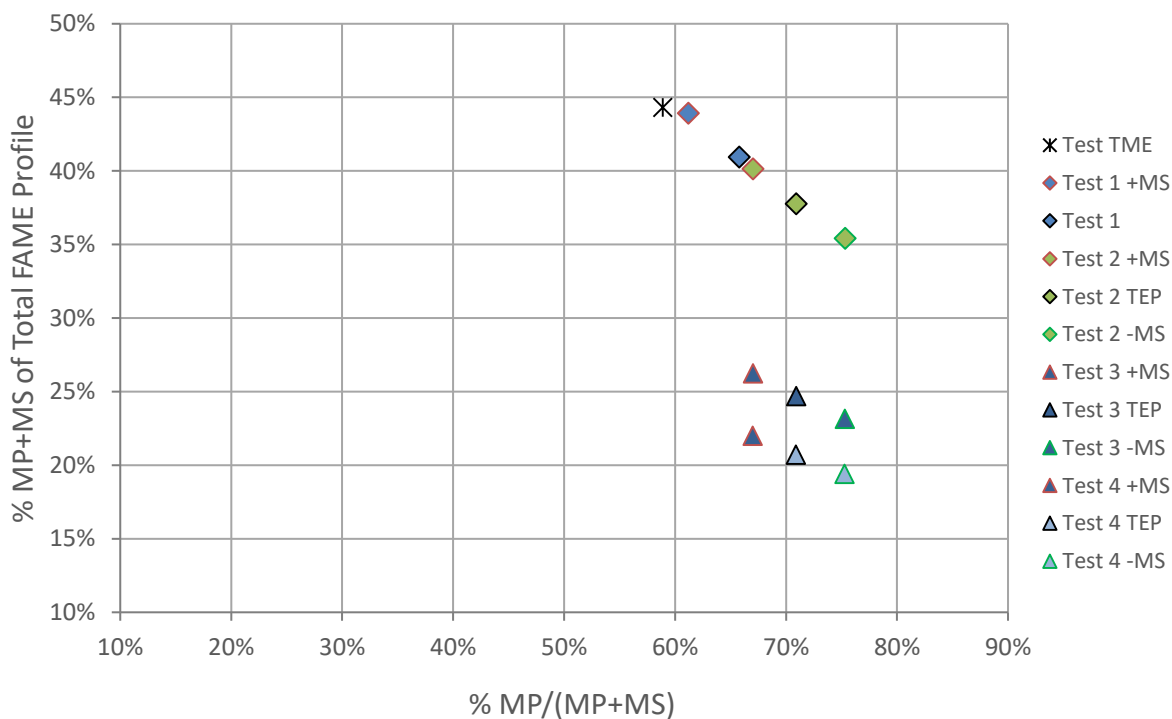


Figure 4.6 – Proposed test points in relation to MP/(MP+MS) ratio and percent MP+MS

4.3.4 Tallow Methyl Ester FAME Profiles

The model TME FAME profile used for all these calculations was based on the average of four distinct TME samples. The first TME FAME profile was from the REG Feedstock report, two samples from Sun West were measured by Westfalia, and two JBS tallow samples were transesterified and measured by Solix. The model TME profile was later compared to the average of all measured TME FAME profiles in Table 4.7. The FAME profile of the average of those TMEs only varied from the model by a maximum of 2.6% for C16:0/MP (CAR-BD-A) and 2.7% for C18:0/MS (JBS-BD-B). Some of the TMEs initially produced in house had their FAME profiles measured in the GC, but since they did not vary significantly from the model TME profile, it was used for all calculations. The FAME profiles of those TMEs are documented in Appendix B.

Table 4.7 - "Model TME Profile" compared with average of other TME profiles

	"Model" TME Profile	Average TME Profile	Max Variation from "Model" TME	Std. Dev. from "Model" TME
FFA %	1.5%	1.4%	0.3%	0.3%
C12:0	0.0%	0.1%	0.3%	0.1%
C14:0	3.5%	3.8%	1.6%	0.7%
C14:1	0.4%	0.7%	1.1%	0.5%
C16:0	26.1%	25.4%	2.6%	1.3%
C16:1	2.5%	2.8%	0.7%	0.6%
C18:0	21.4%	20.6%	2.7%	2.0%
C18:1	40.5%	40.2%	1.7%	1.1%
C18:2	2.1%	2.2%	0.8%	0.7%
C18:3	0.2%	0.4%	0.7%	0.4%
Other FAMES	3.2%	3.9%	3.2%	1.6%

4.3.5 Fractionation FAME Profile Simulation

The next step after determining which FAME profiles to target to reach certain CPs, was to figure out how to make a FAME mixture with that profile. Without the instrumentation to actually fractionate with distillation or crystallization, we initially investigated formulating complete FAME profiles from pure individual FAMES but that was cost-prohibitive. The next best option was use

TME as the base and to blend in high purity methyl esters that would modify the percentages of each FAME to match the target FAME profile. To mimic removing MS from TME, required a methyl ester mix that had a high percentage of MP (C16:0). A high percentage MO (C18:1) mixture and methyl myristate (MM/C14:0) mixture made sure the final FAME profile was as close to the fractionation target FAME profile as possible. This simulation method worked to make the target FAME profiles, but there were natural limits on what FAME profiles could actually be formulated since the mixtures were not pure FAMEs and TME was used as the base. The FAME profiles of the various high concentration methyl ester mixtures are listed below in Table 4.8. All three of these methyl ester mixtures were purchased from Sigma-Aldrich.

Table 4.8 – FAME profiles of Sigma Aldrich FAME mixtures used for fractionation modeling

FAME Type	TME Profile	C14:0 FAME	C16:0 FAME	C18:1 FAME
C14:0	3.5%	99.0%	0.1%	0.3%
C14:1	0.4%	0.0%	0.0%	0.0%
C16:0	26.1%	1.0%	99.9%	5.4%
C16:1	2.5%	0.0%	0.0%	0.0%
C18:0	21.4%	0.0%	0.0%	1.7%
C18:1	40.5%	0.0%	0.0%	81.3%
C18:2	2.1%	0.0%	0.0%	11.0%
C18:3	0.2%	0.0%	0.0%	0.3%
Other	3.2%	0.0%	0.0%	0.0%

To determine how to formulate each test's FAME profile, another Excel Solver function was developed to match the "target" FAME profile by adjusting the mass of each of the four FAME mixtures in Table 4.8. The constraints were that the MM, MP, and MS percentages matched. These constraints were chosen based on the premise that the two FAMEs with the highest CPs are what affect the overall CP, namely MP and MS, and the makeup of the rest of the FAME mixture is not important. Since MM is the FAME with the third highest melting point, and a high purity source was available, matching MM percentages was possible without throwing off the rest of the FAME profile.

4.3.6 Methyl Stearate/Methyl Oleate Carryover

The initial target FAME profiles and yields and were calculated assuming that MS could be perfectly removed. As was discussed previously in Section 1.5.1.1, this is not possible with distillation fractionation since the boiling points of MS and MO are within 3°C, making carryover between the two common. According to the report by PNNL, the minimum reasonable carryover of MO when maximizing MS removal is 4:1 MS/MO [52]. With this in mind, each test also had the yield calculated assuming a 4:1 MS/MO carryover ratio. The comparison between the “ideal” yield and the yield assuming a 4:1 MS/MO carryover ratio is graphed below in Figure 4.7. The target fractionation FAME profiles did not account for the 4:1 MS/MO carryover.

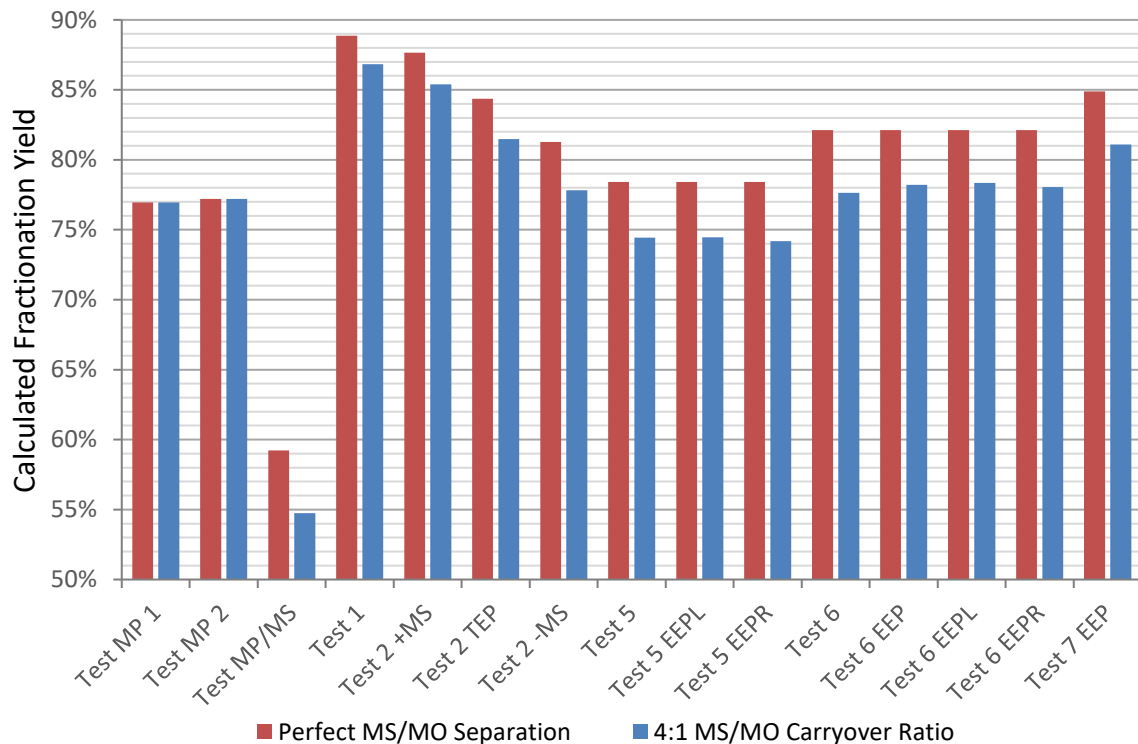


Figure 4.7 – Comparison of ideal yield and 4:1 MS/MO carryover yield for fractionation tests

4.4 Empirical Fractionation Data

Once the FAME profiles were determined that would reach the target CPs with minimal yield loss, they were simulated by mixing together high purity FAMEs with TME in order to mimic the fractionated FAME profile. These FAME mixtures were then tested for CP and CFPP.

4.4.1 Exploratory Fractionation Cloud Point Tests

The very first CP tests that were run early on in this research, were to see what the CPs of a TME mixture would be, when removing large quantities of MP or of MP and MS. The first tests to simulate removing only MP were named “Test MP 1” and “Test MP 2”. “Test MP 1” measured the CP at the maximum MP we could simulate removing (88.4% MP removal), with the constraints that the percentage of MP and of saturated FAMEs would match the “target” FAME profile (Table 4.9). “Test MP 2” also simulated the maximum MP (87.4% MP removal), but had the constraint that the percentages of MP and MS must match the “target” FAME profile. The third test, “Test MP/MS” was to remove the maximum amount of MP and MS that could be simulated (87.8% MP removal, 83.4% MS removal).

Table 4.9 – Initial exploratory CP tests with explanations, calculated CPs, target MP/(MP+MS) ratios and target MP+MS fractions

Test #	Purpose	Calculated Average CP	Target Mole % MP/(MP+MS)	Target Mass % MP + MS	Tested?
Test TME	100% Tallow Methyl Esters	14.5	58.9%	44.3%	Yes
Test MP 1	Max MP Removal, Solving for % MP and % Sats	18.7	13.5%	31.8%	Yes
Test MP 2	Max MP Removal, Solving for % MP and MS	18.7	14.5%	32.0%	Yes
Test MP/MS	Max MP/MS Removal, Solving for % MP and MS	-0.8	49.7%	11.4%	Yes

The initial exploratory tests showed that the counterintuitive results claimed by the thermodynamic models were true. Removing large quantities of the saturated FAME, MP, actually increased the CP of the TME mixture from 14.5°C to 20-22°C by moving the MP/(MP+MS) ratio farther away from the eutectic ratio (Figure 4.8). In this case, the movement from a MP/(MP+MS)

ratio of 59% down to 10.4-13.3% contributed more to the CP than the reduction in the percentage of MP+MS from 47.5% to 32.0-37.7%. Each test formulation was run through the GC so the measured FAME profile could be compared to the “target” FAME and so the CP could be correlated to the actual MP+MS fraction and MP/(MP+MS) ratio of the FAME mixture (see Appendix C for target and actual FAME profiles).

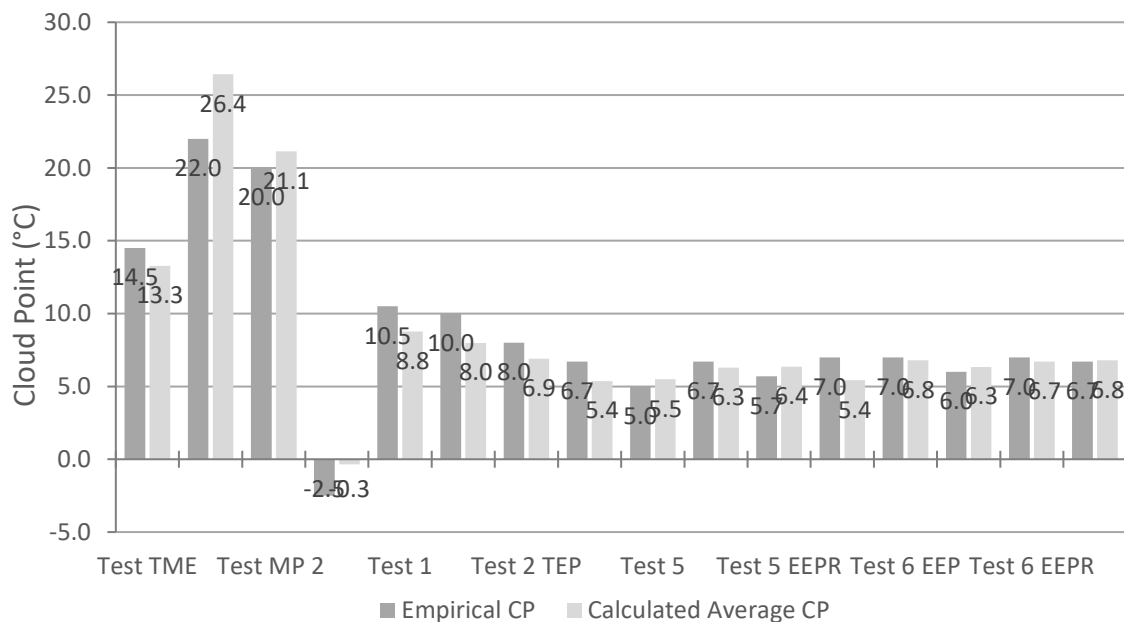


Figure 4.8 – Comparison of calculated and empirical CPs of the initial exploratory tests

The simple explanation that a high level of saturated FAMES cause a high CP is not true, since reducing the total percent of saturated FAMES actually increased the CP. A better explanation is that saturated FAMES do determine the CP, but it is the ratio of the two most prolific, high melting point FAMES, compared to the whole mixture and to each other that determine the CP.

The next test was to remove large amounts of methyl palmitate and methyl stearate (Test MP+MS). Since those are the two saturated FAMES with the highest melting points, the CP dropped significantly from 14.5°C to -2.5°C. If CP was the only concern, this research would be complete. But at that CP, the “ideal” yield is only 59% and with 4:1 MS/MO carryover, the yield drops even further to 55%. That is clearly not economically feasible to effectively throw away half of the product.

4.4.2 Eutectic Fractionation Tests Results

With the initial exploratory tests in mind, the next tests targeted the eutectic ratio to minimize CP and maximize yield while reaching CPs of 10°C, 7°C, 2°C, and 0°C. Additional tests were added on either side of the eutectic ratio to compare the theoretical eutectic point (TEP) to the empirical eutectic point (EEP).

“Test 1 +MS”, in Table 4.10 below, was not conducted since it was likely to be higher than the desired 10°C CP and was too far away from the eutectic ratio to be insightful. “Test 1”, “Test 2 +MS”, “Test 2 TEP” and “Test 2 -MS” were all tested for CP and CFPP.

Table 4.10 – Proposed CP tests with explanations, calculated CPs, target MP/(MP+MS) ratios and target MP+MS fractions

Test #	Purpose	Calculated Average CP	Target Mole % MP/(MP+MS)	Target Mass % MP + MS	Tested?
Test 1 +MS	10°C Calculated CP + 20% MS	12.4	61.2%	43.9%	No
Test 1	10°C Calculated CP	10.0	65.8%	40.9%	Yes
Test 2 +MS	7°C CP @ Theoretical EP + 20% MS	9.3	67.0%	40.1%	Yes
Test 2 TEP	7°C CP @ Theoretical EP	7.0	70.9%	37.8%	Yes
Test 2 -MS	7°C CP @ Theoretical EP - 20% MS	7.5	75.3%	35.4%	Yes
Test 3 +MS	Theoretical EP + 20% MS	4.2	67.0%	26.2%	No
Test 3 TEP	2°C CP, Theoretical EP	2.0	70.9%	24.7%	No
Test 3 -MS	Theoretical EP - 20% MS	0.4	75.3%	23.2%	No
Test 4 +MS	Theoretical EP + 20% MS	2.1	67.0%	22.0%	No
Test 4 TEP	0°C CP, Theoretical EP	0.0	70.9%	20.7%	No
Test 4 -MS	Theoretical EP - 20% MS	-2.3	75.3%	19.4%	No

A look at the results in Figure 4.9 show three things. First, the empirical CPs were all 1-2°C higher than the calculated CPs. Second, “Test 2 -MS” had a lower CP than “Test 2 TEP” showing that the empirical eutectic point was actually at a higher MP/(MP+MS) ratio than the model’s 70.9% eutectic ratio. Finally, after considering that for “Test 2 -MS” to achieve a CP less than 7°C, resulted in a 78% yield, Sun West reevaluated their approach. At that point we chose to forgo the tests at lower calculated CPs (Tests 3 and 4) and look further into finding the EEP.

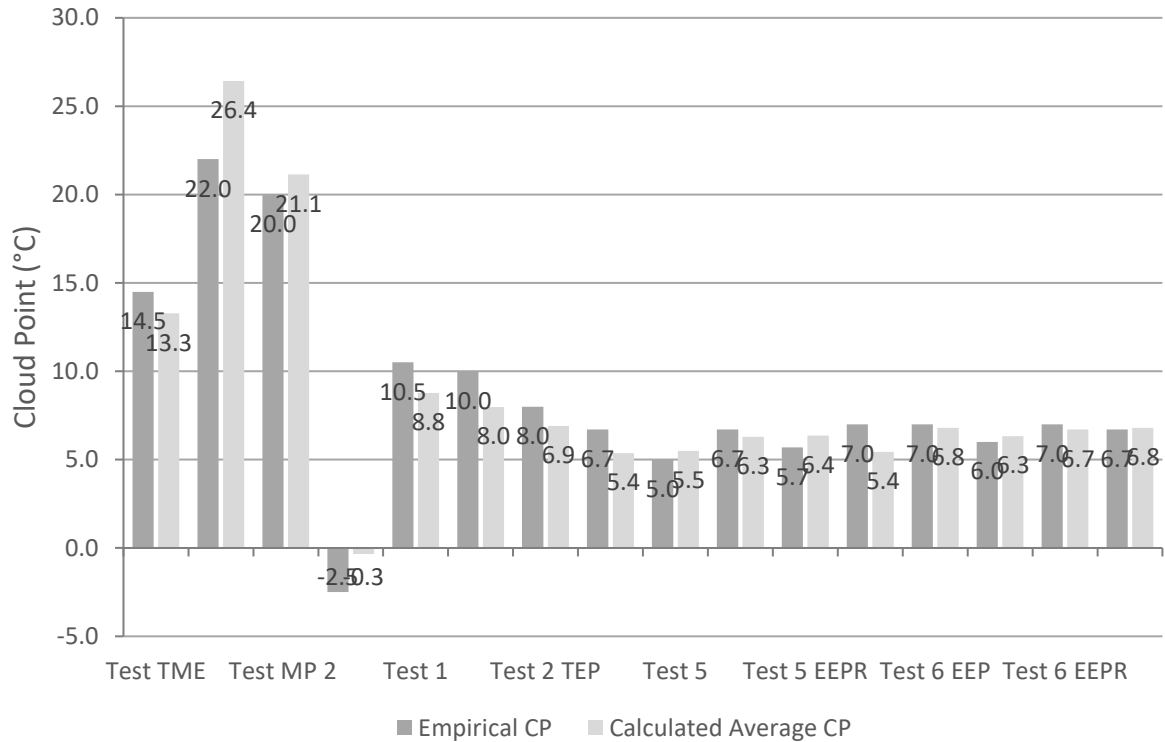


Figure 4.9 – Calculated and empirical CPs of planned test points from Table 4.10

The next tests were conducted for the most part, one at a time with each test informing the next. The first new test, “Test 5” was designed to move the MP/(MP+MS) ratio higher by simulating removing an additional 20% of the MS from “Test 2 TEP”. The CP for “Test 5” was 1.7°C less than “Test 2 –MS” by moving from a MP/(MP+MS) ratio of 75.3% to 80.2% (see Figure 4.10 and Table 4.11). This was a good sign that the eutectic ratio lay in this area, and potentially at an even higher MP/(MP+MS) ratio.

Table 4.11 – Additional CP tests with purpose, calculated CPs, target MP/(MP+MS) ratios and target MP+MS fractions

Test #	Purpose	Calculated Average CP	Target Mole % MP/(MP+MS)	Target Mass % MP + MS	Tested?
Test 5	7°C CP @ Theoretical EP - 40% MS	7.5	80.2%	33.1%	Yes
Test 6	No MP Removed, Highest MP/(MS+MP) possible	11.0	89.0%	36.1%	Yes
Test 7 EEP	No MP Removed, Empirical EP	10.4	82.0%	38.2%	Yes
Test 6 EEPL	Same % MP+MS as Test 5b, Left of Empirical EP	8.9	80.0%	36.1%	Yes
Test 5 EEPL	Same % MP+MS as Test 5a, Left of Empirical EP	7.4	80.0%	33.1%	Yes
Test 6 EEP	Same % MP+MS as Test 5b, at Empirical EP	9.4	82.0%	36.1%	Yes
Test 6 EEPR	Same % MP+MS as Test 5b, Right of Empirical EP	9.9	84.0%	36.1%	Yes
Test 5 EEPR	Same % MP+MS as Test 5a, Right of Empirical EP	8.3	84.0%	33.1%	Yes

“Test 6” came from the realization that the previous tests had the percentage of MP constrained to remain constant at 26.0% of the FAME mixture. Because MS was being removed, some MP also had to be removed to maintain the same percentage of the total FAME mixture. Ideally, to maximize yield, the percentage of MP should not be constrained to its initial percent in the mixture and should be allowed to increase as the MS is removed. “Test 6” was an attempt to remove the maximum amount of MS without removing any MP and therefore, get the highest MP/(MP+MS) ratio (90%) possible with the highest yield. No MP was removed and we were able to simulate up to 83.4% MS removal. The CP increased 2°C from “Test 5” at 80.2% MP/(MP+MS) so the eutectic point was assumed to be at a lower MP/(MP+MS) ratio (see Figure 4.10, Table 4.11, and Figure 4.11).

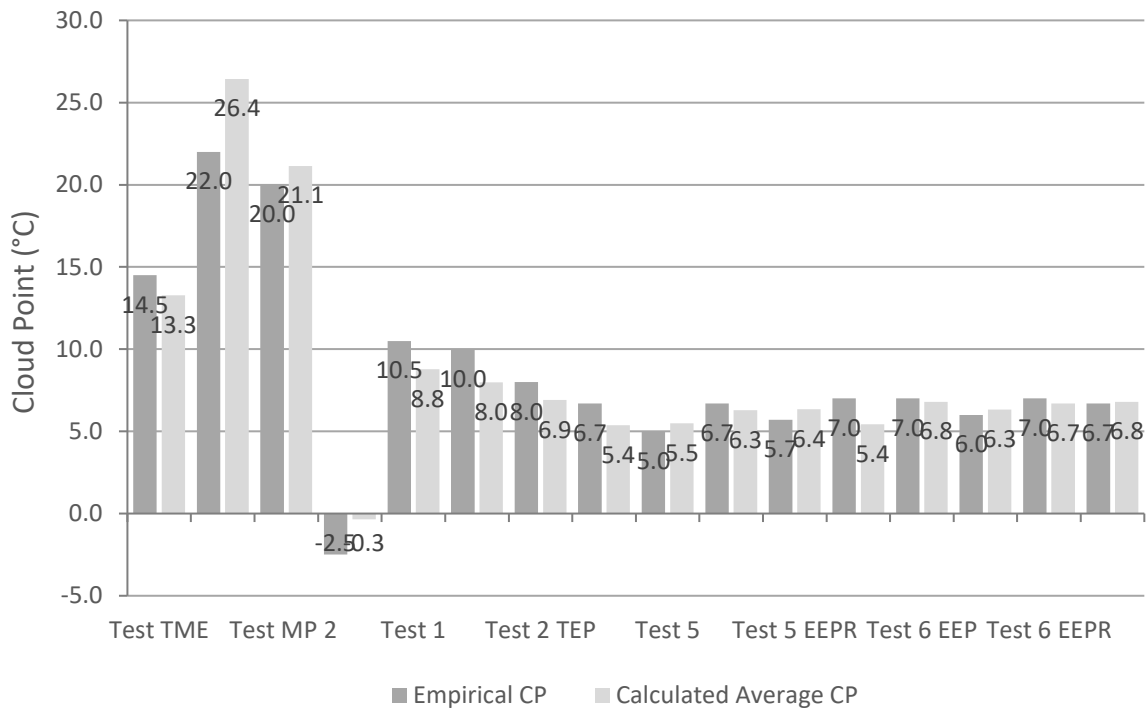


Figure 4.10 – Comparison of calculated and empirical CPs of additional tests

Given these CPs and MP/(MP+MS) ratios, the assumed working EEP looked to be close to 82% MP/(MP+MS). The next test, “Test 7 EEP” was also chosen to only remove MS, but only up the

assumed empirical eutectic point (EEP) of 82%. The CP did decrease slightly compared to “Test 6”, which seemed to confirm the approximate EEP (see Figure 4.10, Table 4.11, and Figure 4.11).

At this point, I came to the realization that I were not making direct comparisons. Even though the MP/(MP+MS) ratios were being compared, the total percent MP+MS in the mixture was changing with each test. The FPDT CP models showed that it is the combination of the MP/(MP+MS) ratio and the total percentage of the two highest melting point saturated FAMES (MP and MS) that determine the CP of the mixture.

With this in mind, the final five tests were constrained to maintain the same overall percent MP+MS in the FAME mixture but varied the MP/(MP+MS) ratio 2% to either side of the EEP. “Test 6 EEPL” was 2% to the “left” or at a lesser MP/(MP+MS) ratio than “Test 6” as was “Test 5 EEPL” compared to “Test 5”. “Test 6 EEPR” was 2% to the “right” or at a greater MP/(MP+MS) ratio than “Test 6” as was “Test 5 EEPR” compared to “Test 5”. “Test 6 EEP” was at the same percent MP+MS as “Test 6” but at the EEP of 82% (see Figure 4.10, Table 4.11, and Figure 4.11).

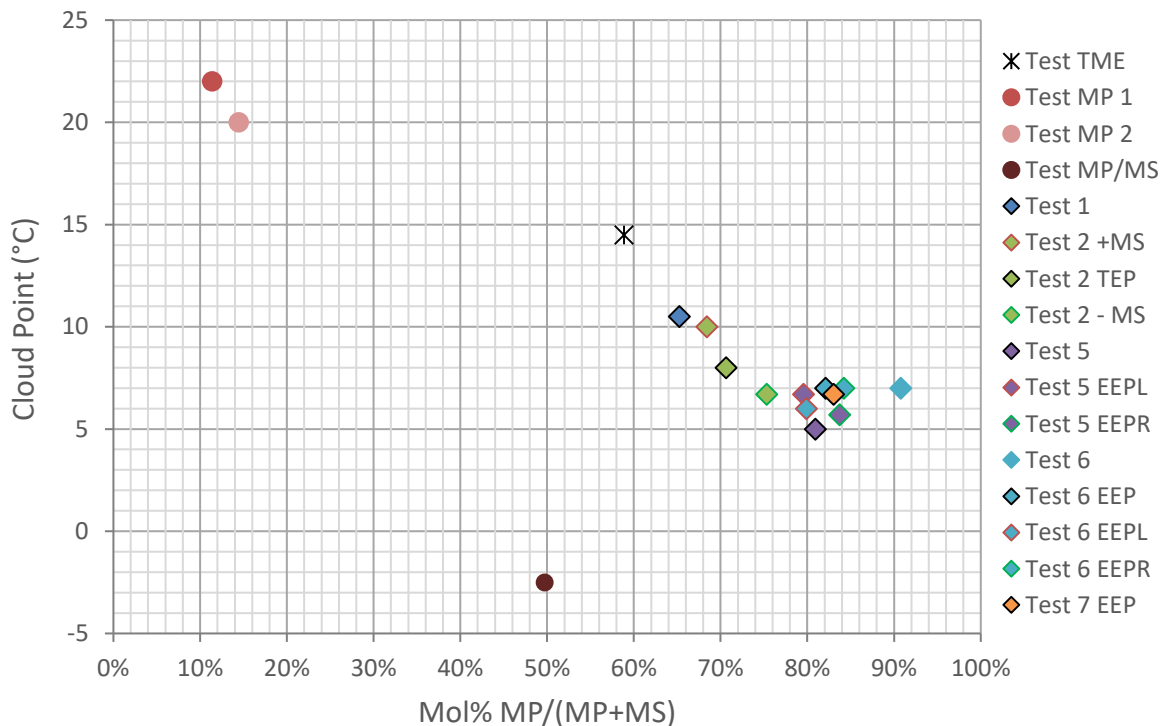


Figure 4.11 - All empirical fractionation CP tests in relation to the MP/(MP+MS) ratio

Figure 4.8, Figure 4.9, and Figure 4.10 show the comparison between the empirical and average calculated CPs for all of the fractionation tests. Without the context of the MP+MS fraction or the MP/(MP+MS) ratio it is difficult to come to many conclusions. Figure 4.12, adds that context to allow better evaluation of the EEP. To create this graph, all of the fractionation tests were sorted within +/-2% MP+MS groupings, and labeled by the average MP+MS fraction of that group. Then the CPs were graphed with each group having its own color, allowing for a better visual representation of the EEP. Group “33%” shows the clearest CP dip, at a MP/(MP+MS) ratio between 80% and 84%, further bolstering the assumed EEP of 82%. The lowest measured CP for that group is at 81% MP/(MP+MS) from “Test 5” but it is also the lowest percent MP+MS in the “33%” MP+MS grouping. Without more detailed testing between 80% to 84% MP/(MP+MS), held to a tighter band than 4% MP+MS it is hard to nail down a more precise EEP percentage.

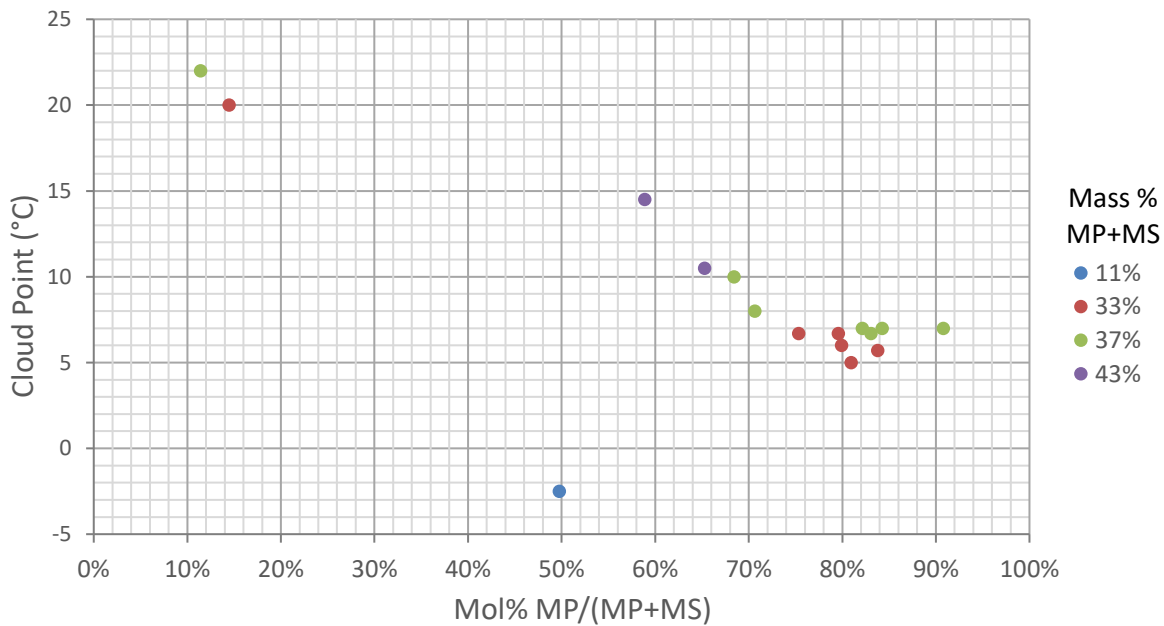


Figure 4.12 – All empirical fractionation CPs in relation to MP/(MP+MS) ratio sorted by MP+MS fraction

The next chart takes this empirical CP data and relates it to the calculated 4:1 MS/MO carryover yield. Out of the empirical data points plotted in Figure 4.13, the best CP/yields combinations are “Test 5”, “Test 6 EEPL”, and “Test 7 EEP”. “Test 5” reached a CP of 5.0°C at a

carryover yield 74%, “Test 6 EEPL” had a CP of 6.0°C with a yield of 78%, and “Test 7 EEP” had a CP of 6.7°C with a carryover yield of 81%. A comparison of “Test 7 EEP” with “Test 2 –MS” perfectly illustrates the advantage to finding the EEP. Both tests reached a CP of 6.7°C but “Test 2 –MS” had a carryover yield of 78% while the yield for “Test 7 EEP” is 81%.

Similar graphs were made for each of the fractionation tests with the cold filter plugging point results. These graphs are presented in Appendix D. Additionally, charts similar to Figure 4.12 were developed, that included measured CP data from this research, Dunn et al., and Imahara et al. The data was sorted by MP+MS fraction to better visualize the eutectic point and the graphs can be found in Appendix K.

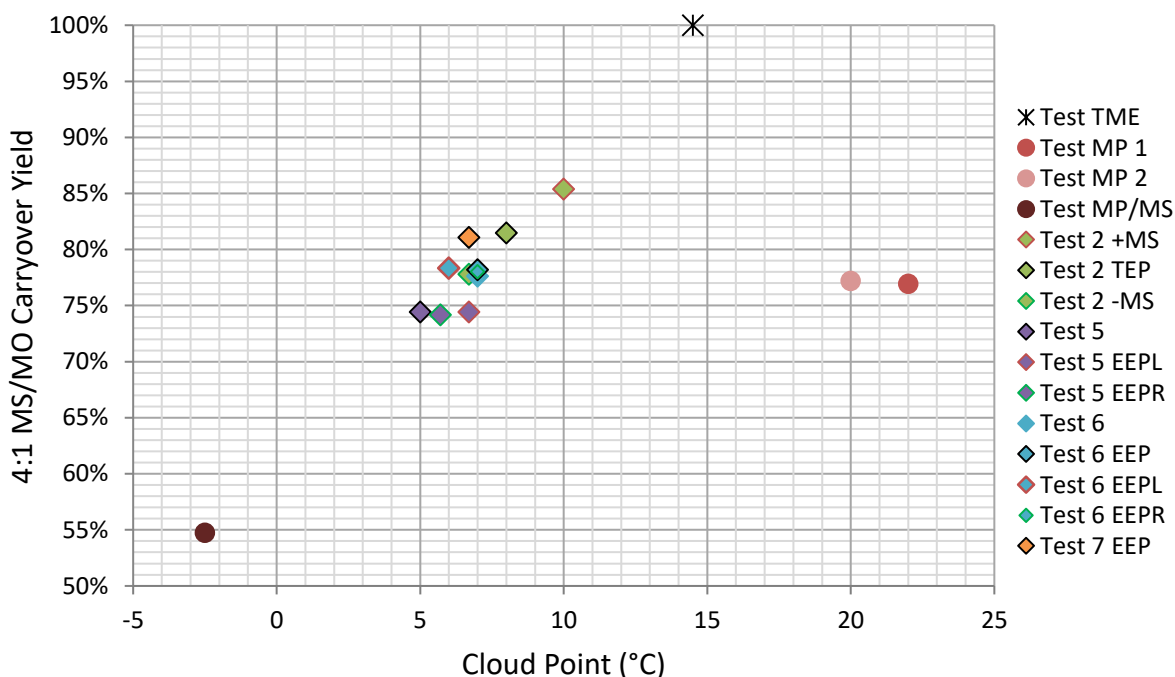


Figure 4.13 – Contrast of empirical fractionation test CPs with 4:1 MS/MO carryover yield

4.4.3 Expanded Cloud Point Data

To truly identify the eutectic ratio, all data points must lie along the same MP+MS fraction line. The initial attempt to sort data points by +/-2% MP+MS groups and plot them together was in Figure 4.12. This was a good preliminary attempt but a better visualization would need to

incorporate all the empirical data points along the same MP+MS curve. The following method was used to “expand” the empirical data points to aid in visualization.

Data points from one MP+MS fraction group could be simulated at the same MP/(MP+MS) ratio but at a different MP+MS fraction group by adjusting them using a calculated differential between MP+MS fractions. To do this required a combination of empirical data and calculated data. First, data points within a +/-2% MP+MS band were sorted into the same group and labeled by the average percent MP+MS of that group, just like in Figure 4.12. These groups were 11%, 33%, 37% and 43% MP+MS. Then a delta was calculated based on the difference between each of the calculated CP curves for MP and MS at those four MP+MS fractions. This difference was based on the average CP of each line between 50% and 85% MP/(MP+MS) as shown by the brackets in Figure 4.14, or between 50% and the maximum MP/(MP+MS) ratio if it was less than 85%. Some of the MP CP curves became unreliable past certain MP/(MP+MS) ratios due to the limitations of the activity coefficients of the Dunn model, which was included in the “Average Calculated CP”.

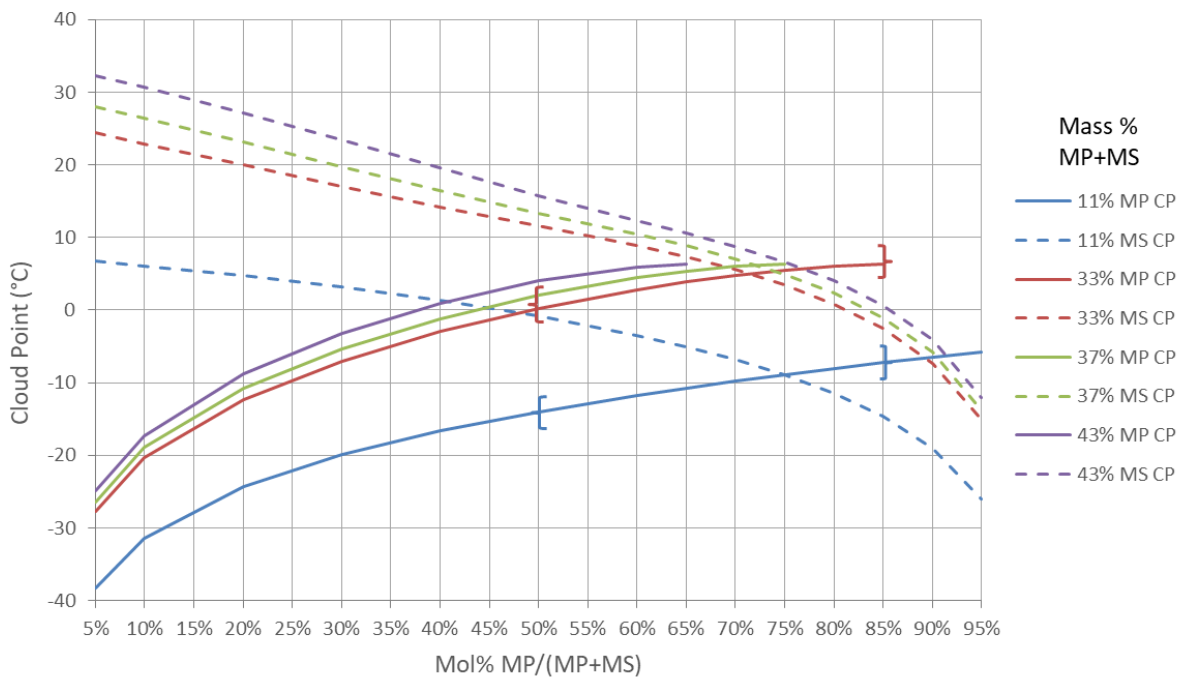


Figure 4.14 – Calculated MP (solid) and MS (dashed) CP curves for MP+MS groups. Brackets show portion of 11% and 33% MP curves where average values were calculated.

Theoretically now, with a known CP delta between the 11% and 33% MP+MS lines, an empirical data point in the 11% MP+MS group could have the delta between the 11 to 33% MP+MS curves added to its value, and create an “adjusted” data point in the 33% MP+MS group, with the same MP/(MP+MS) ratio. This technique was used to adjust every empirical fractionation data point to create new data points in every other percent MP+MS group.

4.4.4 Empirical Eutectic Point

Given this expanded set of data points, better visualizations could be created to see the eutectic point. Figure 4.15 shows two data sets along each line of MP+MS fraction. The circles are the “adjusted” data points made by using the deltas from the MS curves, and are left of the assumed EEP of 82% MP/(MP+MS) since MS is the first FAME to solidify at MP/(MP+MS) ratios lower than the eutectic point. The diamonds are the “adjusted” data points made by using the deltas from the MP curves, and are to the right of the EEP because MP is the first FAME to solidify at MP/(MP+MS) ratios higher than the eutectic point. The “X’s” are the empirical CPs. From this chart, the early assumption that the EEP is around 82% MP/(MP+MS) is supported. Another interesting thing of note, is that the CPs do not seem to rise as quickly to the right of the EEP (MP rich) as it does to the left (MS rich).

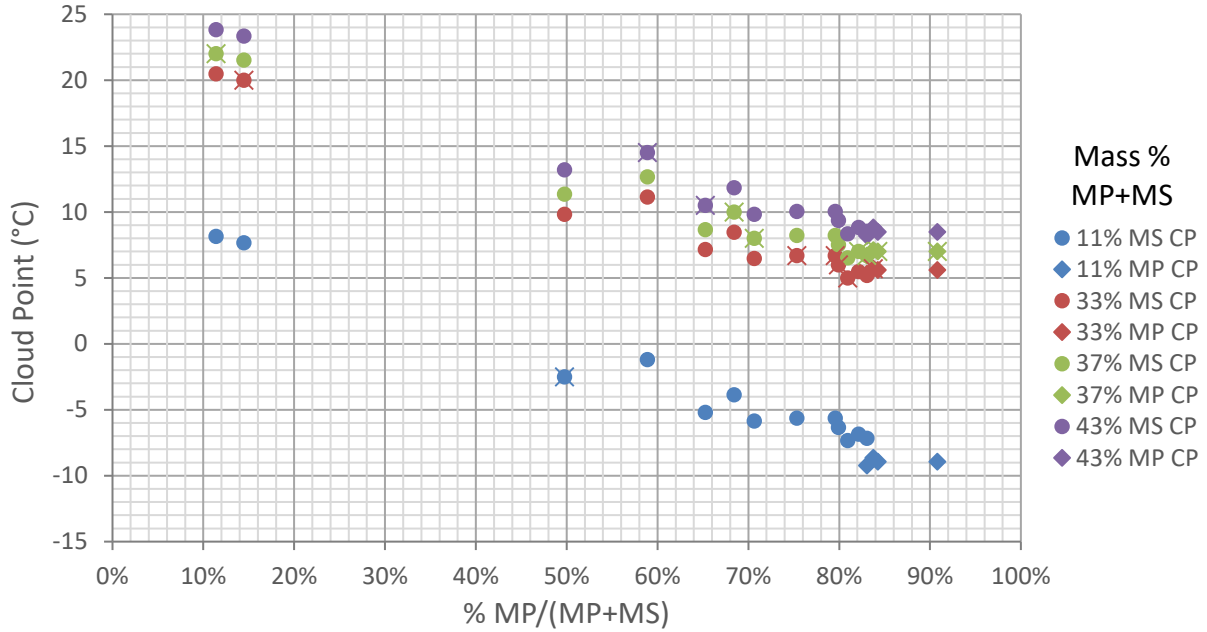


Figure 4.15 - Expanded CPs at various MP+MS fractions with empirical CPs (X's). Diamonds are adjusted using the MP curves and circles are adjusted using the MS curves.

After completing tests that measured the CPs of SME/TME and CME/TME blends I was able to make Figure 4.16 below. Adding all the measured CPs from blending SME and CME, showed similar results for the EEP. The data points at 35% MP+MS give the clearest picture near the eutectic ratio, with an estimated EEP around 80-81% MP/(MP+MS).

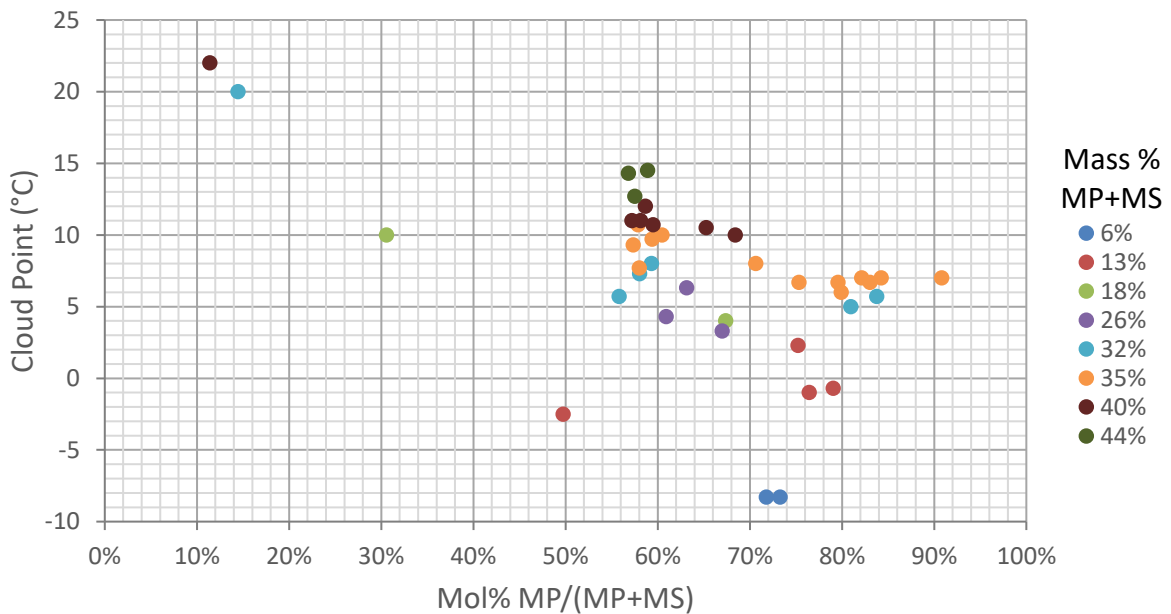


Figure 4.16 - Comparison all empirical CPs (fractionation, and SME and CME blending) of MP/(MP+MS) ratio versus various MP+MS fractions

For Sun West, the most important factor when considering fractionation, was the maximum yield to reach each CP. The chart below (Figure 4.17) directly relates those two. For each percent MP+MS group, the yield decreases from right to left as the CP decreased. At the eutectic point, the yield continues to decrease but the CP actually increases. Therefore, the optimal yield for a specific CP on Figure 4.16, is wherever a line straight above that CP intersects with a eutectic point. For example, the maximum yield with 4:1 carryover for a CP of 7°C, would be around 82% if it was formulated at 82% MP/(MP+MS) with approximately 40% MP+MS. The eutectic yields for 10°C, 2°C, and 0°C would be 90-95%, 60-65% and 55-60% respectively.

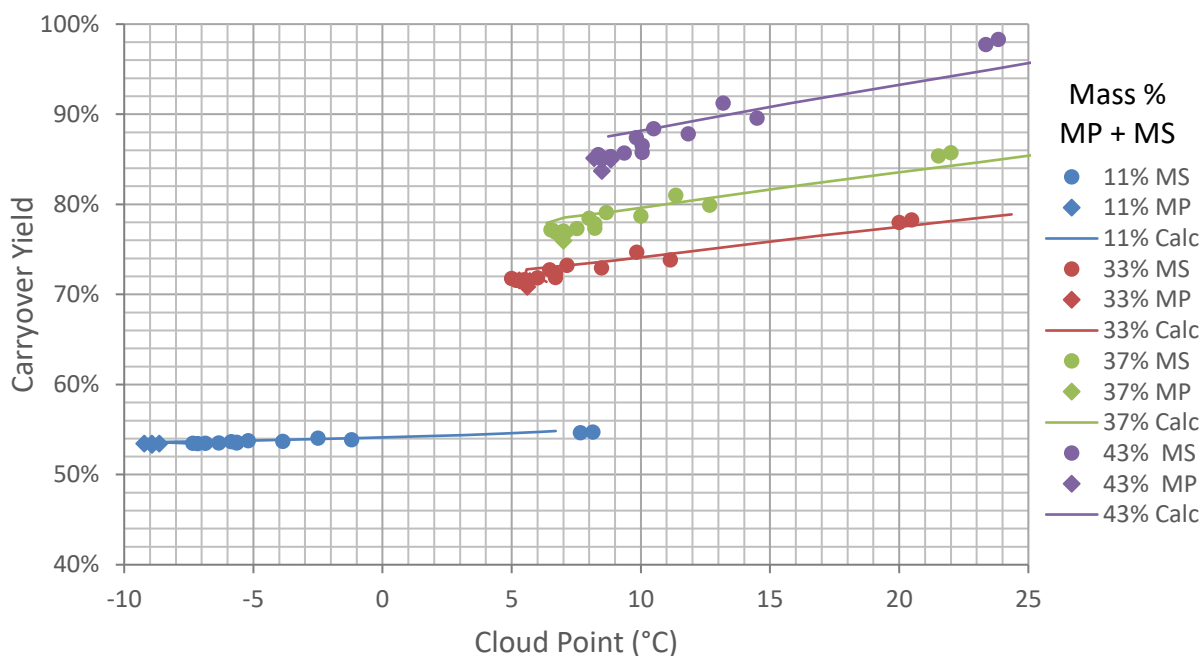


Figure 4.17 – Comparison of expanded CPs versus 4:1 carryover yield (points) with calculated CP/carryover yield curves. Expanded cloud points adjusted with the MP curve are diamonds while those adjusted from the MS curve are circles.

4.5 Comparison of Fractionation Data with Cloud Point Prediction Models

At the beginning of this chapter, a number of thermodynamic models for predicting the CP of a FAME mixture were presented. These models were used to determine what FAME profiles needed to be produced to reach 10°C, 7°C, 2°C and 0°C while maximizing yield. Now with an

abundance of fractionation experimental data, the models can be compared with the empirical CP temperatures to determine the most accurate models for fractionated TME mixtures.

The “Calculated Average CP”, which is the average of the “Dunn”, “Imahara”, “Imahara (Dunn)” and “Ideal” models, seems to do the best overall job of predicting CPs as seen in Figure 4.18, which compares the deviation for each model from each empirical fractionation CP test. While the “Ideal” and “Imahara (Dunn)” methods both decently correlate with the empirical CPs, the “Imahara” model using the Imahara thermodynamic properties did not predict well, and as clearly seen, neither did the Dunn model.

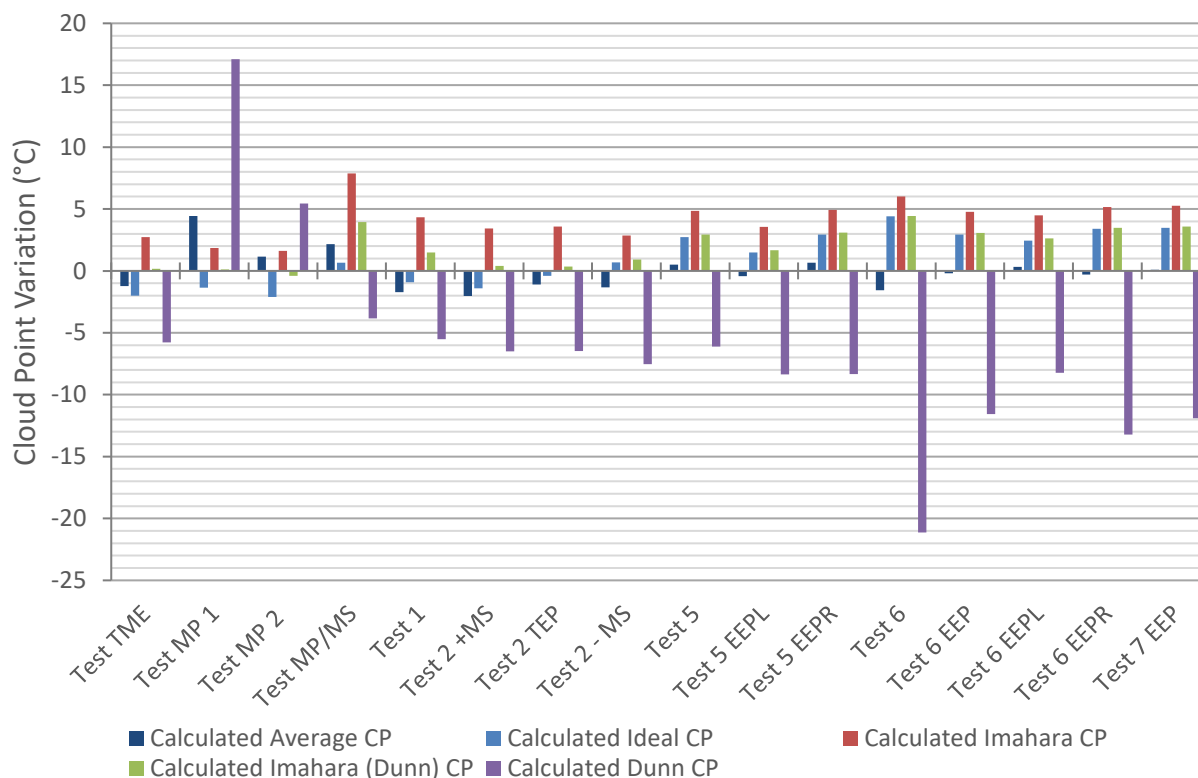


Figure 4.18 - Comparison of the empirical CP for each fractionation test with each CP model

The first few exploratory empirical CPs tests correlated best with the average of the “Dunn” model (with a linearized activity coefficient) and the “Imahara” model so the average of those two CP prediction models was used to determine the FAME profiles that would reach the target CPs.

With additional tests, the “Calculated Average CP”, produced the closest results to the empirical CPs

as seen in Figure 4.19 which compares the average variation of each model to the empirical data. The single model that had the smallest average variation from the empirical CPs was the simple “Ideal” model.

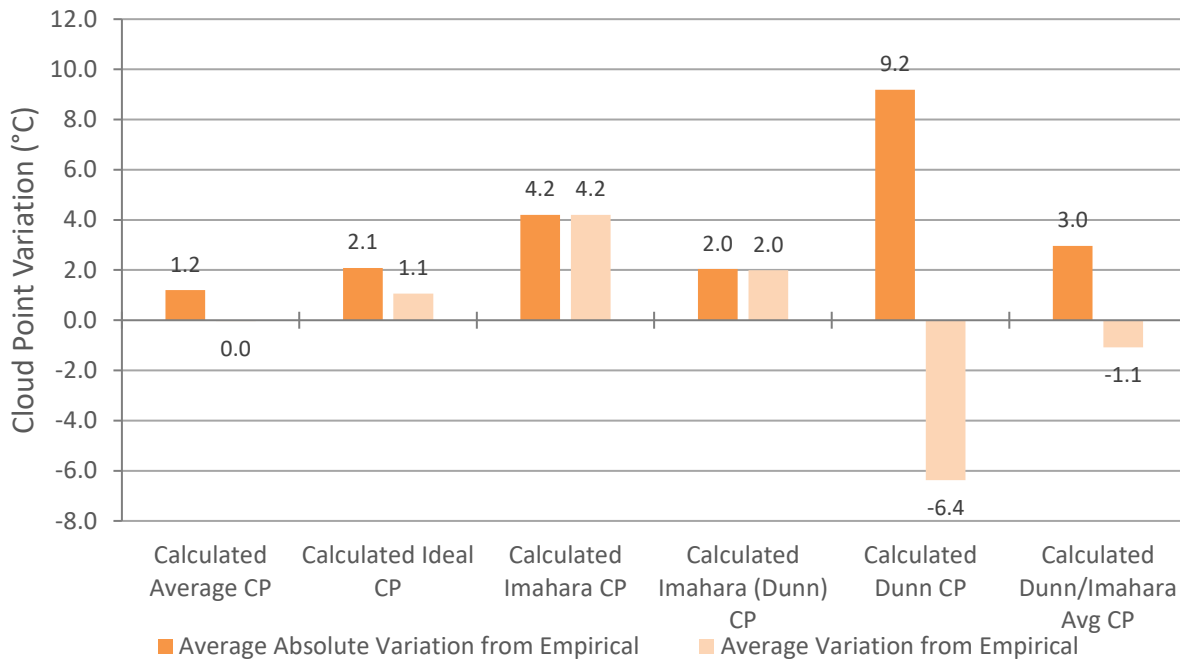


Figure 4.19 – Average variation of FPDT CP models from empirical fractionation test CPs

Figure 4.20 tells a similar story as Figure 4.19, but it displays the maximum variation between the models and the empirical data for all fractionation tests, as opposed to the average. This gives a level of confidence on how far the predicted value could vary from the empirical CP. When comparing the maximum variation, the “Calculated Average CP”, the “Ideal” model and the “Imahara (Dunn)” model all have the same maximum variation of 4.4°C.

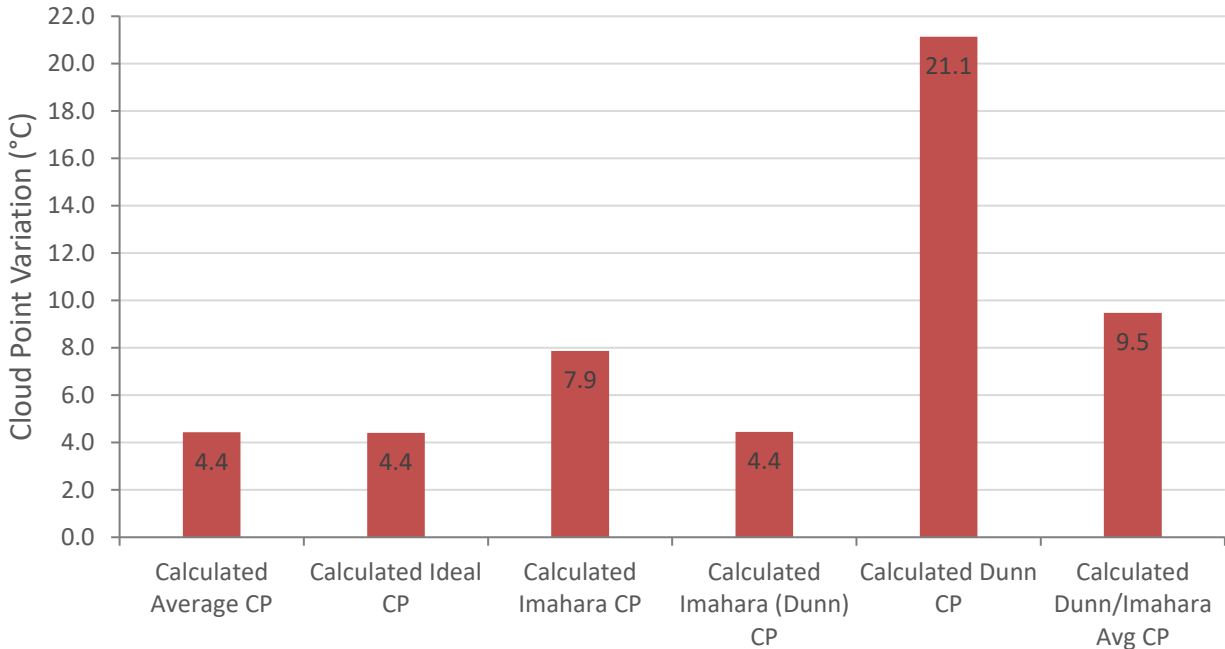


Figure 4.20 – Maximum variation of FPDT CP models from empirical fractionation test CPs

In Figure 4.21, the expanded empirical CP data is overlaid with the “Calculated Average CP” MP and MS curves to give a visual contrast between the calculated and empirical CPs. The correlation is close for the MS curve with 11% MP+MS until it gets close to the EEP, due to the differences between the TEP and the EEP. The other MS curves do well between 40-70% MP/(MP+MS) but also stray near the EEP and at low MP/(MP+MS) ratios. The MP curves are harder to evaluate as many of them are not fully represented due to the “Dunn” model activity coefficient constraints. Only the 11% MP+MS curve is fully represented for MP and it follows the data fairly well with some variance above 90% MP/(MP+MS).

Further charts showing the CP values for each empirical test contrasted with the calculated values from each CP prediction model are presented in Appendix D.

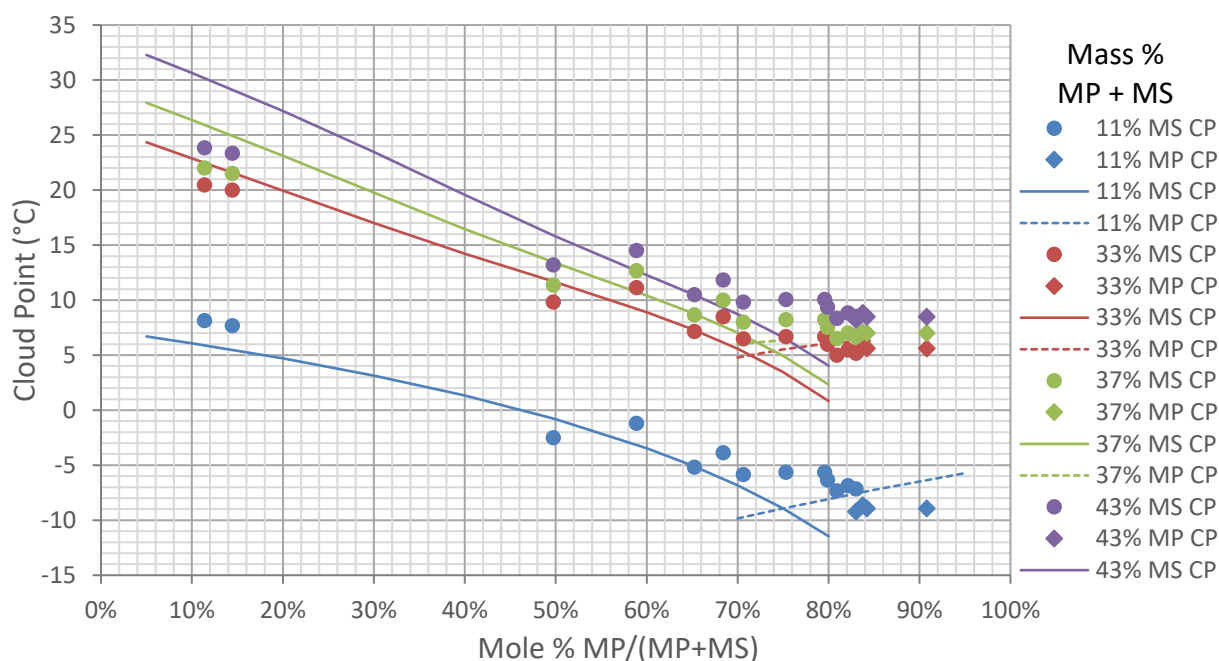


Figure 4.21 – Comparison of calculated CP lines and expanded fractionation CPs. Dashed lines are the MP CP and solid lines are the MS CP. Diamonds are CPs adjusted from the MP curves while circles are CPs adjusted from the MS curves.

4.6 Conclusions

After evaluating the fractionation data there has been quite a lot learned. The major finding is that the eutectic ratio is the key for optimizing CP and yield. Both from the empirical CP data and the expanded CP data, an EEP between 80-84% MP/(MP+MS) is supported. The working assumption of an 82% MP/(MP+MS) EEP would be safe to continue using until more detailed CP data around the EEP is measured. While there is enough information here to make major decisions regarding the economic feasibility of fractionating TME, there are plenty of data points that would need to be filled in to make day to day operating decisions in a tallow biodiesel plant. Testing around the eutectic ratio at varying MP+MS fractions would be the most helpful information since that is where the models are least accurate and it is where fractionation would target.

Chapter 5: Blending with FAMES Cloud Point Reduction

5.1 Introduction

The purpose of fractionation is to reduce the cloud point of TME by reducing the total fraction of MP+MS and to move the MP/(MP+MS) ratio closer to the empirical eutectic point. Another method of achieving a lower CP is by blending TME with other FAME feedstocks that contain high levels of unsaturated FAMES or other FAMES with lower melting points than MP or MS. The melting points for both saturated and unsaturated FAMES were given previously in Figure 1.5. For naturally occurring feedstocks, the most common low melting point FAMES would either be an unsaturated FAME like C18:1 or a shorter chain saturated FAME. Some feedstocks that are high in C18:1 include soybean oil, canola oil, algae oil, corn oil, hemp oil, poultry fat, choice white grease, used cooking oil and yellow grease. Coconut and babassu oil are examples of feedstocks that contain large quantities of shorter chain fatty acids like C12:0 and C14:0 [13].

A second method of reducing CP, could be by blending TME with FAME feedstocks that have MP/(MP+MS) ratios closer to the eutectic point, which for TME is any ratio over 59%. This method does have some effect on CP, especially when the initial MP/(MP+MS) ratio is at the extremes, but in TME it is usually secondary to the effect of reducing the overall mole percent of MP and MS. A few examples of feedstocks that could contribute to moving the FAME profile toward the eutectic ratio are soybean oil, choice white grease, yellow grease, used cooking oil, palm oil, hepar oil and jatropha oil. An exhaustive list of potential feedstock FAME profiles was compiled in the REG Feedstock Report and is included in Appendix I.

For the purposes of this project, the context was to inform a potential biodiesel plant owner and operator what economically feasible ways there were to reduce CP. Because of this, the limitations on blending feedstocks for testing were that they were cost effective and readily

available at large quantities. That left two options, both of which are currently used to make biodiesel – soybean oil and canola oil. Ironically, those are also the two feedstocks tallow that would compete with TME for making biodiesel. Figure 5.1 shows the FAME profiles for TME, SME and CME. SME (CP=2.3°C) and CME (-8.3°C) are both very high in unsaturated C18:1 and C18:2 which is why they have low CPs compared to TME (14.5°C). Additionally, SME has over twice as much MP as it does MS with a MP/(MP+MS) ratio of 75%, meaning it will also contribute to moving the FAME profile closer to the EEP. However, the main mechanism for reducing CP by blending TME with SME and CME seems to be the reduction in the mole fraction of MP and MS in the final FAME profile.

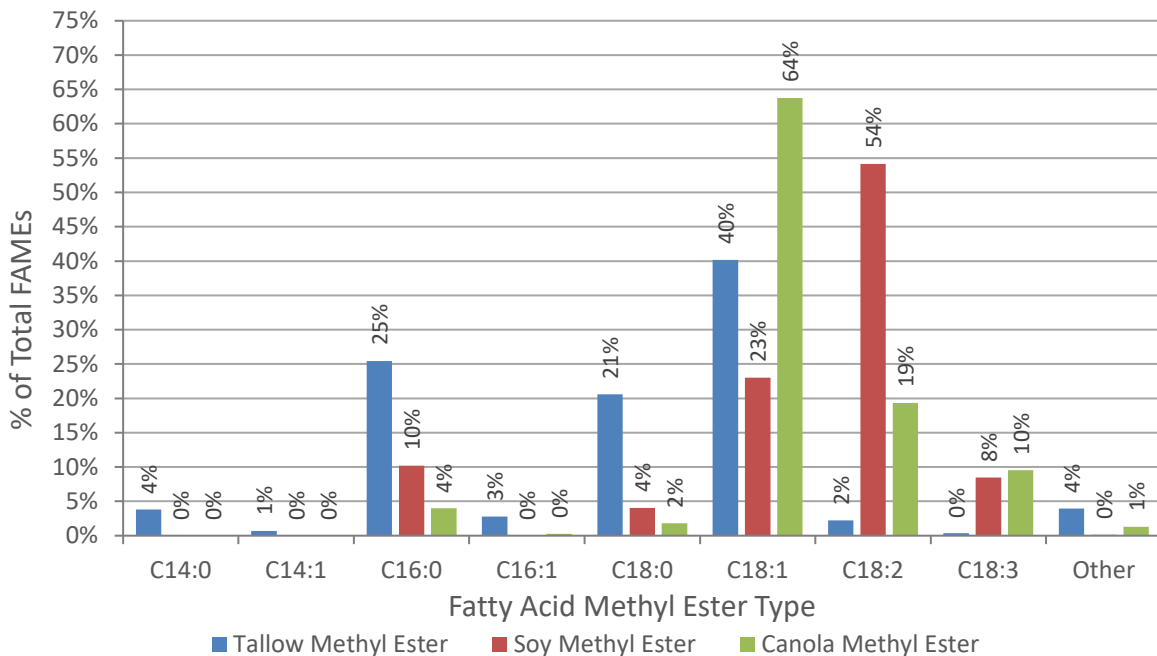


Figure 5.1 – Comparison of tallow, canola and soy biodiesel FAME profiles

Tallow does have a cost advantage of soybean oil or canola oil, but that margin is reduced when blending with a “competing” feedstock. At that point, it is a simple feedstock commodity price vs CP reduction decision. The purpose of this next section is to characterize how blending TME with SME and CME affects CP to aid in future decisions based on real-time commodity prices.

5.2 Soy Methyl Ester Blending

Soy is a readily available feedstock in the U.S. with a CP of 2.3°C due to its high quantities of C18:2 and C18:1. It also has a MP/(MP+MS) ratio of 75%, which is to the left of the EEP, but is closer than the 59% ratio of TME. For these blending tests, SME was mixed with TME from 0-100% at 20% intervals, with an additional test at 30% SME. The CP, CFPP and FAME profiles for each SME/TME blending tests are listed in Table F.1, in Appendix F.

Figure 5.2 shows that the CP is close to a linear function when blending SME in TME. The trend line correlates well with the empirical CPs with a R² value of 0.99. CFPP is always less than the CP for these SME/TME blends but drops off significantly around 60% SME. The CFPP line correlated nicely to a quadratic equation with an R² value of 1.00.

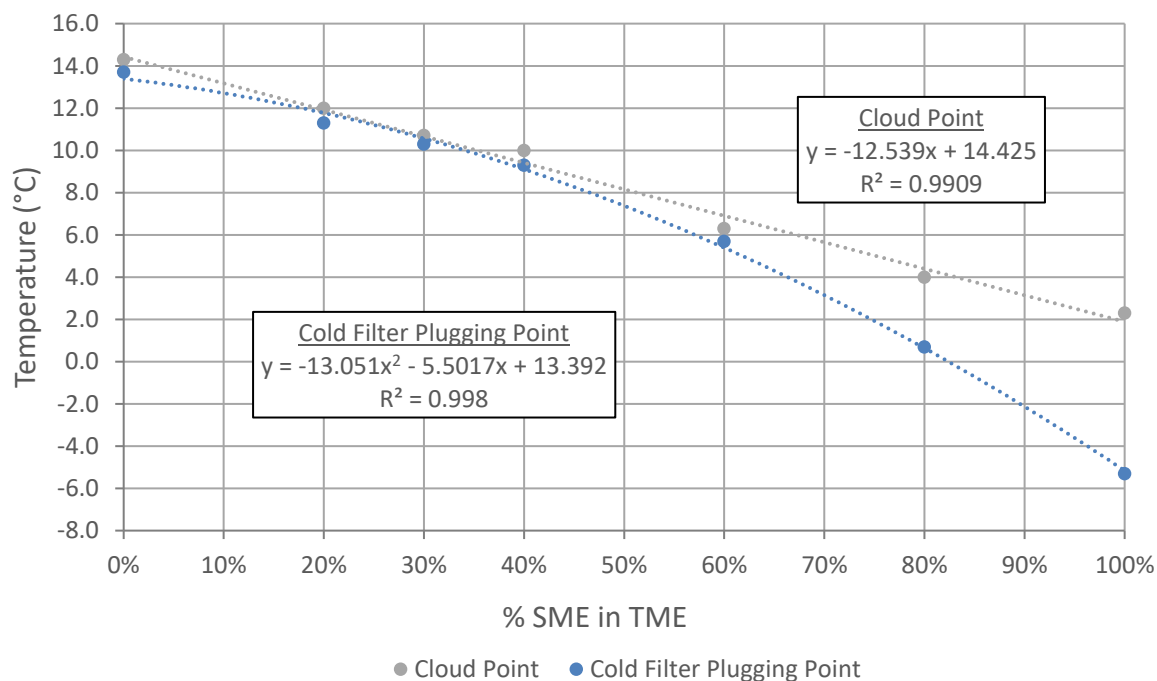


Figure 5.2 - CPs and CFPPs for SME blends in TME with best fit equations

Plotting the CP of the SME blends on a MP/(MP+MS) axis in Figure 5.3 shows that the MP/(MP+MS) ratio seems to move down an exponential curve as it moves closer to the EEP. At low

level blends the ratio changes slowly while at higher level blends the ratio changes much more quickly. Additional graphs showing CFPP results for SME/TME blends are included in Appendix G.

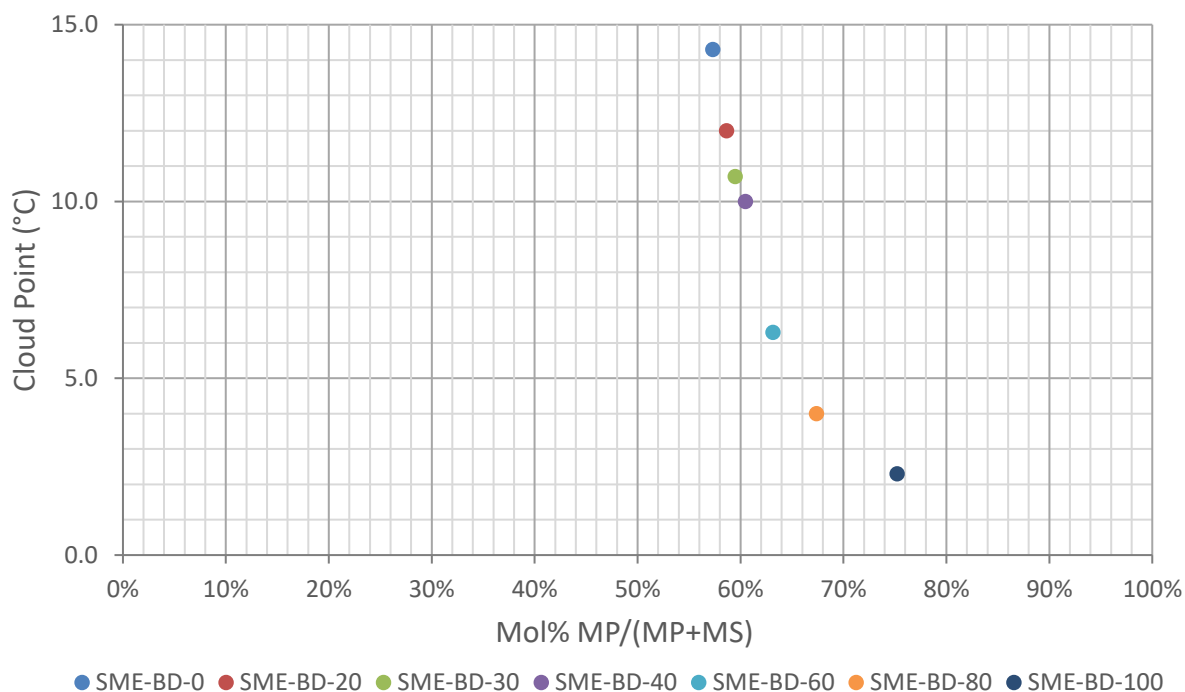


Figure 5.3 – CP variation along MP/(MP+MS) ratio for SME blended in TME

Blending SME in TME does successfully reduce the CP from 100% TME as expected. The economic viability of this method can only be determined with current commodity prices. Outside of the cold temperature properties, modifying the FAME profile also affects other fuel properties. While adding more unsaturated FAMES from SME does reduce the CP of a TME blend, the consequence is that it is detrimental to the oxidative stability. Further tests would need to be conducted to verify that the final FAME mixture meets all ASTM biodiesel standards.

5.3 Canola Methyl Ester Blending

Canola is another biodiesel feedstock grown in North America that is most common in Canada. The cost of canola, like soy, is dependent on the commodities market so there is not an

easy cost comparison between the two. However, this empirical CP data for blending CME in TME can be used for future economic evaluations based on real time commodity prices.

Two sets of canola blending tests were conducted. The first set was from the initial batch of CME called CAN-BD-A with tests from 0-100% at 20% blending intervals and an additional test at 30% CME. The second set was with another batch of CME labeled CAN-BD-B. The CME/TME blends were retested at 10% intervals up to 60% CME/TME, then at 20% intervals thereafter. The CPs, CFPPs, and FAME profiles for both sets of CME/TME blends are in Table F.2 and Table F.3 in Appendix F. Additional CME CFPP charts can be found in Appendix G.

The CP and CFPP data points are plotted below in Figure 5.4 below, with best fit equations relating CME/TME blend with the CP temperature. CME interacts with TME a little differently than SME. The CP best fit line is a quadratic equation, not a linear equation like with SME/TME blending. Because of that, the largest CP changes occur above a 50% CME blend. The CFPP also follows a quadratic line but at 0.5-1.0°C less than the CP. The R² for the CP line is 0.99 and 0.99 for the CFPP.

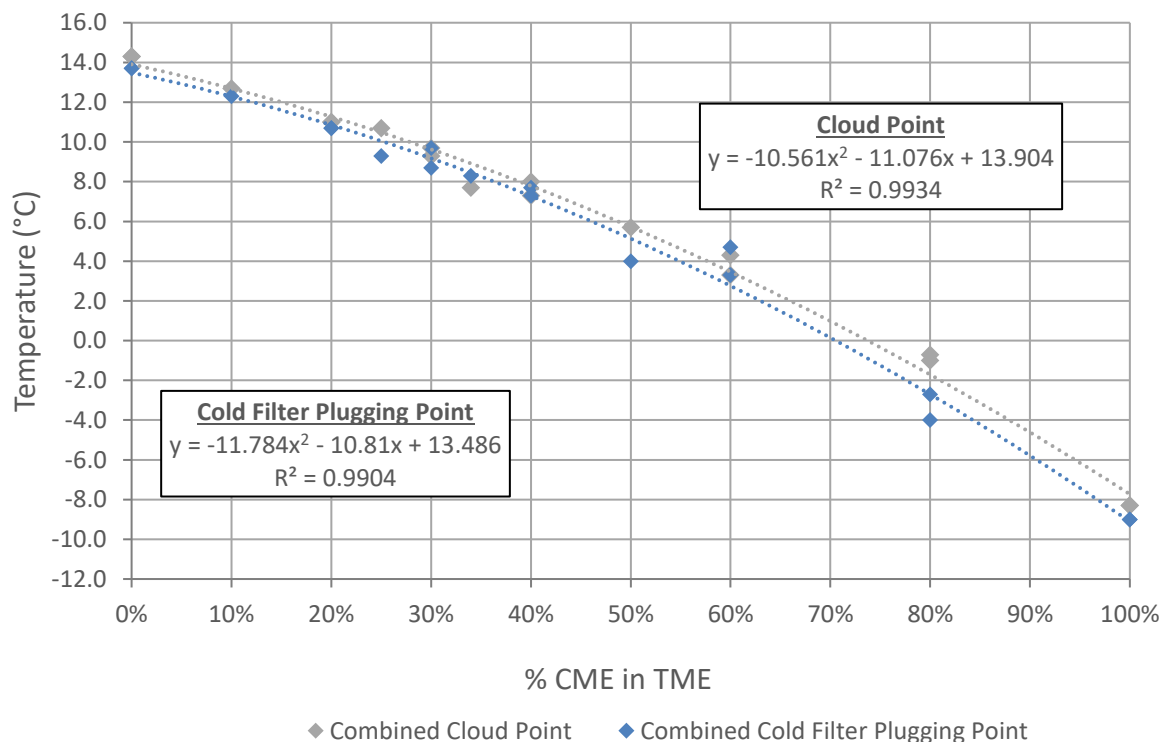


Figure 5.4 - CPs and CFPPs for CME blends in TME with best fit equations

This difference between the SME/TME and CME/TME blend CP curves (Figure 5.5) could be explained by considering the freezing point depression theory CP models. The CP for each individual FAME varies with the natural logarithm of that specie's mole fraction in the FAME mixture (Equation 4.1). Since CME has a higher unsaturated FAME content than SME, this quadratic-appearing effect could potentially be due to the drop-off on the logarithmic curve at lower mole fractions of MP and MS.

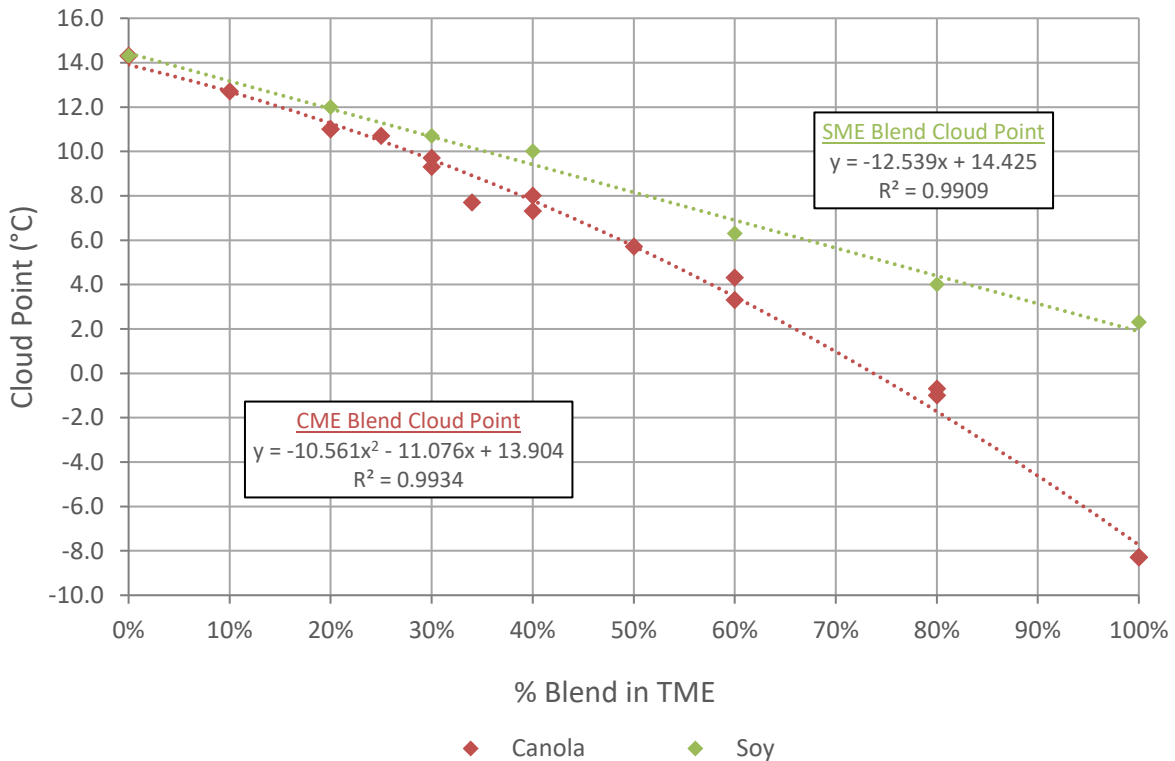


Figure 5.5 – Comparison of SME/TME and CME/TME blend CPs

A comparison of SME and CME blending in TME, in Figure 5.5, shows that 0-40% blends of CME make less than 2°C CP difference than the same SME blend. Beyond a 40% blend, CME blending depressed the CP significantly more than SME, up to 5-10°C. It is safe to say that when canola oil prices are less than, or on par with soybean oil, canola is the more economical option. If soybean oil is less expensive than canola oil, a more in-depth comparison must be done.

Figure 5.6 below plots the CME/TME blends on the MP/(MP+MS) axis versus CP, as was done with SME/TME blends. The MP/(MP+MS) ratio does not change significantly until 60% MP/(MP+MS) then it jumps up quickly before stabilizing again. This relates to the CP which decreases significantly around 60% MP/(MP+MS) in Figure 5.4.

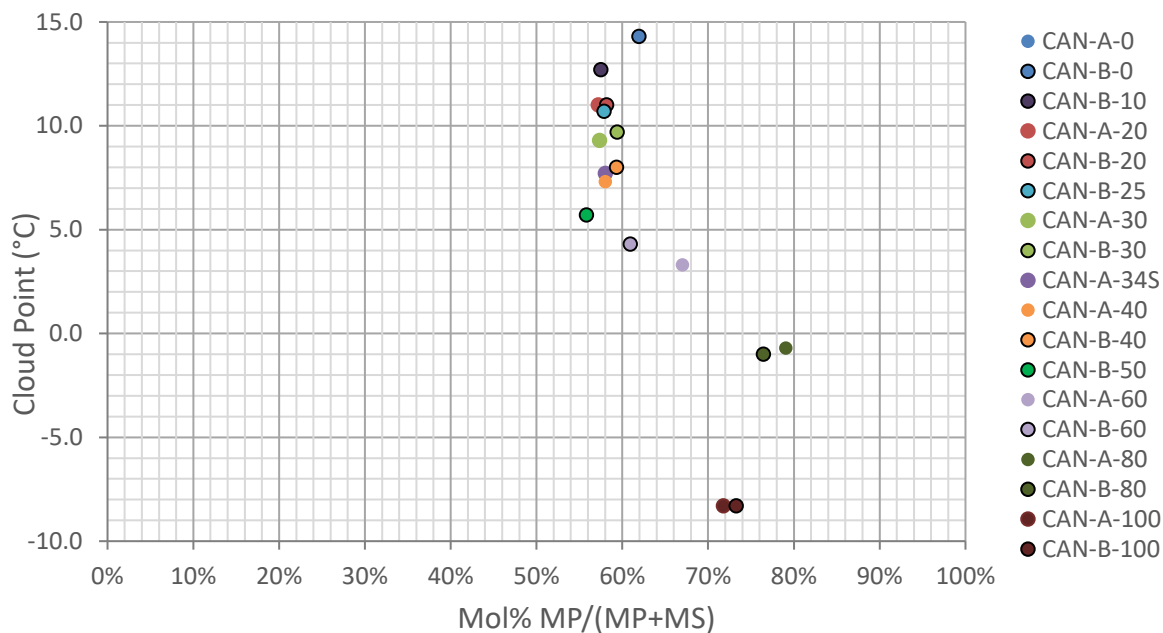


Figure 5.6 - CP variation along MP/(MP+MS) ratio for CME blended in TME

5.4 Comparison of Blending Data with Cloud Point Prediction Models

At the beginning of Chapter 4 on fractionation, a number of thermodynamic models for predicting the CP of a FAME mixture were presented. These models were used to determine what FAME profiles needed to be produced to reach 10°C, 7°C, 2°C, and 0°C at the EEP. Additionally, the CP prediction models were also used to estimate the CPs for each SME/TME and CME/TME blending test.

Analyses of the CP prediction models were conducted comparing the empirical CPs from SME and CME blends in TME. The variations between each model and the empirical CP for each

tested SME/TME blend is delineated below in Figure 5.7. Just like fractionation, most of the models correlated decently to the empirical data but the “Dunn” model is significantly off while the “Imahara” model is not very close.

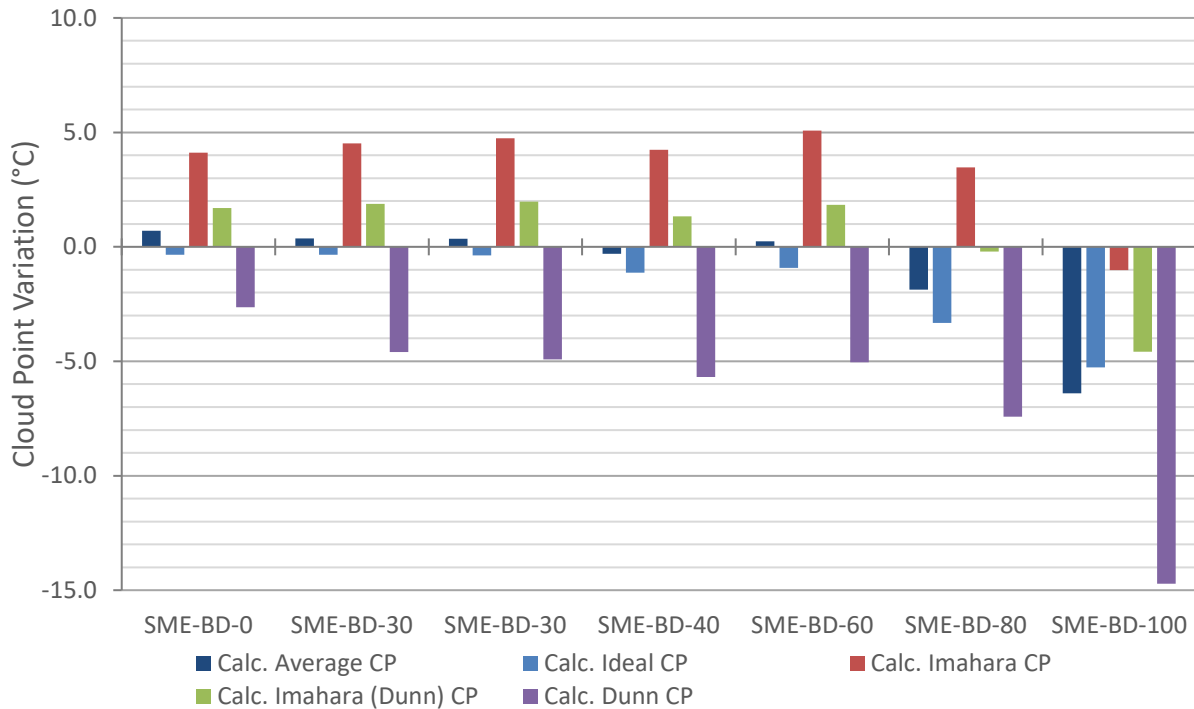


Figure 5.7 – Variation between empirical CPs and CP models for each SME/TME blend

Figure 5.8 also shows similar trends to fractionation with the smallest average absolute variation of 1.5°C held by the “Calculated Average CP”, a 1.7°C variation for the “Ideal” model and 1.9°C variation for the “Imahara (Dunn)” model.

The maximum variation for each model is contrasted in Figure 5.9, and the SME blending tests has different variation results than fractionation. The “Calculated Average CP” actually has the largest maximum variation outside of the “Dunn” model. The “Imahara (Dunn)” model has the smallest maximum variation of 4.6°C.

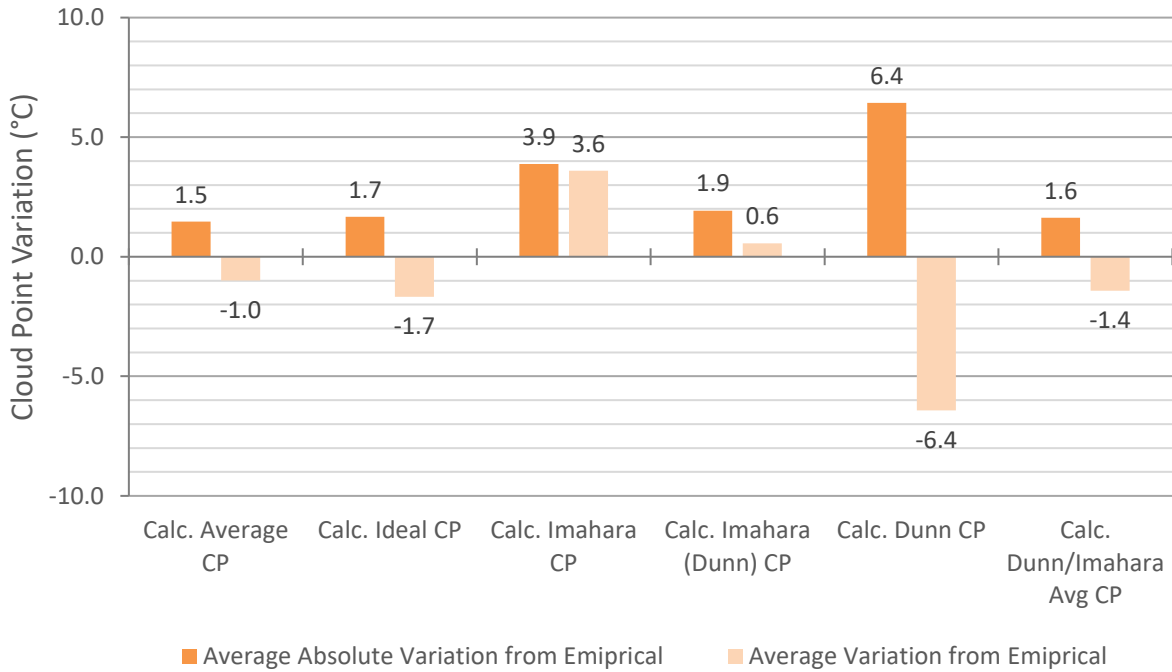


Figure 5.8 – Average variation for all SME/TME blend tests for each CP prediction model

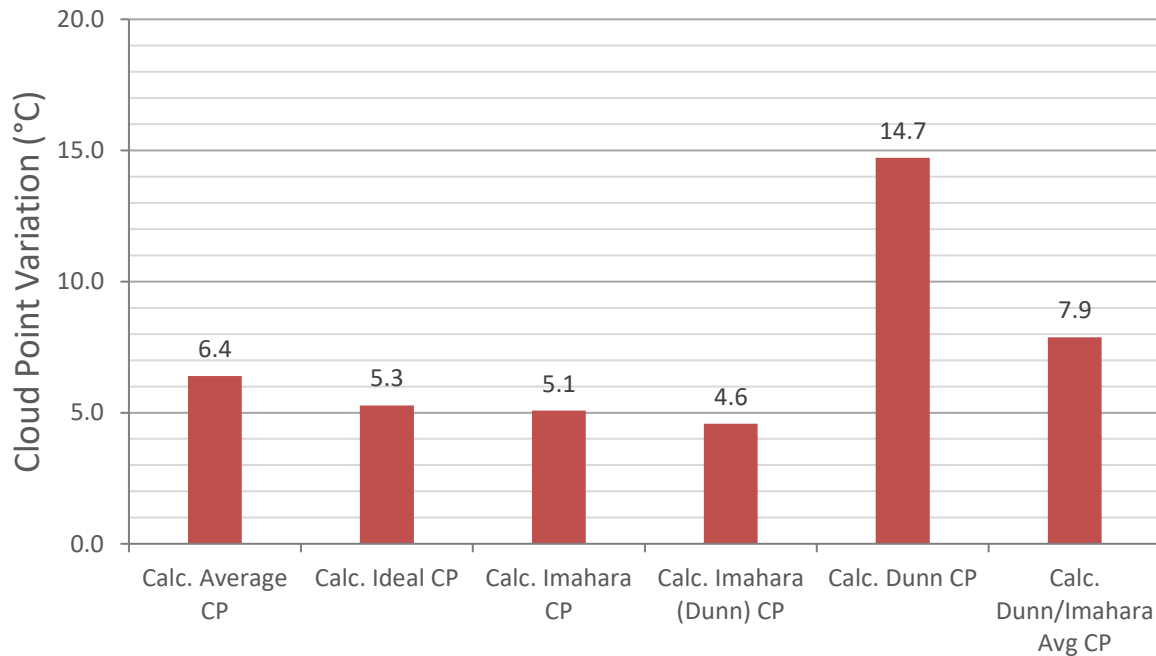


Figure 5.9 – Maximum variation for each CP prediction model for all SME/TME blend tests

Figure 5.10 and Figure 5.11 chart the variation between each model’s calculated CP and the empirical CPs for each CME/TME blend tested for CAN-BD-A and CAN-BD-B, respectively. Once again, the “Dunn” model is a clear outlier.

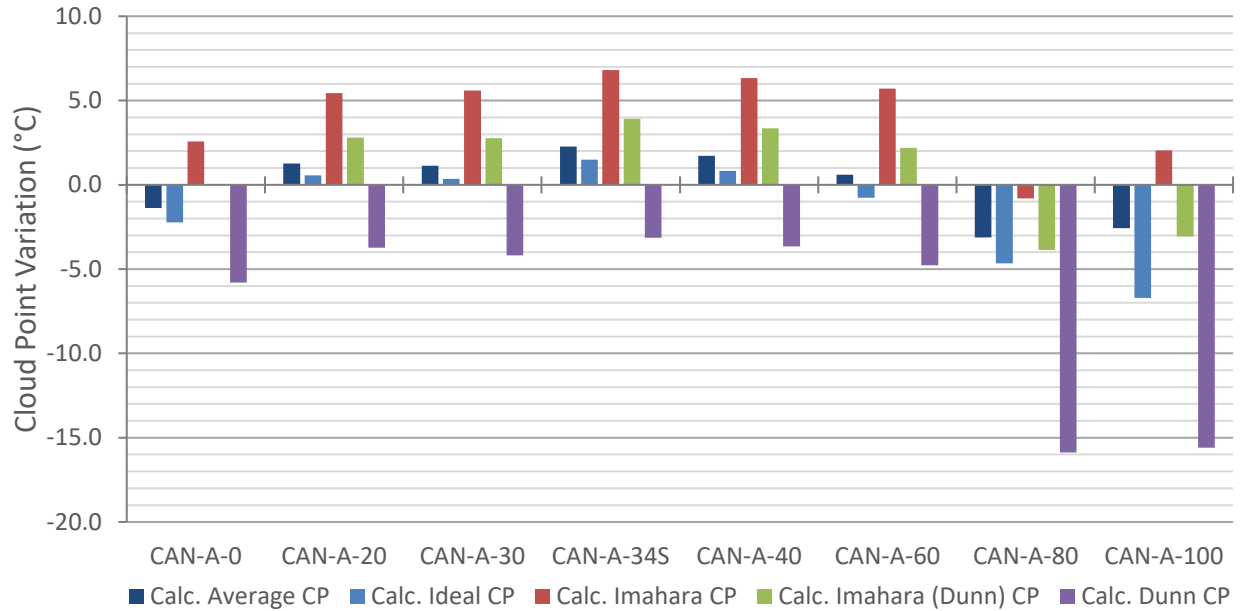


Figure 5.10 – Variation between empirical CPs and CP models for CAN-BD-A/TME blends

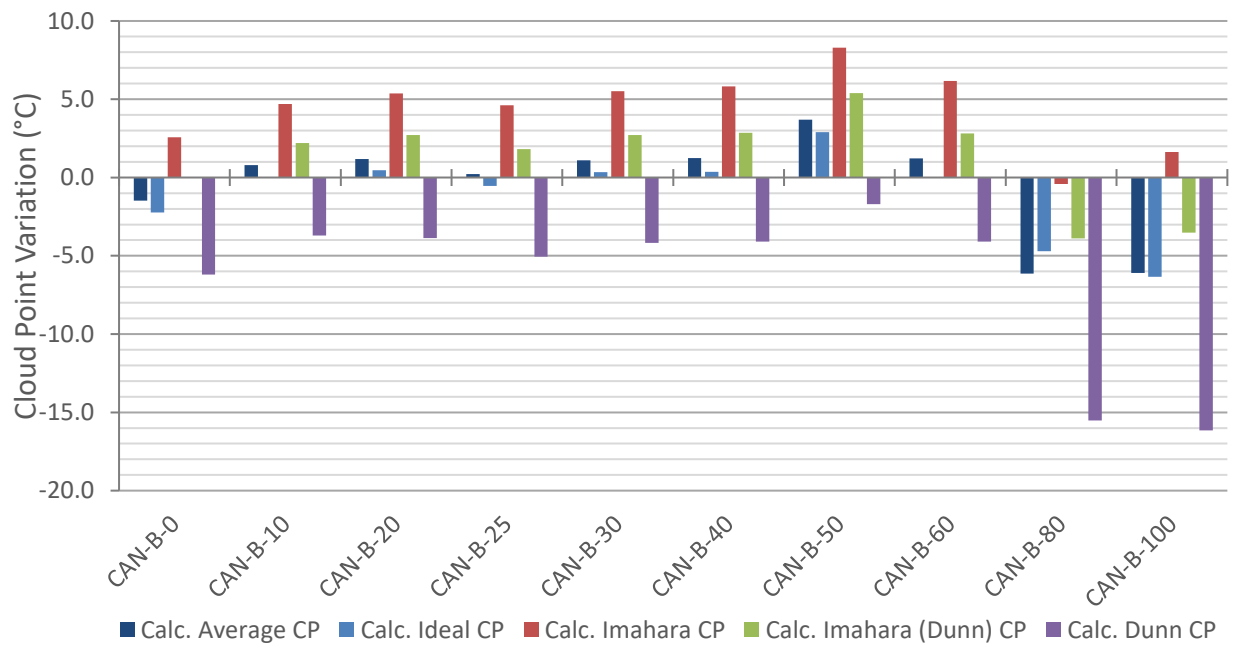


Figure 5.11 – Variation between empirical CPs and CP models for CAN-BD-B/TME blends

The previous two figures are simplified into the average variation of all CME/TME blend tests charted below in Figure 5.12. Unlike fractionation and the SME blending graphs, the smallest average variation of 2.0°C belongs to the “Ideal” model with the “Calculated Average CP” only slightly behind with 2.1°C. “Imahara (Dunn)” is not far behind with 2.8°C average variation from the empirical CPs.

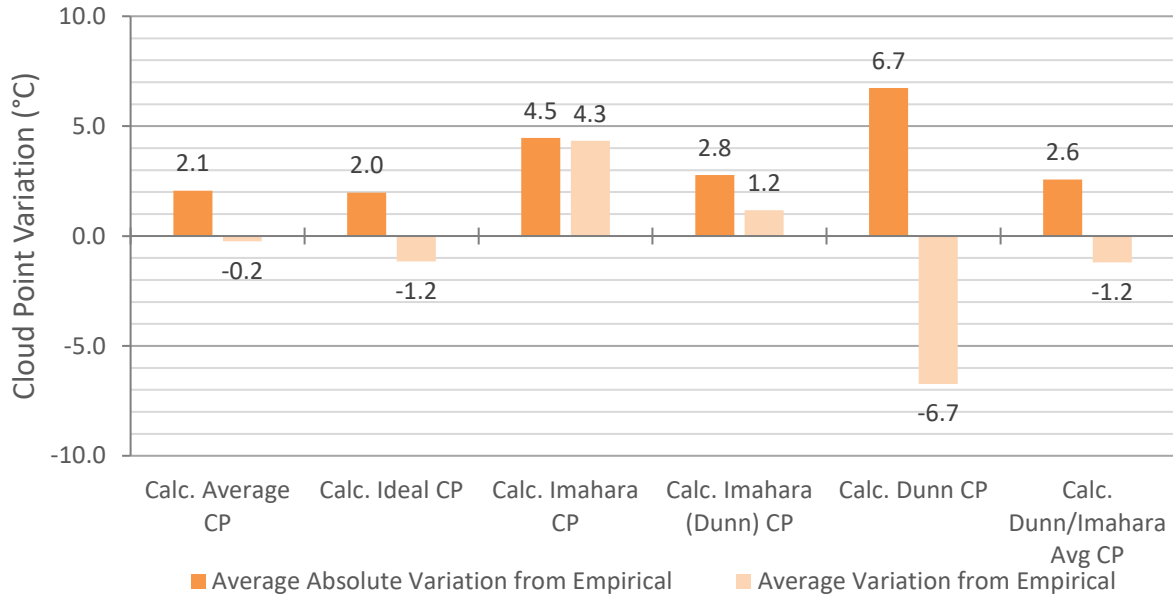


Figure 5.12 – Average variation for all CME/TME blend tests for each CP prediction model

Finally, like fractionation and SME blending, the maximum variation is also displayed for CME/TME blends to give a rough confidence level. Figure 5.13 shows that CME blending had similar results as SME blending with “Imahara (Dunn)” having the smallest maximum variation of 5.4°F. Dissimilar to SME blending, the “Calculated Average CP” had the next smallest variation of 6.1°C. Once again Dunn outsurpassed all other models with a maximum variation of 16.2°C.

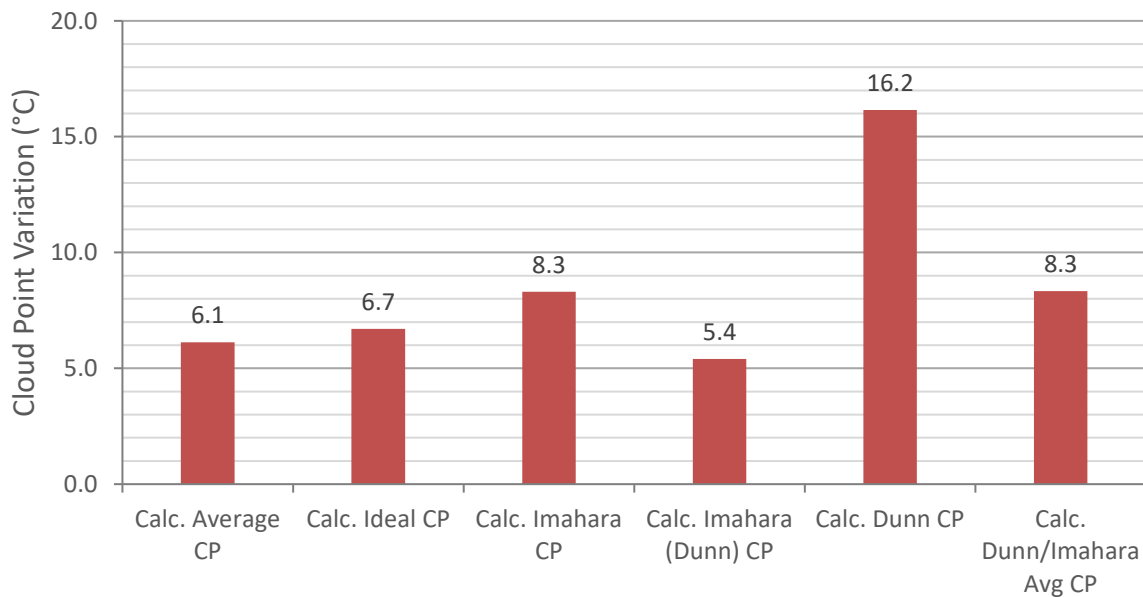


Figure 5.13 – Maximum variation for each CP prediction model for all CME/TME blend tests

In Section 4.5, Figure 4.21 showed a noticeable difference in the theoretical eutectic point (TEP) predicted by the “Calculated Average CP” and the empirical eutectic point (EEP) from the empirical data as well the calculated and empirical CP data at low MP/(MP+MS) ratios. Figure 5.14 validates what can be presumed from Figure 4.21, by plotting the variance along the MP/(MP+MS) axis between the “Calculated Average CP” and the empirical CP for each test. The largest variations between the modeled and empirical CPs occurs at low percentages of MP/(MP+MS). Also, between 60-85% MP/(MP+MS) the variation changes from positive to negative and back to positive due to the differences between the TEP and the EEP.

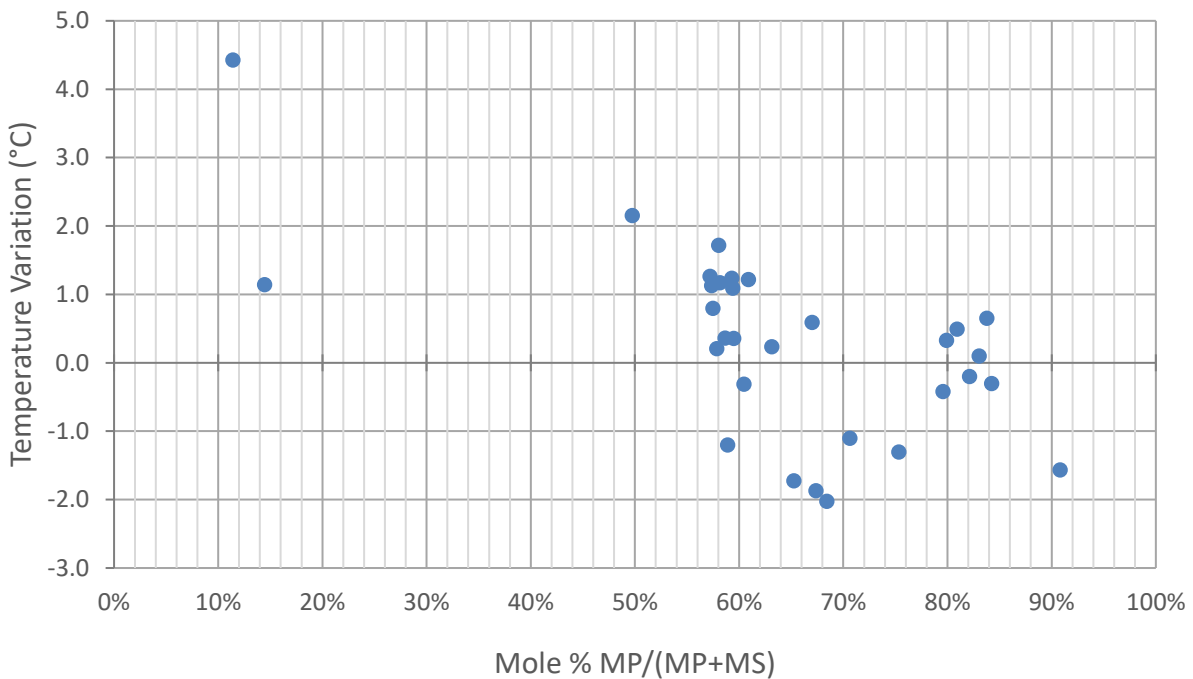


Figure 5.14 -Variation between “Average Calculated CP” and empirical CP for all tests at MP/(MP+MS) fractions

Overall the thermodynamic CP models did a decent job of predicting the CP of fractionated FAME mixtures. The best individual model to use on average would be the Hildebrand “Ideal” model but even better accuracy is achieved by averaging across all four models using the “Calculated Average CP”. However, to achieve the smallest maximum variation, the “Imahara (Dunn)” model is better than them both. The “Dunn” model grossly underperformed all the other

models with the largest average and maximum variations for fractionation, SME blending and CME blending. Significant improvement to the Dunn model could be made by determining the activity coefficients for MP and MS at higher mole fractions. In order to better trust any modeled CP results between 65-85% MP/(MP+MS), empirical validation may be needed because of the variation between the TEP of the models and the EEP.

Additional charts contrasting the empirical CP for each of the SME and CME blends, with each of the CP prediction models, are given in Appendix G.

5.5 Conclusion

Blending both SME and CME in TME is effective at reducing the initial TME CP. Since soybean oil and canola oil are the two competing feedstocks with tallow, the determination of whether to use this method is an economic one. Equations showing the relationship between SME/TME and CME/TME blends with CP are given in Figure 5.5 and can be used to make that economic evaluation. Additionally, this information could be used by a SME or CME producer that would like to reduce costs by blending in TME when initial SME or CME CP is lower than necessary.

Chapter 6: Additive Cloud Point Reduction

6.1 Introduction

A third way of reducing the CP of TME does not modify the FAME profile like fractionation and blending. Polymer additives have been developed to depress the CP and CFPP of methyl esters by modifying the crystal structure size or by delaying the onset of crystallization. Polymer additives are generally known to reduce the CP effectively for a certain number of degrees, and then quickly reach a point of diminishing return. Oftentimes, the polymers are paired with a surfactant that changes the crystal size and decouples CFPP from CP, allowing even lower CFPPs if that is desired [35], [53], [53].

Additives designed to reduce the CP of TME were not very common. The majority of additives designed for biodiesel were for either SME or CME since they are the most common biodiesel feedstocks. Many other additives were designed to improve cold temperature properties of petroleum diesel. From a long list of potential options, we narrowed it down to the eleven additives in Table 6.1 that were either readily available or designed to reduce CP in TME.

Table 6.1 – Tested additives designed to improve various cold temperature properties

Manufacturer	Product	Intended Use	Max Dosage (wt %)
Evonik	Viscoplex 10-530	TME: CP SME: CP, CFPP and PP	1.00%
CorsiTech	4006	Petroleum Oil: PP	0.05%
CorsiTech	4027	Petroleum Oil: PP	0.05%
CorsiTech	4028	Petroleum Oil: PP	0.05%
CorsiTech	6144	Petroleum Oil: PP	0.01%
Infineum	R408	CME: CFPP	0.40%
Infineum	R440	CP	0.10%
Infineum	R511	CP	0.10%
Infineum	R518	SME: PP, CFPP	0.50%
Infineum	R536	FAME: CSFT	0.20%
MLA	-	TME: CP	2.00%

6.2 Evonik Viscoplex 10-530

The Viscoplex 10-530 additive made by Evonik was the first additive that was investigated because it was the only additive initially, that was advertised to influence TME CP. According to Evonik's literature, Viscoplex 10-530 works by "modifying the growth of the crystallizing particles. As crystals form, Cold Flow Improvers act as nucleators and co-crystallize with the saturated hydrocarbon chains, and hence modify the crystal size and shapes typically from plate to needle-like" [53].

Since Viscoplex 10-530 was designed specifically to reduce the CP of TME, testing was very detailed with additive dosages of 0.33%, 0.66% and 1%, repeated at CME/TME blends of 10%, 20%, 25% 30%, 40%, and 50%.

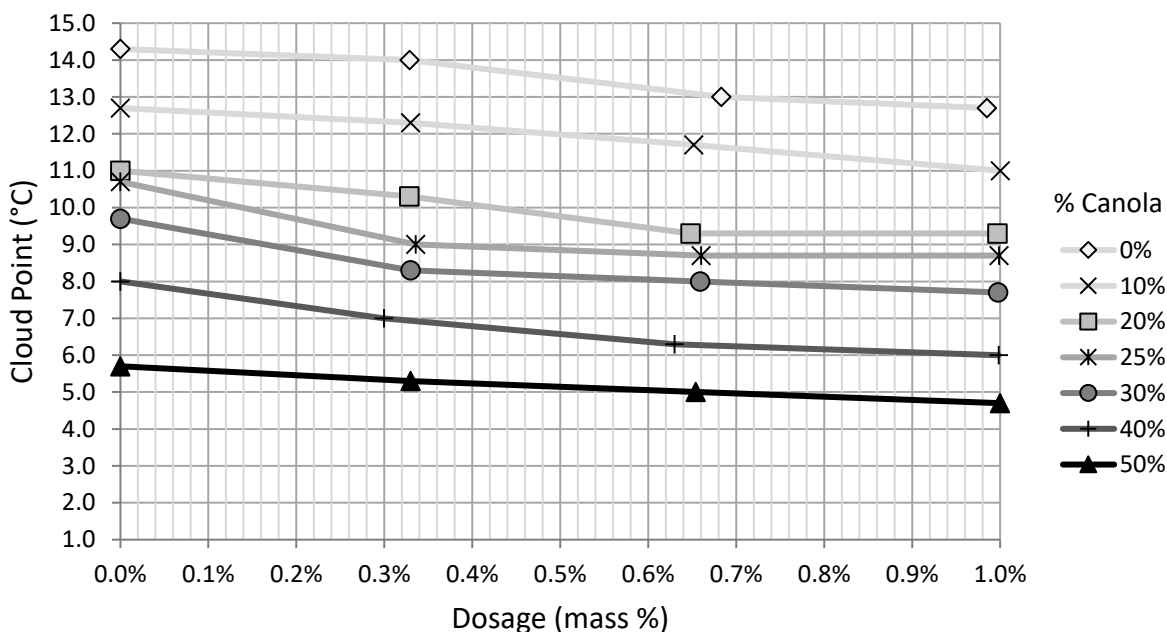


Figure 6.1 – Effect of Evonik's Viscoplex 10-530 dosage on CME/TME blend CPs

The Viscoplex 10-530 additive makes the biggest changes in CP in Figure 6.1 from 0.00% to 0.33% dosage in 25% and 30% CME/TME blends and from 0.33% to 0.66% dosage in the 20% CME/TME blend. The effect of Viscoplex 10-530 on CFPP is shown in Figure 6.2 with the largest change occurring between a 0.00% to 0.33% additive dosage in 40% CME.

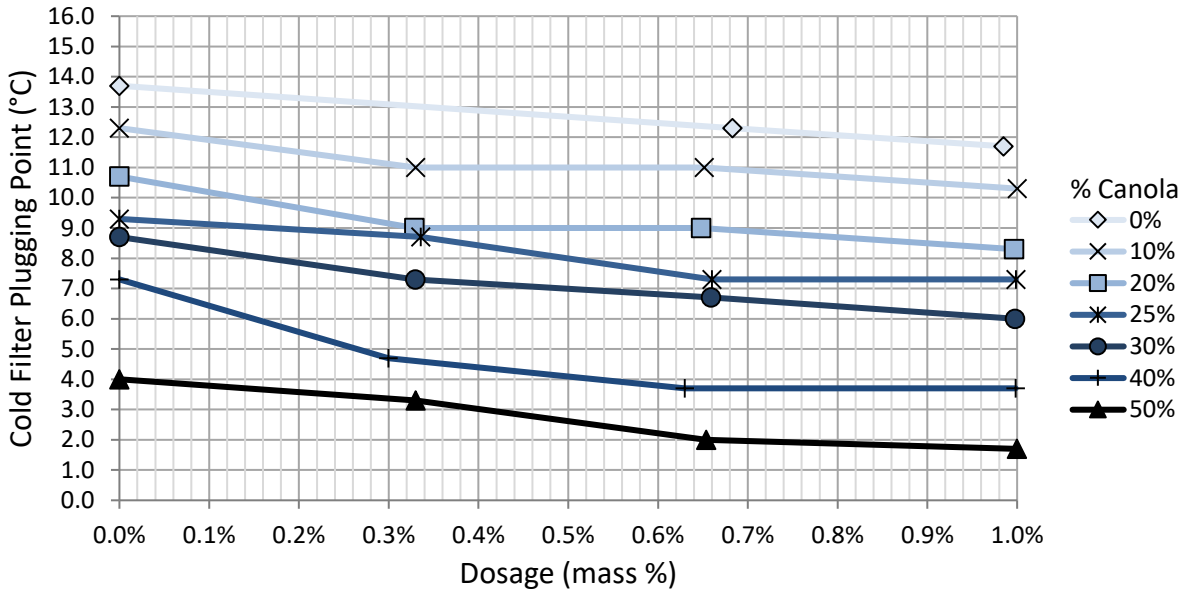


Figure 6.2 – Effect of Evonik’s Viscoplex 10-530 dosage on CME/TME blend CFPPs

To better visualize where the most effective CP and CFPP reduction is taking place, the next two charts show the reduction in CP and CFPP compared to a 0% dosage for each CME/TME blend. Figure 6.3 shows that the most effective CP reductions take place between 20-40% CME blends and at 1-3% dosages with up to 2.0°C drops. The following chart, Figure 6.4, is the corollary for CFPP. In this case, the 40% CME blend has the largest CFPP reduction at 1-3% dosages with up to 3.6°C drops.

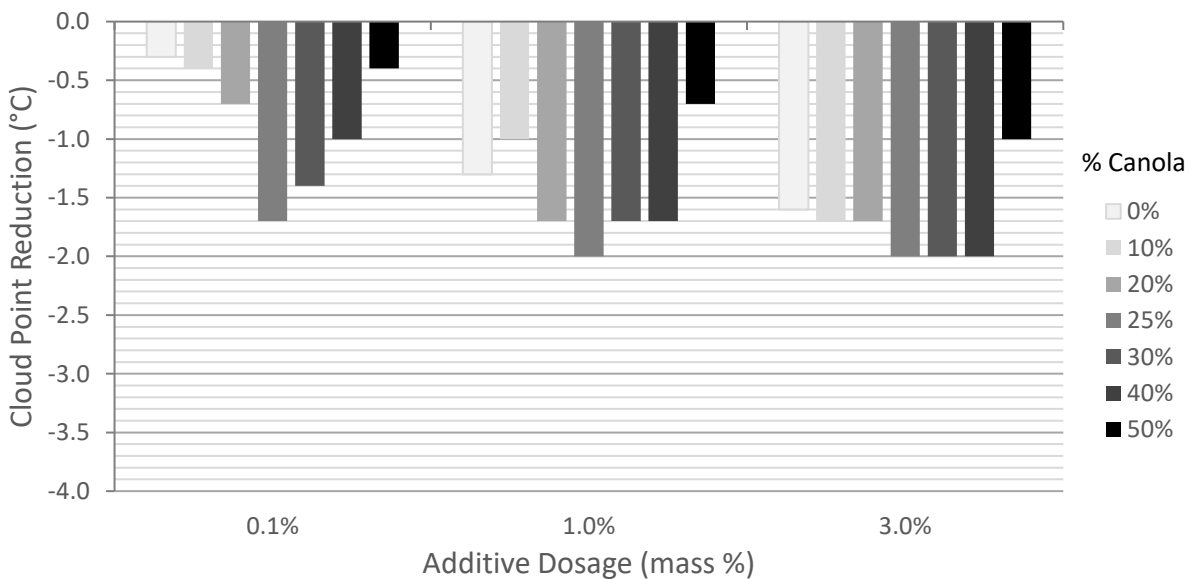


Figure 6.3 – CP reduction by Viscoplex 10-530 from 0% dosage for various CME blends

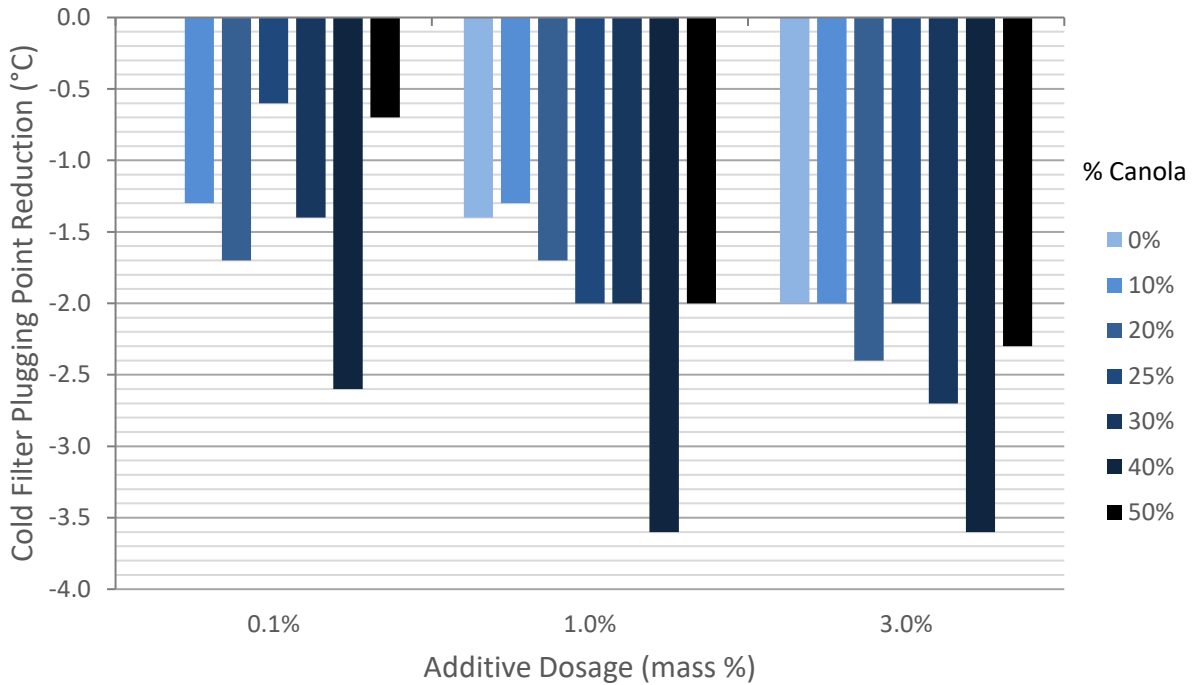


Figure 6.4 – CFPP reduction by Viscoplex 10-530 from 0% dosage for various CME blends

Because CME blending and additive dosage were two variables that both affected CP, the results were examined for synergistic effects between the two. To do this, the reductions in CP at each dosage of Viscoplex 10-530 were first calculated at 100% TME. This accounted for the CP reductions of the additive alone. Then the CP reductions at each CME/TME blend were calculated comparing the CP of each additive dosage to the 0% additive CP at that CME/TME blend. Finally, the additive CP reductions at 10%, 20%, 25%, 30%, 40% and 50% CME/TME blends were subtracted from the additive CP reductions in TME to determine any additional synergistic CP reduction. What these calculations found was that the CP reduction of the additive in TME and the additive in a CME/TME blend is not just the simple addition of the two but the effect of the additive is actually amplified when mixed in a CME/TME blend. This can be visualized in Figure 6.5 below which shows the synergistic CP reduction effect of additive dosages with CME blends. From this chart it is clear that the largest benefit occurred at 25-30% CME blends especially with a 0.1% dosage of Viscoplex 10-530 and produced up to an additional 1.4°C CP drop when paired together.

A detrimental effect occurred at the 50% CME blend, which actually negated some of the additive's CP reduction by 0.6°C at 1% and 3% dosages.

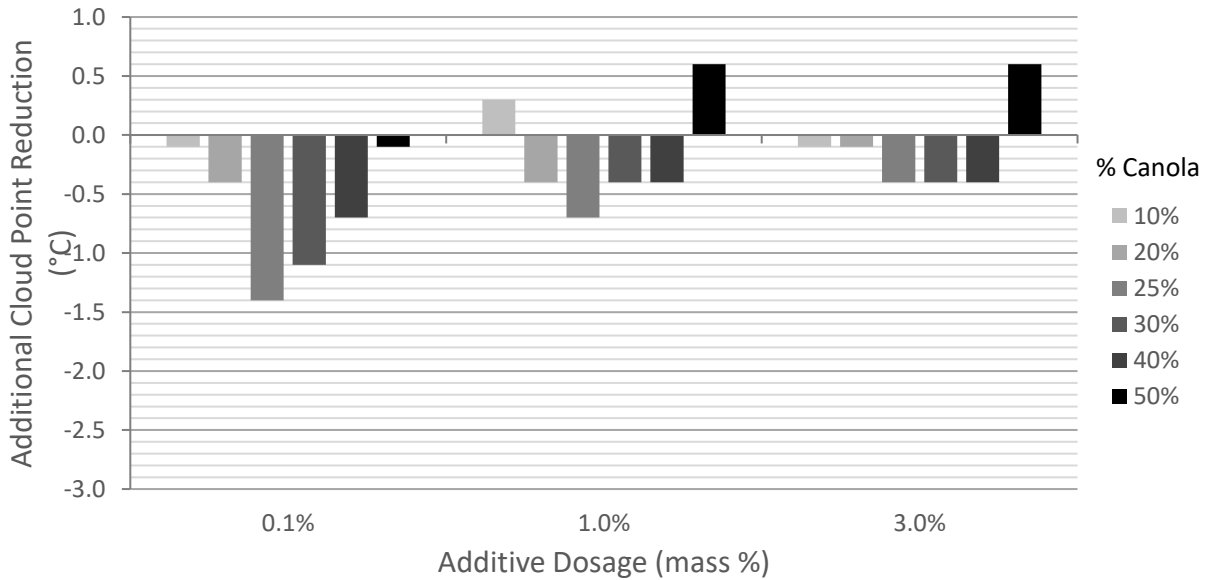


Figure 6.5 – Additional CP reduction from synergy of CME blend and Viscoplex 10-530

The same calculations were completed for CFPP to determine the synergistic effect of additive dosage and CME blend. Those results are shown in Figure 6.6 below. For CFPP it is the 40% CME blend that best interacts with the Viscoplex 10-530, creating an added 1.6-2.6°C CFPP reduction.

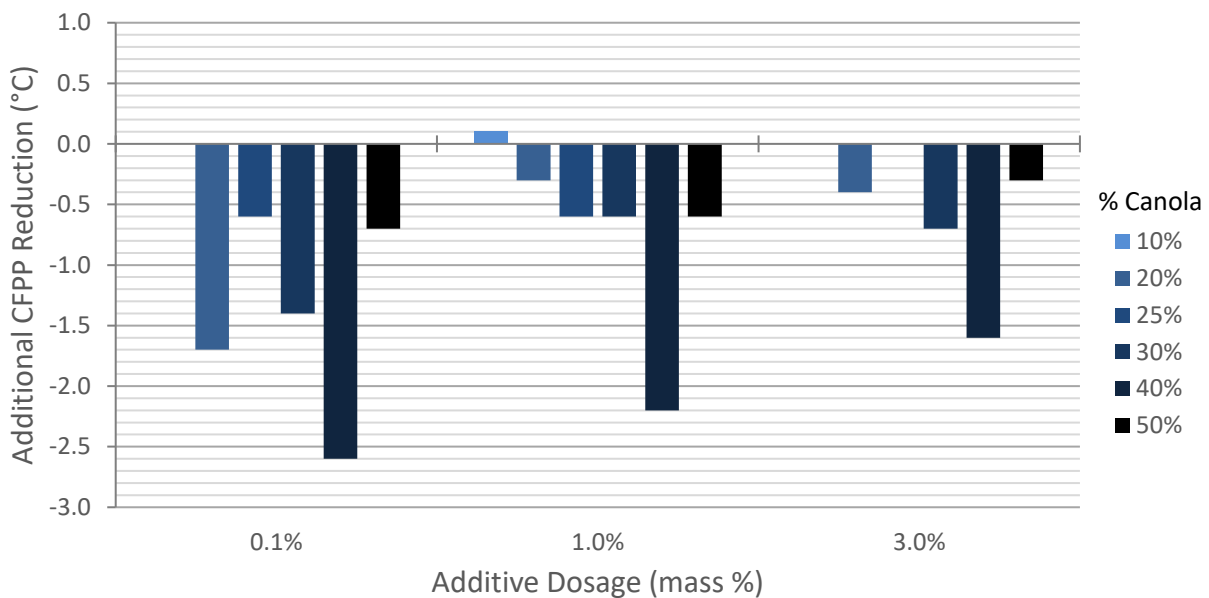


Figure 6.6 - Additional CFPP reduction from synergy of CME blends and Viscoplex 10-530

6.3 CorsiTech Additives

Ideally, to thoroughly test each of these additives, we would see how the CP changes from no additive to the maximum recommended dosage as well as at varying levels of SME or CME blending. Since that would be too time intensive, we quickly screened the non-TME specific additives by testing each additive at its maximum dosage and a midpoint dosage at a 25% CME blend. This made sure we did not miss out on any effect caused by the blending of CME that might not occur with only TME. CME was chosen instead of SME because of its greater effect on CP.

CorsiTech manufactures four of the additives that were tested, and they were all formulated to decrease the pour point (PP) in petroleum oil. The CorsiTech 4006 had a minimal effect on CP with a 0.7°C drop at the 25% CME blend in Figure 6.7 below. Its effect on the CFPP was counterproductive, and actually increased CFPP by 0.4°C as seen in Figure 6.8 below.

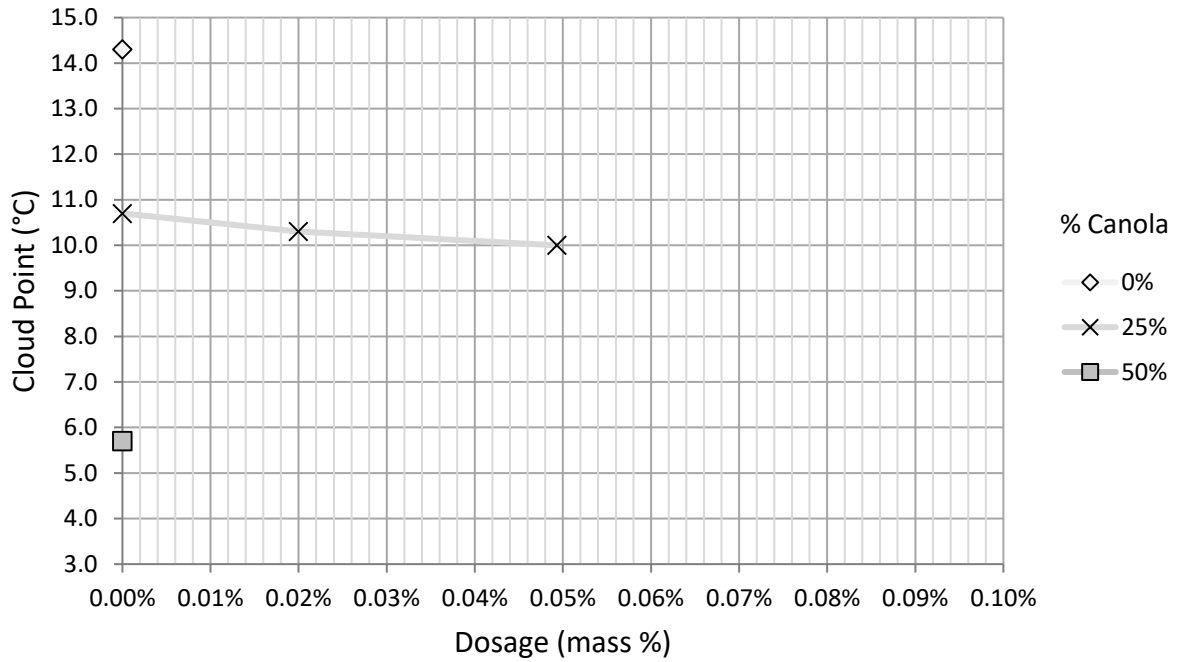


Figure 6.7 - CP effect of CorsiTech 4006 additive in 25% CME/TME blend

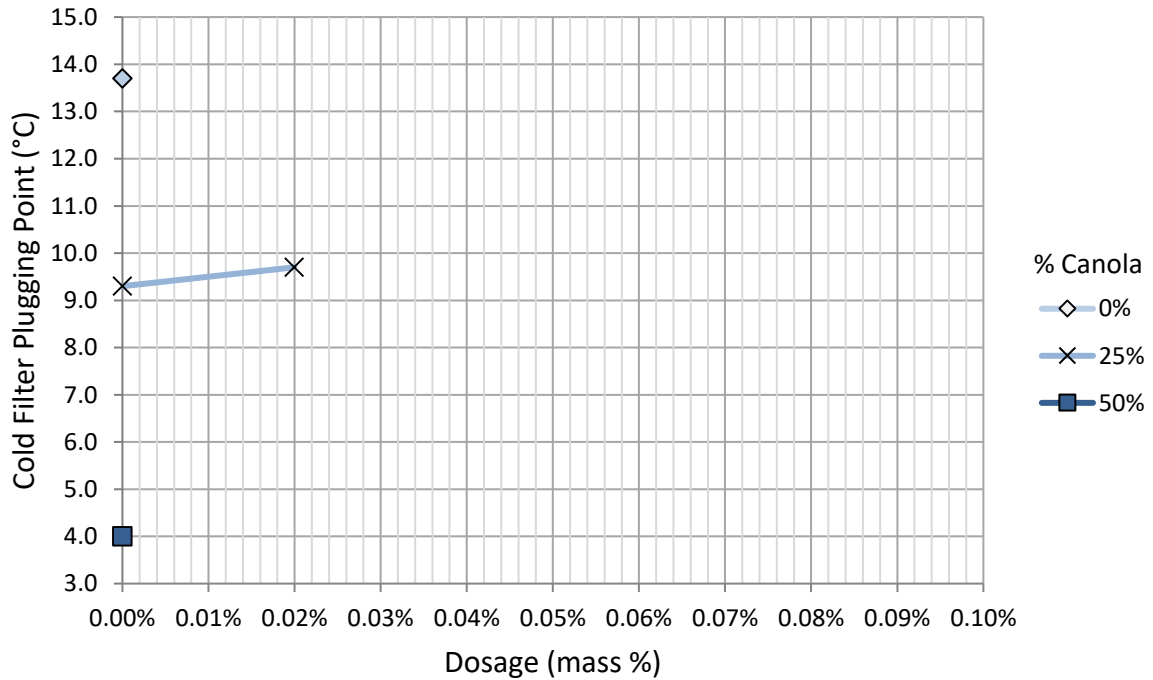


Figure 6.8 - CFPP effect of CorsiTech 4006 additive in 25% CME/TME blend

CorsiTech 4027 performed even worse than the CorsiTech 4006 as seen in Figure 6.9, with the CP at the maximum dosage in the 25% CME blend unchanged and increasing by 4°C at the maximum dosage in the 50% CME blend. The CFPP also increased by 0.4°C at the maximum dosage in a 25% CME blend as shown in Figure 6.10.

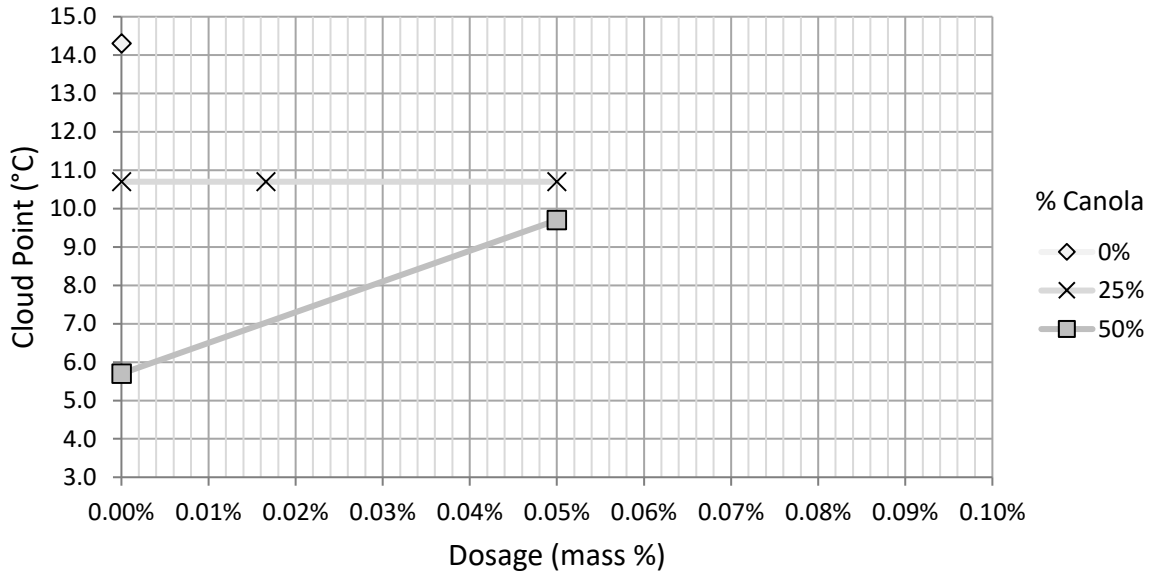


Figure 6.9 - CP effect of CorsiTech 4027 additive in CME/TME blends

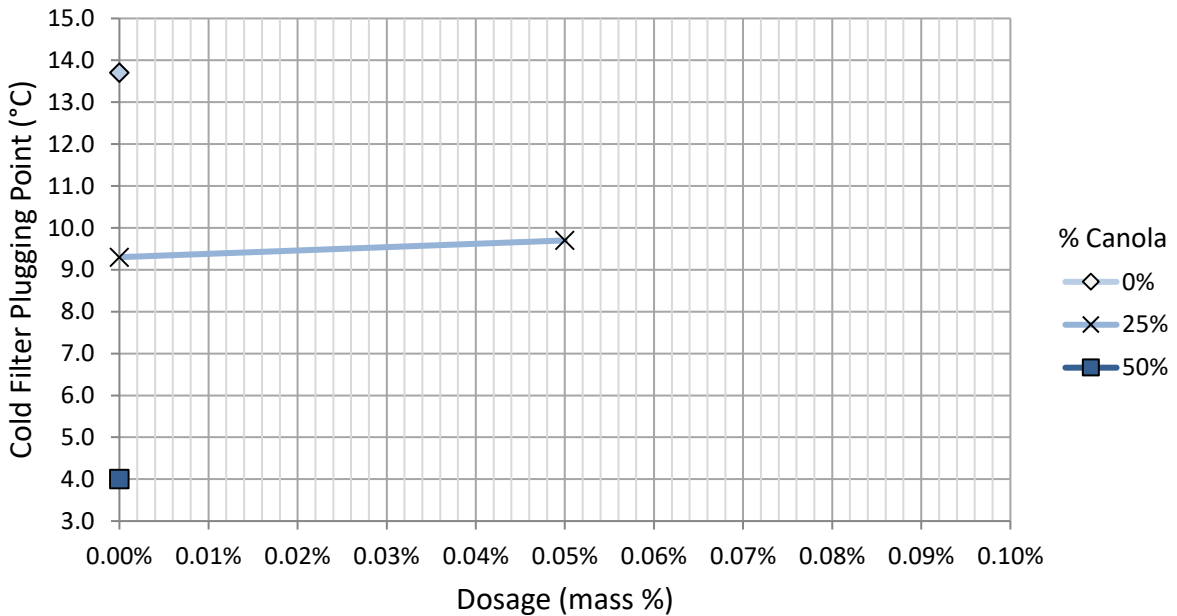


Figure 6.10 - CFPP effect of CorsiTech 4027 additive in 25% CME/TME blend

The next additive, CorsiTech 4028, was also not very successful with a maximum CP depression of 0.7°C and an increase in CFPP of 0.4°C charted in Figure 6.11 and Figure 6.12.

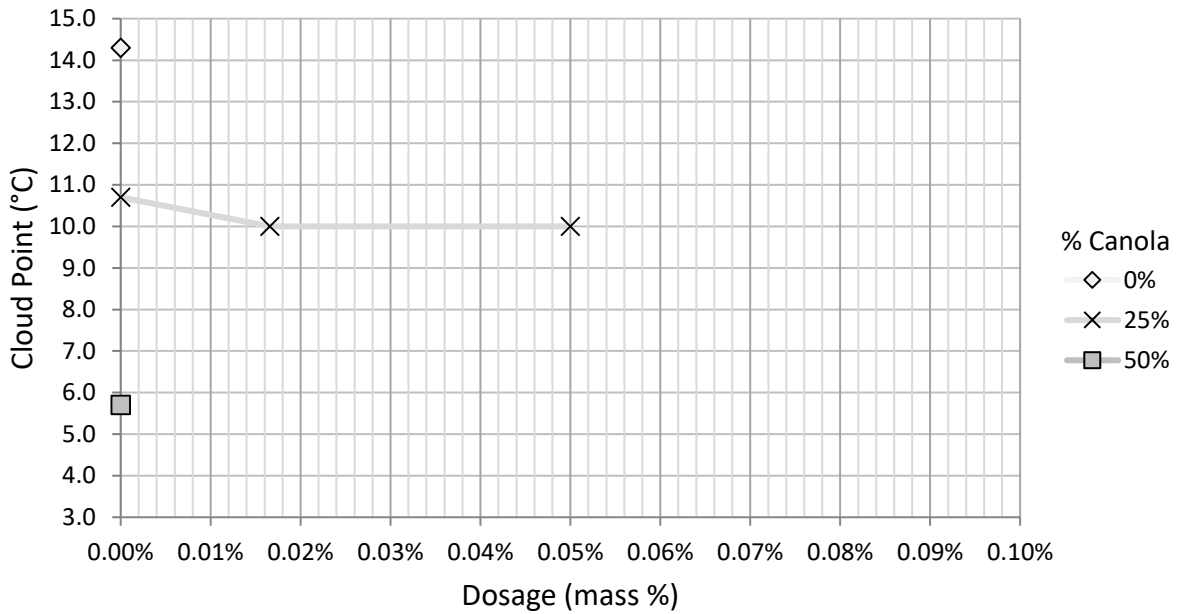


Figure 6.11 - CP effect of CorsiTech 4028 additive in 25% CME/TME blend

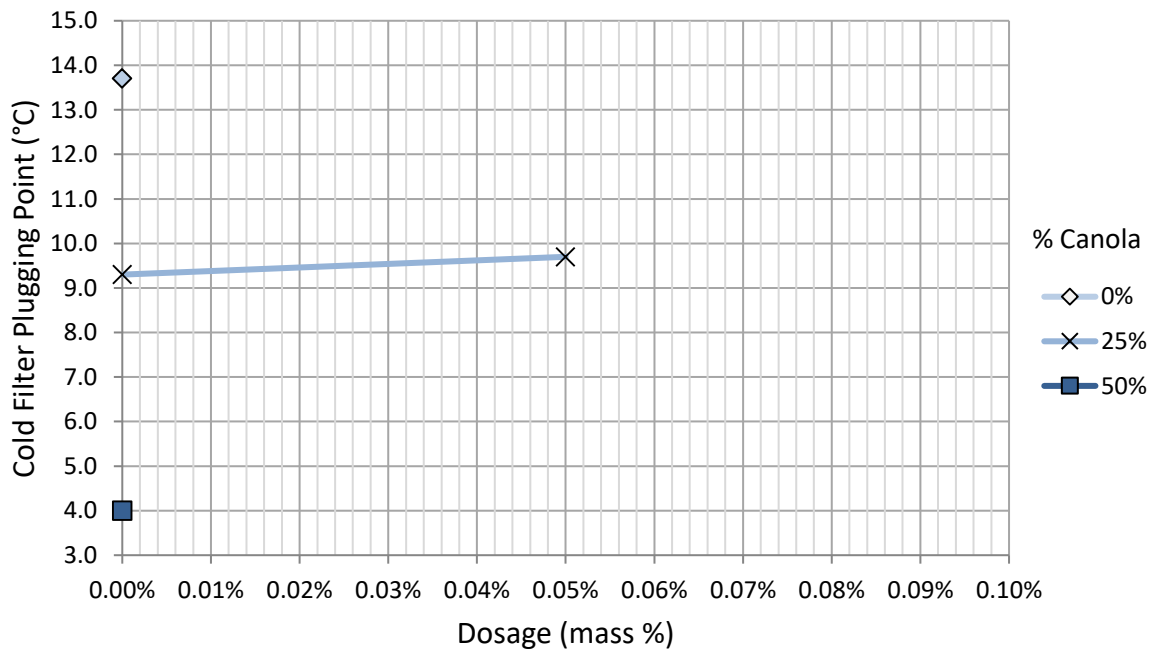


Figure 6.12 - CFPP effect of CorsiTech 4028 additive in 25% CME/TME blend

CorsiTech 6144 was the final CorsiTech additive tested. This one only decreased CP by 0.4°C at a 0.01% dose (Figure 6.13) then increased back to the starting CP at a 0.05% dose which is above the recommended maximum of 0.01%. In Figure 6.14, the CFPP initially rose 1°C at the 0.017% dose then decreased 0.3°C at the 0.05% dose.

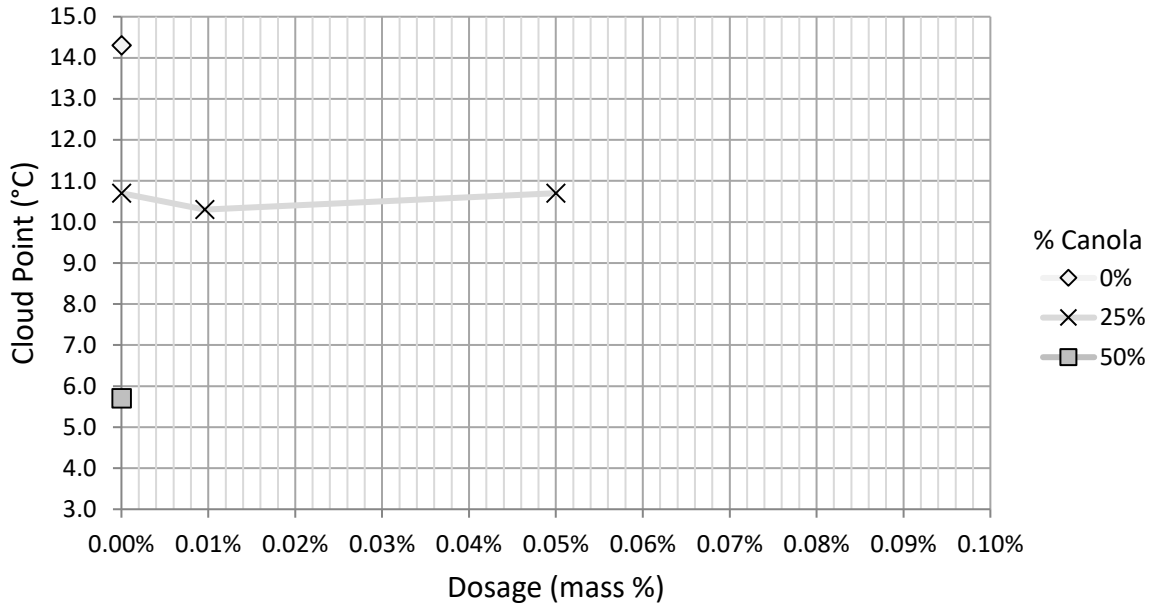


Figure 6.13 - CP effect of CorsiTech 6144 additive in 25% CME/TME blend

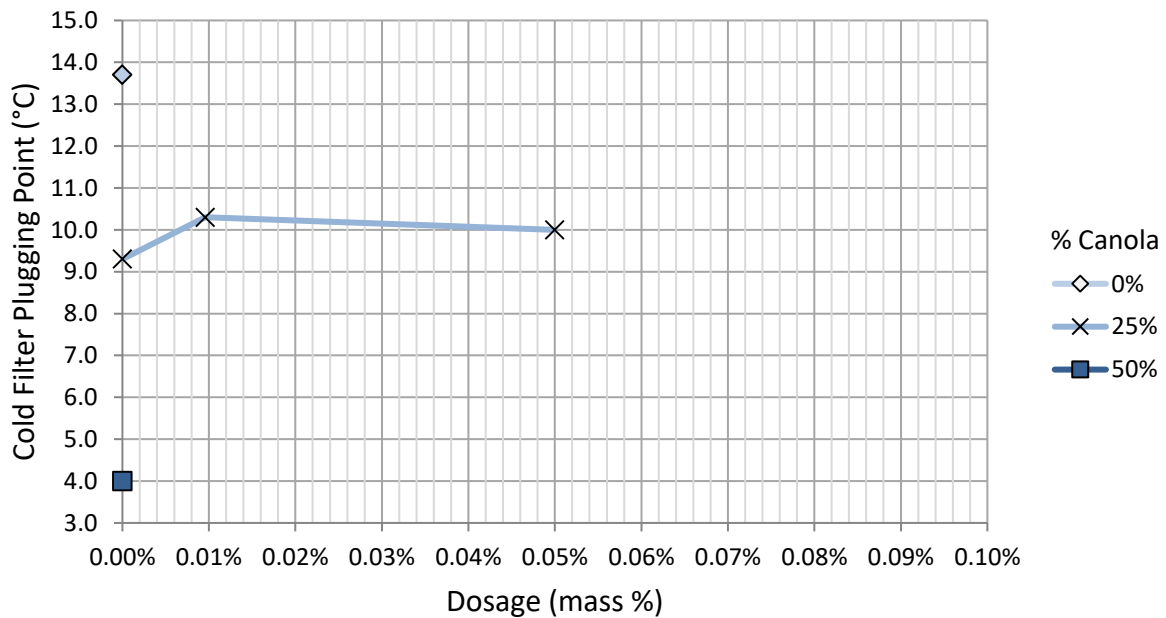


Figure 6.14 - CFPP effect of CorsiTech 6144 additive in 25% CME/TME blend

6.4 Infineum Additives

The next group of additives was made by Infineum. These additives were designed for a variety of fuels: SME, CME, general FAMES and some that were not specified. Additionally they span the range of reducing CP, CFPP, PP and CSFT.

Infineum R408 was made to reduce the CFPP in CME. At a 25% blend of CME, the CP only lowered 0.7°C at a 0.1% dose shown in Figure 6.15. In Figure 6.16, at the 25% CME blend, the CFPP actually increased 0.7°C with an additive designed to reduce CFPP in CME. To be fair, the maximum recommended dosage for R408 is 0.4%, and the maximum tested was 0.1%.

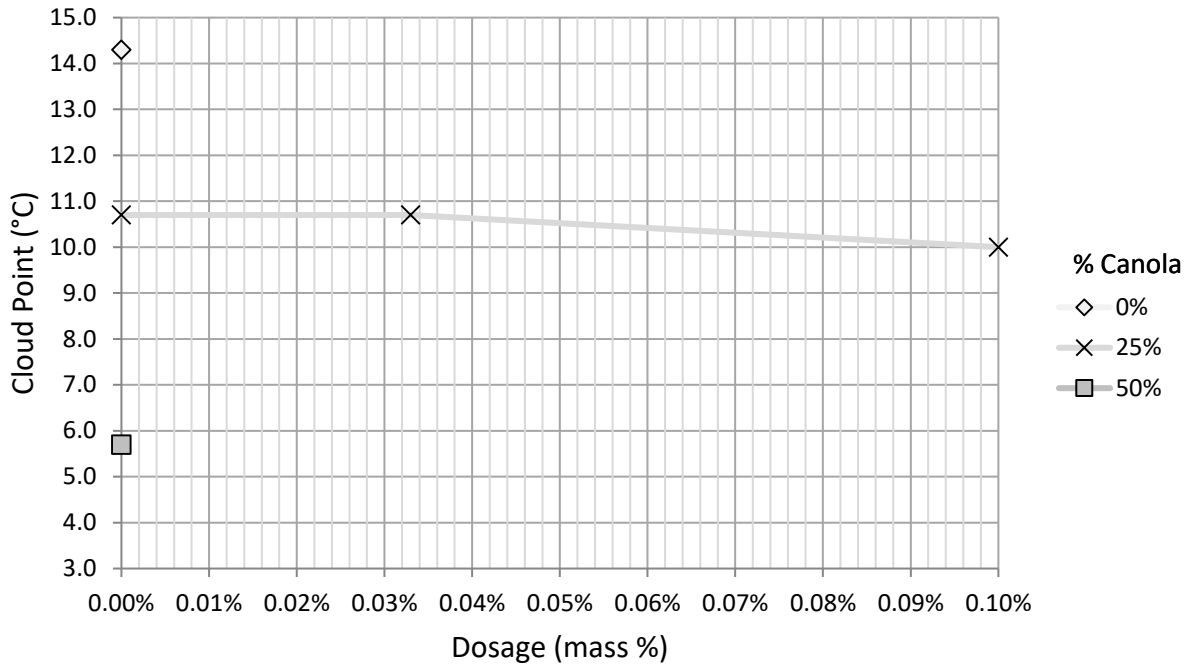


Figure 6.15 - CP effect of Infineum R408 additive in 25% CME/TME blend

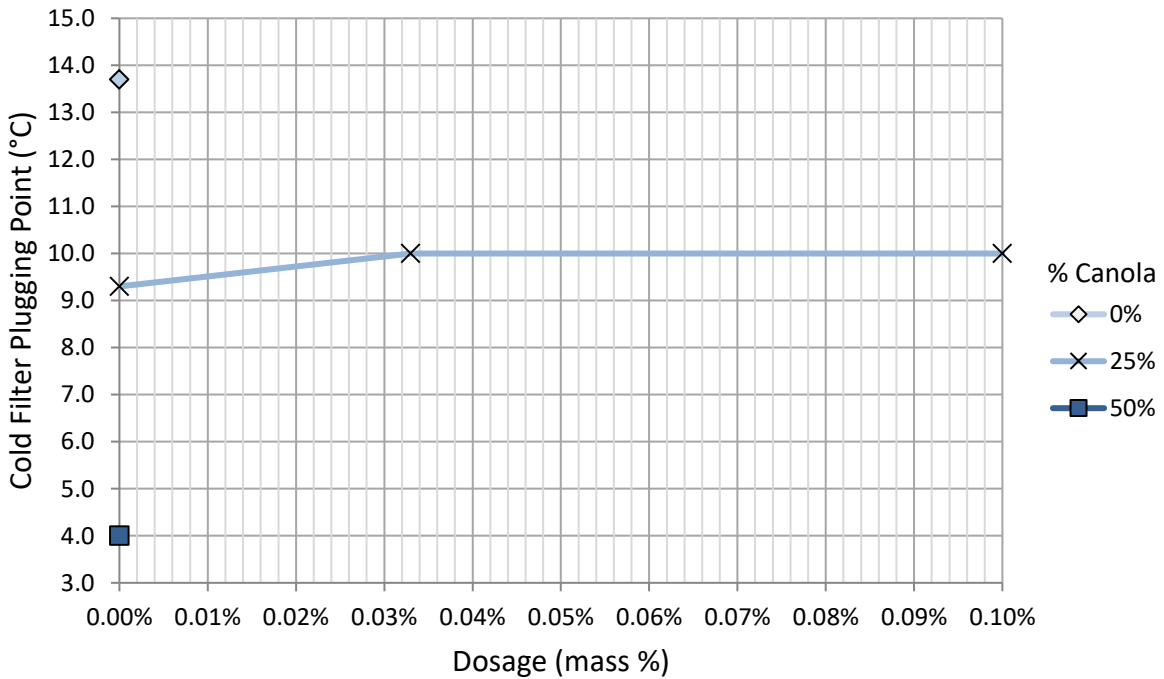


Figure 6.16 - CFPP effect of Infineum R408 additive in 25% CME/TME blend

Infineum R440 was created to reduce CP, but the intended fuel type is unknown. R440 was shown in Figure 6.17 to be even less effective than R408 since the CP increased 0.3°C at 0.033%

dose and 4°C at a 0.330% dose, which is over 3x the recommended dose of 0.100%. The CFPP also increased from 0.000% to 0.033% additive dosage (Figure 6.18).

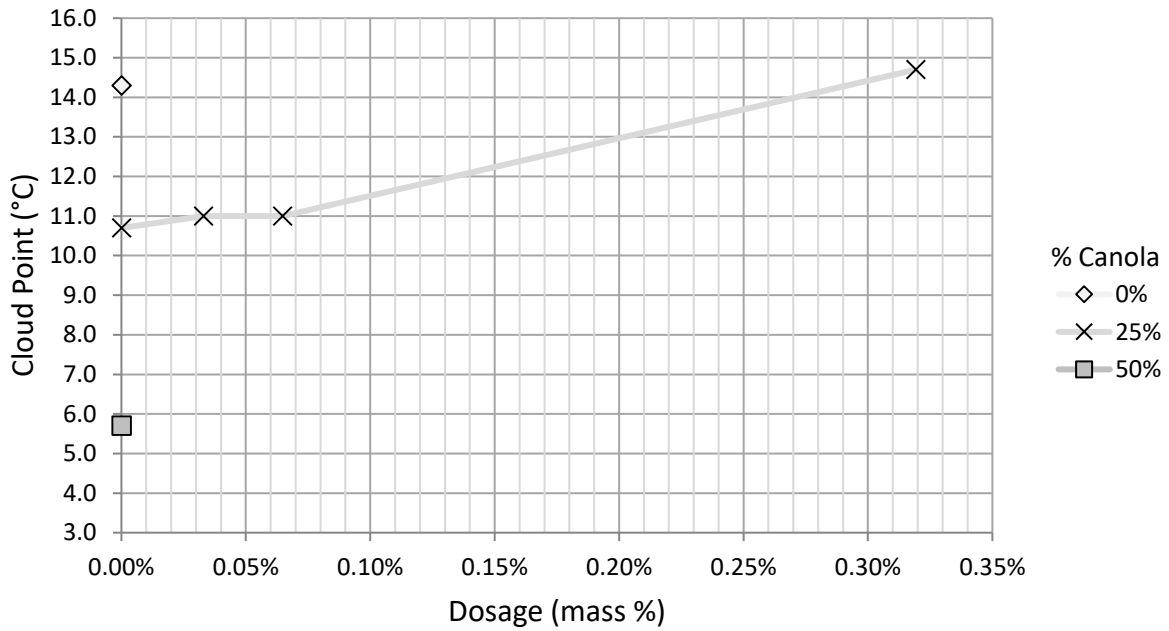


Figure 6.17 - CP effect of Infineum R440 additive in 25% CME/TME blend

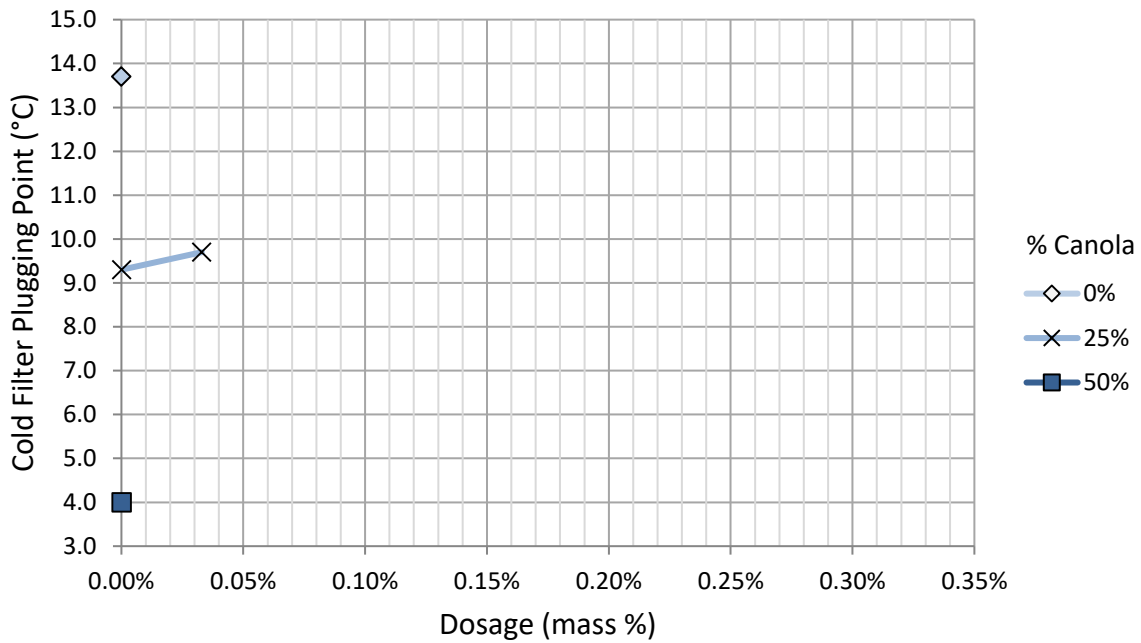


Figure 6.18 - CFPP effect of Infineum R440 additive in 25% CME/TME blend

The next Infineum additive tested was R511. The fuel this additive was designed for is unknown, but it is designed for CP reduction. Within its recommended dosage range of 0.1%, the maximum CP reduction was only 0.4°C as seen in Figure 6.19. Outside of the recommended dosage range, the CP increased 0.7°C at 0.33% additive. Figure 6.20 shows the CFPP was unchanged at a 0.33% dosage.

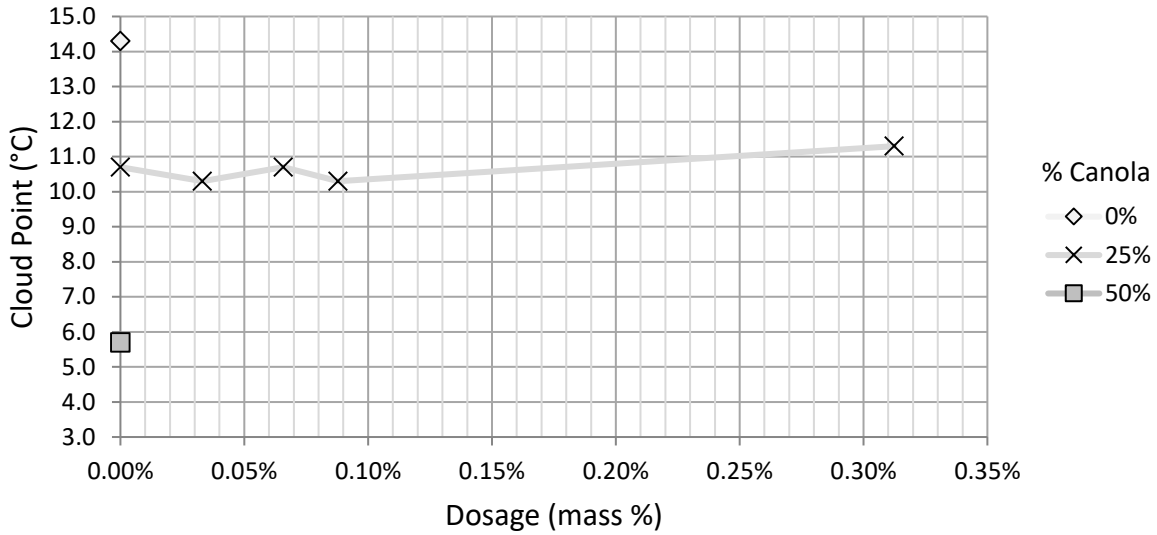


Figure 6.19 - CP effect of Infineum R511 additive in 25% CME/TME blend

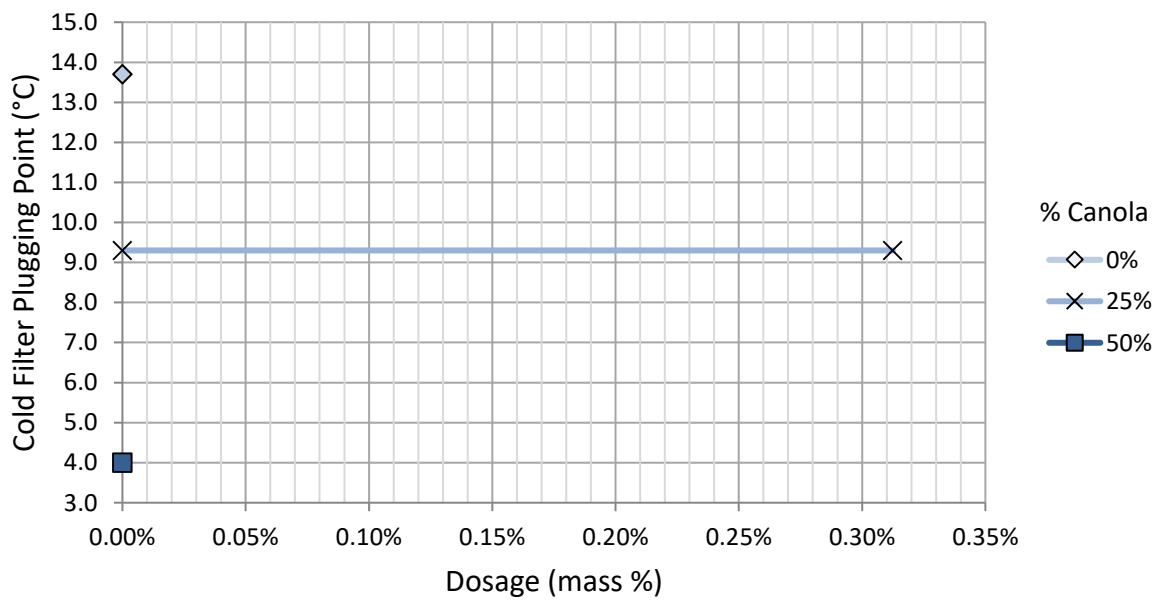


Figure 6.20 - CFPP effect of Infineum R511 additive in 25% CME/TME blend

Out of curiosity, I wanted to see if Infineum R511 would have any effect on SME or if it would be virtually the same as the CME/TME blends. It was disappointing to see so many of these additives have so little effect on CME/TME blends so this was sanity check of sorts. Sure enough, the Infineum R511 had a significant 4.3°C CP reduction in 100% SME at a 0.066% additive dose. The effect on CFPP was the reverse and increased it 2°C from 0.033% to 0.066% additive. These results are graphed below in Figure 6.21

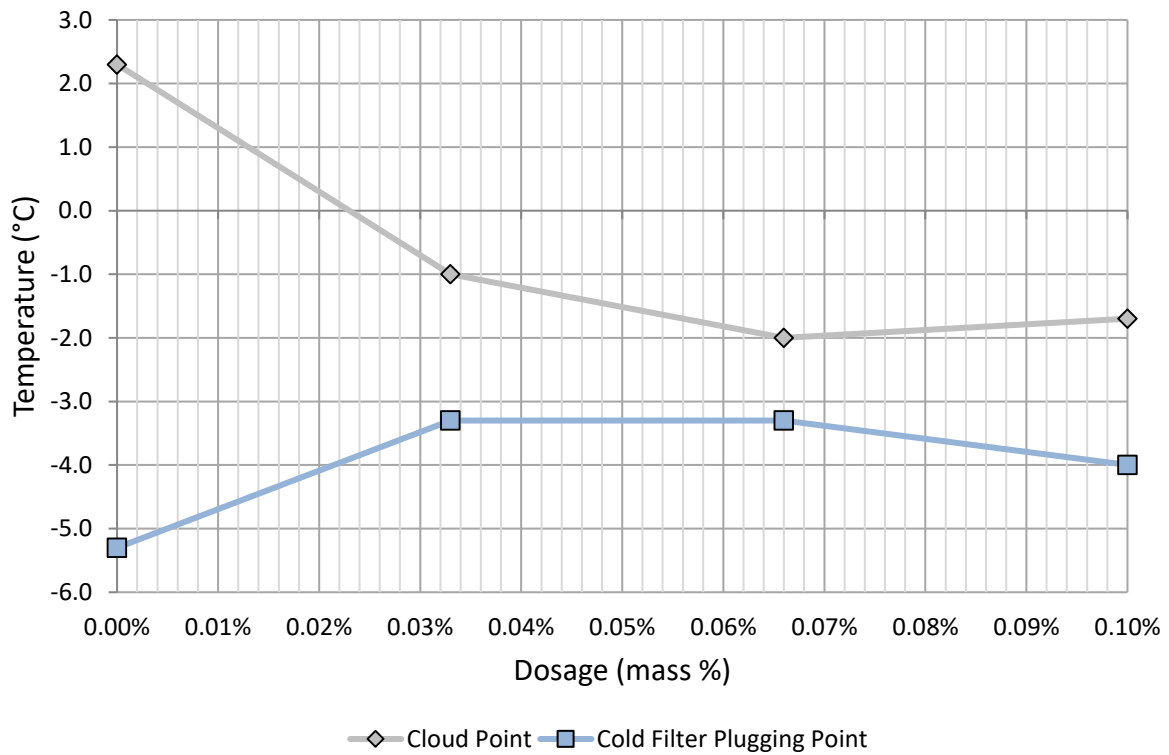


Figure 6.21 – CP and CFPP effect of Infineum R511 additive in SME

Infineum R518 was designed to reduce PP and CFPP in SME and had a minimal effect on CP with only a 0.4°C reduction (Figure 6.22) and increased CFPP by 1.0°C (Figure 6.23).

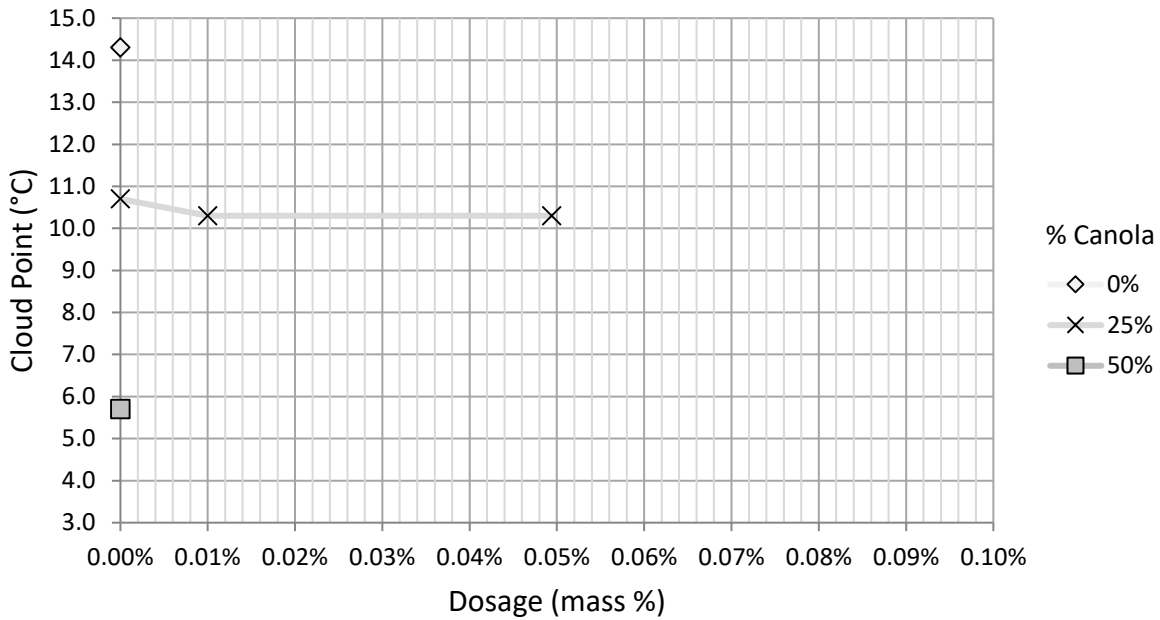


Figure 6.22 - CP effect of Infineum R518 additive in 25% CME/TME blend

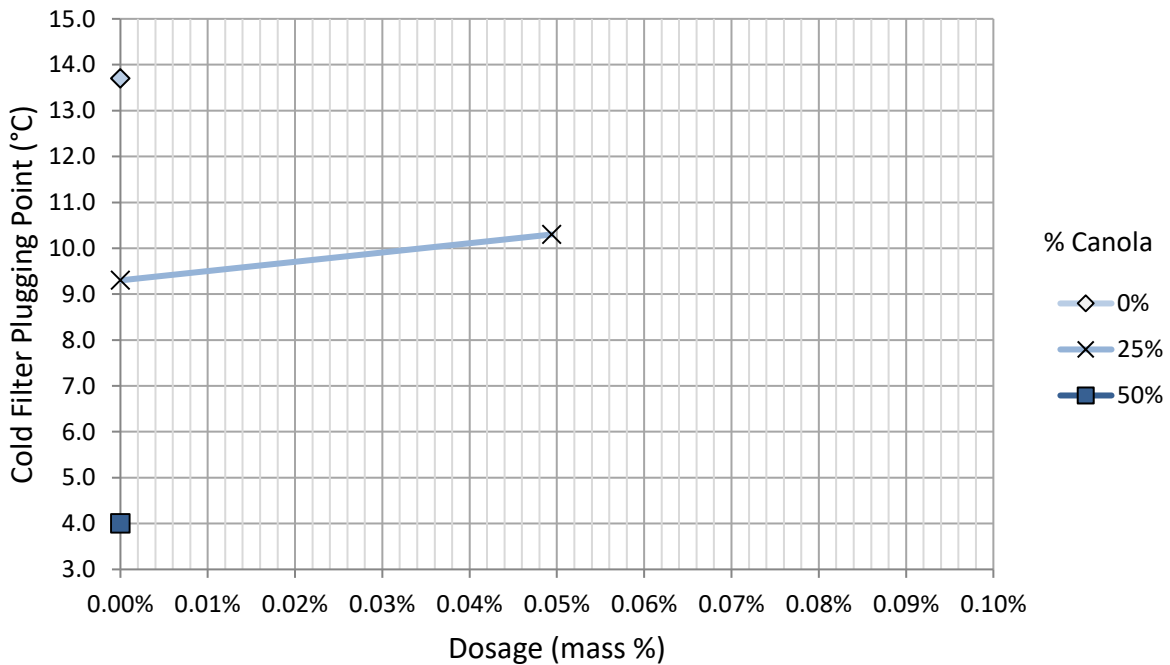


Figure 6.23 - CFPP effect of Infineum R518 additive in 25% CME/TME blend

The final Infineum additive evaluated was R536 which was formulated to improve the cold soak filtration test (CSFT) in FAMES. This additive also did not perform well with only a 0.4°C reduction in CP (Figure 6.24) and a 1.0°C increase in CFPP (Figure 6.25).

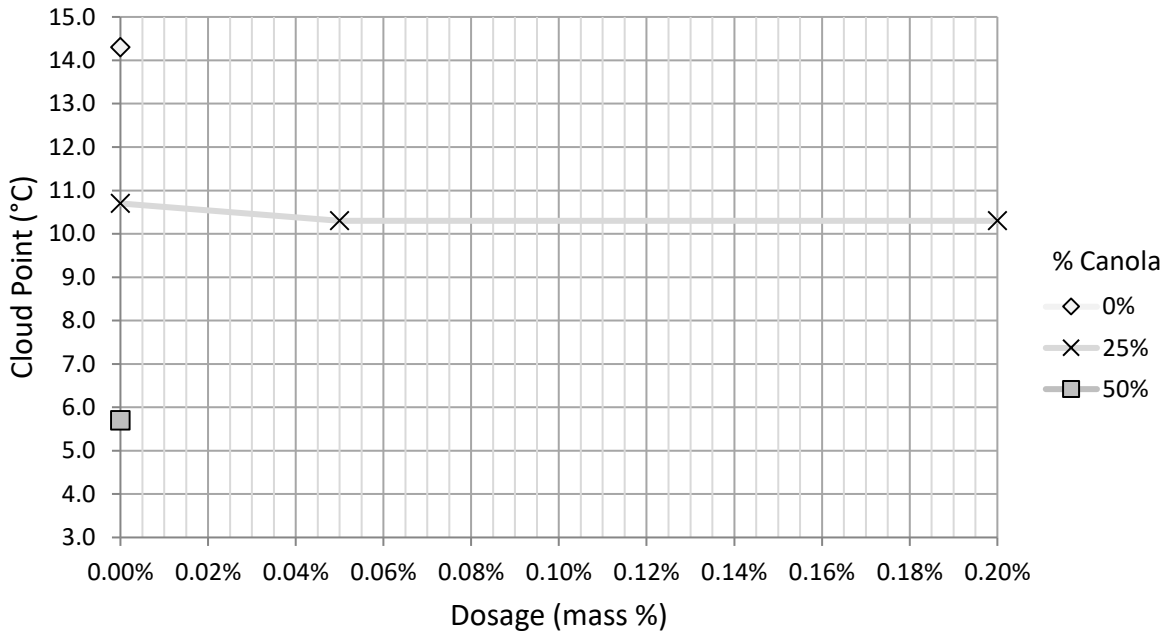


Figure 6.24- CP effect of Infineum R536 additive in 25% CME/TME blend

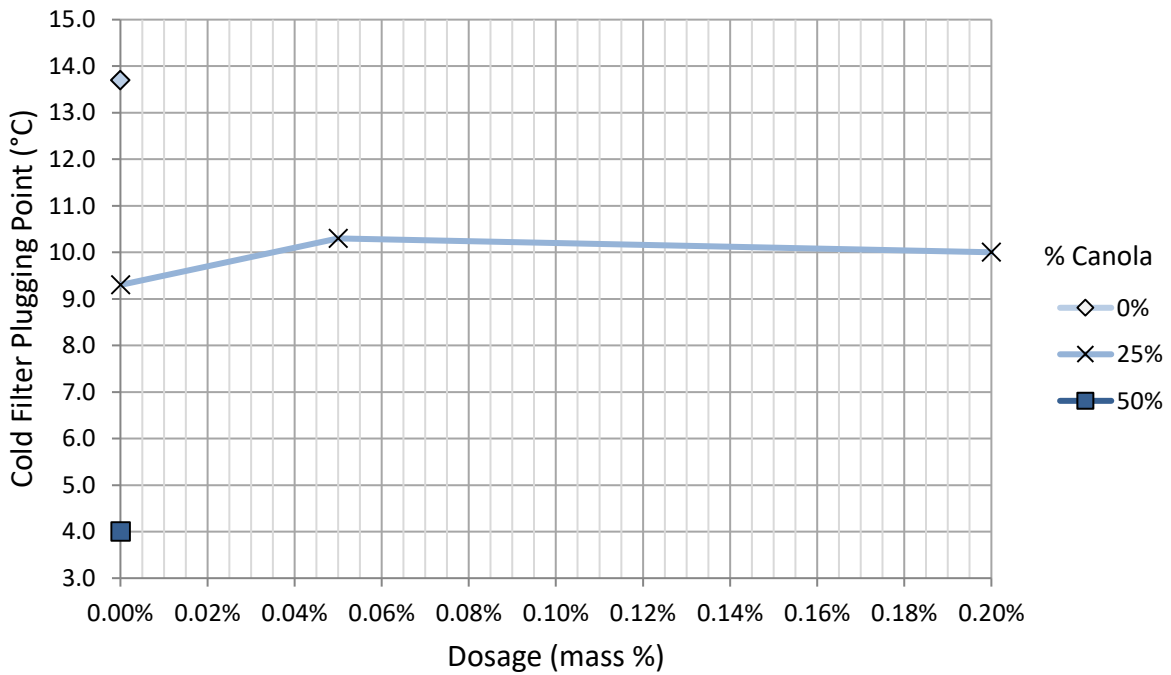


Figure 6.25 - CFPP effect of Infineum R536 additive in 25% CME/TME blend

6.5 MLA Additive

After testing all ten of the previous additives, it was disappointing that only the Viscoplex 10-530 made much of a change in CP for CME/TME blends, with only a 2°C maximum CP reduction. At that point, Sun West provided a sample of a proprietary additive that was designed specifically to reduce CP in TME. This additive was developed at Flinders University in Adelaide, Australia through research funded by the Meat and Livestock Australia (MLA), a red-meat industry group. According to an article published in Biodiesel Magazine in 2008, MLA has partnered with The Midfield Group and Food Processing Equipment to commercialize this additive but when conducting this research in 2012 it was not commercially available [54].

6.5.1 MLA Additive Makeup

According to the MLA report, the additive blend was 25% active ingredients (polymers and surfactants) mixed with 75% petroleum diesel and intended for use with B5, B20 and B100. The report claims the additive produced CP reduction from 10°C to -6°C in an animal fats based biodiesel. This would likely be biodiesel made from choice white grease or pork fat since the initial CP was 10°C [52]. Either way, that is still a 16°C CP reduction, which in TME would result in a final CP of -1.5°C if the same results hold true.

A closer look at their chart, in Figure 6.26, shows the claims are overstated. The bars in blue are the CP and the bars in red represent CFPP. There are two biodiesels they tested this additive on, one from the EU with a B100 CP of 14°C and one from Australia with a B100 CP of 17°C. The EU B100 and the Australian B100 were blended with petroleum diesel to make B20. That initial CP drop shown was solely from mixing biodiesel with petroleum diesel (CP=2°C) at a 20/80 mix. After the biodiesel was blended to B20, they then mixed in the MLA additive. Both the EU and the Australian biodiesels drop from 4°C at B20 to 0°C with the additive for a 4°C CP reduction. The -6°C

temperature from the report is actually the CFPP of B20 with the MLA additive. This is a 5°C CFPP reduction with the additive. While the 16°C CP drop was misleading, a 4°C in B20 is still intriguing.

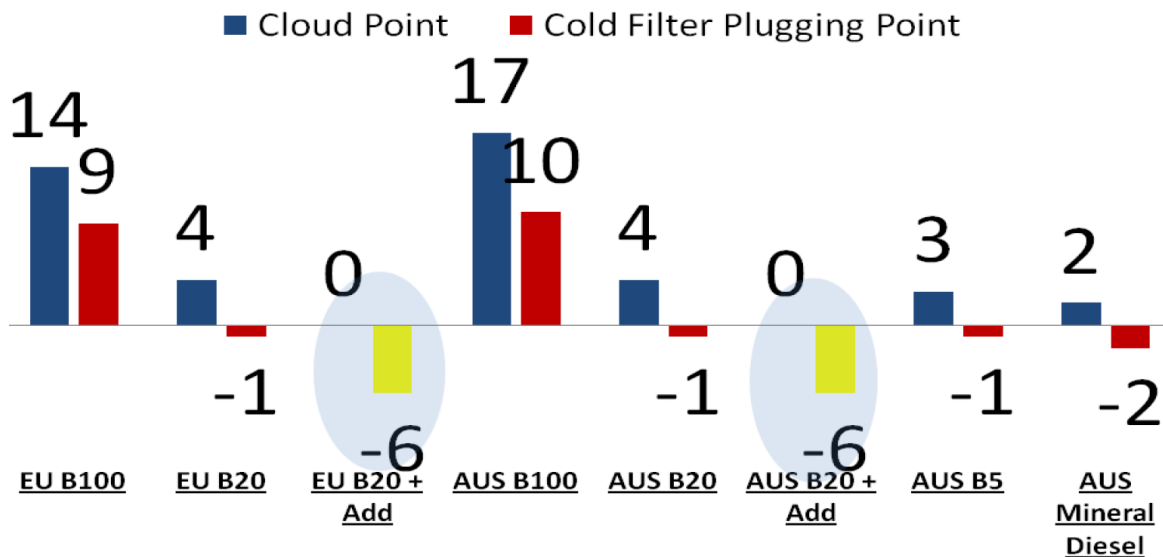


Figure 6.26 – Chart from MLA report showing CP and CFPP reduction in B20 biodiesel. CP (blue), CFPP (red) and CFPP with additive (yellow) [53]

6.5.2 MLA Additive and CME Blending

Because the MLA additive had significant promise we decided to do thorough testing at 0%, 25%, and 50% CME/TME blends with dosages up to and beyond the recommended 2.0%. The results were quickly promising with a sharp 1.0-1.3°C drop with only a 0.1% dose across all CME blends and up to a 3.6°C drop at a 5% dose in 100% TME (Figure 6.27). The additive was not tested higher than 5% because doses higher than that would likely not be cost effective. Additionally, with 75% of the additive blend being diesel, a 5% additive dosage meant there was already 3.75% diesel in the TME, potentially enough to start affecting the CP. The CFPP dropped even more than CP with between 1.0-3.7°C drops at a 0.1% dose and a maximum of 6.3°C at the 50% CME blend with 3% additive (Figure 6.28).

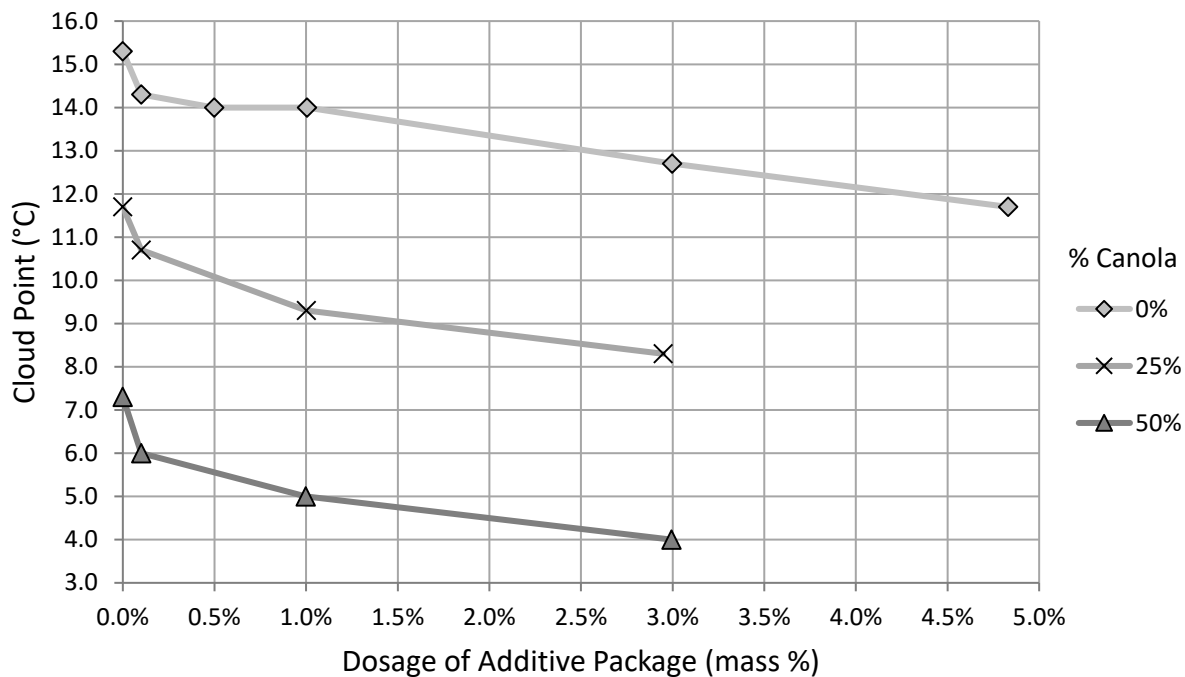


Figure 6.27 - CP effect of MLA additive in CME/TME blends

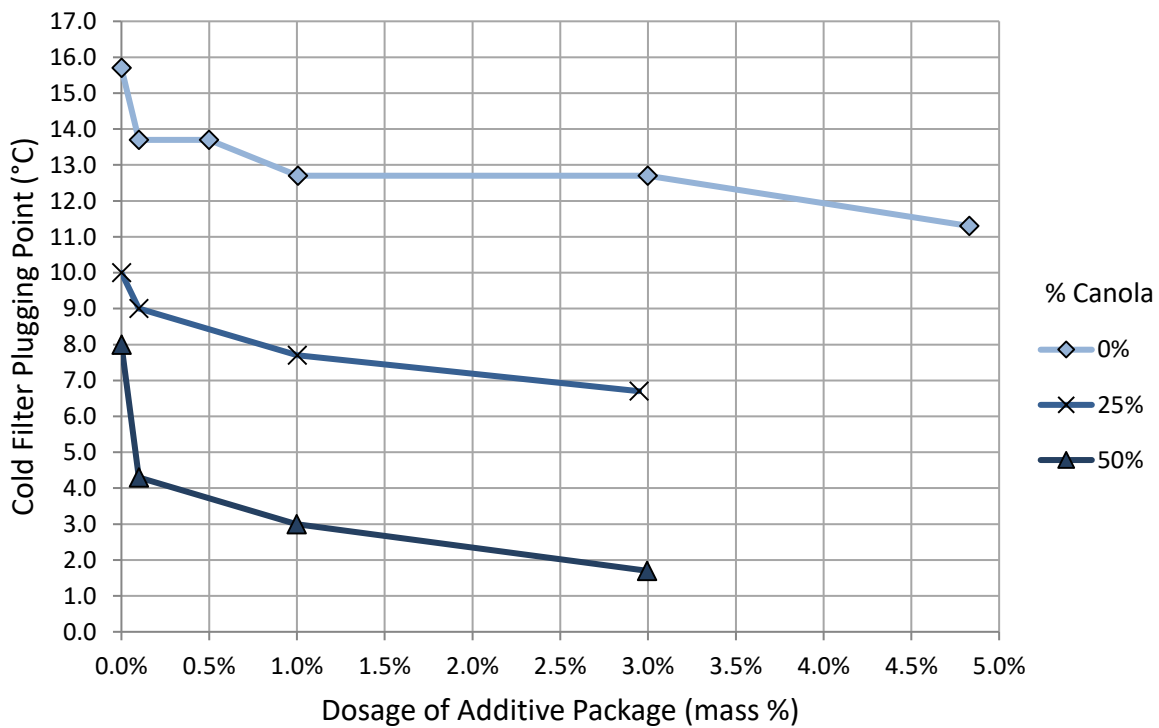


Figure 6.28 - CFPP effect of MLA additive in CME/TME blends

According to Figure 6.29 below, the greatest CP reductions happened expectedly at the higher dosages of 3-5%. At a 1% or 3% additive dosage, the CP reduction at the 25% CME blend tended to be slightly more than at the 50% CME blend.

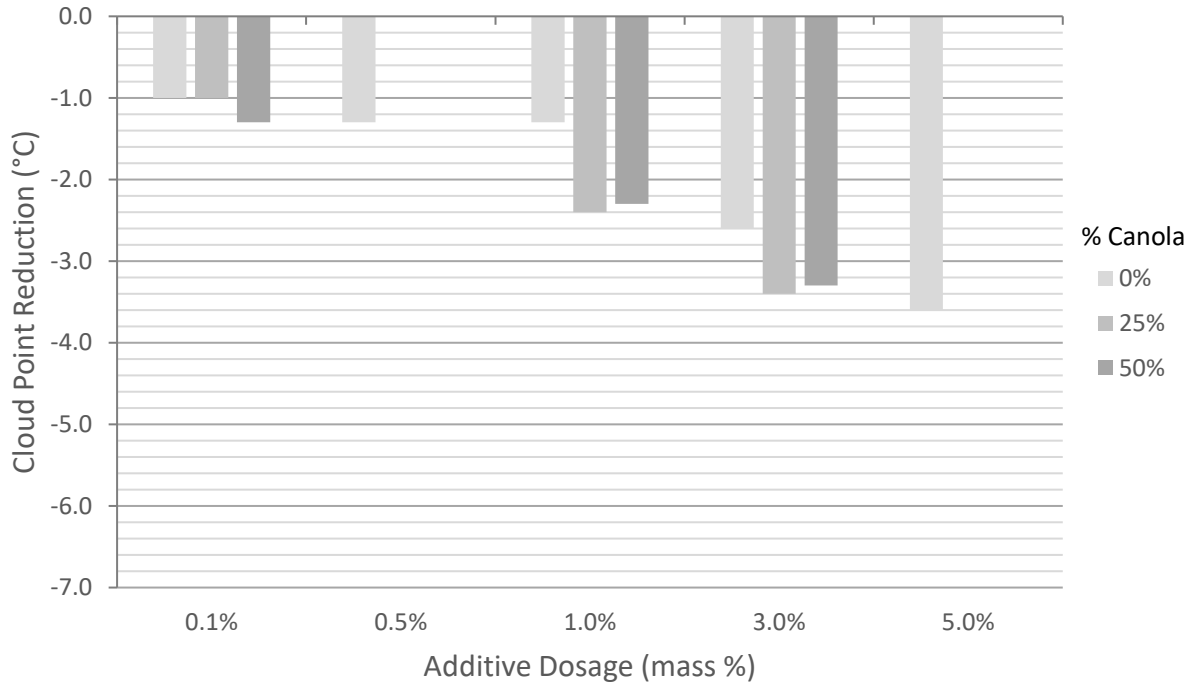


Figure 6.29 – CP reduction by MLA additive from 0% dosage for various CME/TME blends

Given the additional reduction in CP between 3% and 5% MLA dosage in TME, it would be interesting to test if that trend would repeat if the 25% and 50% CME/TME blends were tested with 5% MLA additive. Assuming the deltas from 3% to 5% additive dosage were similar, a 5% dosage with 25% CME could reduce CP over 4°C.

As far the CFPP, the MLA caused a greater effect as the dosages increased up to 5%. The additive produced a greater CFPP reduction at 0% CME than 25% CME blends but both were out surpassed at the 50% CME blend with up to a 6.3°C drop at 3% MLA additive (Figure 6.30).

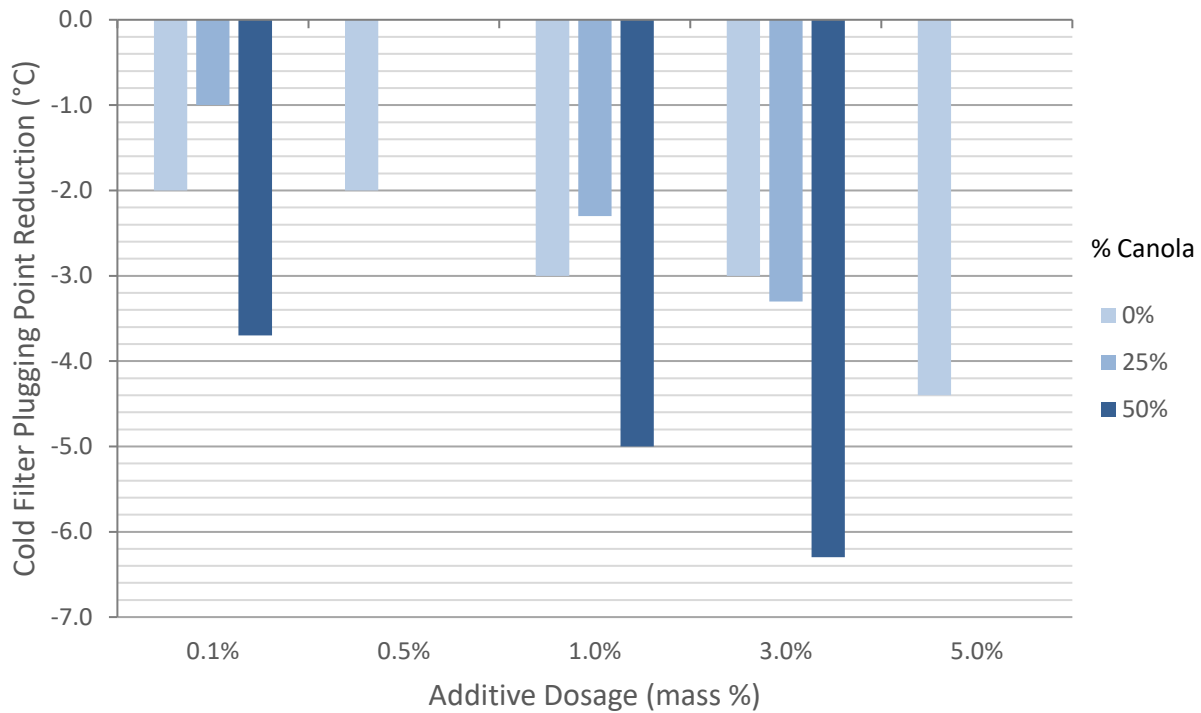


Figure 6.30 - CFPP reduction by MLA additive from 0% dosage for various CME/TME blends

When testing the Viscoplex 10-530 a synergistic effect was found between the additive and CME/TME blends. To see if a similar effect happened with the MLA additive, the same calculations were carried out, as with the Viscoplex 10-530, to find any additional CP and CFPP reduction.

Figure 6.31 and Figure 6.32 show a picture of how different CME/TME blends compound the CP reduction when paired with the MLA additive. The biggest synergy occurred at a 1% dosage, with an additional 1.1°C CP drop compared to the addition of the CME blend CP reduction and the additive CP reduction in TME. The synergistic effect is slightly less at 50% CME with a 1.0°C drop. With the CFPP, the additive actually did better with 100% TME than with the 25% CME/TME blend. At 50% CME though, the synergy created a 1.7°C to 3.3°C drop, with the highest drop at a 3% dosage.

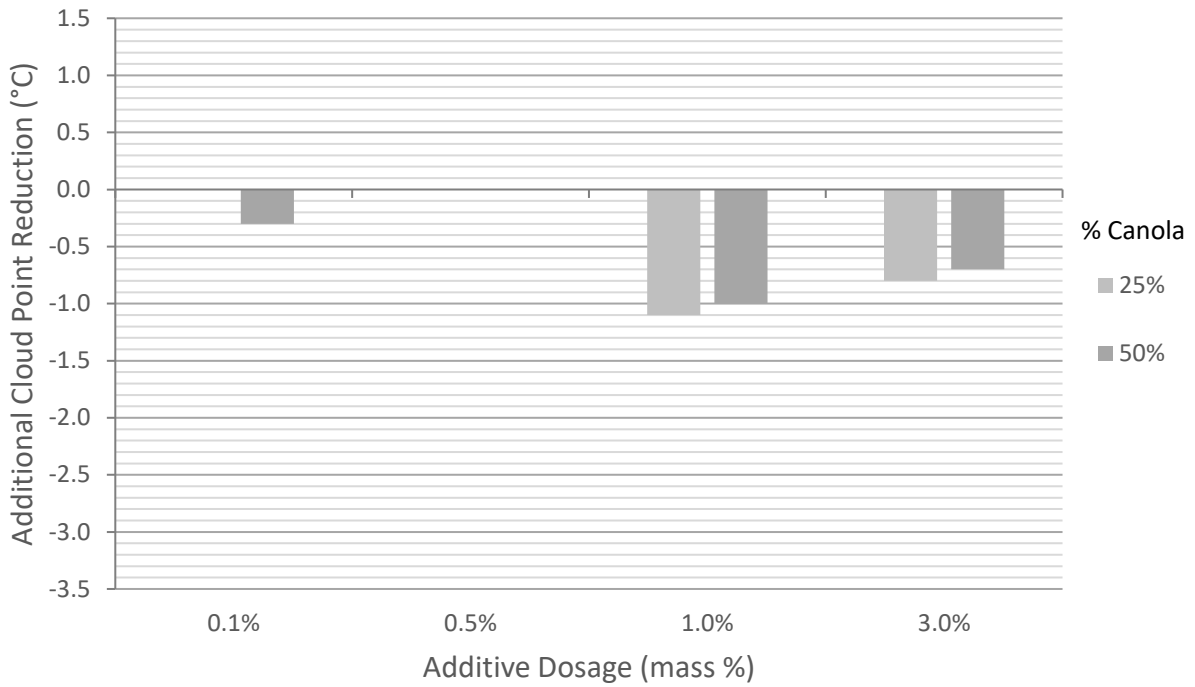


Figure 6.31 - Additional CP reduction from synergy of CME blend and MLA additive

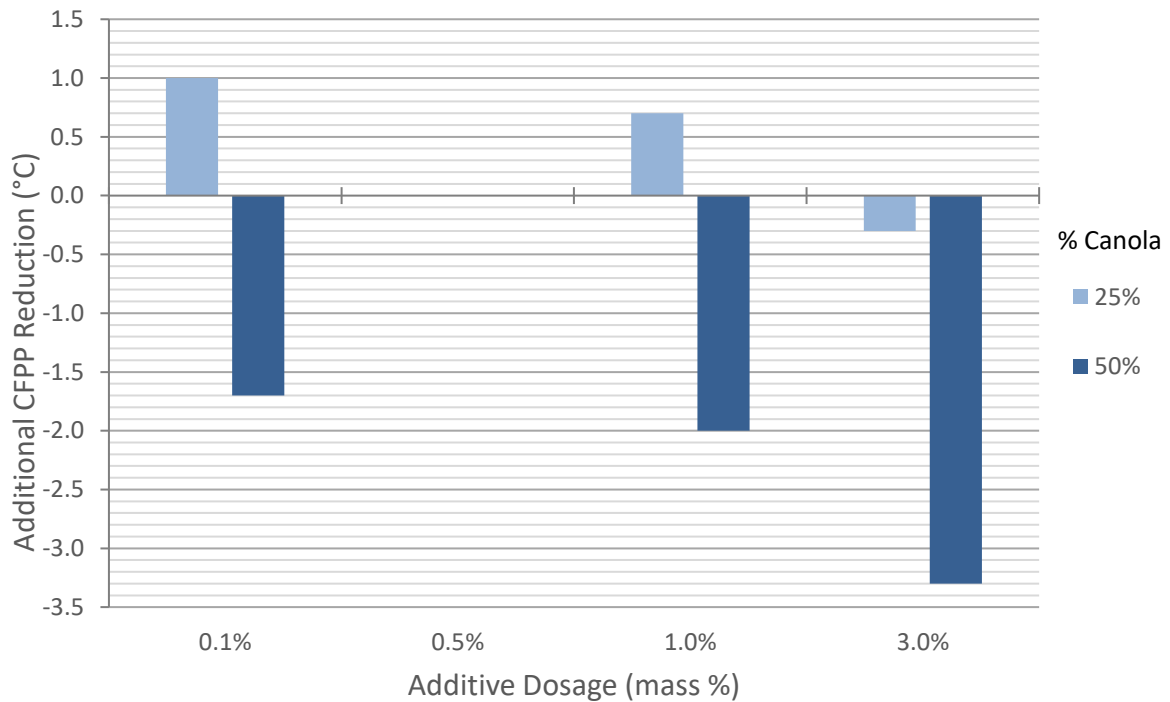


Figure 6.32- Additional CFPP reduction from synergy of CME blend and MLA additive

This last figure, Figure 6.33, was created to make it easier to visualize the three variable interaction of additive dosage, CME/TME blend and CP.

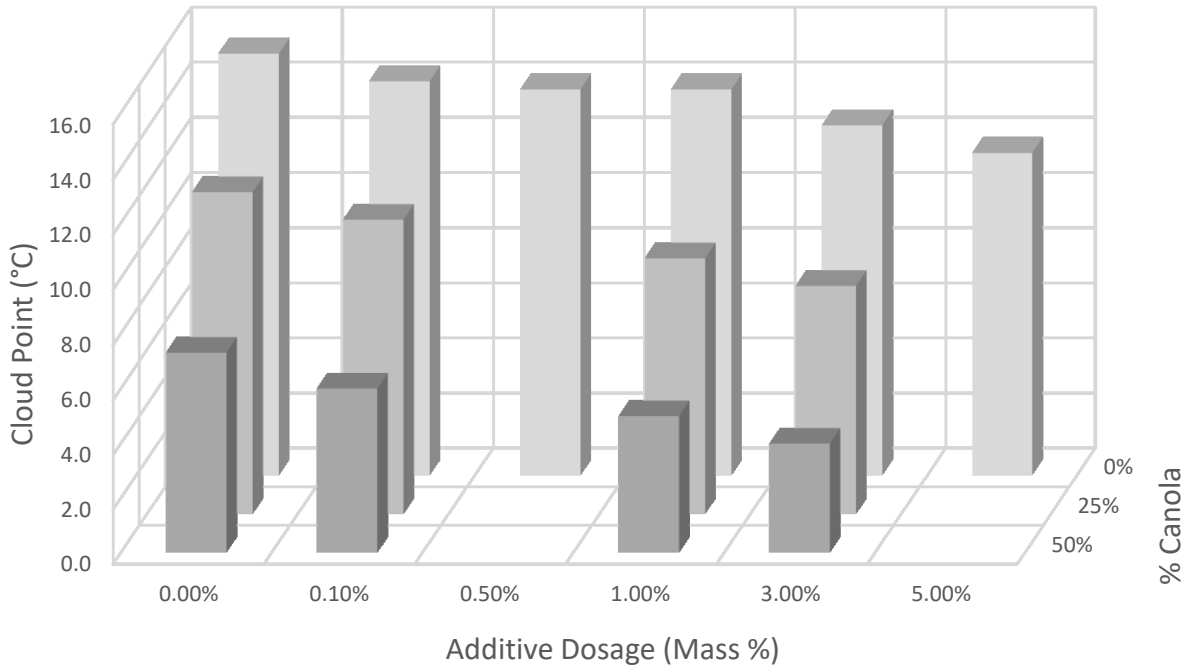


Figure 6.33 – Visualization of CME blending and MLA additive CP reduction

6.5.3 MLA Additive Components

The MLA additive had the most promising results of all the additives that were tested. In the patent for the MLA additive, the majority of the testing was at a 1% dosage, but it mentioned tests run from 0.1% up to 3.5%. We tested the MLA additive with dosages from 0.1% up to 5% but the active components were dissolved in diesel for a 25% active additive/75% diesel mixture. This means the active additive dosages actually varied from 0.25% to 1.25%.

From the MLA report, the active part of the additive from Meat and Livestock Australia is made up of two parts: a polymer and a surfactant (Figure 6.34) [52]. According to the patent, the polymer depresses the onset of crystal formation which reduces both CP and CFPP. The surfactant

then further reduces the CFPP by causing the fuel to form smaller crystals which pass through the filter easier [56] This means if CP is paramount, the surfactant is not necessary. If only the polymer is needed, the additive cost could be reduced.

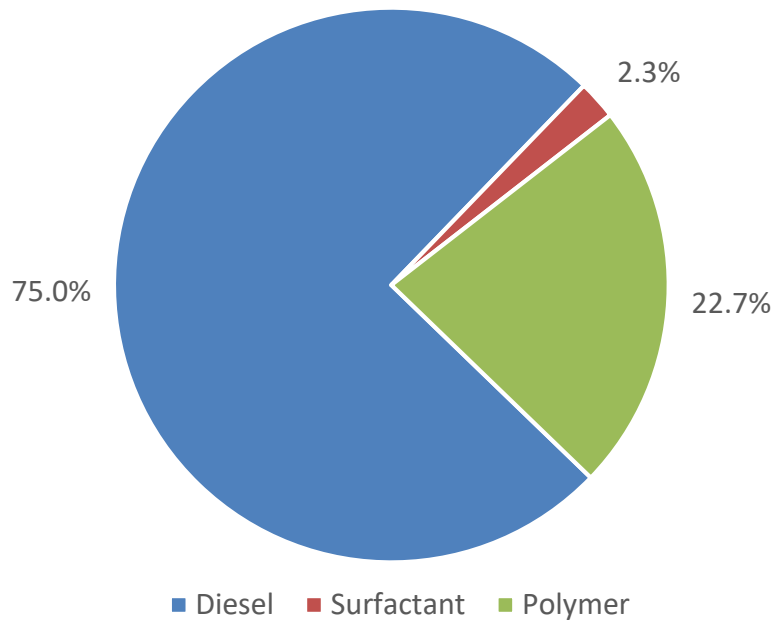


Figure 6.34 - Percentage breakdown of diesel, surfactant and polymer in MLA additive

To determine the specific constituent makeup required more digging into the patent. The polymer is made up of three monomers in various ratios for different “polymer packages”. The monomers are lauryl acrylate, stearyl methacrylate and maleic anhydride and for the B20 “optimized package” they are mixed in a 1:2:0.5 ratio. The surfactant is made up of two esters: sucrose myristate and sucrose oleate at a 2:1 ratio. The ratio of polymers to surfactants is most likely 1:0.1 but could vary up to 1:0.5. From reading the patent, the ratios that were probably used in the additive sample are listed below (see Table 6.2 and Figure 6.35).

Table 6.2 – Percentage breakdown of MLA additive components

Additive Package	100.0%
Diesel	75.0%
Active Additive	25.0%
Surfactant	2.3%
Sucrose Myristate	1.5%
Sucrose Oleate	0.8%
Polymer	22.7%
Lauryl Acrylate	6.5%
Stearyl Methacrylate	13.0%
Maleic Anhydride	3.2%

When the MLA additive mixture settles, a sediment forms. In the patent it mentions that maleic anhydride is insoluble in diesel, so it may be that polymer dropping out. The patent also mentions the surfactants are not dissolvable in biodiesel but are in diesel. After centrifuging the additive, the solid portion was 1.4% mass percent.

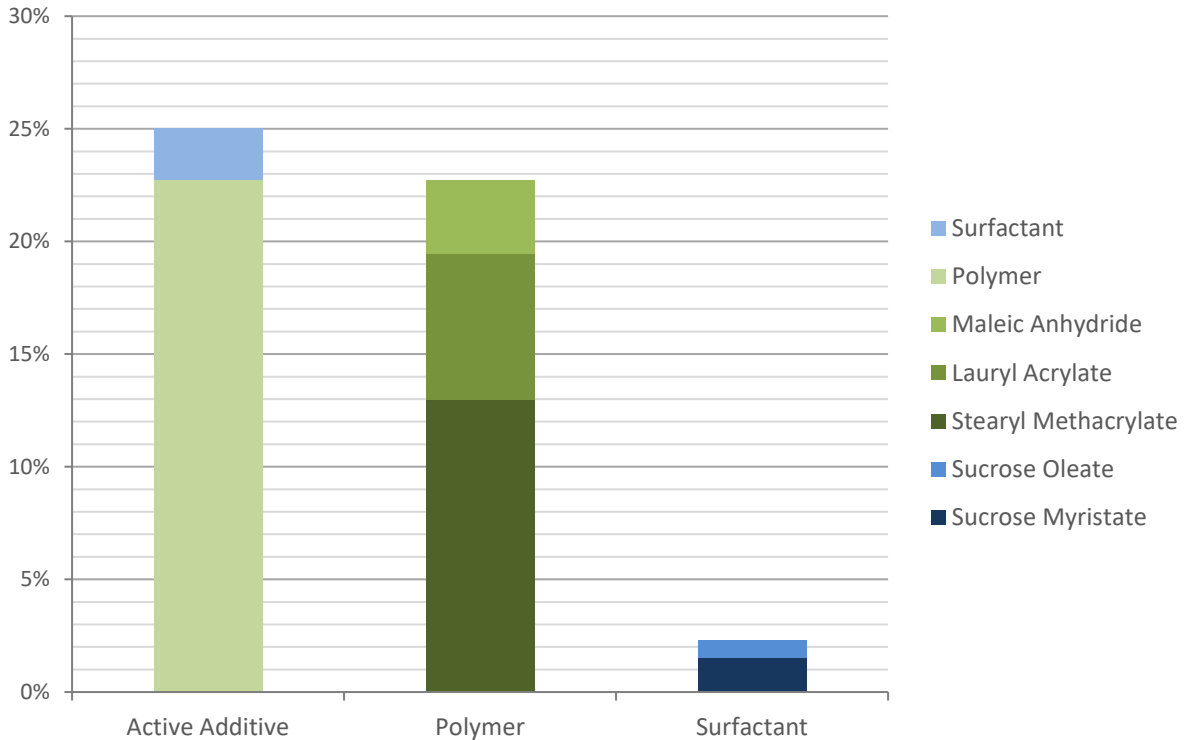


Figure 6.35 – Breakdown of polymer and surfactant constituent percentages

The solid portion was mixed in biodiesel and did dissolve, but settled out of petroleum diesel, making it likely that this was the maleic anhydride monomer. The most likely components

for the solid precipitate of the additive after comparing the weight percent with Table 6.2 is either sucrose myristate or maleic anhydride. While the weight percent measured for the solid portion was 1.4% instead of 3.2%, it is possible that some of the maleic anhydride stayed in solution or was not completely separated. A quick test with the solid and liquid portions of the separated additive had some interesting results.

The solid component of the MLA additive had no effect on CP and increased CFPP by 1.7°C at 1% dosage, so no additional tests were conducted with the solid portion. The liquid component had quite the opposite effect. At the 1% dosage CP dropped 2.0°C and CFPP dropped 1.3°C. They both had their maximum effect at a 3.1% dosage with a 3.0°C CP drop and 2.3°C drop in CFPP. In comparison, the complete additive package at a 3.0% dose reduced CP by 2.6°C and CFPP by 3°C. All of this is charted below in Figure 6.36.

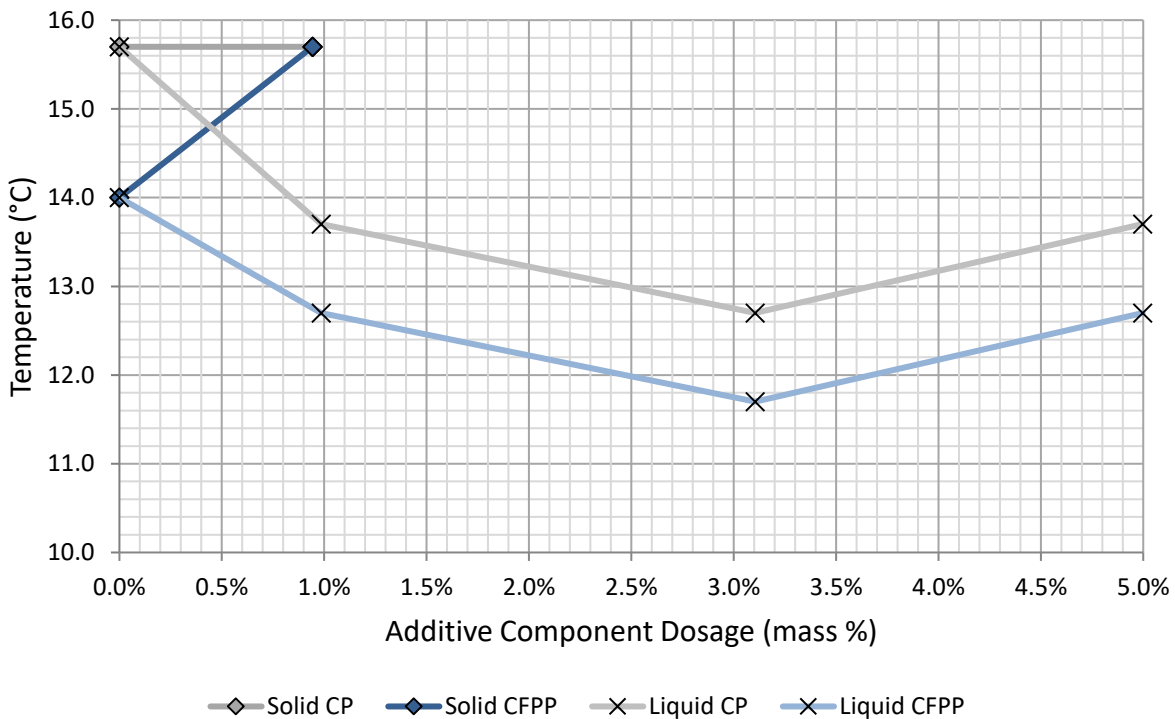


Figure 6.36 – CP and CFPP reduction from solid and liquid portions of MLA additive

These results seem to contradict the assumption that the solid component is a polymer, since it had no effect on CP, but maleic anhydride could be ineffective by itself. Potentially it was a

surfactant since the CFPP temperature reduction with the liquid portion was diminished after it was removed. Either way, the liquid portion outperformed the complete additive in regard to CP reduction making further investigation valuable.

6.6 Conclusion

After testing a lot of different additives, we found out a few things. First, none of the additives that were designed to improve the cold temperature properties of petroleum oil did much to reduce CP in CME/TME blends. Likewise, additives formulated to improve CP, CFPP, PP or CSFT for other methyl esters besides TME, had little to no effect on TME CP. The only additives that had any effect $>1^{\circ}\text{C}$ on TME CP were Viscoplex 10-530 and the MLA additive, both of which were specifically designed for TME CP reduction. A side-by-side comparison of the two (Figure 6.37) shows a clear advantage to using the MLA additive especially above 1% dosage and also for 50% CME blends.

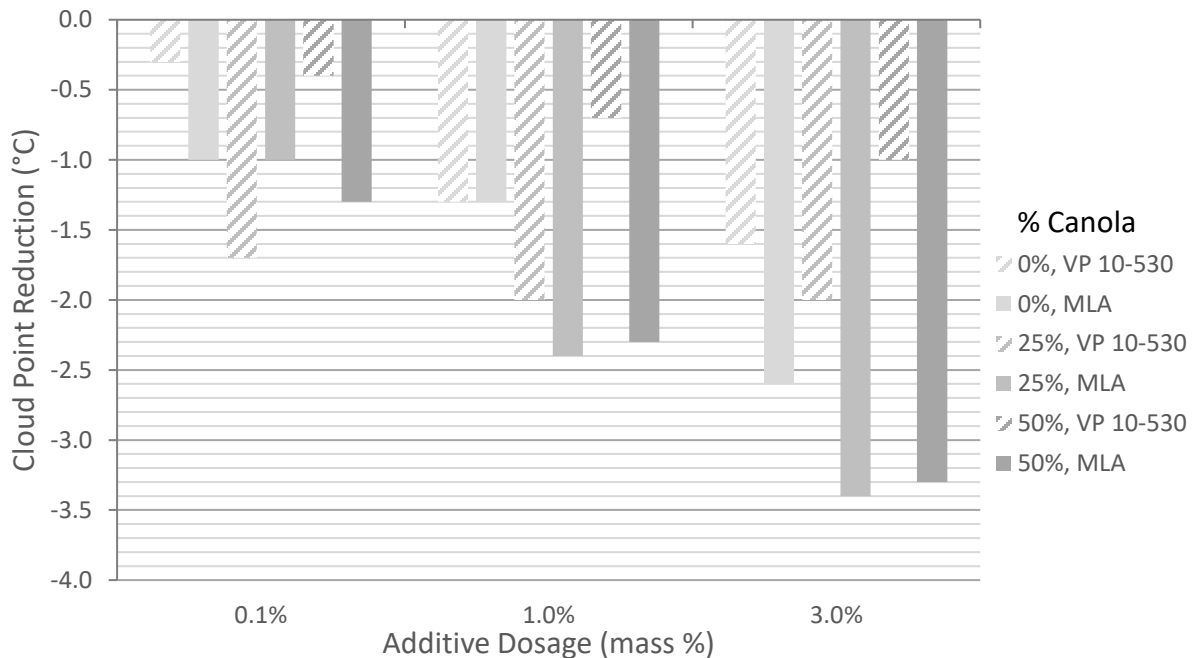


Figure 6.37 – Comparison of CP effect of Viscoplex 10-530 and MLA additives in CME blends

There are two things to note with the MLA additive. First, additional CP reduction could occur beyond the 5% dosage, but the additive would need to be formulated without diesel to verify that the diesel is not reducing the CP. Second, the MLA additive had even more impressive CFPP reductions than the CP reductions. This is likely due to the inclusion of surfactants in the additive package that are designed to “decouple” CFPP from CP to reduce CFPP further, which may not be necessary for CP reduction alone.

Without knowing the cost of the MLA additive it is hard to compare whether MLA or Viscoplex 10-530 would be more economically advantageous. If the prices are on par, or if more than a 2°C CP reduction is desired, MLA is the better choice. Because of its limitation in reducing CP, the MLA additive is best suited for small CP changes or to get the last 2-3°C after using blending or fractionation to get close to the desired CP.

One other thing to note about these additive tests is that all of these tests used CME/TME blends besides Infineum’s R511 which was also blended into SME. It could be beneficial to rerun tests in SME/TME blends, with the additives designed for FAMES, to see if there is significant CP reduction. The Viscoplex 10-530 and MLA additives are the primary two candidates to test with SME/TME blends due to their success in reducing CP in CME/TME blends.

Chapter 7: Blending with Diesel Fuel

7.1 Diesel Blended with Tallow Biodiesel

While the foremost goal of this research was to reduce the CP of tallow biodiesel to be on par with SME or CME, eventually all of those biodiesel mixtures would be blended with petroleum diesel. Therefore, characterizing the TME/diesel blends is helpful for a TME producer. If additives have a synergistic effect on CP when mixed with diesel fuel, there is a chance a higher CP TME mixture could have a similar final CP when blended with diesel compared with SME or CME blended at the same ratio in diesel.

The diesel fuel used for these tests had a CP of -18.3°C and a CFPP of -16.7°C. In Figure 7.1 below, the CP and CFPP temperatures for TME/diesel blends are graphed.

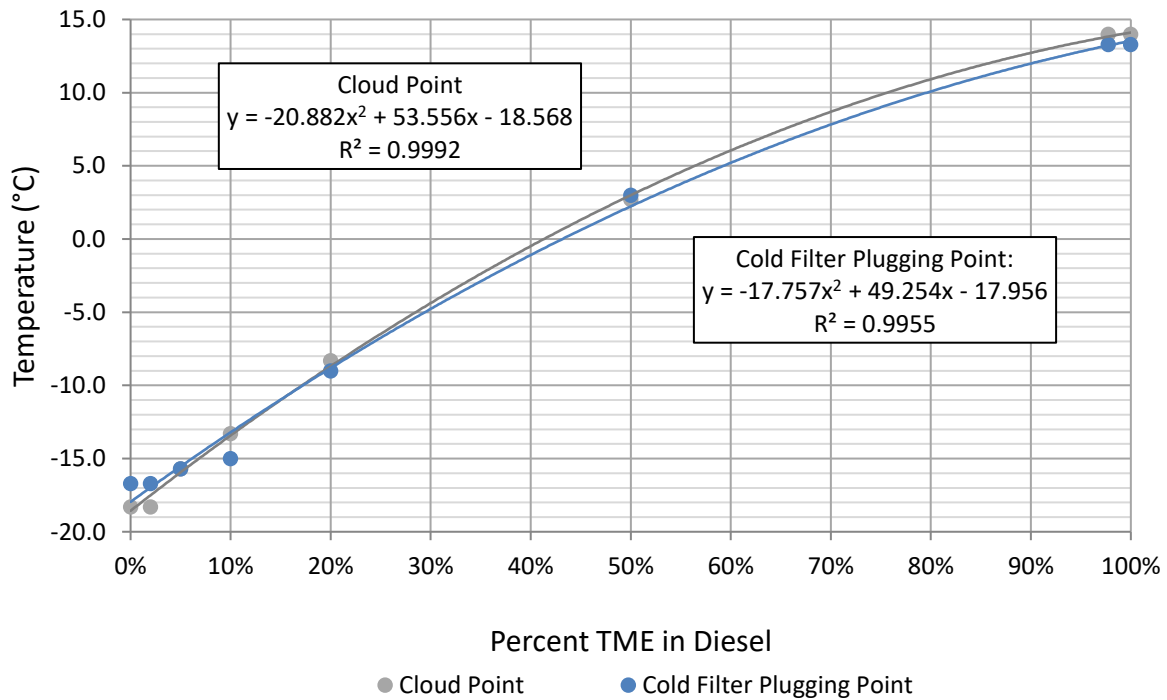


Figure 7.1 – CP and CFPP for TME/diesel blends with best fit equations

Two quadratic equations were able to correlate well enough to the empirical data points that the cloud point's R² value was 1.00 and the R² for cold filter plugging point was also 1.00. A close look at the CPs and CFPPs show no change between B0 and B2 as well as B98 and B100. The CP and CFPP temperatures for the TME/diesel blends are listed below in Table 7.1.

Table 7.1 – Table of CP and CFPP for TME/Diesel blends

	Diesel	B2	B5	B10	B20	B50	B98	B100
Cloud Point	-18.3	-18.3	-15.7	-13.3	-8.3	2.7	14.0	14.0
Cold Filter Plugging Point	-16.7	-16.7	-15.7	-15.0	-9.0	3.0	13.3	13.3

7.2 MLA Additive in TME/Diesel Blend

Once the TME/diesel blends were characterized for CP and CFPP, the next step was to add in the MLA additive. The TME/diesel blends from the previous section were reused and had the MLA additive mixed into the TME/diesel blends at doses of 0.1%, 1%, 3% and 5%. Looking at Figure 7.2 shows a quick CP drop at 0.1% MLA with a more gradual drop continuing until a 5% dose. The additive appears to be more effective with higher quantities of diesel.

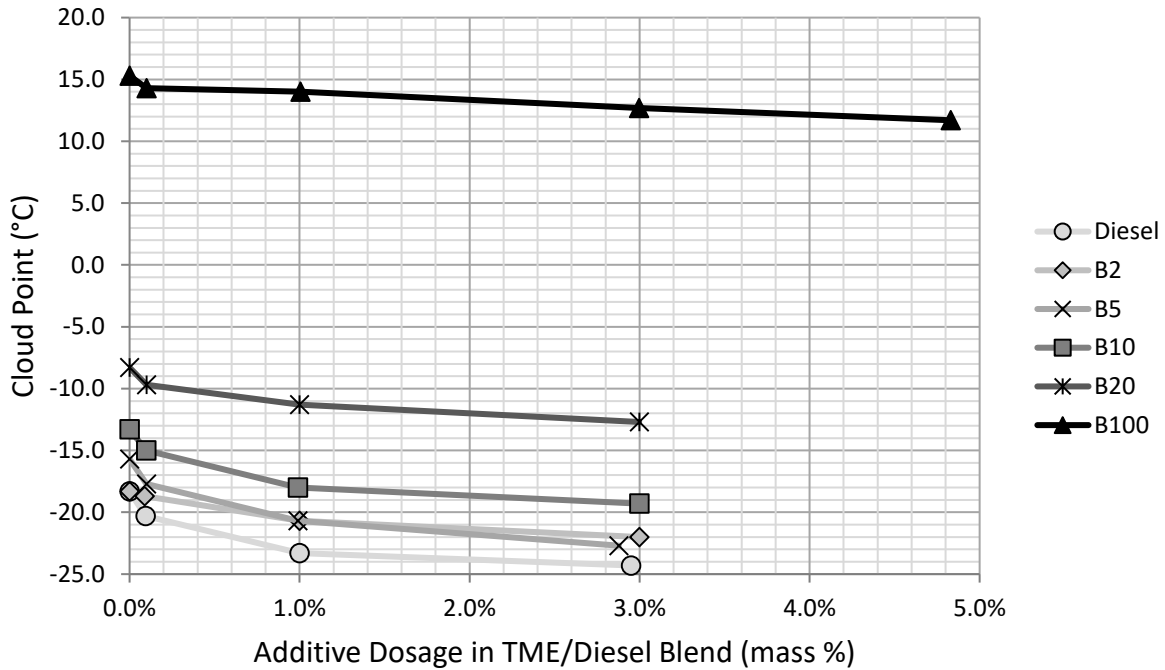


Figure 7.2 - CP effect of MLA additive mixed with various TME/diesel blends

The CFPP of the TME/diesel blends with MLA additive had similar trends (Figure 7.3), however, for B2, B10 and B20 the CFPP initially increased at a 0.1% dose, but then decreased with additional additive. The largest drops appear to be from 1.0% to 3.0% with B20.

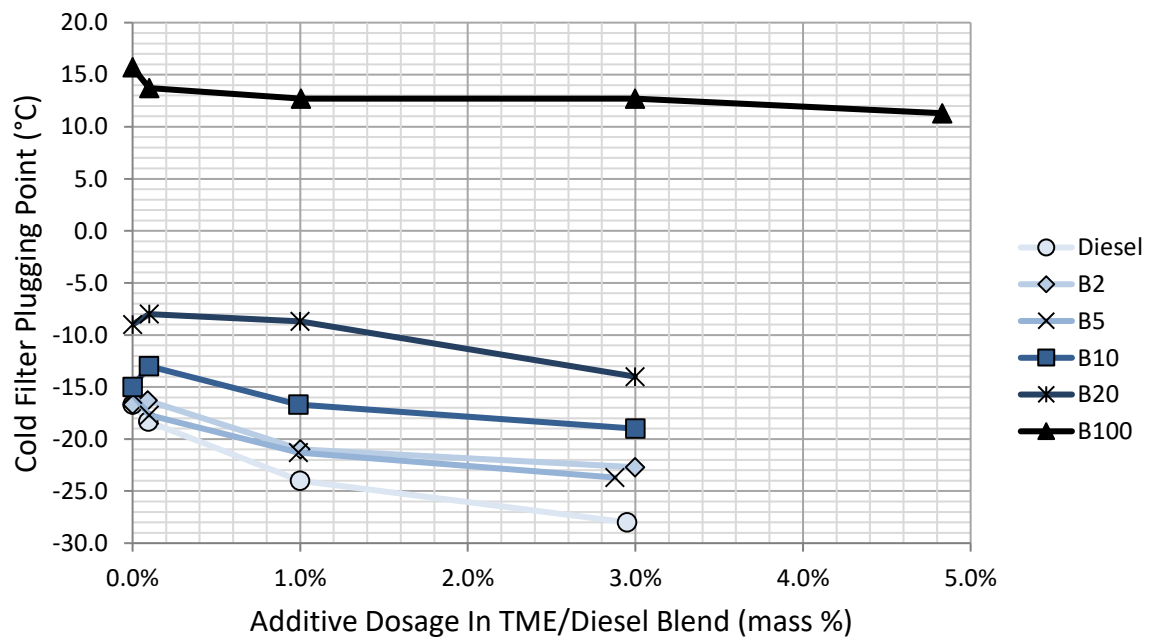


Figure 7.3 - CFPP effect of MLA additive mixed with various TME/diesel blends

The next two charts (Figure 7.4 and Figure 7.5) show the drop in CP and CFPP for each TME/diesel blend compared to 0% MLA additive. The largest CP drop realized is 7.0°C at a 3% dosage in B5. For B100, the addition of the MLA additive continues to drop the CP at a 3% dose, and even further at a 5% dose hinting at the possibility of further reducing CP at 5% dosage for the TME/diesel blends. The MLA additive is most effective with straight diesel, B5 and B10. Interestingly, the B2 blend performs worse than both straight diesel and B5.

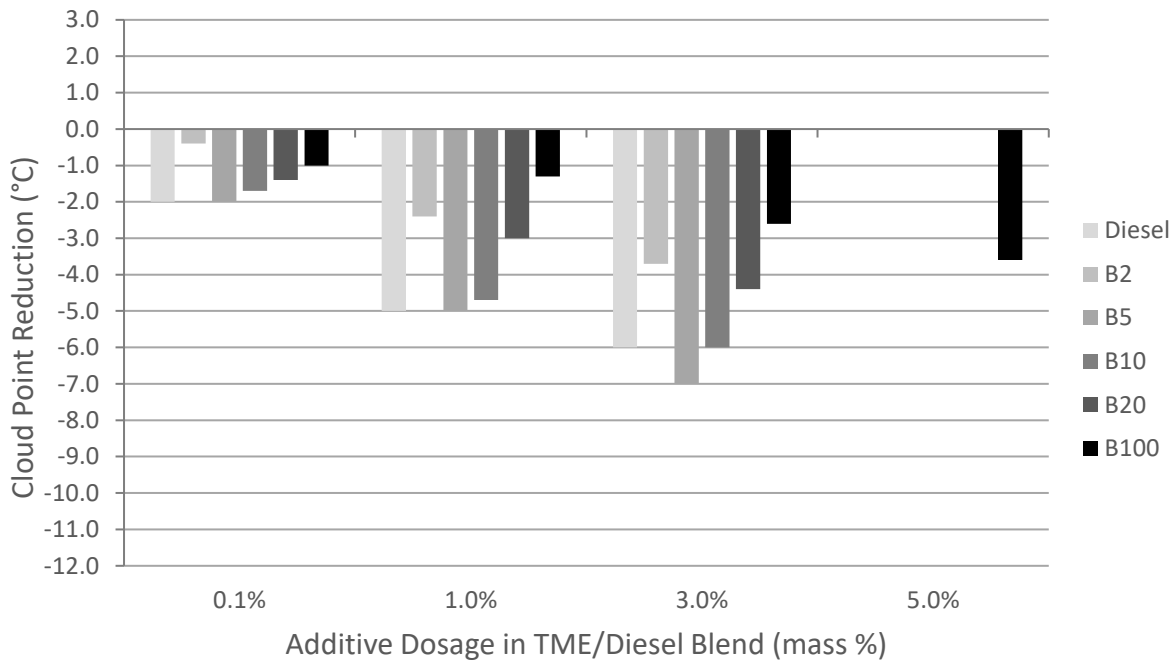


Figure 7.4 – CP reduction from MLA additive mixed with TME/diesel blends

Similar trends occur with CFPP, which also decreases with additional MLA additive up to 5% dosage. The most noteworthy difference is that the CFPP actually increases for some TME/diesel blends at a 0.1% dose. The maximum CFPP reduction of 11.3°C occurs with straight diesel at a 3% dose of MLA. The MLA additive works best for CFPP with straight diesel and B5.

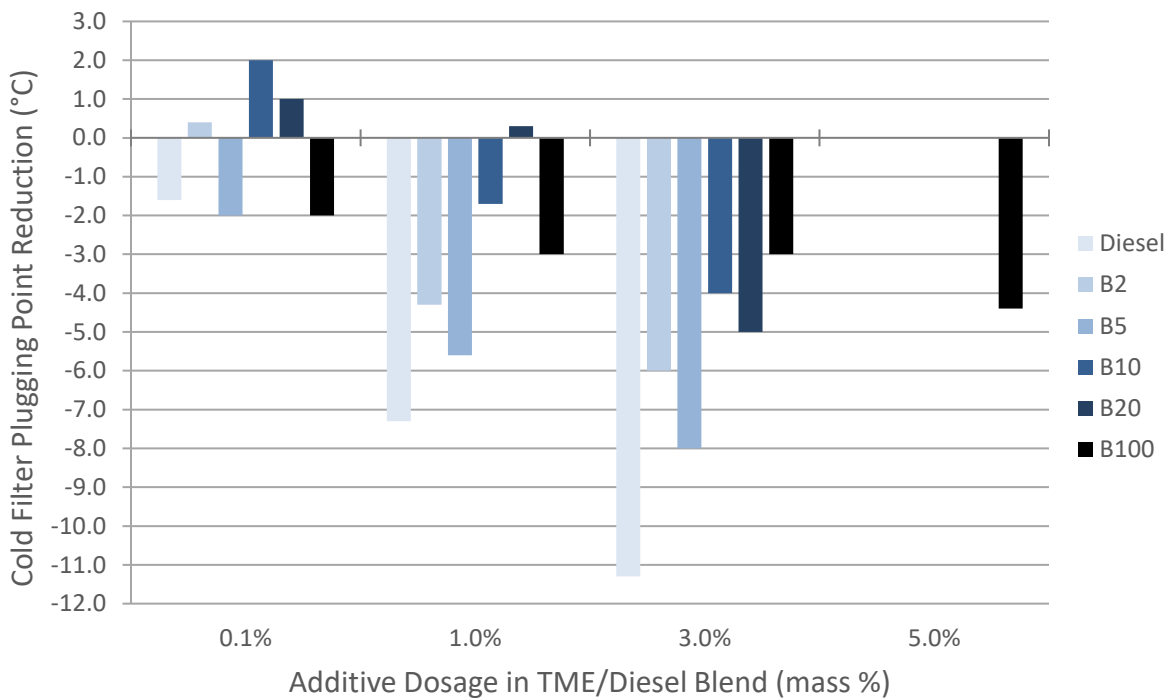


Figure 7.5 – CFPP reduction from MLA additive mixed with TME/diesel blends

As was done earlier with the Viscoplex 10-530 and MLA additive in CME/TME blends, the synergistic effect of the MLA additive with diesel blends was teased out by removing the additive’s CP drop at each TME/diesel blend from the CP reduction caused by the additive in B100 (Figure 7.6). For all but one case (0.1% MLA in B2), the MLA and diesel CP effects compounded and produced a greater CP drop than simply adding them together. The largest synergistic effect occurred with straight diesel, B5 and B10. B10 with 3% MLA had an additional 4.4°C CP reduction beyond the reduction from the B10 TME/diesel blend combined with the reduction from 3% MLA in TME. B2 had the smallest synergistic effect.

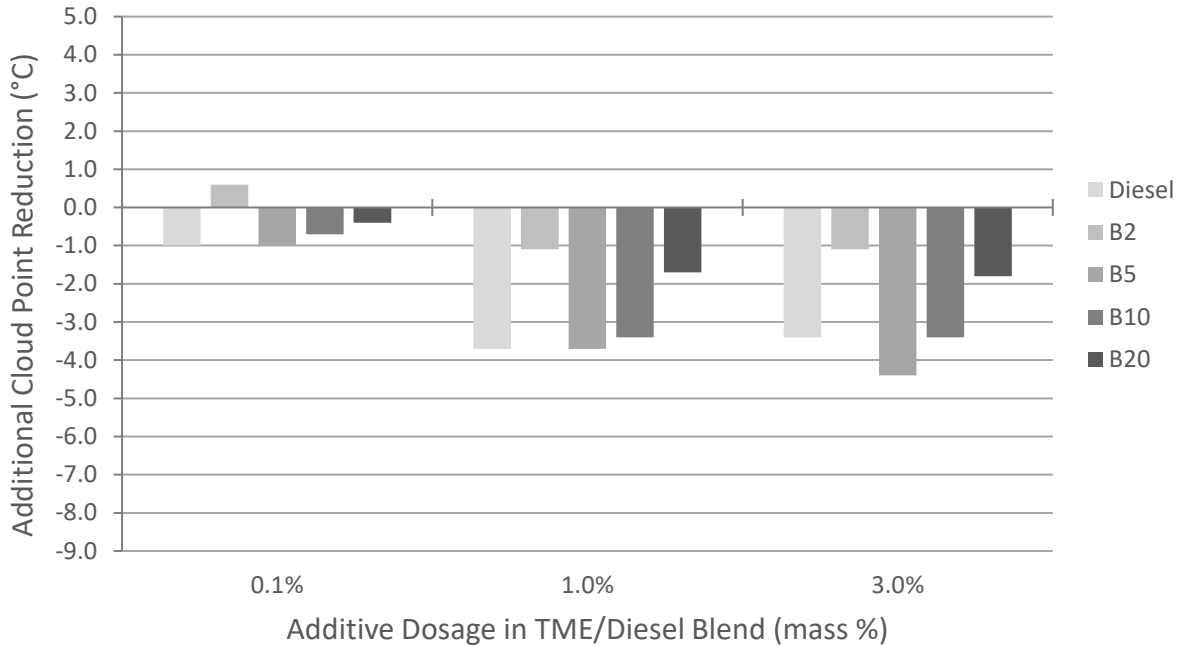


Figure 7.6 - Synergistic effect on CP from diesel blend interaction with MLA additive

The synergistic effects were not as consistent with CFPP, and at 0.1% MLA additive for all blends and at 1% additive for B10 and B20 it actually had a negative effect (Figure 7.7). However, the maximum additional CFPP was as high as -8.3°C for a 3% dose of MLA in straight diesel.

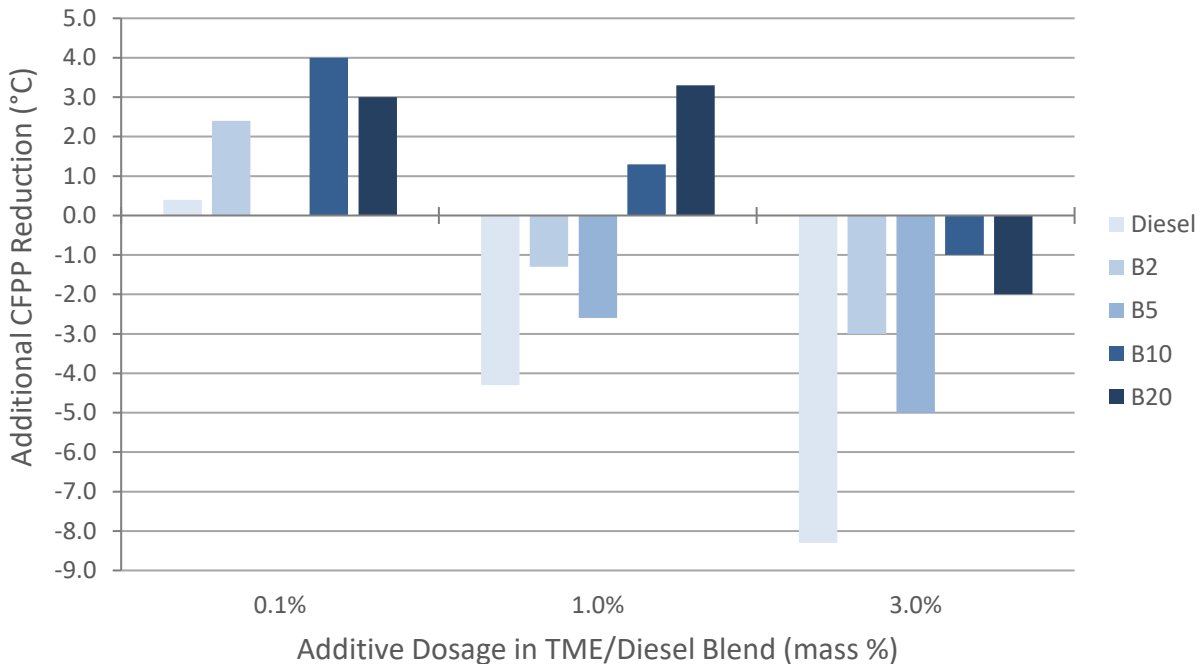


Figure 7.7 - Synergistic effect on CFPP from diesel blend interaction with MLA additive

7.3 MLA Additive in TME then Blended with Diesel

After completing all the prior tests in Section 7.2, of mixing MLA into TME/diesel blends, I realized that that information would not be very helpful for a TME biodiesel producer. Generally, a biodiesel producer would sell their TME with a declared CP to a distributor who would then blend it with diesel to the desired BXX blend. It is the biodiesel producer who would have incentive to reduce the CP of their TME, or at least show a distributor that when it is blended with diesel, the CP of the BXX blend will be on par with one made from SME or CME.

This next set of CP tests switched up the order of the previous set of tests. First, the MLA is mixed with the tallow at set dosages and tested at B100. Then, that TME/MLA mixture is blended with diesel fuel to make B20, B10, B5, or B2. In Figure 7.8, the 0.1% MLA dosage was a unreliable for reducing CP, with some instances raising the CP and others lowering it no more than 1.0°C. The addition of the MLA additive up to 3% in TME decreased the CP for all TME/diesel blends, up to 4.4°C at 3% MLA in TME blended at B5.

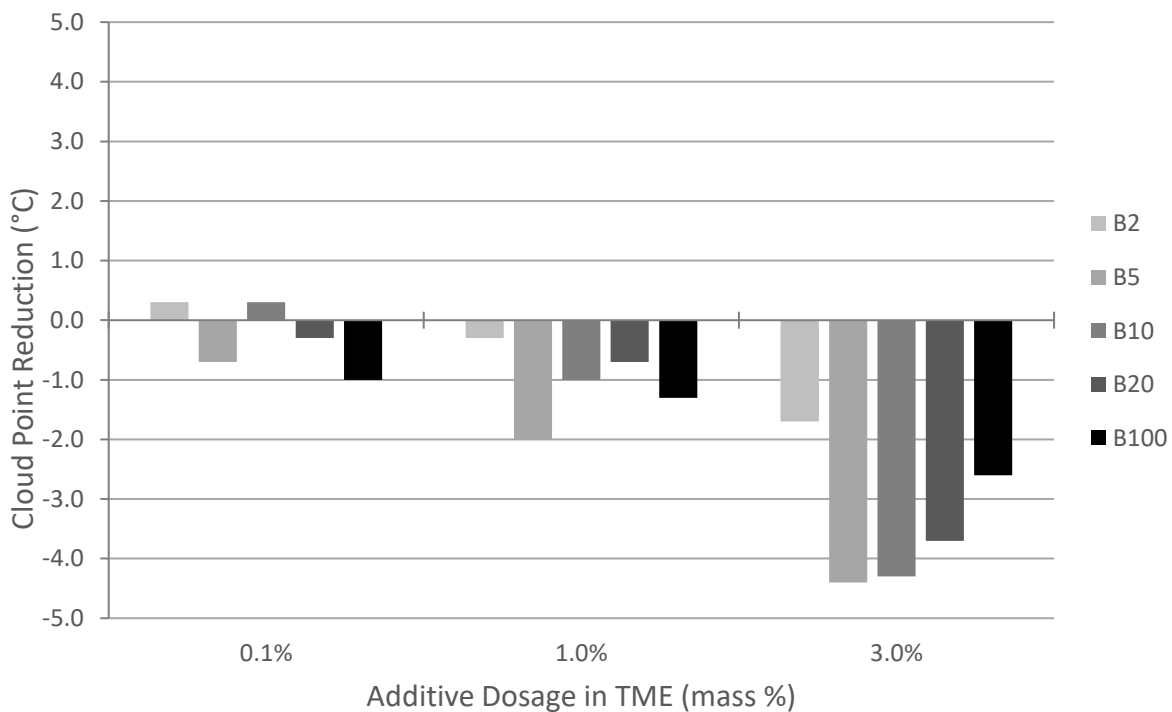


Figure 7.8 – CP reduction from MLA additive mixed with TME then blended with diesel

The CFPP was also unpredictable at 0.1% MLA as well as 1% MLA in TME. At 3% MLA in TME, all BXX blends realized a CFPP decrease, with the maximum of 3.6°C occurring with 3% MLA and a B5 blend (Figure 7.9).

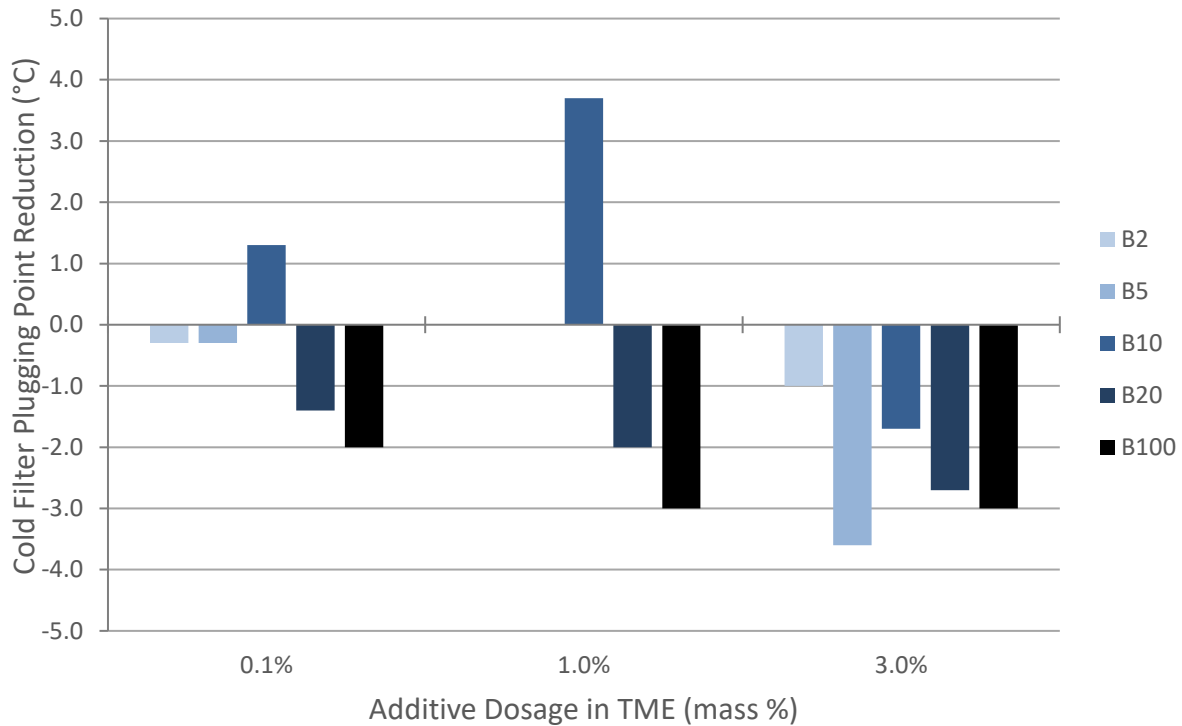


Figure 7.9 – CFPP reduction from MLA additive mixed with TME then blended with diesel

Once again we investigated the synergistic effect of MLA additive with diesel fuel, only this time with the MLA additive dosage referenced to its percentage in the TME, not the whole TME/diesel mixture. In Figure 7.10, at 0.1% MLA in TME, the CP was negatively affected by mixing MLA and diesel. At 1.0%, the results were varied, but mainly negative. By 3%, the results were mainly positive with the notable outlier being B2. The maximum additional CP drop was 1.7°C at B5 with 3% MLA in TME. Every CFPP test in Figure 7.11 had a harmful synergistic effect besides 3% MLA in TME blended at B5 which had a minimal reduction of 0.6°C. The worst instance occurred in a B10 with 1% MLA in TME and increased CP by 6.7°C. These trends are not surprising because a similar result occurred at low MLA dosages when mixed into TME/diesel blends. In these

cases, where MLA is mixed into TME then blended with diesel, the additive percent of the whole mixture is less - 1/5th for B20 and up to 1/50th for B2.

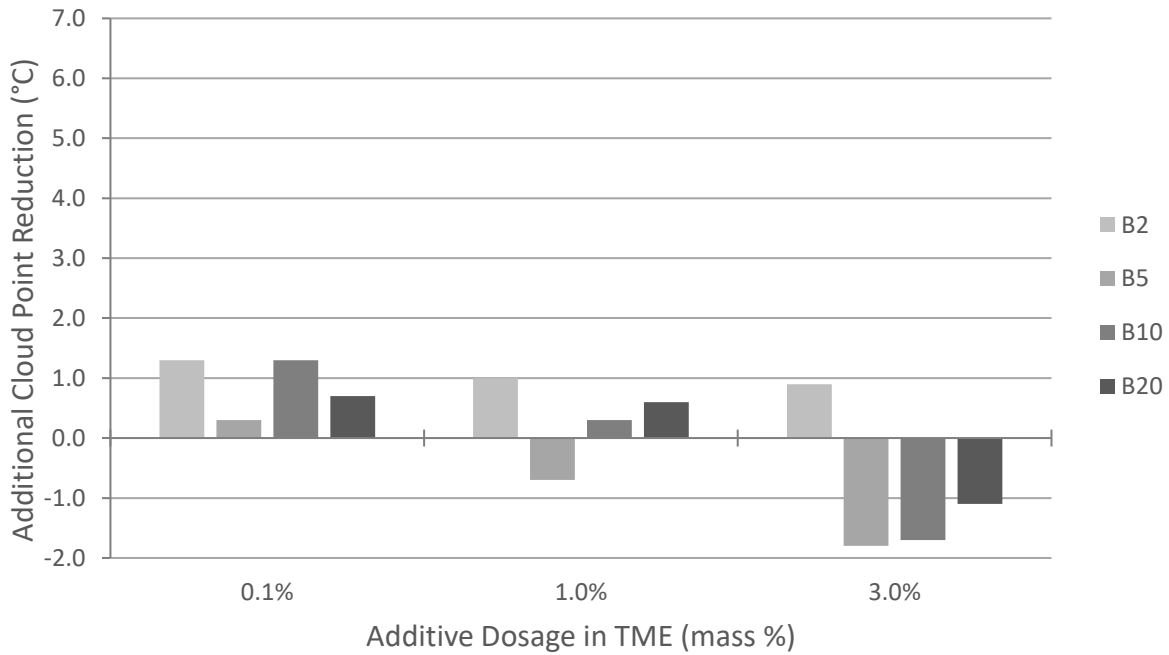


Figure 7.10 - Synergistic effect on CP from MLA additive in TME, then blended with diesel

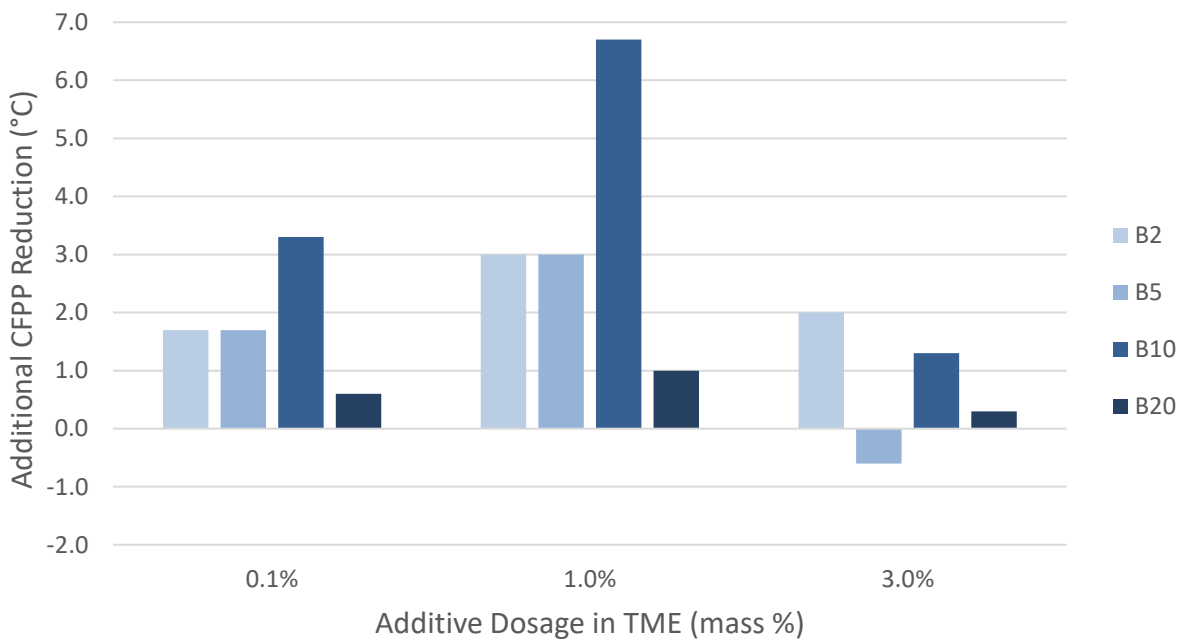


Figure 7.11 - Synergistic effect on CFPP from MLA additive in TME, then blended with diesel

Whether the MLA additive is mixed in as a percentage of the TME/diesel blend, or as a percent of the TME which is then blended with diesel, both can have the MLA dosage expressed as a percent of the whole. For the first set of data, nothing has to be calculated. For the tests that had the MLA dosage reported as a percent of the TME, it is simple multiplication. Take the dosage in TME and then multiply it by the percent of TME in the TME/diesel blend to get the percentage of MLA in the whole mixture. Charts comparing all of these data points can be found in Appendix J.

7.4 Conclusion

For a biodiesel producer who is using tallow as a feedstock, it is worth a look at using the MLA additive to reduce the CP of straight TME and blended in petroleum diesel. In a B10 blend the MLA additive was able to drop the CP by 7.0°C. Using MLA in the presence of diesel had a favorable synergistic effect, in some cases reducing CP by an additional 4.4°C past the reduction from the diesel blend and the additive in TME alone. The highest CP reductions happened at 3-5% doses of the entire mixture so there would have to be an economic analysis conducted to see if the cost would be worth it. The cost of the MLA additive and the diesel would need to be compared to the cost of SME or CME required to reach the same CP at that BXX blend. Further testing can always be done. In this case, adding a third variable by blending MLA in CME/TME or SME/TME blends that were then mixed into BXX blends with diesel would be necessary for a complete economic analysis for any producer seeking to use these methods.

Chapter 8: Economic Comparison of CP Reduction Methods

8.1 Economic Motivation to Tallow Research

In order to approach this next section, which considers the economics of tallow CP reduction, the context of this research should be restated. Sun West Biofuels funded this research because they saw an opportunity to produce biodiesel, with the readily available and inexpensive feedstock source of tallow, due to the large slaughterhouses in the Front Range. The major obstacle was the CP of TME is significantly higher than SME and CME, the two major feedstocks used to make biodiesel. While this research can aid other pursuits, the end goal in this situation was to inform an economic decision and it would be remiss to not include that information in this paper.

In order to compare these diverse CP reduction methods, their cost needed to be reduced to a standardized metric. A direct comparison required that each of these methods was reduced to the cost it takes to reduce a gallon of completed biodiesel by 1°C (\$/gal/°C). Because only the CP reduction methods are being compared, things that are common between them need not be quantified, like overall capital costs and regular operating expense.

It is also important to note that with all economic decisions, what holds true at one point in time is not necessarily true at another. While the hard fractionation, blending, and additive CP data does not change, the price inputs are heavily dependent on the commodities market, causing a very fluid economic outlook.

8.2 Distillation Fractionation Standardized Cost

The main drivers of the cost of distillation fractionation are heating costs and yield loss, as well as the amortized capital costs of the distillation columns. The first two costs will be considered

but the amortization will be left for future analysis. Determining the \$/gal/°C for distillation fractionation requires the input cost of tallow (\$/gal), the cost of natural gas or other heating fuel (\$/Btu), the price for selling any removed methyl esters (\$/gal), and the initial and desired CP temperatures.

First, the heating cost needs to be calculated. With distillation fractionation, all of the TME would need to be heated so this is a fairly simple calculation. The energy it takes to heat a gallon of TME (kBtu/gal) can be calculated given the percentages of the major FAMES (MP, MS and MO), their specific heats, and their enthalpies of vaporization (since they must all boil), as well as the preheated temperature of the FAMES entering the column and the boiling temperatures of each FAME at the column's reduced pressure. According to the Aspen model prepared by Dr. T. Gordon Smith, the preheated temperature coming into the column would be 300°C with the temperature of the distilled components at 572°C under a reduced pressure of 2 psia [39]. The heating value per gallon is multiplied by the cost of energy (\$/kBtu) to find the cost it takes to heat a gallon of FAME for distillation fractionation.

The next step is to calculate the cost due to the loss of yield. With the initial CP and the desired CP given, the change in CP can be calculated. Then the CP change can be subtracted from the model's initial CP (13.3°C in Figure 8.1) to find the adjusted final CP in the model. With the adjusted final CP, Figure 8.1 below, can be used to find the yield with a 4:1 MS/MO carryover ratio at that CP. To optimize yield, this model first mimics removing only MS until it reaches the eutectic point around 10°C. At that point, the model relates the yield if MP and MS were both removed to maintain the assumed empirical eutectic point at 82%.

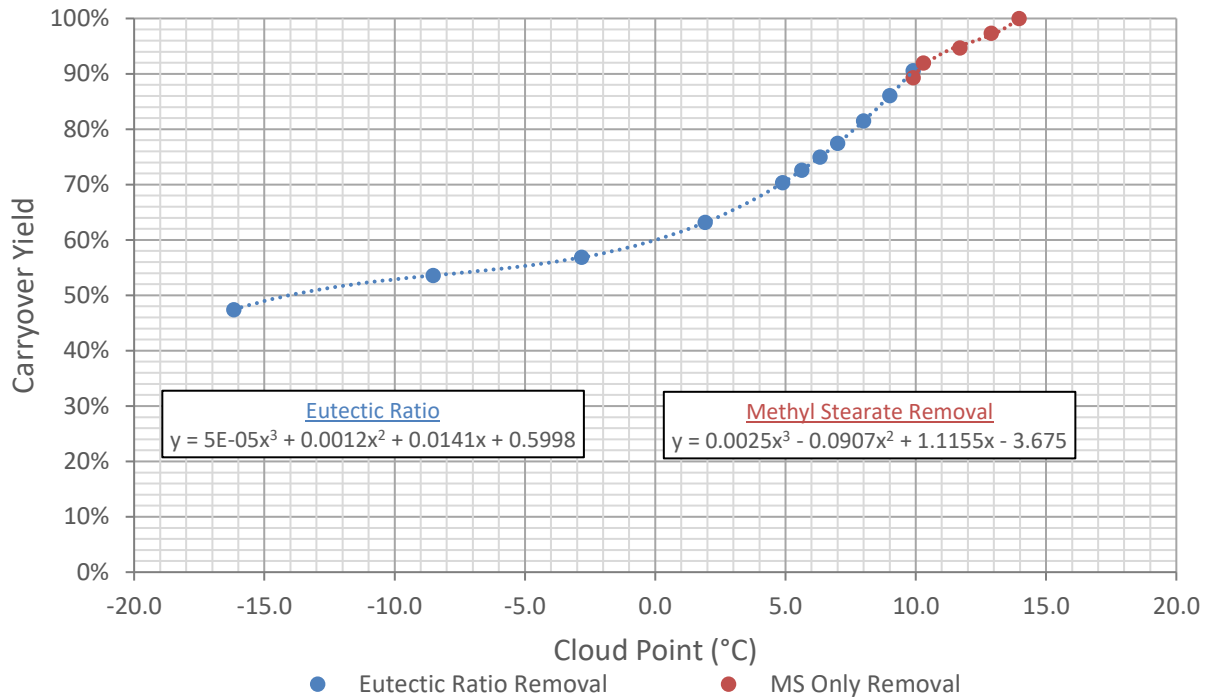


Figure 8.1 – Model for finding fractionation yield from desired CP with best fit equations

Once the yield is determined from the model, the “additional cost” of fractionation (\$/gal) can be determined by first finding the “real cost” of the tallow by dividing the purchase price (\$/gal) of tallow by the yield. Subtracting the purchase price from the “real cost” results in the “additional cost” of fractionation (\$/gal). To account for any offset from selling the fractionation byproduct, the yield loss is multiplied by the price it is sold for to find the “byproduct price”. The total cost (\$/gal) is simply the energy cost (\$/gal) + the yield loss cost (\$/gal) – the byproduct price (\$/gal). Once the total costs is calculated, it is then divided by the CP change to find the \$/gal/°C as demonstrated in Equation 8.1 below.

$$\$/gal/°C = \frac{(Heating \$/gal) + (Yield Loss \$/gal) - (Byproduct ME \$/gal)}{\Delta CP}$$

Equation 8.1 – General equation to find standardized cost of fractionation

8.3 Crystallization Fractionation Standardized Cost

Crystallization fractionation was not extensively considered in this research so its economic analysis will be a little less defined. Overall, it had a similar model as distillation fractionation. The inputs would be tallow cost (\$/gal), FAME byproduct price (\$/gal), electricity costs (\$/kWh), and the initial and desired CPs.

The cooling costs would first need to be calculated on a \$/gal basis. The cooling load would need to apply to the whole of the TME flow, accounting both for the specific heat for all FAMEs and the enthalpy of fusion for the FAMEs that solidify. Once the required energy change is determined, actual energy requirements (kWh/gal) would need to be calculated knowing the efficiency of the chillers. From there the energy cost can be found (\$/gal).

Like distillation, the next step would be to determine yield based on the CP. Only this graph would be much closer to the “ideal” yield since there would not be any MO carryover with the MS. The total cost would once again be determined with energy costs (\$/gal) + the fractionation (yield loss) cost (\$/gal) – the byproduct price (\$/gal). From there the standardized cost (\$/gal/°C) can be found by dividing by the CP change.

If there is any MP/MS carryover with crystallization, that small fraction could be run through a single distillation column and separated quite easily without much energy costs compared to distilling the whole product stream. The same steps as fractionation would be followed to find the “additional cost” from the yield loss.

The main reason we did not investigate crystallization fractionation was due to the high costs of chilling 60 MGY. However, at that time we did not consider the fact that the temperature differential from ambient temperature to 14.5°C, where MS starts to precipitate, is much less than heating the product stream by 272°C to fractionate using distillation [39]. We also did not consider that there would be MS/MO carryover issues with distillation that would not occur with crystallization. Because of those two reasons, it would be worth taking a second look and doing a

more detailed economic analysis into crystallization fractionation versus distillation fractionation of TME, especially considering the carryover yield losses.

8.4 SME Blending Standardized Cost

After fractionation, the next CP reduction method that was investigated was blending. From an economic standpoint, blending TME with SME or CME is a little ironic. The economic feasibility of producing biodiesel from tallow is dependent on its cost in comparison to SME and CME. The potential with SME/TME blends is if a biodiesel distributor would accept a biodiesel with a CP higher than SME, but not as high as 14.5°C. Another scenario that could maintain the cost differential, would be blending to reduce the CP initially, then using an additive to complete the drop to the desired CP.

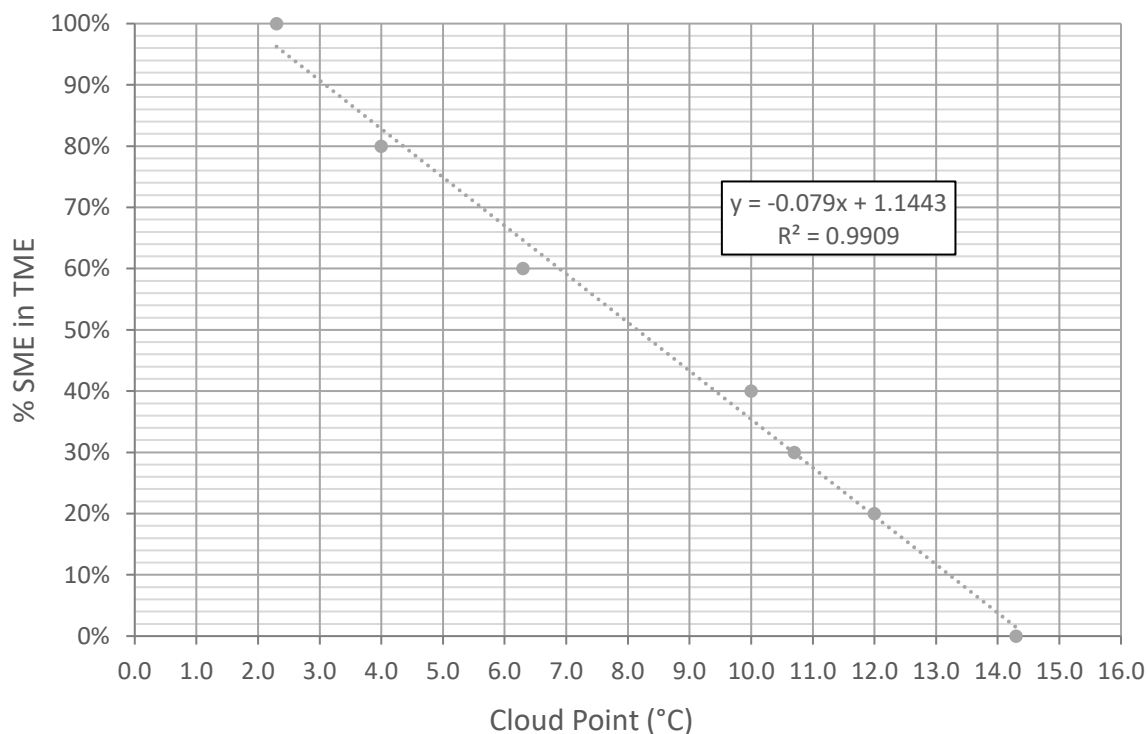


Figure 8.2 – Correlation between CP and SME/TME blend with best fit equation

Determining the standardized cost of blending SME in TME is fairly simple. The inputs are the \$/gal for tallow and for soy, and the initial and final CPs. Like with fractionation, the CP is converted to a “CP drop” which is then subtracted from the model’s initial CP (14.5°C for Figure 8.2) to find the “adjusted target CP”. With the “adjusted target CP” the SME/TME blend can be determined from Figure 8.2 above.

From there, finding the standardized cost is simple. The percent of SME is multiplied by the difference in SME and TME price. That is all divided by the CP reduction to get the \$/gal/°C for SME blending (Equation 8.2).

$$\$/gal/°C = \frac{\% SME * (\$/gal SME - \$/gal TME)}{\Delta CP}$$

Equation 8.2 – Standardized cost for SME/TME blending

8.5 CME Blending Standardized Cost

Determining the standardized cost of CME blending is exactly the same as with SME. However, it is a different CP versus CME/TME blend graph presented in Figure 8.3 below.

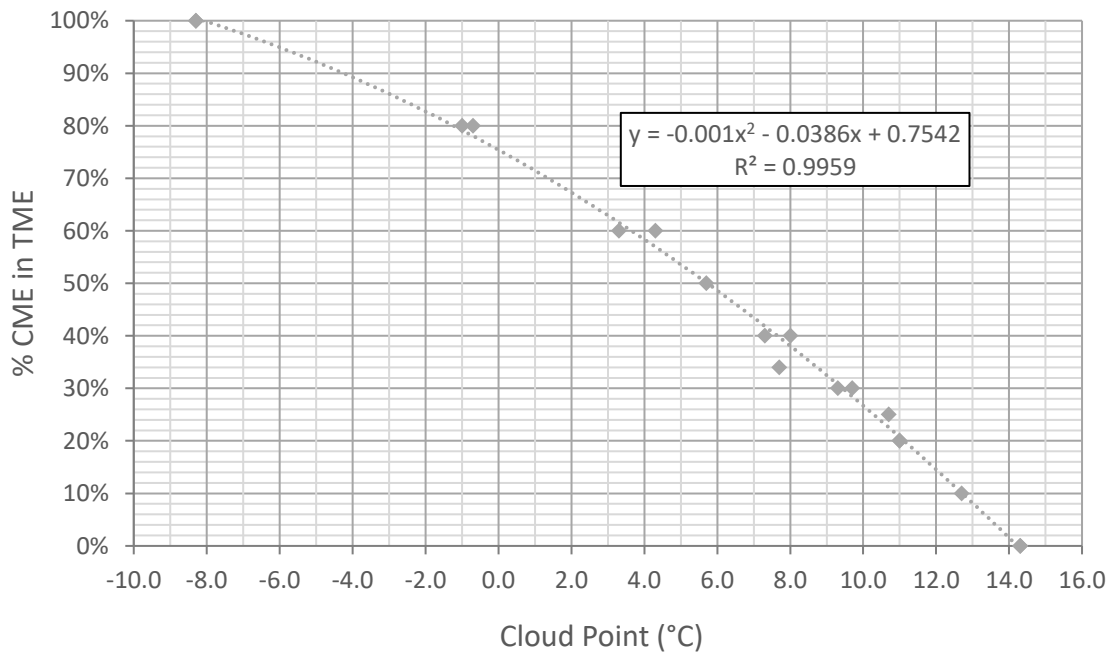


Figure 8.3 – Correlation between CP and CME/TME blend with best fit equation

In the case of CME, instead of a linear fit like SME, it is a quadratic equation that fits best. As explained in Section 5.3, this is likely due to the logarithmic relationship between the CP of a mixture and the mole fraction of the high melting point constituents. The equation to calculate the standardized cost for CME/TME blending is presented below in Equation 8.3.

$$\$/gal/^\circ C = \frac{\% CME * (\$/gal CME - \$/gal TME)}{\Delta CP}$$

Equation 8.3 - Standardized cost for CME/TME blending

8.6 MLA Additive in TME Standardized Cost

Calculating the standardized cost of the MLA additive in TME is straightforward and similar to blending. The inputs are simply the MLA additive \$/gal, and the initial and final CPs.

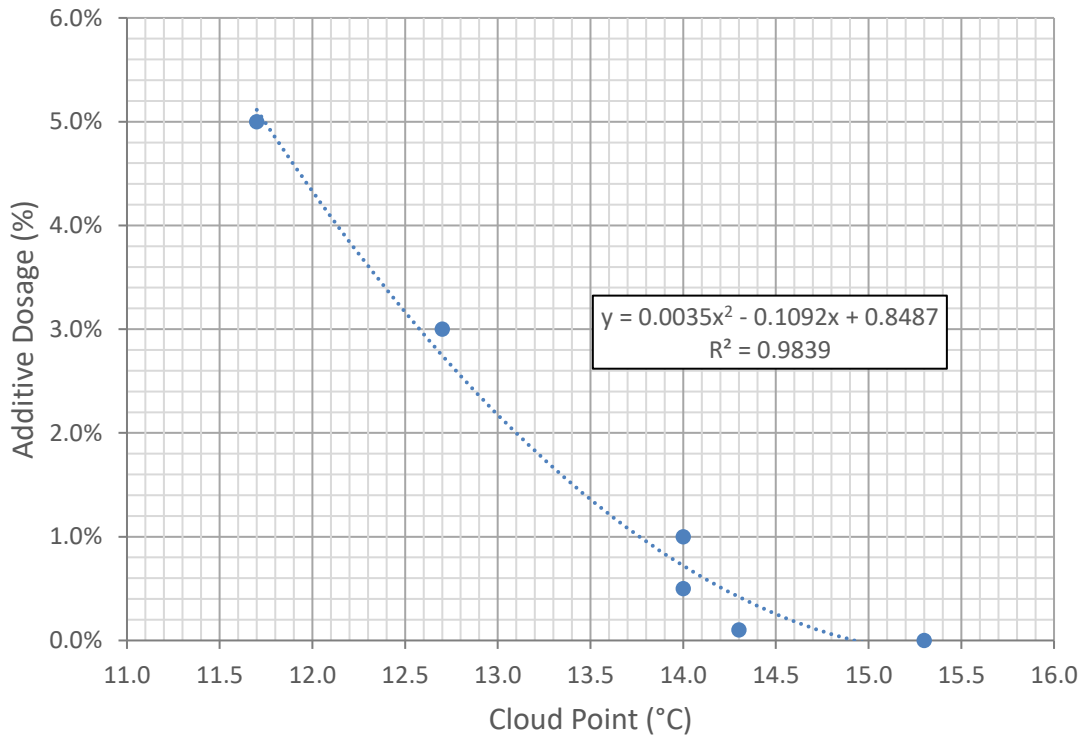


Figure 8.4 - Correlation between CP and MLA additive dosage with best fit equation

Once again the “adjusted target CP” is subtracted from the model’s initial CP (14.7°C for Figure 8.4) to find the final CP, then the additive dosage at that CP is found using Figure 8.4. The percent of active polymer is determined to be 0.25/1.1 times the additive dosage (based off of the constituent percentages in Table 6.2), taking into account the additive dosage includes the diesel fuel and the surfactants which do not reduce CP. The standardized cost is calculated in Equation 8.4 below.

$$\$/gal/^{\circ}C = \frac{(Additive\ dosage * 0.25/1.1) * (Additive\ cost\ \$/gal)}{\Delta CP}$$

Equation 8.4 - Equation to find the standardized cost of MLA additive in TME

8.7 MLA Additive in CME/TME Blends Standardized Cost

The next step of determining the standardized cost of MLA additive in CME/TME blends is a little more complicated. The inputs are the TME, CME, and MLA additive prices (\$/gal), and the initial and final CP. Due to a multi-variable matrix, one simple equation will not suffice. Because of the limited data points, the model can only predict either at 0%, 25% and 50% CME blends along varying additive dosages or at 0.0%, 0.1%, 0.5%, 1.0%, 3.0% and 5.0% additive dosages and along varying % CME.

The general equation to calculate the cost of varying MLA dosage for specific CME blends is the same as Equation 8.4 but uses the correlations between CP and additive dosage found in Figure 8.5 below. The equations are solved for any of the CME/TME blend and MLA additive dosage combinations that successfully reaches the target CP.

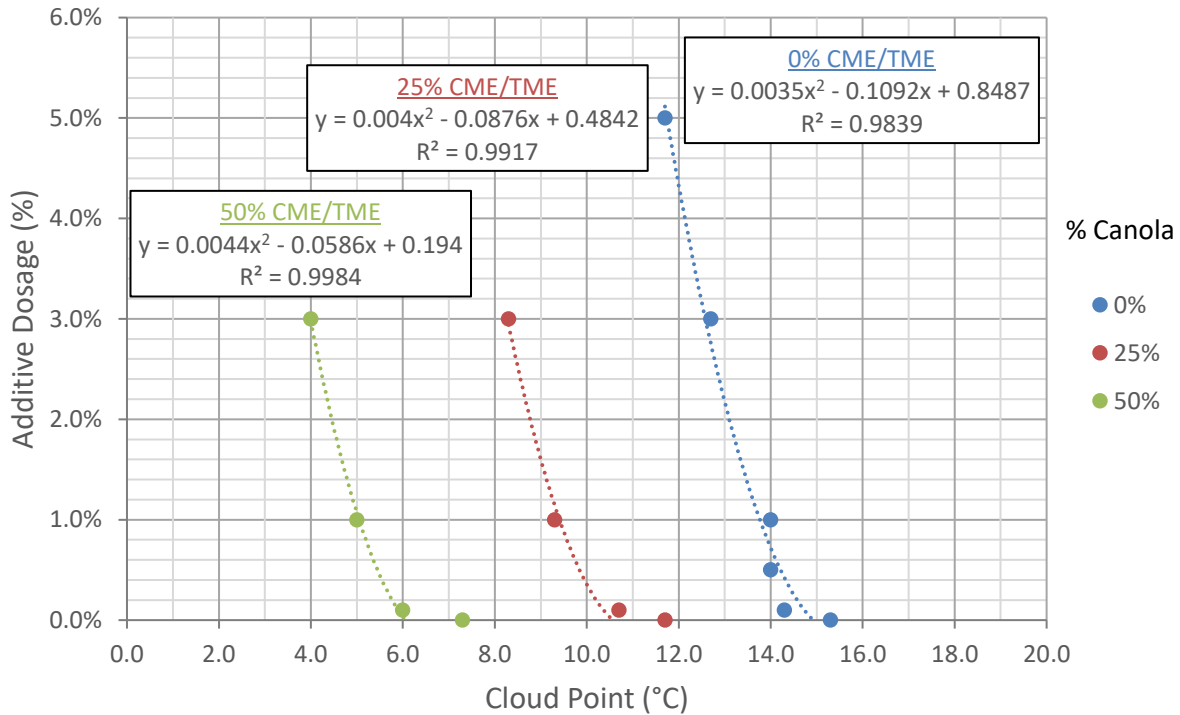


Figure 8.5 – Correlation between CP and MLA additive dosage at different CME/TME blends

Similarly, the equations to calculate the cost for varying CME blends with distinct additive dosages, is identical to the CME blending cost equation (Equation 8.3), just repeated at the six different additive dosages. The correlations relating CP to CME blend at the six additive dosages are below in Figure 8.6.

Using the “adjusted target CP” for each of those nine equations in Figure 8.5 and Figure 8.6, the standardized costs for the CME blend and the MLA dosage are calculated individually, then added together to get the total \$/gal/°C for each case. The overall model then compares the standardized cost for those nine different possibilities, chooses the minimum cost, and reports the additive dosage, CME/TME blend and the standardized cost for that case.

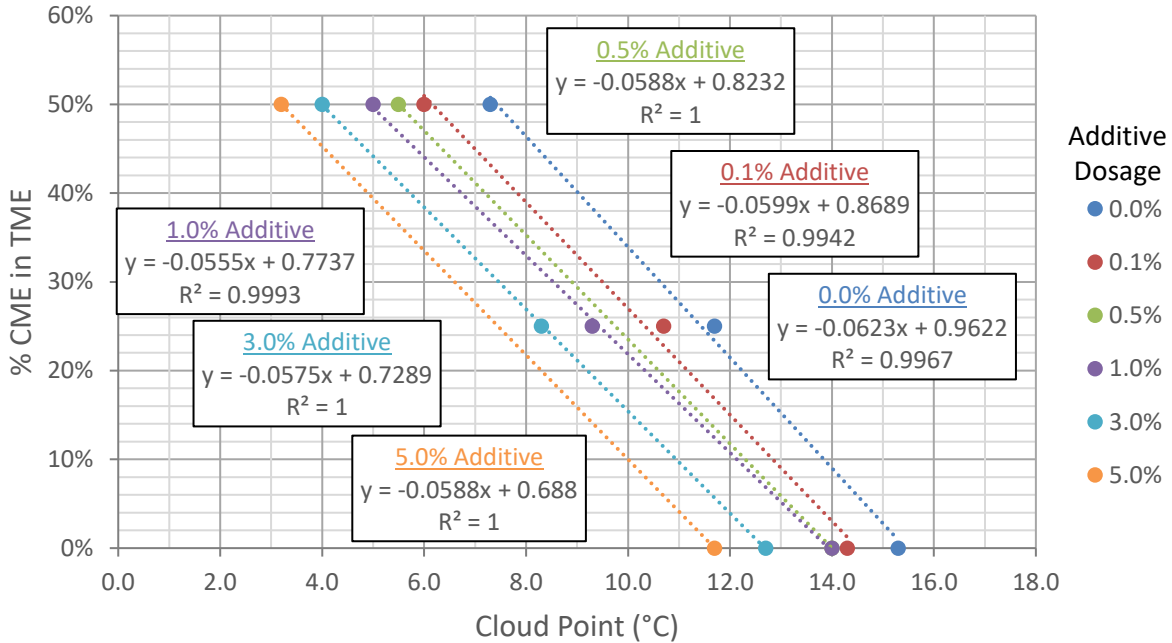


Figure 8.6 – Correlation between CP and CME/TME blends at different MLA additive dosages

8.8 Economic Decision Making for Multiple Methods

Because there are a number of pathways to achieve the same CP, each method must be simplified to a standardized \$/gal/°C to allow comparison between each method. Then, the method with the lowest \$/gal/°C should be implemented. Furthermore, a master model needs to allow real time pricing updates to provide instantaneous economic comparison of CP reduction methods. In the master model I created in Excel, the input interface looks like Figure 8.7 below.

INPUTS		
Cloud Points		
Initial Tallow CP (°C)	14.3	
Desired CP (°C)	7.0	
Prices		
	\$/lb	\$/gal
Tallow	\$0.49	\$3.55
Soy	\$0.55	\$4.06
Canola	\$0.60	\$4.42
MLA Additive	\$0.42	\$3.00
Tallow Byproducts	\$0.25	\$1.78
	\$/kWh	
Electricity	\$0.073	
	\$/kSCF	\$/kBTU
Natural Gas	\$5.33	\$0.005

Figure 8.7 – Example of input interface for economic comparison model

In this case, all highlighted cells required a user input for the model to function. The inputs are initial and desired CPs and estimated prices for tallow, soy, canola, the MLA additive, electricity and natural gas. The next figure (Figure 8.8) shows a standardized cost table for each specific method, with its blend percent and additive dosage if applicable. If a specific method could not reach the desired CP it displayed “N/A”. In this example case, a desired CP of 7.0°C could not be reached using only the MLA additive.

Costs of Various Methods			
	\$/gal/°C	% Blend	% Additive
Distillation	\$0.110	-	-
MLA Additive	N/A	-	N/A
SME Blending	\$0.040	58%	-
CME Blending	\$0.052	44%	-
CME and MLA	\$0.038	28%	5.0%

Figure 8.8 – Example of standardized cost comparison with blend and additive percentages for economic comparison model

Finally, the standardized cost for each individual method was compared and the most cost effective method was displayed on a results table (Figure 8.9) with its standardized cost, the total

cost per gallon based on the desired CP reduction, and the blend and additive percentages required to reach that CP.

Results	
Min \$/gal/°C	\$0.038
\$/gal	\$0.274
Method	Canola and MLA
% Blend	28%
% Additive	5%

Figure 8.9 – Example of a results table for economic comparison model showing most cost effective method

When the input prices are known, the methods can also be graphically compared. In Figure 8.10, the models are graphed using feedstock, energy and estimated MLA prices from 2012.

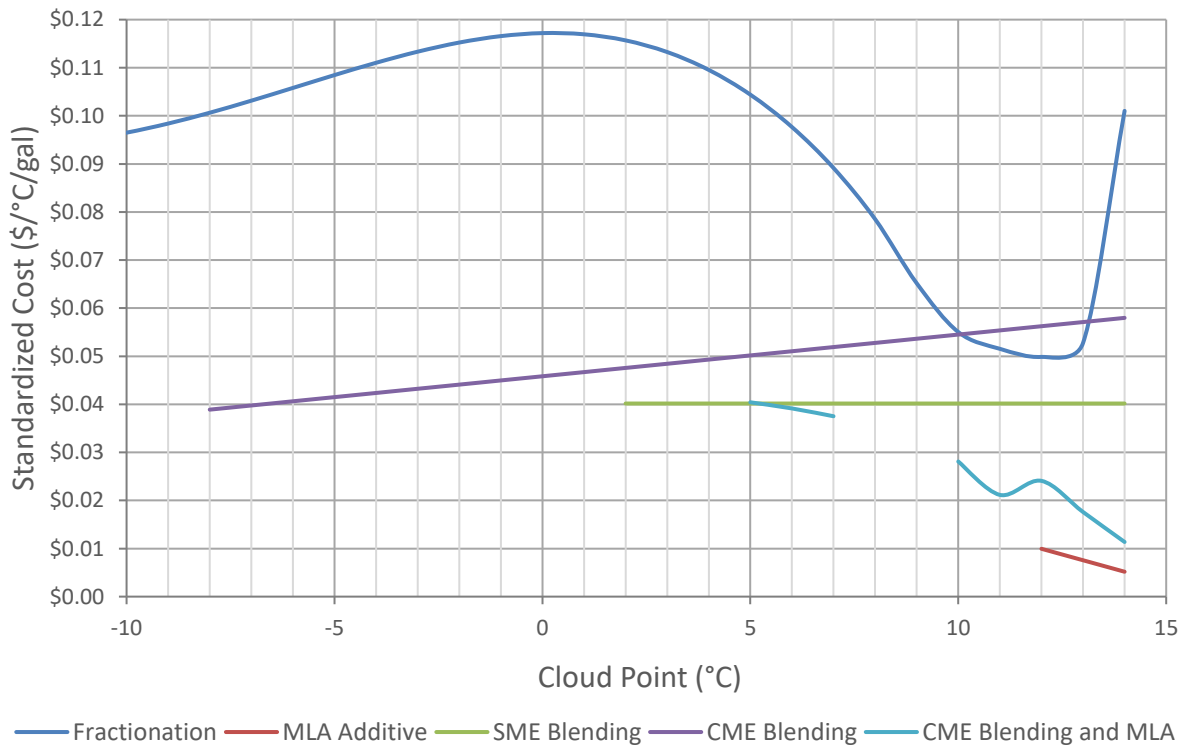


Figure 8.10 – Economic comparison of CP reduction methods with 2012 prices

From the highest to the lowest CPs, the most economic option was the MLA additive until 12°C. Below 12°C, the most cost effective option was CME blending with the MLA additive, then

SME blending, then CME only blending and finally distillation fractionation once the desired CP was below -8°C.

In Figure 8.11, the prices are updated to reflect the economics in June 2017. Over those five years, the soy prices have actually fallen below tallow prices causing a negative standardized price, effectively stating that it is cheaper to make SME biodiesel compared to TME biodiesel given the current commodity prices.

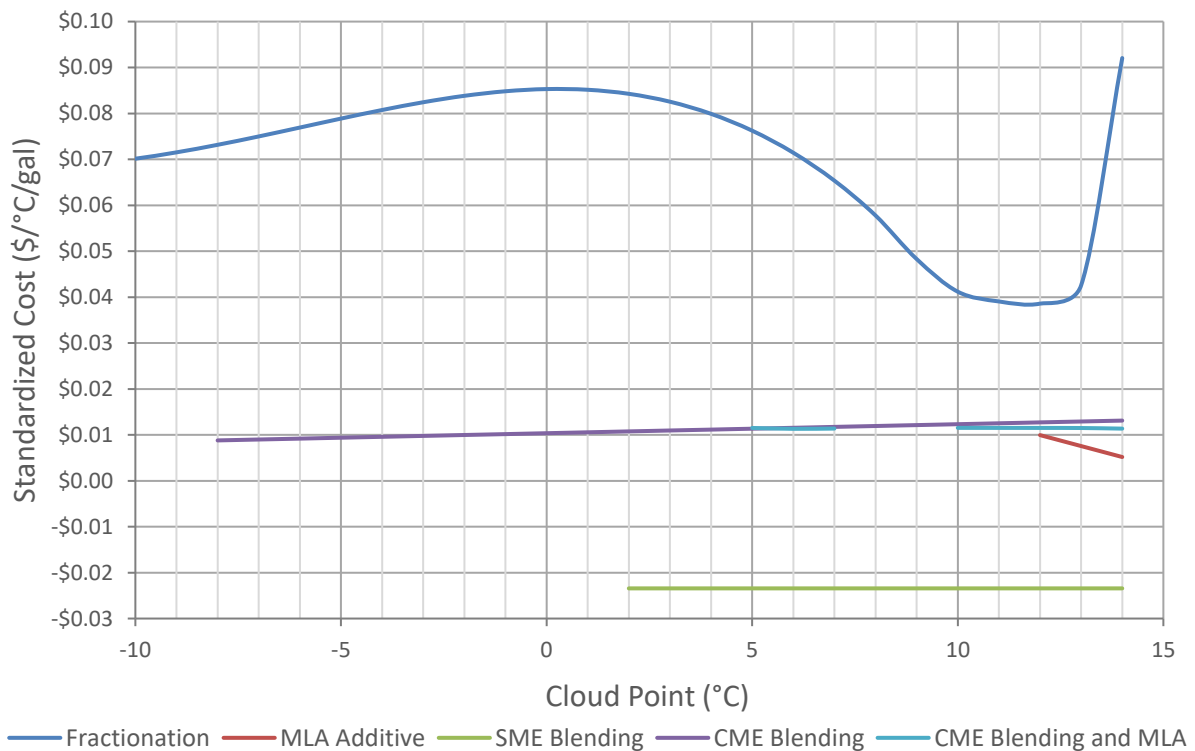


Figure 8.11 – Economic comparison of CP reduction methods with 2017 prices

As a disclaimer, this economic model only shows what the least expensive CP reduction option is and does not determine if a tallow biodiesel plant will be profitable overall.

Chapter 9: Conclusions and Future Work

This research was sponsored by Sun West Biofuels to determine what methods would be necessary to reduce the CP of TME to make it on par with SME and CME in order to capitalize on the lower cost feedstock of tallow. However, the fractionation yield loss required to reach between 0-2°C CP would be in the range of 35-45%. Blending with SME and CME, and using additives were successful in reducing the CP of TME, but blending minimized the cost advantage and additives alone, could not depress the CP low enough. The major finding from this research for Sun West was that with the current prices (in 2012) of tallow in relation to soybean oil and canola oil, it was not economically feasible due to the high yield loss required to fractionate TME to reach 0-2°C. Based on these findings, Sun West abandoned their plans to build a tallow biodiesel plant.

While the outcome of this research for Sun West was not ideal, it did prevent them from building a biodiesel plant that would not be profitable. Additionally, this research still has great value to provide the data required for future economic decisions on tallow biodiesel. As commodity prices change this could become a viable feedstock source. Finally, the data contained in this thesis can be used for other applications, like blending TME into CME to make it cost competitive with SME while maintaining similar CPs.

There are three main contributions of this thesis to a greater understanding of tallow derived biodiesel. The first is the improved pretreatment and transesterification processes tailored specifically for tallow. Then, the characterization of CP reduction methods for TME including fractionation, blending and additives. The final contribution is the framework for an economic analysis to determine if TME can be produced at a cost lower than SME or CME with comparable CPs.

9.1 Improved Fuel Production Steps

In Chapter 3, the steps to produce TME were presented and broken into two main processes. A pretreatment process is first required to prepare the tallow to be converted into biodiesel. Then, transesterification, the actual conversion process, turns the raw triglycerides into FAMES. Over the course of 10 pretreatment attempts, the metals content (sulfur especially) was reduced below the biodiesel standard levels and the yield was improved to as high as 85% in the laboratory. The final recipe, given in Table 3.7, requires 25% excess citric acid, 25% excess NaOH and 20% extra Trisyl 300B and diatomaceous earth. A similar optimization process was carried out with transesterification. Using a typical transesterification recipe, modifications were made over 14 attempts to improve yield, by varying methanol content, reaction time, number of reactions and separation methods. The final optimized transesterification recipe is detailed in Table 3.9, and achieved a maximum of 82% yield. The major changes were that the catalyst was switched from KOH to NaOH to mimic plant scale production, the reaction time was increased to 45 minutes, the excess MeOH was reduced from 60% to 20%, the glycerin was separated using a centrifuge instead of a separatory funnel and the water wash step was repeated 15 times.

9.2 Comparing Cloud Point Reduction Methods

In order to compete with SME and CME, TME must have its CP reduced to a similar temperature. The three methods that were researched to reduce TME CP were fractionation, blending with other FAMES and using polymer additives.

9.2.1 Fractionation

Fractionation was shown to be successful at reducing the CP of TME. In order to retain the maximum yield while reducing the CP, the empirical eutectic ratio (EEP) of 82% MP/(MP+MS)

needs to be reached then maintained when removing FAMEs. When starting with pure TME, the MP/(MP+MS) ratio is 59%, meaning MS must be removed at first to bring it to the EEP. After that, MP and MS need to be removed at an 82% MP/18% MS ratio to remain at the EEP. According to Figure 4.17, which accounts for the 4:1 MS/MO carryover, reducing CP to 10°C requires a yield loss of 5-10%, 7°C takes a 15-20% yield loss, 2°C has a 35-40% loss and 0°C would create a 40-45% yield loss. Losing that much product makes fractionation difficult to justify unless the cost of tallow is significantly less than soy or canola oil.

9.2.2 Blending

Blending TME with SME and CME, which have lower CPs, did successfully reduce the methyl ester blends' overall CPs, as would make sense. The pathway for the CP reduction was both a result of a decrease in overall saturated FAMEs by mixing in high levels of unsaturated FAMEs as well as moving the MP/(MP+MS) ratio closer to the EEP.

CME was more successful at reducing CP than SME, as seen in Figure 5.5, as would be expected given the -8.3°C CP of CME compared to 2.3°C for SME. With equal or lesser feedstock costs, it would be better to use CME to blend with TME than SME. In other cost scenarios, the equations in Figure 5.5 could be used to determine the better economic option.

Considering that the purpose behind researching TME is the cost advantage it has over SME and CME, it could be self-defeating to blend with SME or CME as the cost advantage dwindles at higher blend proportions. On the flip-side, there may be an economic advantage for a SME or CME producer to mix in a percentage of TME to reduce their costs if their CP requirement is at a higher temperature than the CP of the methyl esters.

9.2.3 Additives

Chapter 6 investigated eleven different additives. Some of those additives were designed for petroleum diesel, others for FAMES and two specifically to reduce the CP of TME. Out of all eleven, only the two designed for TME had any significant reduction in CP. Out of those two, the MLA additive clearly outperformed Evonik's Viscoplex 10-530 additive.

The maximum CP reduction the MLA additive was able to produce in pure TME was 3.6°C at a 5% dose (Figure 6.27). CME/TME blends were only tested up to a 3% MLA dose but were able to come close with a 3.4°C drop for 25% CME/TME and 3.3°C drop for 50% CME/TME. In contrast, at a 3% MLA dose, TME had a 2.6°C CP drop. This comparison, along with additional analysis demonstrated that the CME/TME blends had a synergistic effect on the MLA additive effectiveness compared to pure TME.

A few cursory tests were conducted to investigate if all components of the MLA additive were necessary to achieve reduced CPs. A solid portion of the additive naturally settles, and was found to have minimal effect on CP, while the liquid portion produced greater CP reduction results (CP drop = 3°C) than the combined MLA additive (CP drop = 2.6°C). If the MLA additive were to be used for only CP reduction, and CFPP was not a concern, the liquid portion would produce a greater CP reduction, with less material, making it more economical to purchase only the liquid portion.

9.2.4 Combination of Methods

In all likelihood, for a biodiesel plant to produce TME with acceptable CPs, all three methods would need to be used at different times dependent on feedstock, additive and energy prices. In some situations it may be worth fractionating to the EEP, then using the MLA additive or blending to reach the last few degrees. In other cases, blending then using the MLA additive might be the best answer. For larger CP drops, all three methods may need to be employed.

Determining the theoretical CPs when pairing blending and fractionation can be done by coupling the fractionation FAME profile solver with the blending solver to find the combined FAME profile, then calculating the CP. Using the MLA additive with CME/TME blends has already been characterized, but further tests with SME/TME blends would need to be carried out. The most difficult method combination to determine, would be mixing the MLA additive into fractionated blends. In order to properly map the MLA additive effect, it would likely need to be tested at varying MP/(MP+MS) ratios and percent MP+MS.

9.2.5 Diesel Blends

All these FAME mixtures and their respective CPs need to be characterized well when mixed at blends in diesel fuel. For pure methyl esters either from fractionation, SME/TME blends or CME/TME blends, a given FAME mixture CP likely relates well to a specific CP at a BXX blend as long as the diesel CP is consistent. It gets more complicated when the MLA additive is included because Chapter 7 revealed that the CP reduction effect of the MLA additive is compounded when mixed in diesel blends. This characterization with the MLA additive would need to be explored further to include data on MLA/CME/TME/Diesel blends and MLA/SME/TME/Diesel blends.

9.3 Economics

As technical as the research might be, it all converges to a simple economic evaluation. The economic advantage of tallow as a less expensive feedstock compared to soy or canola is what prompted Sun West to fund this research. An economic evaluation of each CP reduction method is the means to determine if producing TME to sell as biodiesel is worthwhile.

Each CP reduction method was compared using a standardized cost of reducing one gallon of produced biodiesel by 1°C (\$/gal/°C). The means to calculate this standardized cost for each

method were outlined in Chapter 8, and can be carried out to determine the current economic situation, in regards to using tallow as a biodiesel feedstock. Additionally, it allows real-time decisions to be made on which combination of methods will reduce the CP of the TME mixture at the minimum cost. This economic model could be taken a step further by running stochastic simulations to determine if there are likely cost scenarios where TME, with a reduced CP, would have a cost advantage over SME or CME, and the probability those scenarios would occur.

9.4 Future Work

As usual, there is always more research that can be done. For a potential tallow biodiesel producer to implement this research they would need to characterize a few more things.

First, the empirical eutectic point could be better defined. From the data points in the fractionation tests, along with the expanded data, there is a good working empirical eutectic ratio of 82% MP/(MP+MS). To better characterize the EEP, CPs could be tested at regular spaced MP+MS fraction intervals, and from 80 to 85% MP/(MP+MS) at 1% intervals. Testing for the EEP at varied MP+MS fractions is important because according to the models, the eutectic point actually shifts as the MP+MS fraction changes. From that information, the graph contrasting the EEP CP vs yield could be updated providing a much more accurate cost assessment.

One weakness in all this research is that all the fractionation tests were simulated. Verifying the CP of some simulated fractionation tests using distillation would increase confidence in them all. For a company planning to fractionate tallow biodiesel, it would be worth conducting small scale pilot tests to verify the results.

A few areas that could be researched to increase the options available for a TME producer would be testing additional blends. This paper investigated MLA additive mixed into CME/TME blends but not with SME/TME. Having this data allows more CP reduction flexibility, and

potentially, the MLA additive has an even greater synergistic effect in SME/TME blends than the CME/TME blends. Another variant of previous testing could be combining the MLA additive in diesel, with SME/TME or CME/TME blends and TME/diesel blends to determine the CP effect of blending the MLA additive with SME/TME/diesel or CME/TME/diesel mixtures.

Additionally, crystallization fractionation could be explored further. There are two main areas to investigate, to determine the viability of crystallization fraction compared to distillation fractionation. First, CHEMCAD or Aspen models could be run to see if there is any carryover when removing MS, with another FAME (potentially MP). Then, the cost of cooling the FAME stream at a smaller temperature differential would need to be compared to the heating costs of distillation.

Another CP reduction method that was not explored at all was using ethanol in the transesterification process instead of methanol. As the whole gist of this thesis is dedicated to comparing CP reduction methods on a cost basis, characterizing the CP reduction of FAEEs over FAMES with a cost comparison model would be a logical addition to these results.

With all of these tests, the only properties largely measured were CP and CFPP. As the FAME profile changes by fractionation or blending, other properties like oxidative stability and cetane number are affected. It would be wise to test for these properties at the extremes of fractionation, blending and additive dosages to verify that they remain within ASTM specs.

The FAME profile of any biodiesel is a balance of saturated/unsaturated and high/low melting point FAMES that must be within certain limits to meet ASTM and producer standards. One other area that could be researched would answer the question, "What is the ideal biodiesel FAME profile range?" This FAME profile range would meet all specifications for cold temperature properties, cetane number, oxidative stability and any other key fuel property requirements. From there, either an "ideal feedstock" or ideal blends of common feedstocks could be offered. This idea was prompted by the graphic shown below in Figure 9.1 [18].

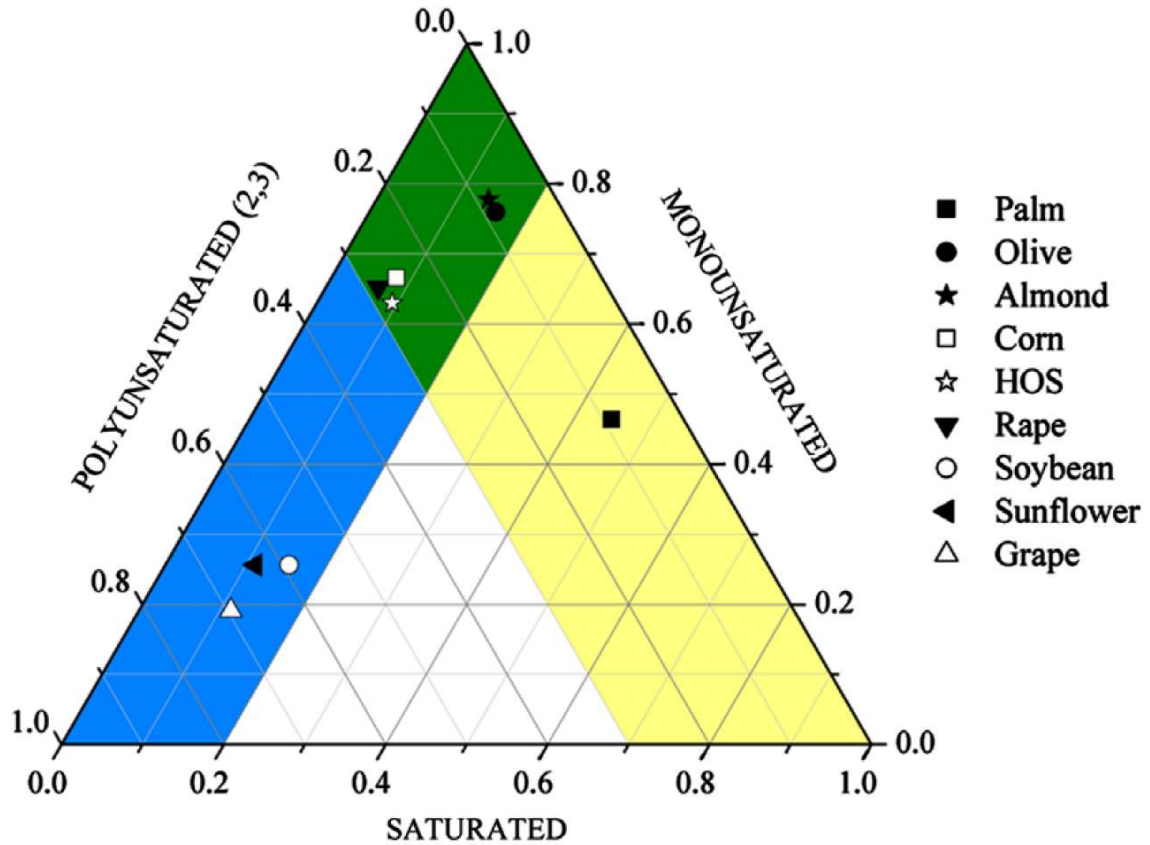


Figure 9.1 – Biodiesel sorted by monounsaturated, polyunsaturated and saturated methyl esters. Areas satisfying parameter of the European Standard UNE-EN 14214: yellow (right), good cetane number and iodine value; blue (left), good CFPP; green (intersection), biodiesel that satisfied UNE-EN 14214. [18]

References

- [1] T. Grossenbacher, "Global Oil Production & Consumption since 1965." [Online]. Available: <https://labs.timogrossenbacher.ch/worldoil/>. [Accessed: 07-Sep-2017].
- [2] J. Tsao, N. Lewis, and G. Crabtree, "Solar FAQs," 2006. [Online]. Available: <http://www.sandia.gov/~jytsao/Solar%20FAQs.pdf>. [Accessed: 08-Sep-2017].
- [3] M. S. Graboski and R. L. McCormick, "Combustion of fat and vegetable oil derived fuels in diesel engines," *Prog. Energy Combust. Sci.*, vol. 24, no. 2, pp. 125–164, 1998.
- [4] S. C. Davis, S. E. Williams, and R. G. Boundy, "Transportation Energy Data Book: Edition 35," ORNL/TM--2016/470, 1357967, Oct. 2016.
- [5] "Alternative Fuels Data Center: Biodiesel Vehicle Emissions," *Alternative Fuels Data Center*. [Online]. Available: https://www.afdc.energy.gov/vehicles/diesels_emissions.html. [Accessed: 08-Sep-2017].
- [6] "Highway and Nonroad Diesel Fuel Standards," *United States Environmental Protection Agency*, Jan-2011. [Online]. Available: <https://www.epa.gov/sites/production/files/2015-08/documents/420b11003.pdf>. [Accessed: 14-Sep-2017].
- [7] D. Reece and C. Peterson, "ACUTE TOXICITY OF BIODIESEL TO FRESHWATER AND MARINE ORGANISMS," *Biodiesel Education*. [Online]. Available: <http://biodieseleducation.org/LITERATURE/index.html>. [Accessed: 28-Sep-2017].
- [8] X. Zhang, C. Peterson, D. Reece, R. Haws, and G. Möller, "BIODEGRADABILITY OF BIODIESEL IN THE AQUATIC ENVIRONMENT," *Trans. ASAE*, vol. 41, no. 5, pp. 1423–1430, 1998.
- [9] R. McCormick and T. Allenman, "Renewable Diesel Fuel," *Clean Cities*, 18-Jul-2016. [Online]. Available: https://cleancities.energy.gov/files/u/news_events/document/document_url/182/McCormick__Alleman_RD_Overview_2016_07_18.pdf. [Accessed: 14-Sep-2017].
- [10] "Renewable Diesel Fuels," *Diesel Technolgy Forum*. [Online]. Available: http://www.dieselforum.org/files/dmfile/RenewableFuelsFactSheet_01.30.13.pdf. [Accessed: 28-Sep-2017].
- [11] "Air Product's U.S. Gulf Coast hydrogen network." [Online]. Available: <http://www.airproducts.com/microsite/h2-pipeline/pdf/air-products-US-gulf-coast-hydrogen-network-dataSheet.pdf>. [Accessed: 15-Sep-2017].
- [12] "U.S. Biodiesel Plants," *Biodiesel Magazine*, 11-May-2017. [Online]. Available: <http://www.biodieselmagazine.com/plants/listplants/USA/>. [Accessed: 15-Sep-2017].
- [13] S. D. Sanford, J. M. White, P. S. Shah, C. Wee, M. A. Valverde, and G. R. Meier, "Feedstock and biodiesel characteristics report," *Renew. Energy Group*, vol. 416, pp. 1–136, 2009.
- [14] R. D. O'Brien, *Fats and oils: formulating and processing for applications*, 3rd ed. Boca Raton: CRC Press, 2009.
- [15] J. V. Gerpen, "Biodiesel processing and production," *Fuel Process. Technol.*, vol. 86, no. 10, pp. 1097–1107, Jun. 2005.
- [16] D. Y. C. Leung, X. Wu, and M. K. H. Leung, "A review on biodiesel production using catalyzed transesterification," *Appl. Energy*, vol. 87, no. 4, pp. 1083–1095, Apr. 2010.
- [17] H. Bucy, "Oxidative stability and ignition quality of algae derived methyl esters containing varying levels of methyl eicosapentaenoate and methyl docosahexaenoate," Colorado State University, 2011.

- [18] M. J. Ramos, C. M. Fernández, A. Casas, L. Rodríguez, and Á. Pérez, "Influence of fatty acid composition of raw materials on biodiesel properties," *Bioresour. Technol.*, vol. 100, no. 1, pp. 261–268, Jan. 2009.
- [19] W. Brorsen, "Projections of US Production of Biodiesel Feedstock," *Rep. Prep. Union Concerned Sci. Int. Counc. Clean Transp.*, 2015.
- [20] "Feedstocks - The Future of Biodiesel," *Biodiesel Sustainability Blog*. [Online]. Available: <http://www.biodieselsustainability.com/feedstocks/>. [Accessed: 08-Sep-2017].
- [21] J. Van Gerpen, "Cetane number testing of biodiesel," in *Proceedings of the third liquid fuels conference*, 1996, pp. 197–206.
- [22] "NIST Chemistry WebBook." [Online]. Available: <http://webbook.nist.gov/chemistry/>. [Accessed: 15-Sep-2017].
- [23] "POCKET INFORMATION MANUAL A BUYER'S GUIDE TO RENDERED PRODUCTS," *National Renderers Association*, 2008. [Online]. Available: http://assets.nationalrenderers.org/pocket_information_manual.pdf. [Accessed: 15-Sep-2017].
- [24] "Biodiesel Demand for Animal Fats and Tallow Generates an Additional Revenue Stream for the Livestock Industry," *Biodiesel*, Sep-2014. [Online]. Available: <http://biodiesel.org/docs/default-source/news---supporting-files/animal-fats-and-tallow-bd-demand-impact-report.pdf?sfvrsn=2>. [Accessed: 08-Sep-2017].
- [25] "Fuel Properties Comparison," *Alternative Fuels Data Center*, 29-Oct-2014. [Online]. Available: https://www.afdc.energy.gov/fuels/fuel_comparison_chart.pdf. [Accessed: 08-Sep-2017].
- [26] "Standard Specification for Biodiesel Fuel Blend Stock (B100) for Middle Distillate Fuels," ASTM D6751-15c, ASTM, 2015.
- [27] J. C. A. Lopes *et al.*, "Prediction of Cloud Points of Biodiesel †," *Energy Fuels*, vol. 22, no. 2, pp. 747–752, Mar. 2008.
- [28] R. O. Dunn, "Improving the cold flow properties of biodiesel by fractionation," in *Soybean Applications and Technology*, InTech, 2011.
- [29] R. O. Dunn, "Crystallization Behavior of Fatty Acid Methyl Esters," *J. Am. Oil Chem. Soc.*, vol. 85, no. 10, pp. 961–972, Oct. 2008.
- [30] H. Imahara, E. Minami, and S. Saka, "Thermodynamic study on cloud point of biodiesel with its fatty acid composition☆," *Fuel*, vol. 85, no. 12–13, pp. 1666–1670, Sep. 2006.
- [31] R. A. Davis, S. Mohtar, and B. Y. Tao, "Production of low-temp biodiesel through urea clathration," in *2007 ASAE Annual Meeting*, 2007, p. 1.
- [32] "Characterization of Biodiesel Oxidation Products," *National Renewable Energy Laboratory*, Nov-2005. [Online]. Available: <https://www.nrel.gov/docs/fy06osti/39096.pdf>. [Accessed: 28-Sep-2017].
- [33] A. I. Bamgboye, A. C. Hansen, and others, "Prediction of cetane number of biodiesel fuel from the fatty acid methyl ester (FAME) composition," *Int. Agrophysics*, vol. 22, no. 1, p. 21, 2008.
- [34] "Animal and vegetable fats and oils -- Determination of iodine value," ISO 3961:2013, International Organization for Standardization, 2013.
- [35] P. C. Smith, Y. Ngothai, Q. Dzuy Nguyen, and B. K. O'Neill, "Improving the low-temperature properties of biodiesel: Methods and consequences," *Renew. Energy*, vol. 35, no. 6, pp. 1145–1151, Jun. 2010.
- [36] R. O. Dunn and M. O. Bagby, "Low-temperature properties of triglyceride-based diesel fuels: transesterified methyl esters and petroleum middle distillate/ester blends," *J. Am. Oil Chem. Soc.*, vol. 72, no. 8, pp. 895–904, 1995.
- [37] T. A. Foglia, L. A. Nelson, R. O. Dunn, and W. N. Marmer, "Low-temperature properties of alkyl esters of tallow and grease," *J. Am. Oil Chem. Soc.*, vol. 74, no. 8, pp. 951–955, 1997.
- [38] R. O. Dunn, "Cold-Flow Properties of Soybean Oil Fatty Acid Monoalkyl Ester Admixtures †," *Energy Fuels*, vol. 23, no. 8, pp. 4082–4091, Aug. 2009.

- [39] T. G. Smith, "Preliminary Process Design for Vacuum Distillation of C16/C18." 17-Jan-2012.
- [40] "Standard Test Method for Cloud Point of Petroleum Products and Liquid Fuels," ASTM D2500-17, ASTM, 2017.
- [41] "Standard Test Method for Cloud Point of Petroleum Products and Liquid Fuels (Optical Detection Stepped Cooling Method)," ASTM D5771-17, ASTM, 2017.
- [42] "Operating Manual for Lawler Model DR4-14 H and L Automated Cold Filter Plugging Point and Cloud Point Analyzer." Lawler.
- [43] "Flame Ionization Detector - FID," *SRI Instruments*. [Online]. Available: <http://www.sri-instruments-europe.com/en/pdf/FID-mdi.pdf>. [Accessed: 28-Sep-2017].
- [44] "MXT-WAX Columns (70655-271)," *RESTEK*. [Online]. Available: <http://www.restek.com/catalog/view/1429>. [Accessed: 16-Sep-2017].
- [45] "Bulletin 907: Comparison of 37 Component FAME Standard on Four Capillary GC Columns," *Sigma Aldrich*. [Online]. Available: <https://www.sigmaaldrich.com/content/dam/sigma-aldrich/docs/Supelco/Bulletin/t196907.pdf>. [Accessed: 28-Sep-2017].
- [46] "Spectro GENESIS Manual." Spectro, 2013.
- [47] "VHG-SB100-100-100- Sulfur Standard: S @ 100 µg/g in B100 Biodiesel," *VHG Labs*. [Online]. Available: <https://www.lgcstandards.com/AZ/en/Sulfur-Standard-S-100-g-g-in-B100-Biodiesel/p/VHG-SB100-100-100>. [Accessed: 16-Sep-2017].
- [48] "V23 Wear Metal Standards - 10 µg/g," *VHG Labs*. [Online]. Available: <https://vhglabs.com/products/wear-metal-standards/VHG-V23>. [Accessed: 16-Sep-2017].
- [49] "Manual 743 Rancimat." Metrohm.
- [50] "PetroTest PMA 4 User Manual." Petrotest® Instruments GmbH & Co. KG.
- [51] A. Meyer, K. Albrecht, and R. Hallen, "Preliminary Case Study: Distillation of Beef Tallow Methyl Esters," Pacific Northwest National Laboratory, Feb. 2012.
- [52] R. Hallen, A. Meyer, and K. Albrecht, "Brief Technical Update: Distillation of Beef Tallow Methyl Esters," Pacific Northwest National Laboratory, Feb. 2012.
- [53] "Biodiesel Additive Final Report," Meat & Livestock Australia Limited, A.MDC.0003, Jul. 2011.
- [54] "VISCOPLEX® CFIs - Cold Flow Improvers for Biodiesel." Evonik Industries.
- [55] R. C. Christiansen, "Additive lowers tallow-based biodiesel cloud point," *Biodiesel Magazine*, 14-Oct-2008. [Online]. Available: <http://www.biodieselmagazine.com/articles/2908/additive-lowers-tallow-based-biodiesel-cloud-point->. [Accessed: 23-Sep-2017].
- [56] A. Westlake *et al.*, "Biodiesel Additive," US 20110232159 A1, May-2009.

Appendix A: Cloud Point Models' Calculated Curves

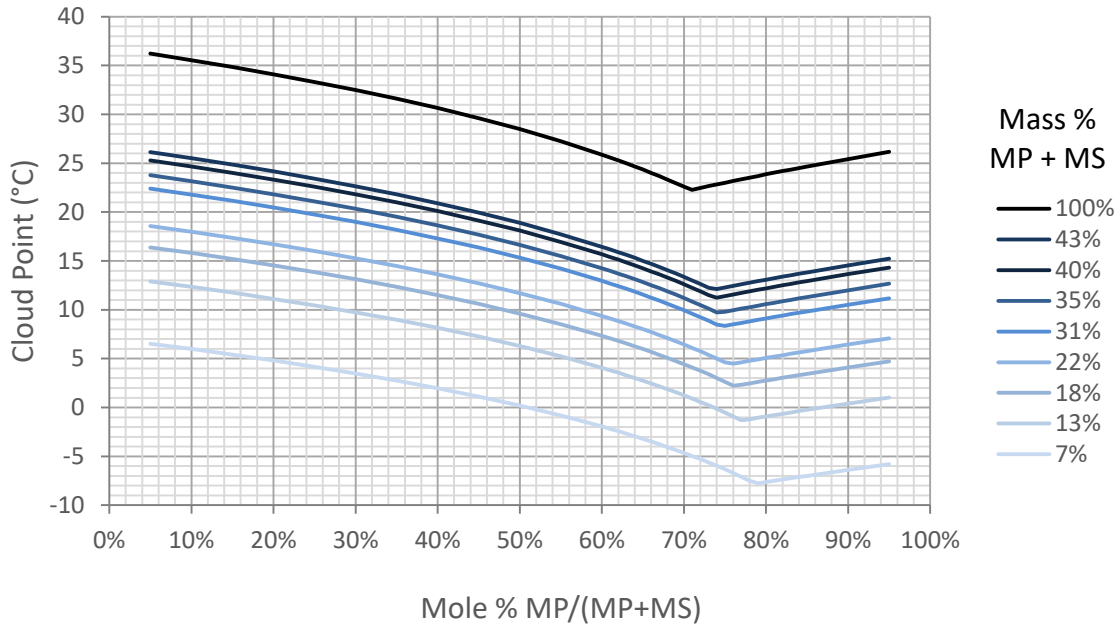


Figure A.1 - CP vs MP/(MP+MS) ratio for the “Imahara” model at varying MP+MS fractions

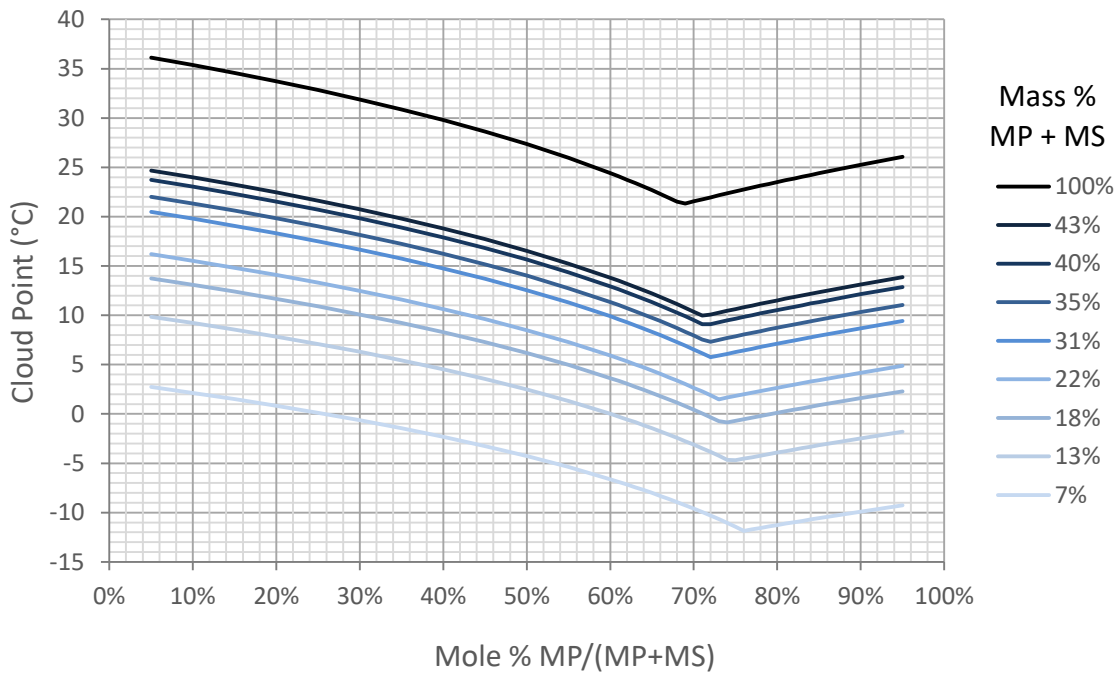


Figure A.2 - CP vs MP/(MP+MS) ratio for the “Imahara (Dunn)” model at varying MP+MS fractions

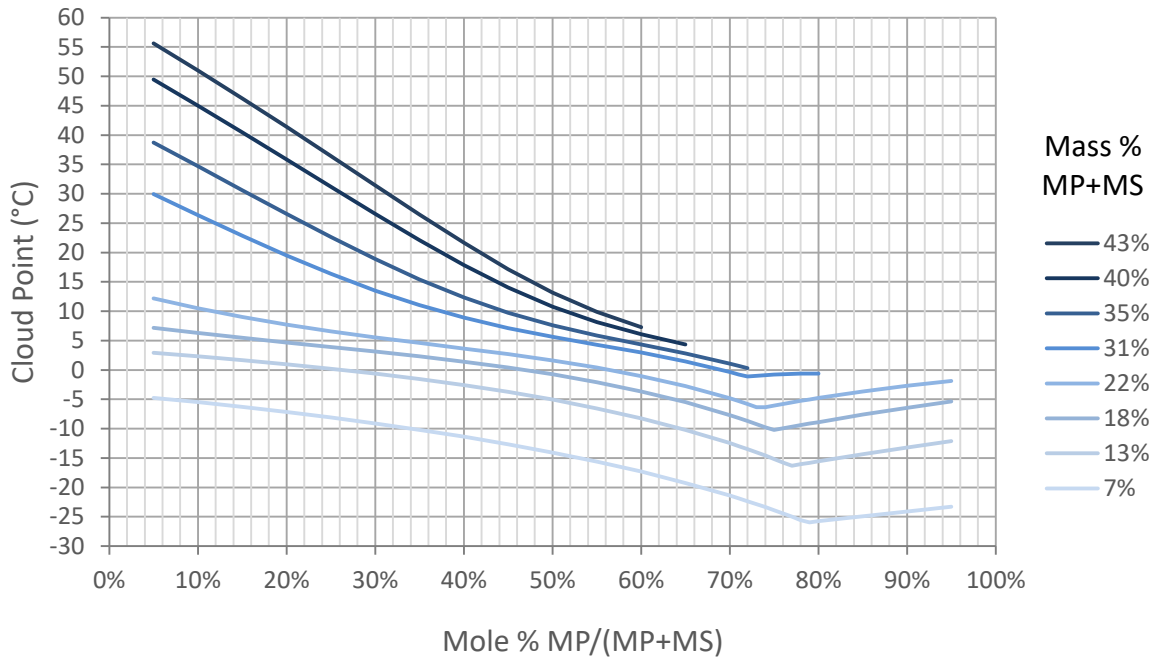


Figure A.3 - CP vs MP/(MP+MS) ratio for the “Dunn (Simple)” model at varying MP+MS fractions

Appendix B: Comparison of TME FAME Profiles

Table B.1 – FAME profiles of different TME samples used to make “Standard TME Profile”

TMEs Measured By:	REG Report	Westfalia	Solix	In House	In House	Average Profile of TMEs
TMEs Provided By:		JBS	JBS	JBS	Cargill	
FFA %	1.61%	1.22%				1.41%
C12:0	0.2%	0.1%	-	0.1%	0.3%	0.1%
C14:0	2.9%	3.7%	3.5%	4.8%	3.3%	3.8%
C14:1	0.0%	0.6%	0.4%	1.2%	0.9%	0.7%
C16:0	24.3%	25.1%	26.8%	25.8%	23.5%	25.4%
C16:1	2.1%	3.4%	2.3%	3.2%	3.0%	2.8%
C18:0	22.8%	18.6%	22.4%	19.1%	19.7%	20.6%
C18:1	40.2%	39.6%	40.8%	38.9%	41.9%	40.2%
C18:2	3.3%	2.6%	1.7%	1.7%	2.9%	2.2%
C18:3	0.7%	0.0%	0.1%	0.4%	0.9%	0.4%
Other FAMES	3.5%	6.4%	2.0%	4.8%	3.7%	3.9%

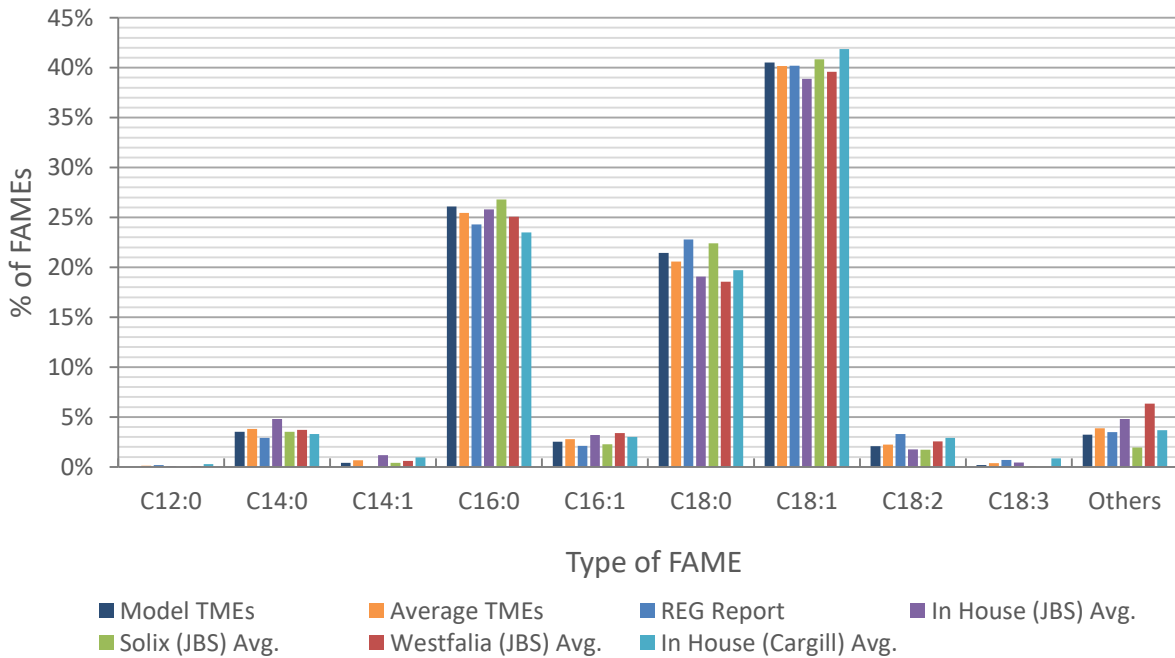


Figure B.1 – Comparison of FAME profiles of various TME sources

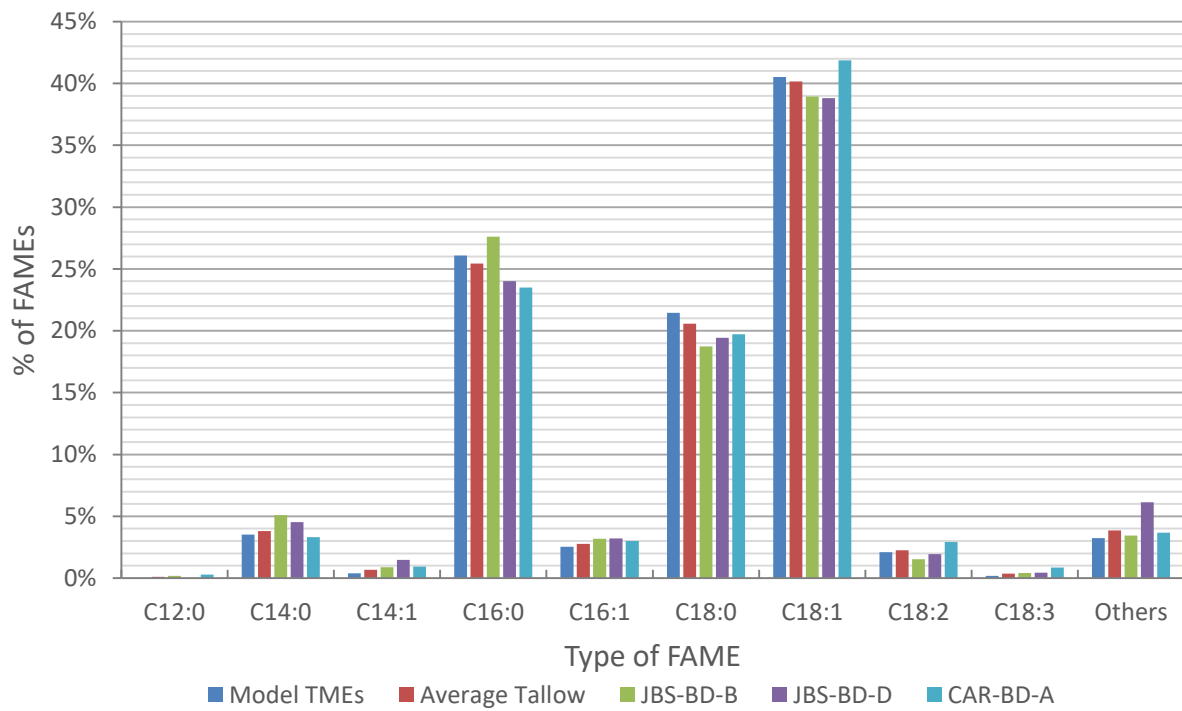


Figure B.2 – Comparison of “Model TME Profile” with measured TME profiles

Appendix C: FAME Profiles of Fractionation Tests

Table C.1 – CP, CFPP, yields and GC FAME profile results of exploratory fractionation tests

	Test TME	Test MP 1	Test MP 2	Test MP/MS				
% MP of Total FAMES	26.1%	3.9%	4.3%	5.4%				
% MS of Total FAMES	21.4%	27.9%	27.8%	6.0%				
% MP Removed	0.0%	88.4%	87.4%	87.8%				
% MS Removed	0.0%	0.0%	0.0%	83.4%				
% Yield	0.0%	77.0%	77.2%	59.2%				
% Yield with 4:1 Carryover	100.0%	77.0%	77.2%	54.8%				
Max Empirical CP (°C)	14.5	22.0	20.0	-2.5				
Max Empirical CFPP (°C)	14.2	23.0	21.0	2.2				
Comparison of Target vs. Expected FAME Profiles								
	Expected	Measured	Target	Expected	Target	Expected	Target	Expected
Mass % Saturated FAMES	52.7%	51.0%	38.0%	38.0%	38.2%	32.3%	18.3%	11.7%
Mass % MP + MS	47.5%	44.3%	31.8%	37.7%	32.0%	32.0%	11.4%	11.4%
Mol% MP of (MP + MS)	57.3%	58.9%	12.4%	10.4%	13.3%	13.3%	47.3%	47.3%
Mass % of C14:0	3.5%	4.3%	4.6%	0.2%	4.5%	0.2%	5.9%	0.3%
Mass % of C14:1	0.4%	1.1%	0.5%	0.0%	0.5%	0.0%	0.7%	0.0%
Mass % of C16:0	26.1%	25.0%	3.9%	3.9%	4.3%	4.3%	5.4%	5.4%
Mass % of C16:1	2.5%	3.1%	3.3%	0.0%	3.3%	0.0%	4.3%	0.0%
Mass % of C18:0	21.4%	19.3%	27.9%	33.8%	27.8%	27.8%	6.0%	6.0%
Mass % of C18:1	40.5%	39.9%	52.7%	54.2%	52.5%	59.3%	68.4%	77.5%
Mass % of C18:2	2.1%	2.1%	2.7%	7.3%	2.7%	8.0%	3.5%	10.5%
Mass % of C18:3	0.2%	0.6%	0.2%	0.5%	0.2%	0.4%	0.3%	0.3%
Mass % of Other FAMES	3.2%	4.6%	4.2%	0.0%	4.2%	0.0%	5.5%	0.0%

Table C.2 – CP, CFPP, yields and measured FAME profiles of fractionation test groups 1 and 2

	Test 1	Test 2 +MS	Test 2 TEP	Test 2 -MS				
% MP of Total FAMES	26.0%	26.0%	26.0%	26.0%				
% MS of Total FAMES	14.9%	14.1%	11.8%	9.4%				
% MP Removed	11.4%	12.6%	15.9%	19.0%				
% MS Removed	38.1%	42.2%	53.6%	64.3%				
% Yield	88.9%	87.7%	84.4%	81.3%				
% Yield with 4:1 Carryover	86.8%	85.4%	81.5%	77.8%				
Max Empirical CP (°C)	10.5	10.0	8.0	6.7				
Max Empirical CFPP (°C)	11.0	10.3	8.0	6.7				
Comparison of Target vs. Measured FAME Profiles								
	Target	Measured	Target	Measured	Target	Measured	Target	Measured
Mass % Saturated FAMES	44.9%	45.8%	44.1%	44.3%	41.9%	40.1%	39.7%	39.3%
Mass % MP + MS	40.9%	41.6%	40.1%	40.0%	37.8%	36.0%	35.4%	33.2%
Mol% MP of (MP + MS)	63.5%	63.0%	64.8%	66.3%	68.8%	68.6%	73.4%	73.5%
Mass % of C14:0	3.9%	4.1%	4.0%	4.3%	4.2%	4.1%	4.3%	6.2%
Mass % of C14:1	0.5%	0.4%	0.5%	0.4%	0.5%	0.4%	0.5%	0.3%
Mass % of C16:0	26.0%	26.2%	26.0%	26.5%	26.0%	24.7%	26.0%	24.4%
Mass % of C16:1	2.9%	1.4%	2.9%	1.4%	3.0%	1.5%	3.1%	1.1%
Mass % of C18:0	14.9%	15.4%	14.1%	13.5%	11.8%	11.3%	9.4%	8.8%
Mass % of C18:1	45.6%	47.6%	46.2%	47.6%	48.0%	50.1%	49.9%	50.5%
Mass % of C18:2	2.4%	1.9%	2.4%	3.5%	2.5%	5.2%	2.6%	5.6%
Mass % of C18:3	0.2%	0.0%	0.2%	0.1%	0.2%	0.2%	0.2%	0.2%
Mass % of Other FAMES	3.7%	2.9%	3.7%	2.7%	3.9%	2.4%	4.0%	2.9%

Table C.3 – CP, CFPP, yields and measured FAME profiles of fractionation test group 5

	Test 5	Test 5 EEPL	Test 5 EEPR			
% MP of Total FAMES	26.0%	25.9%	27.3%			
% MS of Total FAMES	7.1%	7.2%	5.7%			
% MP Removed	21.8%	22.1%	17.8%			
% MS Removed	74.1%	73.8%	79.0%			
% Yield	78.4%	78.4%	78.4%			
% Yield with 4:1 Carryover	74.4%	74.5%	74.2%			
Max Empirical CP (°C)	5.0	6.7	5.7			
Max Empirical CFPP (°C)	5.7	6.7	6.3			
Comparison of Target vs. Measured FAME Profiles						
	Target	Measured	Target	Measured	Target	Measured
Mass % Saturated FAMES	37.6%	39.0%	37.6%	41.9%	37.6%	40.1%
Mass % MP + MS	33.1%	31.5%	33.1%	33.3%	33.1%	32.5%
Mol% MP of (MP + MS)	78.6%	79.4%	78.4%	77.9%	82.6%	82.4%
Mass % of C14:0	4.5%	7.5%	4.5%	8.6%	4.5%	7.6%
Mass % of C14:1	0.5%	0.1%	0.5%	0.5%	0.5%	0.3%
Mass % of C16:0	26.0%	25.0%	25.9%	26.0%	27.3%	26.8%
Mass % of C16:1	3.2%	0.5%	3.2%	1.2%	3.2%	0.9%
Mass % of C18:0	7.1%	6.5%	7.2%	7.4%	5.7%	5.7%
Mass % of C18:1	51.7%	52.8%	51.7%	47.4%	51.7%	49.5%
Mass % of C18:2	2.7%	5.8%	2.7%	5.0%	2.7%	5.9%
Mass % of C18:3	0.2%	0.1%	0.2%	0.1%	0.2%	0.1%
Mass % of Other FAMES	4.1%	1.7%	4.1%	4.0%	4.1%	3.2%

Table C.4 – CP, CFPP, yields and measured FAME profiles of fractionation test groups 6 and 7

	Test 6	Test 6 EEP	Test 6 EEPL	Test 6 EEPR	Test 7 EEP					
% MP of Total FAMES	31.8%	29.1%	28.3%	29.8%	30.7%					
% MS of Total FAMES	4.3%	7.0%	7.8%	6.3%	7.4%					
% MP Removed	0.0%	8.5%	10.9%	6.1%	0.0%					
% MS Removed	83.4%	73.0%	70.1%	76.0%	70.5%					
% Yield	82.1%	82.1%	82.1%	82.1%	84.9%					
% Yield with 4:1 Carryover	77.6%	78.2%	78.4%	78.0%	81.1%					
Max Empirical CP (°C)	7.0	7.0	6.0	7.0	6.7					
Max Empirical CFPP (°C)	8.3	7.7	6.7	7.3	7.0					
Comparison of Target vs. Measured FAME Profiles										
	Target	Measured	Target	Measured	Target	Measured	Target	Measured	Target	Measured
Mass % Saturated FAMES	40.4%	43.9%	40.4%	44.0%	40.4%	41.7%	40.4%	43.8%	44.0%	47.0%
Mass % MP + MS	36.1%	36.3%	36.1%	36.5%	36.1%	33.8%	36.1%	36.6%	38.2%	36.8%
Mol% MP of (MP + MS)	88.0%	89.9%	80.5%	80.6%	78.4%	78.3%	82.6%	82.9%	82.0%	83.0%
Mass % of C14:0	4.3%	7.5%	4.3%	7.5%	4.3%	8.0%	4.3%	7.2%	4.1%	9.2%
Mass % of C14:1	0.5%	0.1%	0.5%	0.1%	0.5%	0.3%	0.5%	0.1%	0.5%	0.2%
Mass % of C16:0	31.8%	32.7%	29.1%	29.4%	28.3%	26.4%	29.8%	30.3%	30.7%	30.0%
Mass % of C16:1	3.1%	0.3%	3.1%	1.0%	3.1%	0.9%	3.1%	0.8%	3.0%	0.7%
Mass % of C18:0	4.3%	3.7%	7.0%	7.1%	7.8%	7.3%	6.3%	6.3%	7.4%	6.8%
Mass % of C18:1	49.3%	47.7%	49.4%	52.2%	49.4%	48.9%	49.4%	52.9%	47.7%	46.6%
Mass % of C18:2	2.6%	5.7%	2.6%	0.0%	2.6%	5.0%	2.6%	0.0%	2.5%	4.2%
Mass % of C18:3	0.2%	0.0%	0.2%	0.1%	0.2%	0.5%	0.2%	0.1%	0.2%	0.1%
Mass % of Other FAMES	3.9%	2.3%	3.9%	2.6%	3.9%	2.7%	3.9%	2.3%	3.8%	2.3%

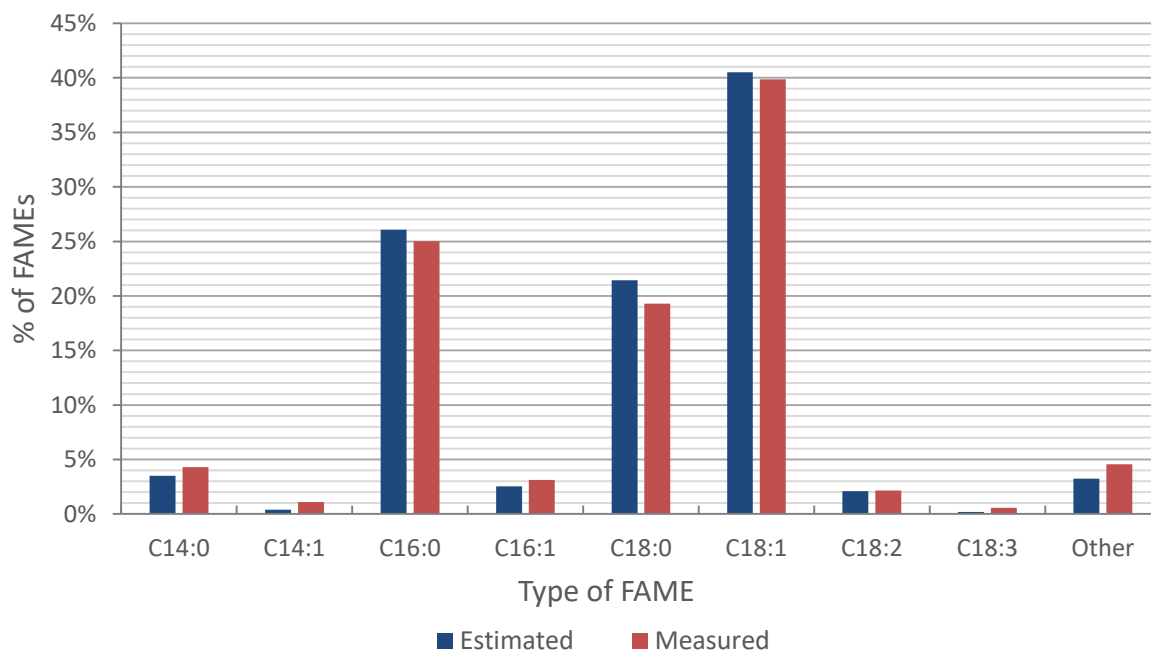


Figure C.1 – Estimated and measured FAME Profile for “Test TME”

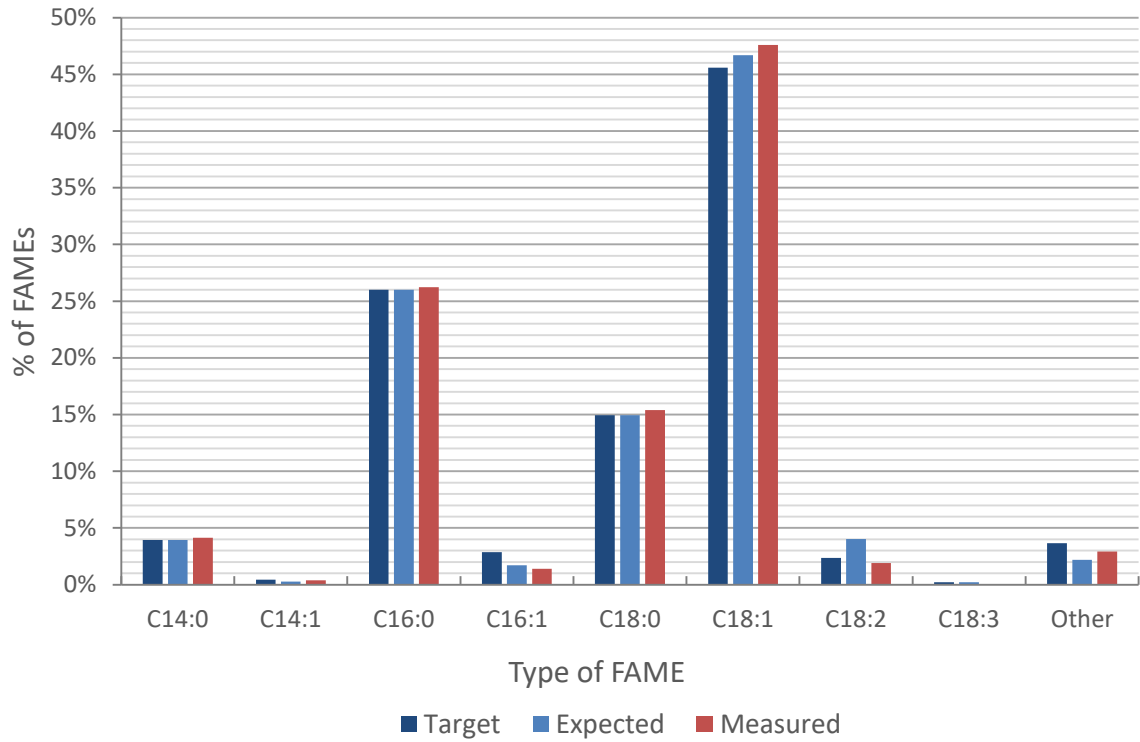


Figure C.2 – Target, expected and measured FAME Profile for “Test 1”

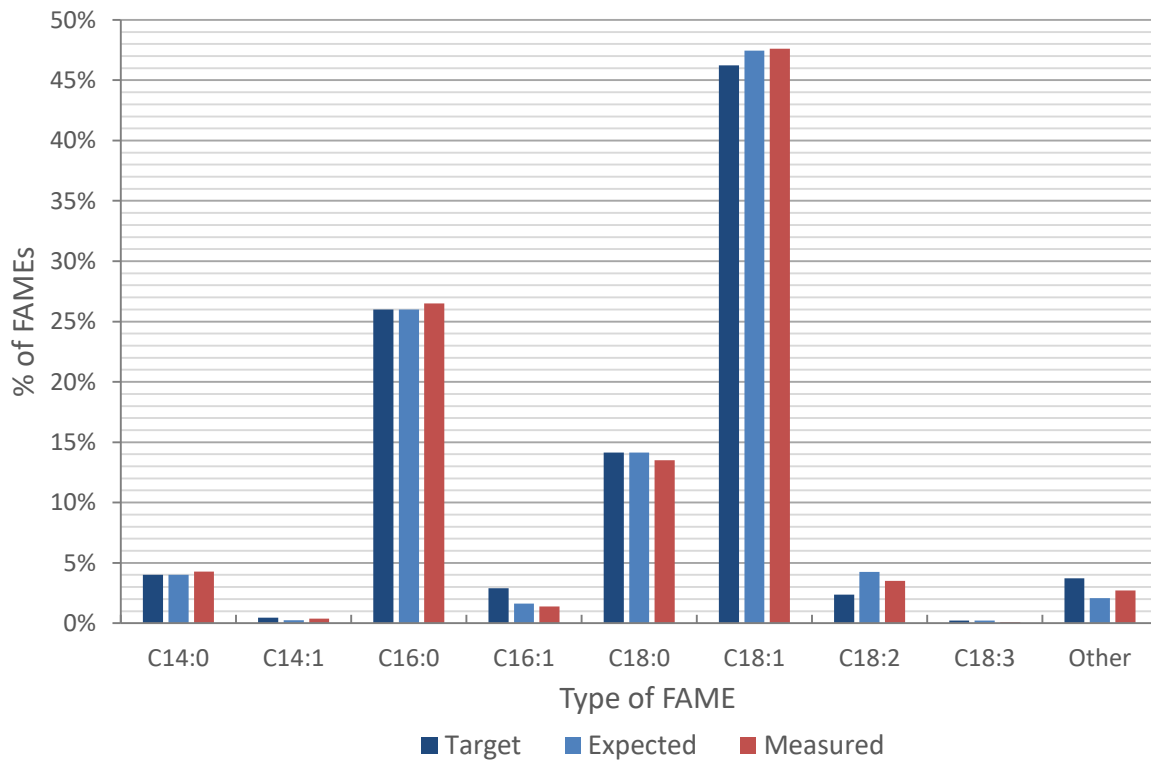


Figure C.3 – Target, expected and measured FAME Profile for “Test 2 +MS”

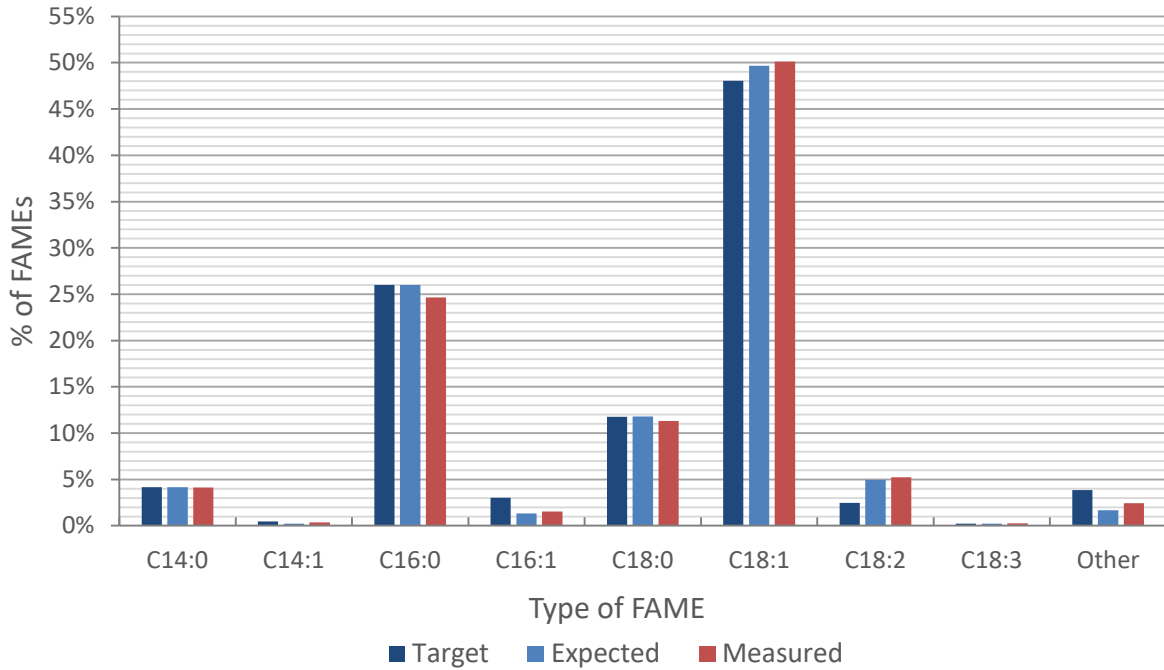


Figure C.4 – Target, expected and measured FAME Profile for “Test 2 TEP”

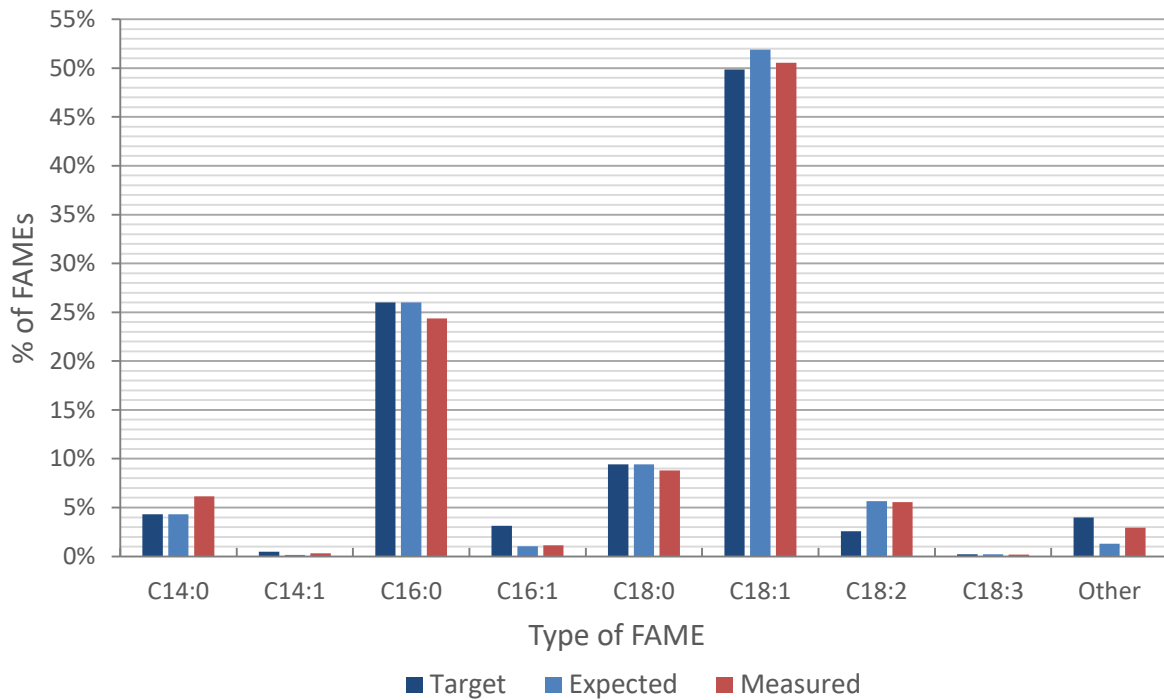


Figure C.5 – Target, expected and measured FAME Profile for “Test 2 -MS”

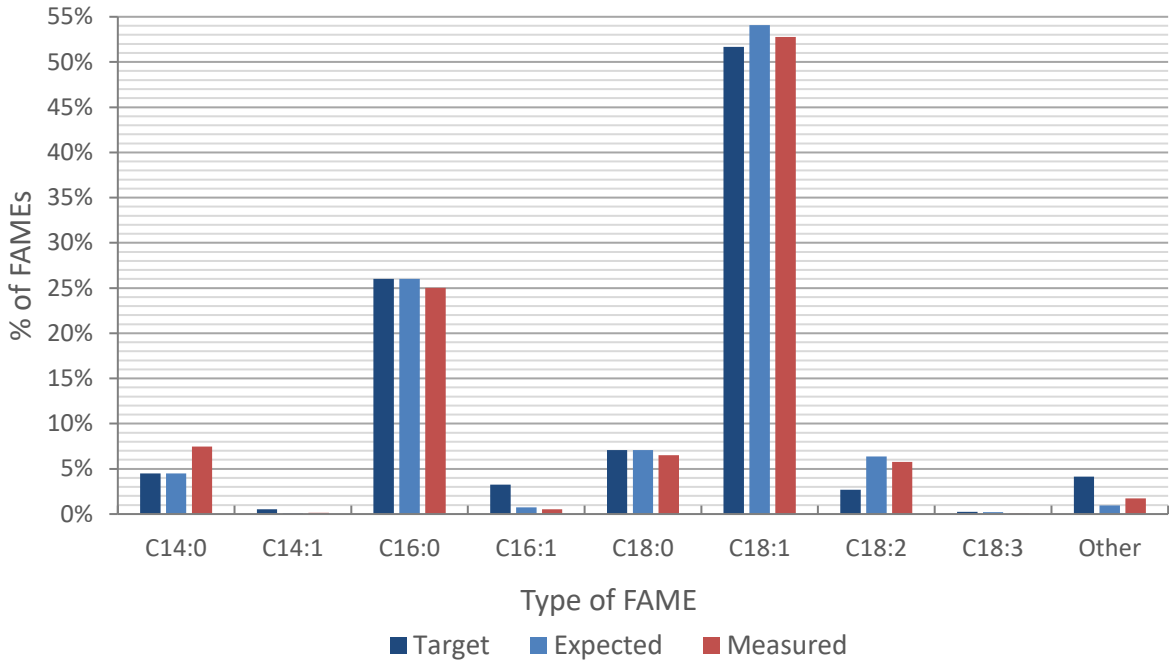


Figure C.6 – Target, expected and measured FAME Profile for “Test 5”

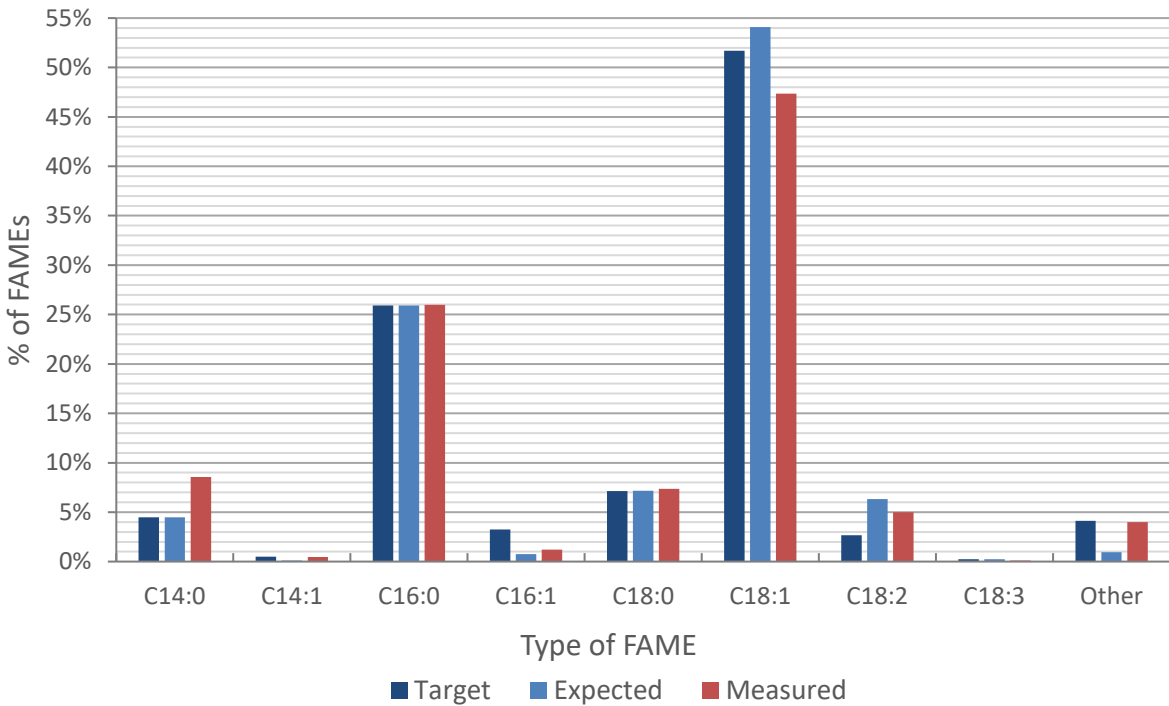


Figure C.7 – Target, expected and measured FAME Profile for “Test 5 EEPL”

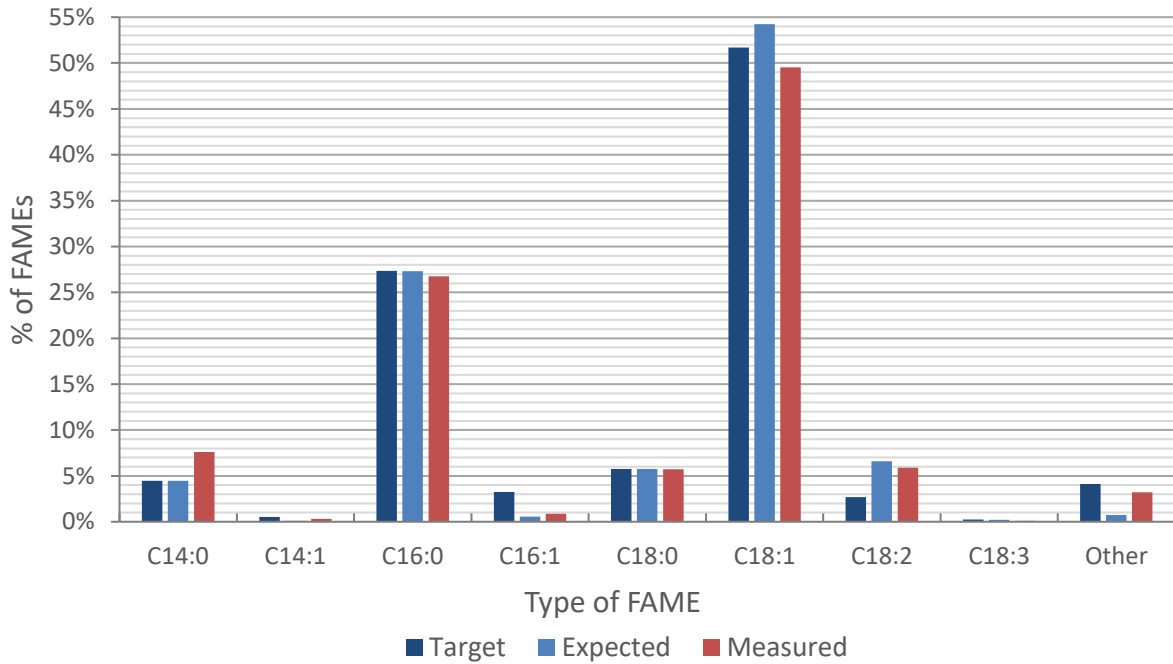


Figure C.8 - Target, expected and measured FAME Profile for "Test 5 EEPR"

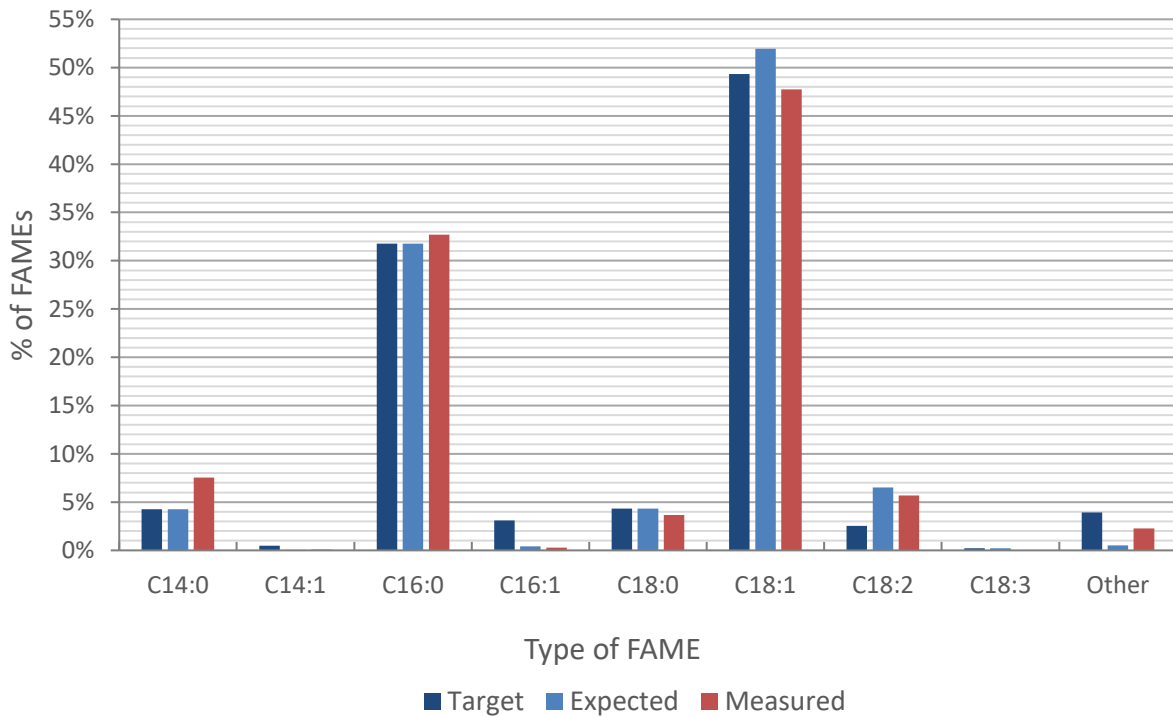


Figure C.9 - Target, expected and measured FAME Profile for "Test 6"

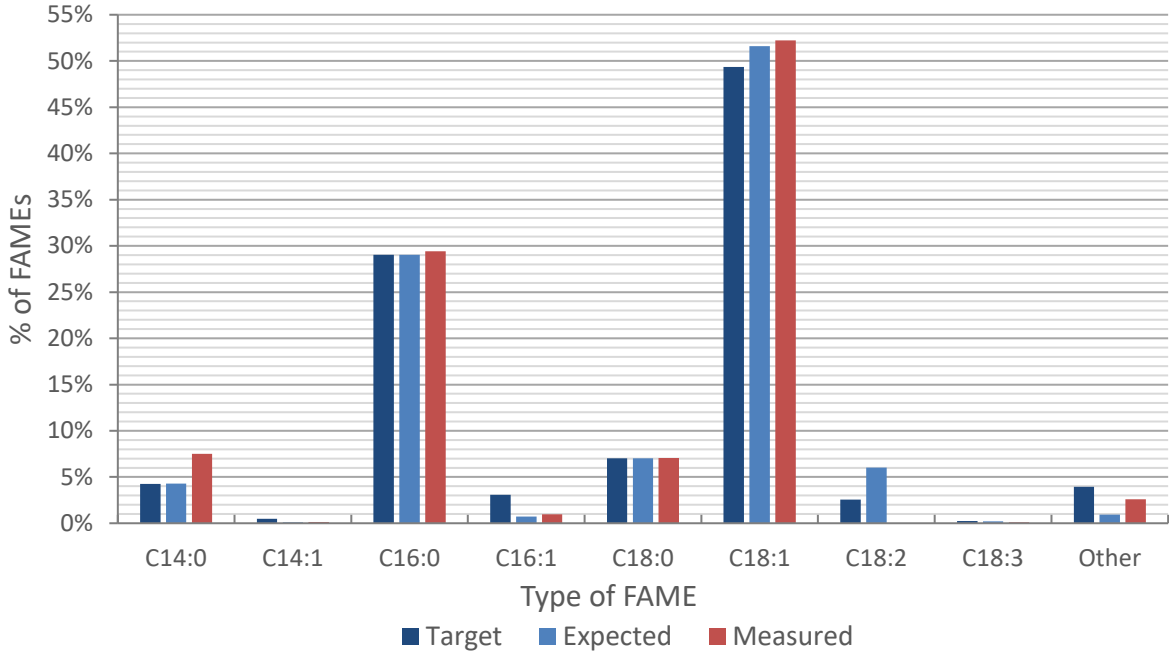


Figure C.10 – Target, expected and measured FAME Profile for “Test 6 EEP”

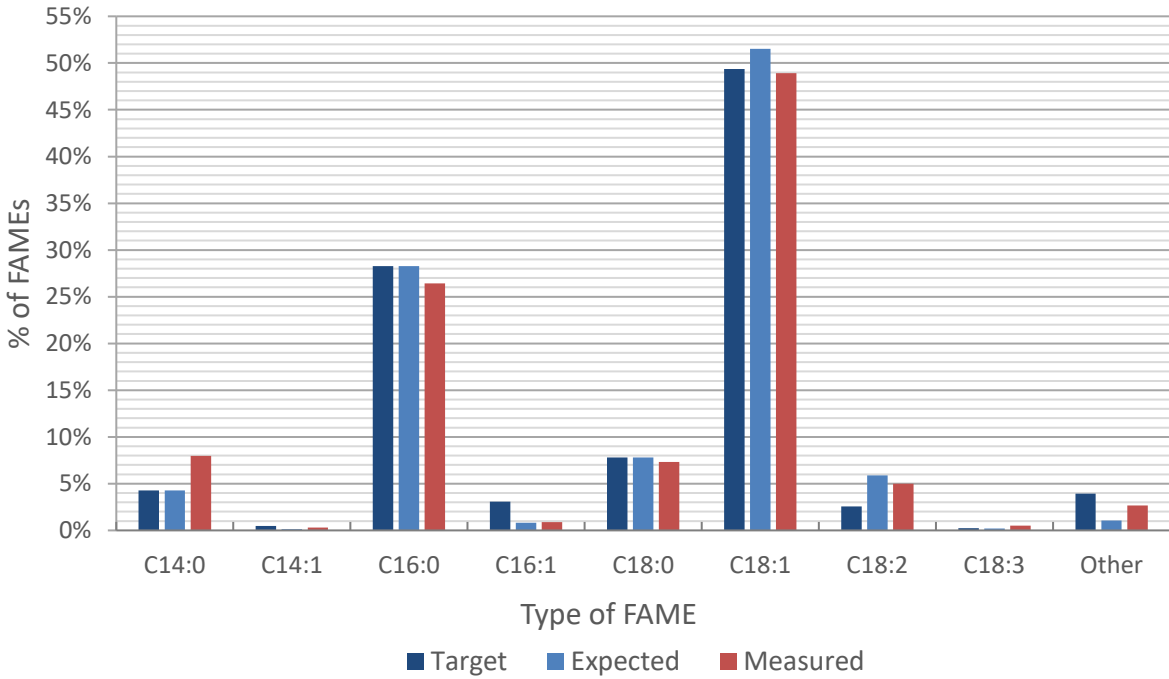


Figure C.11 – Target, expected and measured FAME Profile for “Test 6 EEPL”

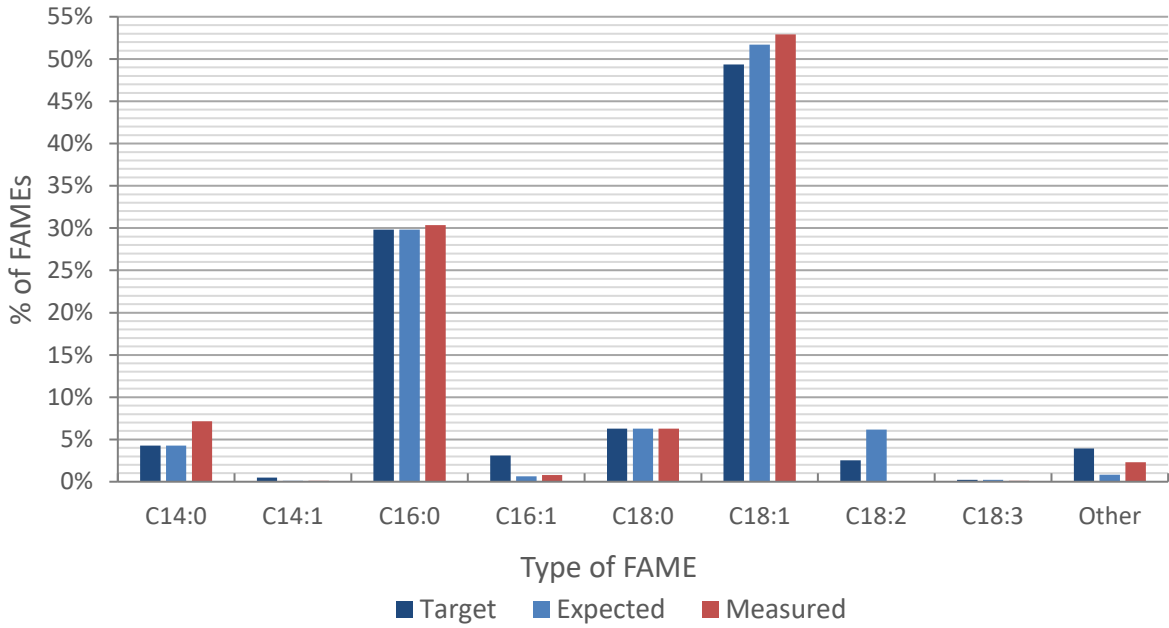


Figure C.12 - Target, expected and measured FAME Profile for "Test 6 EEPR"

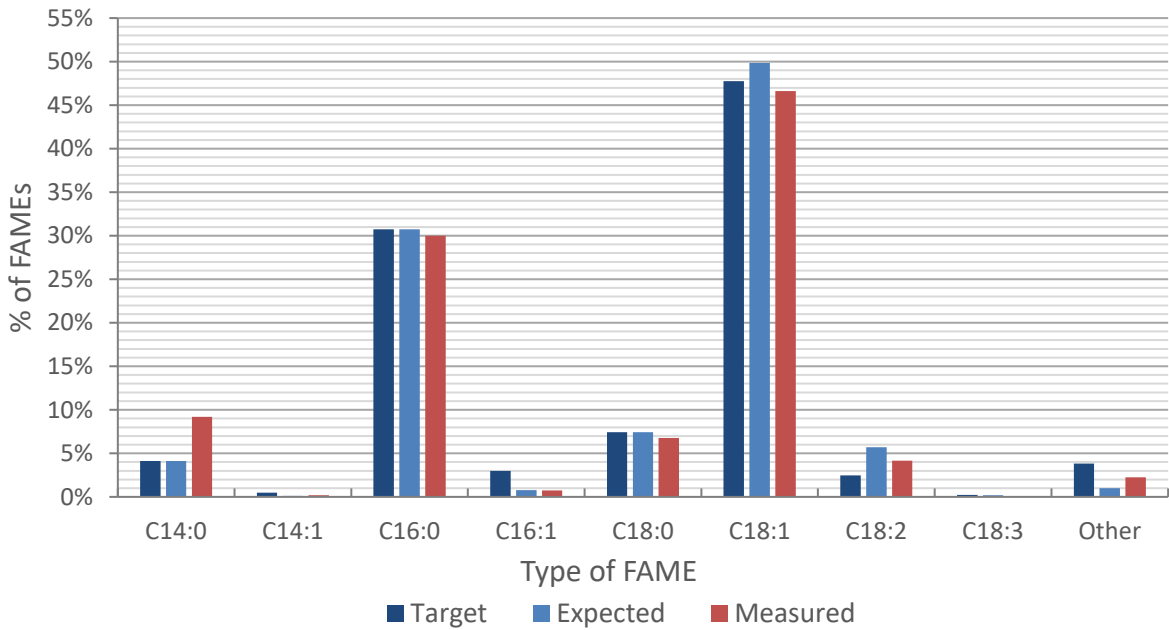


Figure C.13 - Target, expected and measured FAME Profile for "Test 7 EEP"

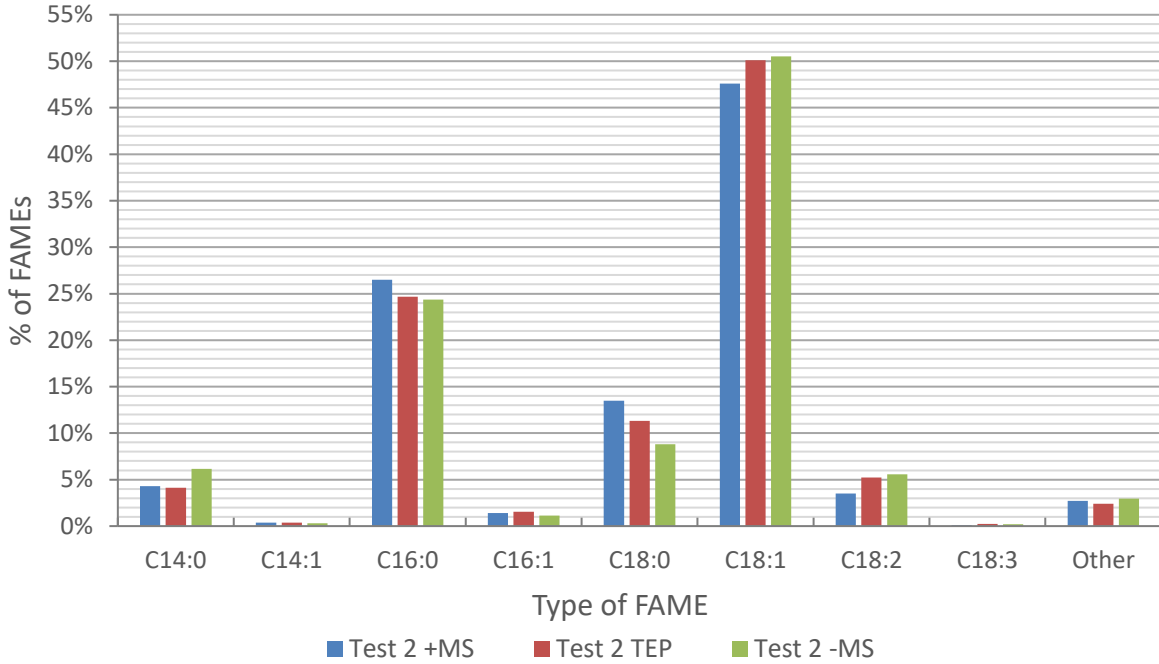


Figure C.14 - Comparison of FAME Profiles for Test 2 group

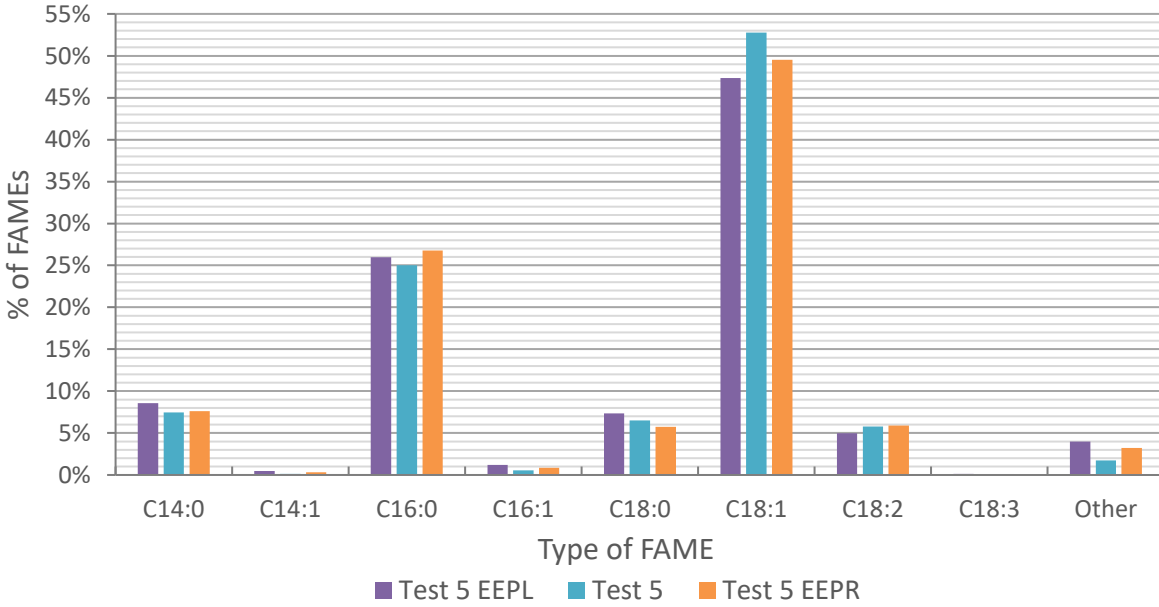


Figure C.15 - Comparison of FAME Profiles for Test 5 group

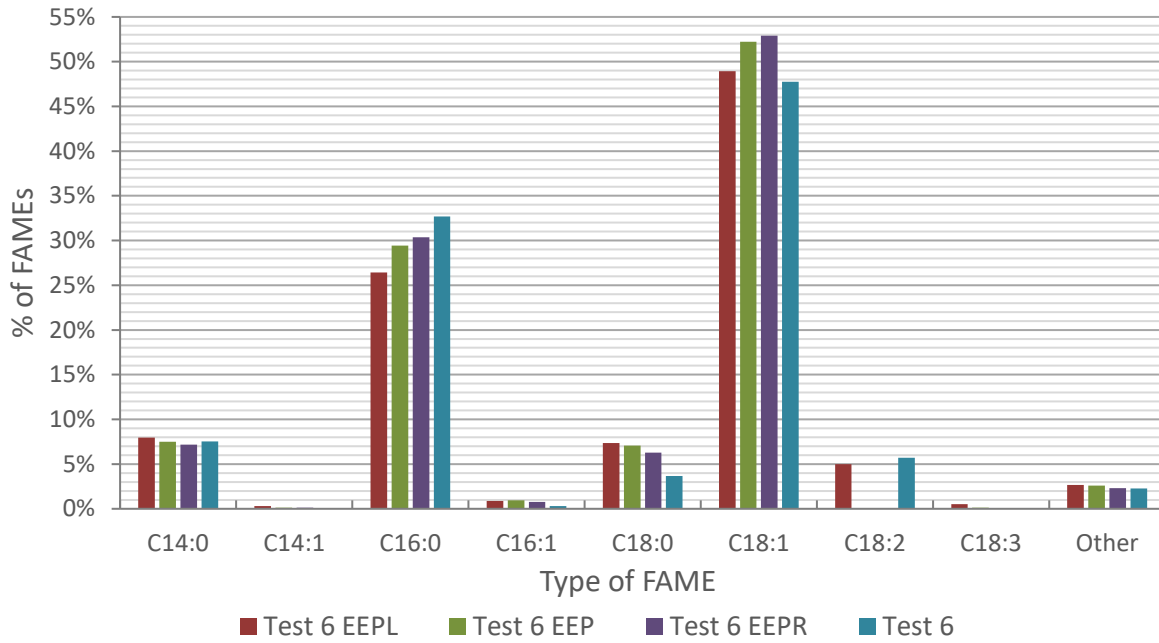


Figure C.16 - Comparison of FAME Profiles for Test 6 group

Appendix D: Fractionation Cold Filter Plugging Point Results

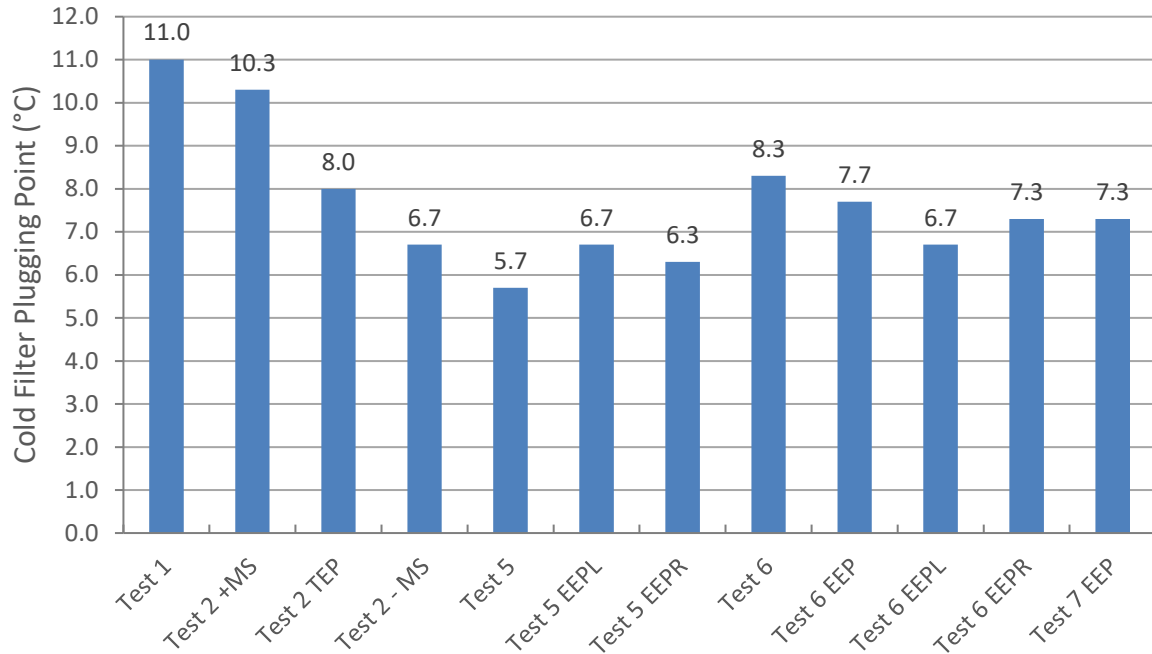


Figure D.1 - Cold filter plugging point for fractionation tests

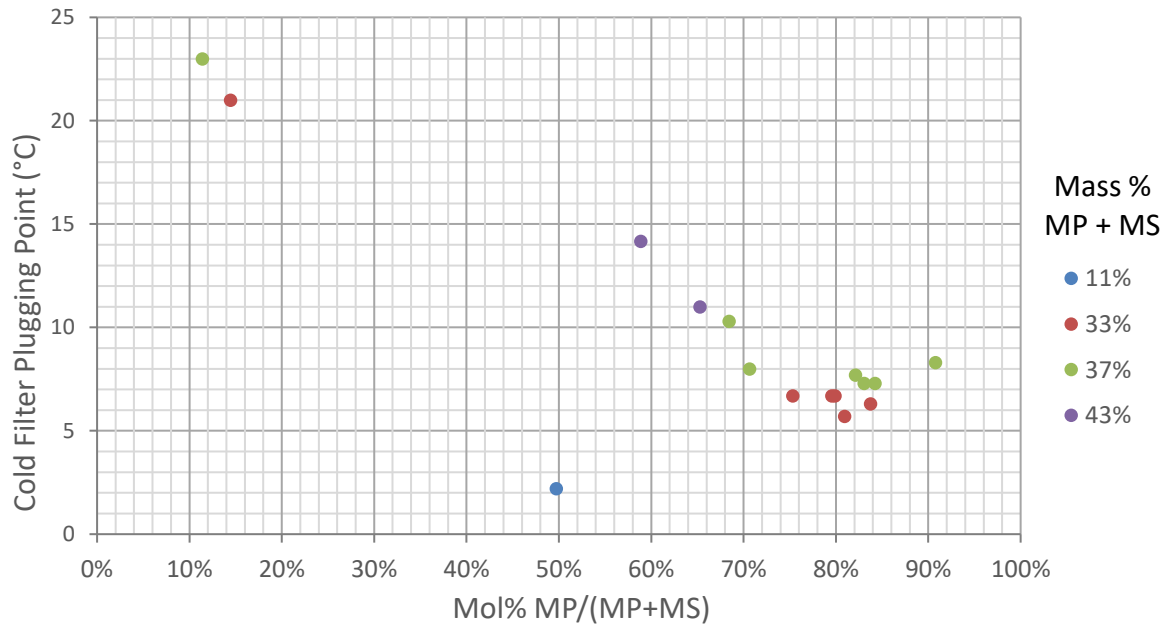


Figure D.2 - All empirical fractionation CFPPs in relation to MP/(MP+MS) ratio and sorted by MP+MS fraction

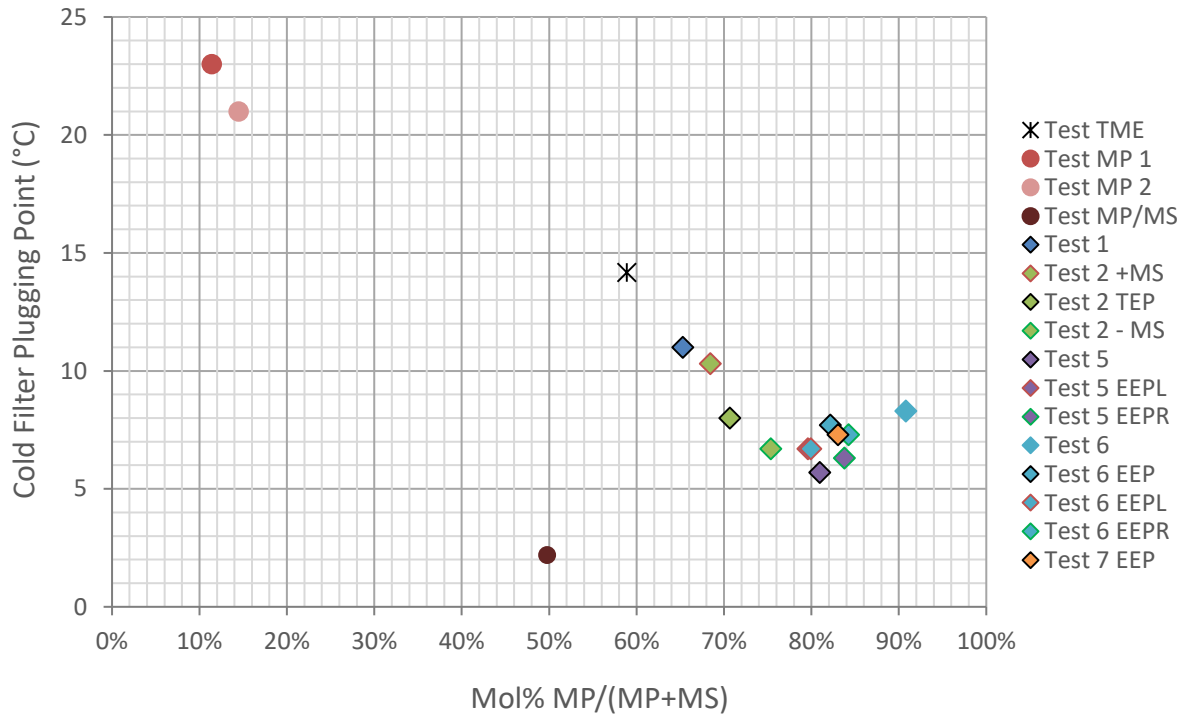


Figure D.3 - All empirical fractionation CFPPs in relation to MP/(MP+MS) ratio

Appendix E: Comparison of Fractionation Tests with CP Models

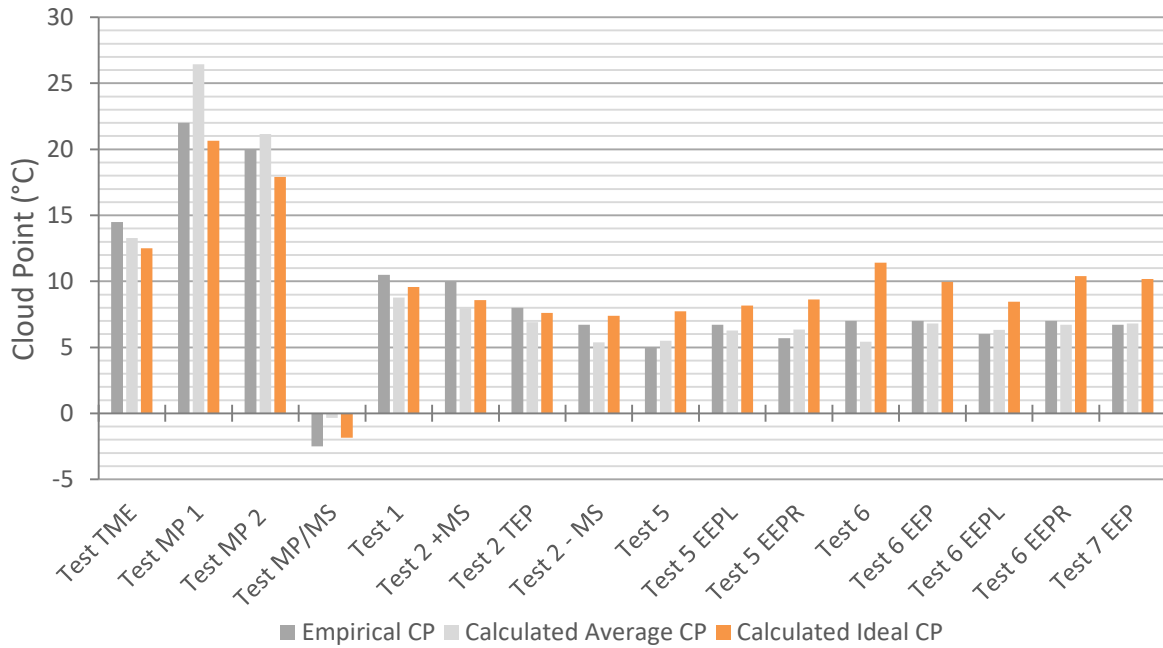


Figure E.1 – Comparison of fractionation tests’ empirical, calculated average and “Ideal” CPs

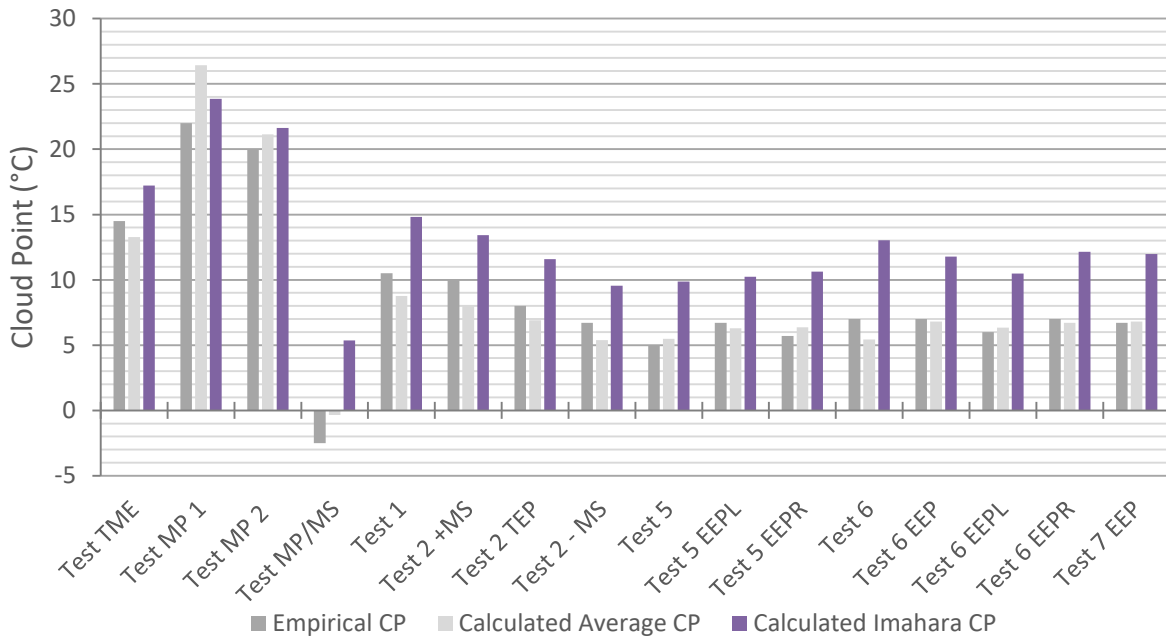


Figure E.2 – Comparison of fractionation tests’ empirical, calculated average and “Imahara” CPs

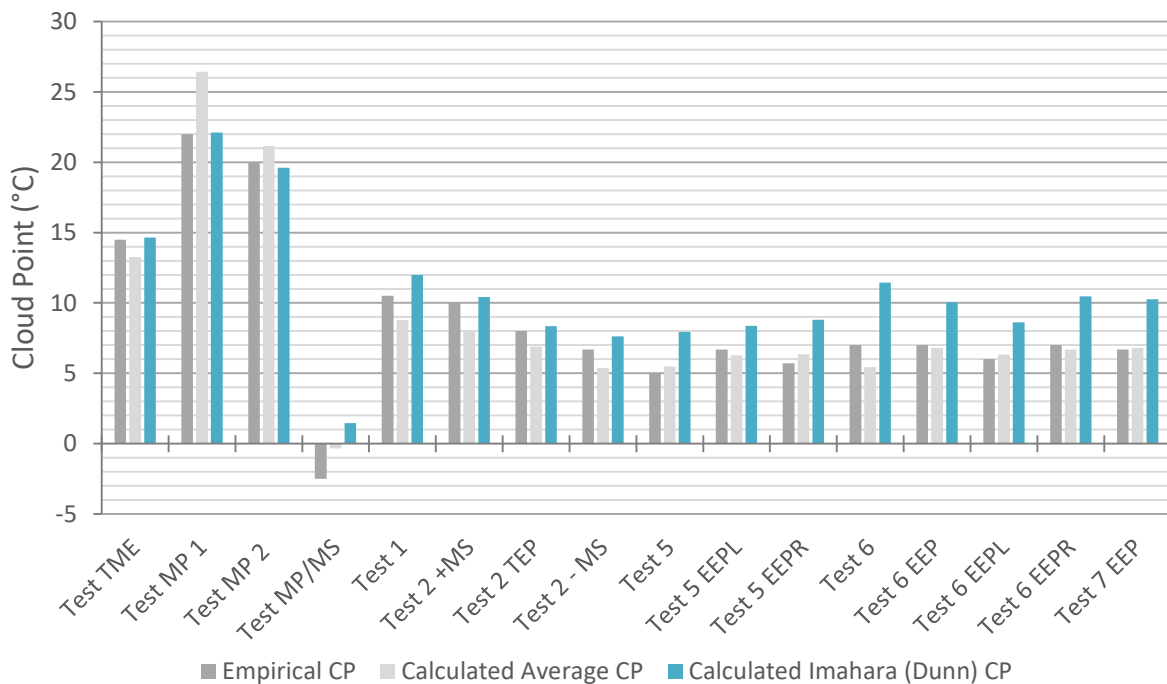


Figure E.3 – Comparison of fractionation empirical, calculated average and “Imahara (Dunn)” CPs

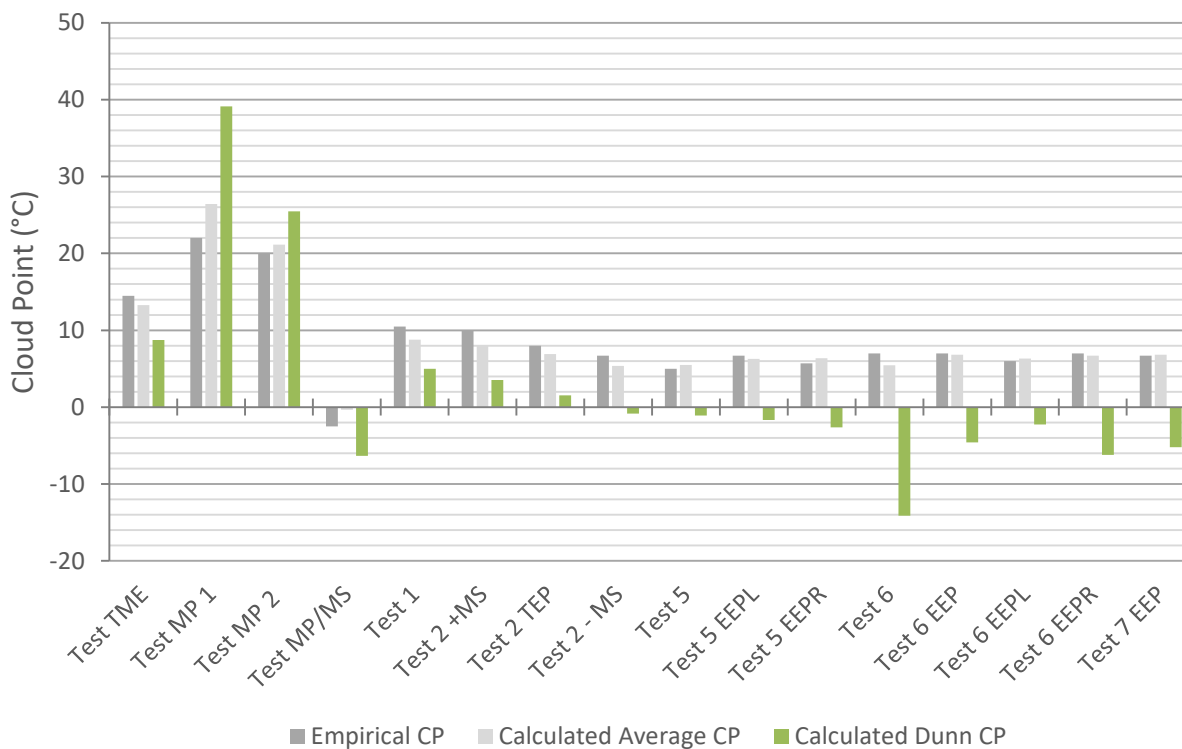


Figure E.4 – Comparison of fractionation tests’ empirical, calculated average and “Dunn” CPs

Appendix F: FAME Profiles of Blending Tests

Table F.1 – CP, CFPP and FAME profiles for SME in TME blending tests

	SME-BD-0	SME-BD-30	SME-BD-30	SME-BD-40	SME-BD-60	SME-BD-80	SME-BD-100
Max Empirical CP	14.3	12.0	10.7	10.0	6.3	4.0	2.3
Max Empirical CFPP	13.7	11.3	10.3	9.3	5.7	0.7	-5.3
Molar % MP/(MP+MS)	57%	59%	59%	60%	63%	67%	75%
Mass % MP+MS	48%	41%	38%	35%	28%	22%	15%
Measured FAME Profiles							
Mass % C14:0	3.5%	2.8%	2.5%	2.1%	1.4%	0.7%	0.0%
Mass % C14:1	0.4%	0.3%	0.3%	0.2%	0.2%	0.1%	0.0%
Mass % C16:0	26.1%	23.1%	21.6%	20.0%	17.0%	14.0%	11.0%
Mass % C16:1	2.5%	2.0%	1.8%	1.5%	1.0%	0.5%	0.0%
Mass % C18:0	21.4%	18.0%	16.2%	14.5%	11.0%	7.5%	4.0%
Mass % C18:1	40.5%	37.2%	35.6%	33.9%	30.6%	27.3%	24.0%
Mass % C18:2	2.1%	12.3%	17.4%	22.5%	32.6%	42.8%	53.0%
Mass % C18:3	0.2%	1.8%	2.5%	3.3%	4.9%	6.4%	8.0%
Mass % Other FAMES	3.2%	2.6%	2.3%	1.9%	1.3%	0.6%	0.0%

Table F.2 – CP, CFPP and FAME profiles from CME blending with TME using CAN-BD-A

	CAN-A-0	CAN-A-20	CAN-A-30	CAN-A-40	CAN-A-60	CAN-A-80	CAN-A-100
Max CP	14.3	11.0	9.3	7.3	3.3	-0.7	-8.3
Max CFPP	13.7	10.7	9.7	7.7	4.7	-2.7	-9.0
Molar % MP/(MP+MS)	62%	57%	57%	58%	67%	79%	72%
Mass % MP+MS	46%	39%	34%	31%	25%	12%	6%
Measured FAME Profiles							
Mass % C14:0	5.1%	2.9%	2.6%	2.1%	2.7%	0.9%	0.0%
Mass % C14:1	0.9%	0.5%	0.6%	0.4%	0.5%	0.2%	0.0%
Mass % C16:0	27.6%	21.6%	18.7%	17.1%	16.1%	9.1%	4.1%
Mass % C16:1	3.2%	1.9%	2.1%	1.4%	1.4%	0.7%	0.2%
Mass % C18:0	18.7%	17.8%	15.4%	13.6%	8.8%	2.7%	1.8%
Mass % C18:1	38.9%	46.7%	47.8%	51.0%	52.3%	61.3%	64.1%
Mass % C18:2	1.5%	4.3%	6.5%	8.3%	11.5%	16.8%	19.9%
Mass % C18:3	0.4%	1.3%	2.4%	3.1%	4.2%	6.0%	9.4%
Mass % Other FAMES	3.6%	3.1%	3.8%	3.1%	2.5%	2.3%	0.5%

Table F.3 - CP, CFPP and FAME profiles from CME blending with TME using CAN-BD-B

	CAN-B-0	CAN-B-10	CAN-B-20	CAN-B-30	CAN-B-40	CAN-B-50	CAN-B-60	CAN-B-80	CAN-B-100
Max CP	14.3	12.7	11.0	9.7	8.0	5.7	4.3	-1.0	-8.3
Max CFPP	13.7	12.3	10.7	8.7	7.3	4.0	3.3	-4.0	-9.0
Molar % MP/(MP+MS)	62%	57%	58%	59%	59%	56%	61%	76%	73%
Mass % MP+MS	46%	43%	40%	37%	32%	30%	24%	12%	6%
Measured FAME Profiles									
Mass % C14:0	5.1%	3.2%	3.1%	2.9%	2.5%	1.8%	1.7%	1.7%	0.1%
Mass % C14:1	0.9%	0.4%	0.7%	0.5%	0.4%	0.2%	0.2%	5.0%	0.0%
Mass % C16:0	27.6%	23.9%	22.3%	21.0%	18.3%	16.1%	14.2%	9.0%	4.2%
Mass % C16:1	3.2%	2.3%	2.2%	1.7%	1.5%	1.4%	1.1%	0.6%	0.2%
Mass % C18:0	18.7%	19.5%	17.7%	15.9%	13.9%	14.1%	10.0%	3.1%	1.7%
Mass % C18:1	38.9%	42.7%	45.1%	46.3%	49.2%	50.3%	54.1%	56.7%	63.2%
Mass % C18:2	1.5%	3.8%	4.4%	5.9%	8.0%	9.4%	11.5%	15.1%	19.4%
Mass % C18:3	0.4%	1.3%	0.8%	2.6%	3.4%	4.6%	5.4%	7.2%	9.4%
Mass % Other FAMES	3.6%	2.9%	3.9%	3.2%	2.6%	2.2%	1.8%	1.6%	1.7%

Appendix G: Blending Cold Filter Plugging Point Results

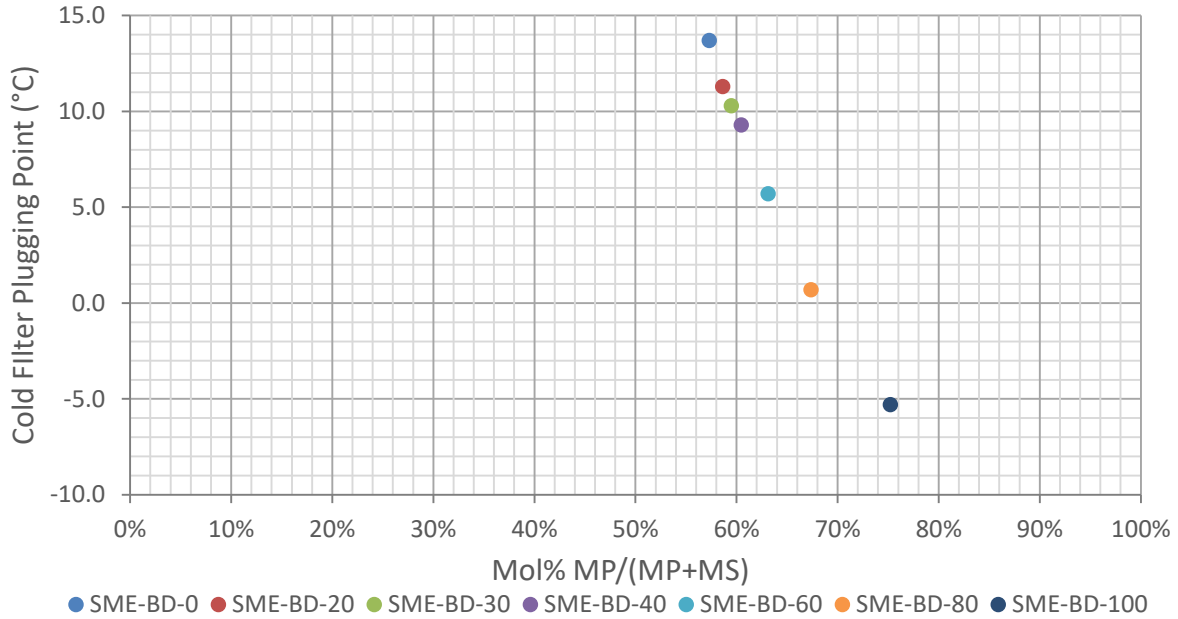


Figure G.1 – SME blending CFPPs in relation to MP/(MP+MS) ratio

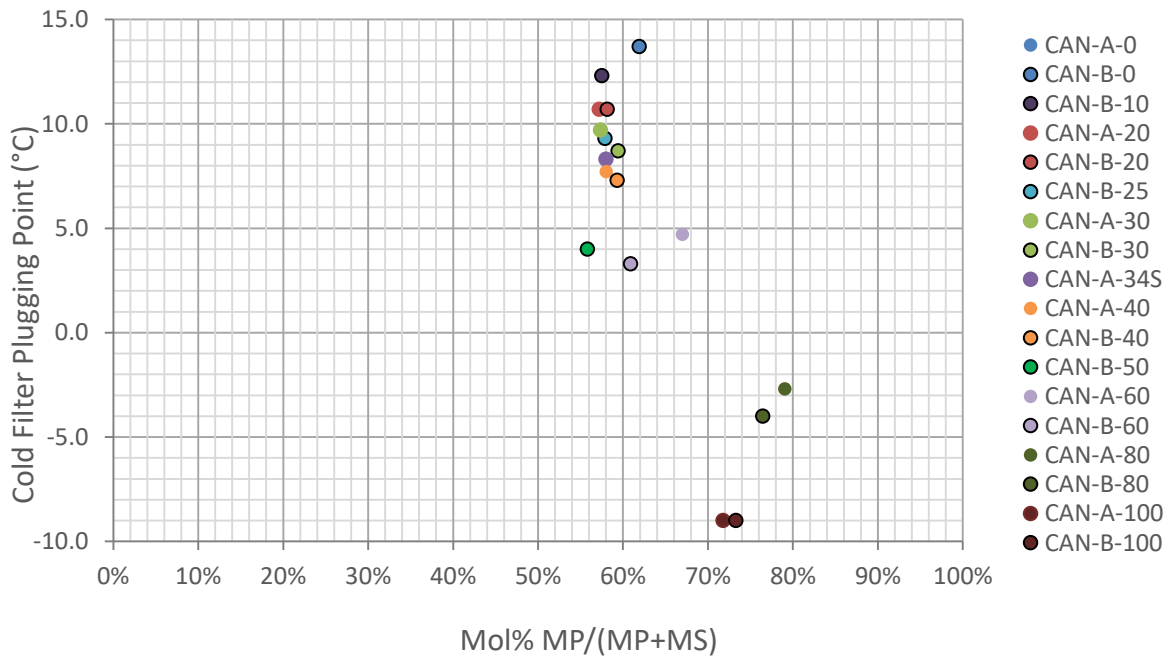


Figure G.2 – CME blending CFPPs in relation to MP/(MP+MS) ratio

Appendix H: Comparison of Blending Tests with CP Models

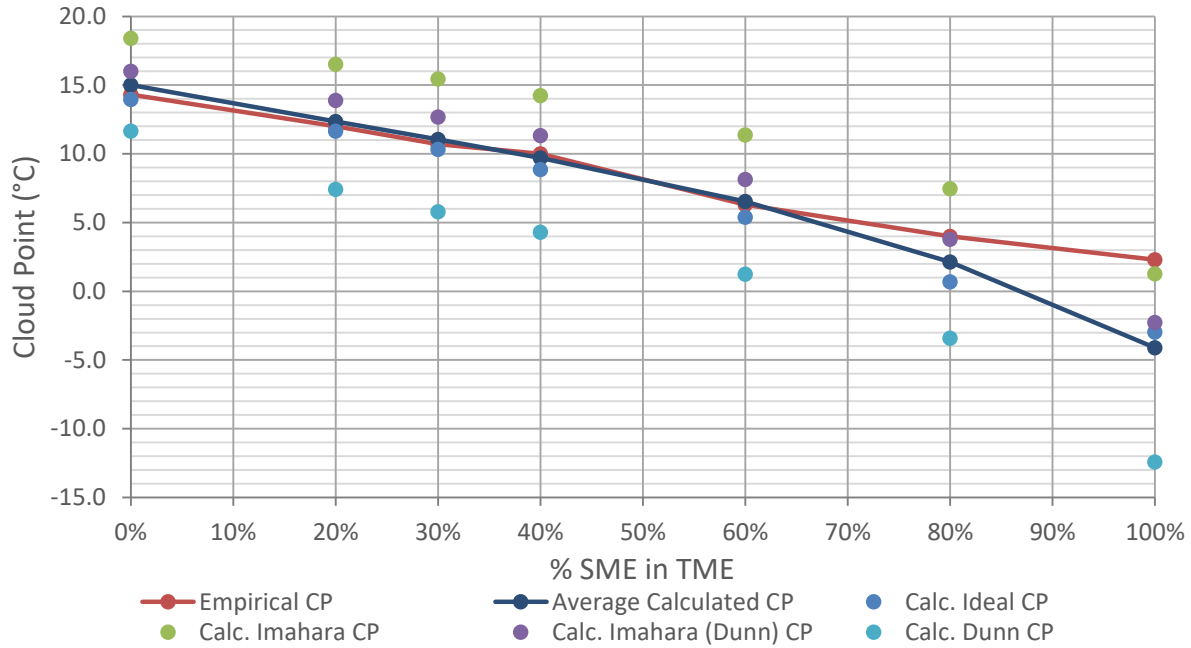


Figure H.1 - Comparison of empirical CPs with CP models for each SME/TME blend

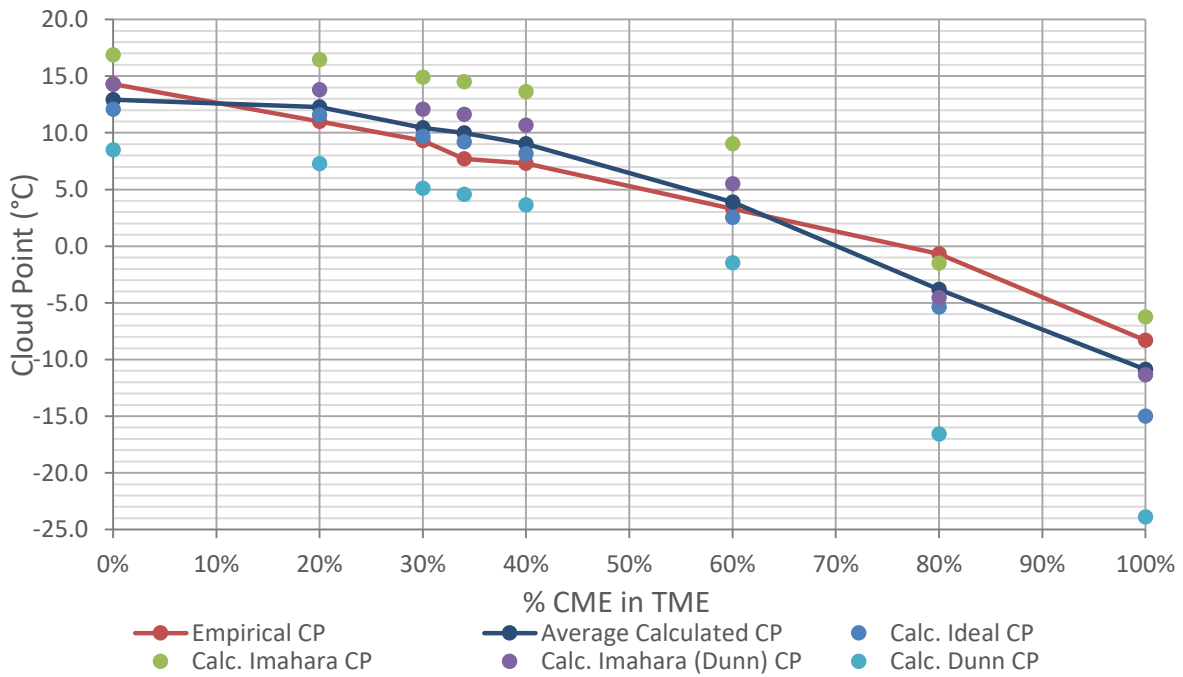


Figure H.2 - Comparison of empirical CPs with CP models for each CAN-A-BD/TME blend

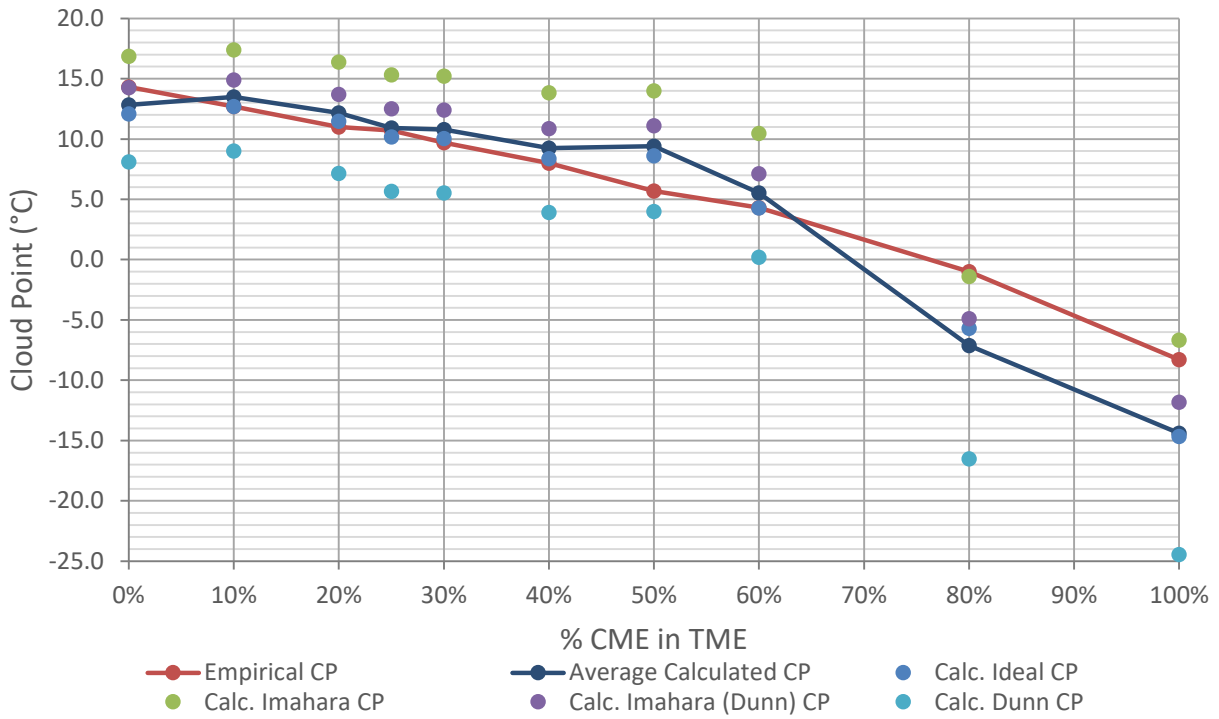


Figure H.3 - Comparison of empirical CPs with CP models for each CAN-B-BD/TME blend

Appendix I: FAME Profiles of Various Feedstocks

Feedstock	C8:0	C10:0	C12:0	C14:0	C15:0	C16:0	C16:1	C17:0	C17:1	C18:0	C18:1	C18:1n-3(OH)	C18:2	C18:3	C18:3n-3,11,13 ^a	C20:0	C20:1	C20:1n-7(OH)	C20:2	C20:5	C22:0	C22:1	C24:0	C24:1	UNKNOWN
Algae 1				0.6		6.9	0.2			3.0	75.2		12.4	1.2		0.4					0.1				
Babassu	0.5	3.8	48.8	17.2		9.7				4.0	14.2		1.8												
Beef Tallow			0.2	2.9	0.6	24.3	2.1	1.2	0.4	22.8	40.2		3.3	0.7		0.2	0.6								0.5
Borage						9.3				3.8	17.1		38.7	26.1							0.2	2.5		1.5	0.8
Camelina Oil						5.0				2.2	17.7		18.0	37.9		1.4	9.8		1.6		0.4	4.5	0.3	0.2	1.0
Canola Oil						3.8	0.3			1.9	63.9		19.0	9.7		0.6					0.4		0.2	0.2	
Castor ^a						0.9				1.1	3.1	90.3	4.0	0.6											
Choice White Grease				1.3		21.6	2.8	0.2	0.3	9.0	50.4		12.2	1.0		0.2	0.5					0.3			0.2
Coconut	6.3	6.0	49.2	18.5		9.1				2.7	6.5		1.7												
Coffee						11.0	0.5			3.4	70.0		12.7	0.8		0.6	0.1				0.2		0.1		0.6
Corn						12.1	0.1		0.1	1.8	27.2		56.2	1.3		0.4					0.2				0.6
<i>Cuphea Viscosissima</i>				4.7		18.2				3.5	46.9		22.8	2.3		0.6					0.4		0.6		
Evening Primrose				6.0		6.0				1.8	6.6		76.3	9.0		0.3									
Fish			0.2	7.7		18.8	9.3	0.3	0.3	3.9	15.0		4.6	0.3		0.2	1.4			25.1	0.7	1.3		0.4	10.5
Hemp						5.2				2.4	13.1		57.1	20.0		0.7					0.5		0.3		0.7
Hepar, High IV			0.2	1.0		20.7	2.7	0.3	0.3	8.9	46.7		15.6	0.5		0.2	0.8		1.3		0.2	0.4		0.1	0.1
Hepar, Low IV		0.1	0.1	1.5		28.0	1.9	0.3	0.2	20.2	36.1		9.7	0.3		0.2	0.7		0.4			0.3			
Jatropha						12.7	0.7			5.5	39.1		41.6	0.2		0.2									
<i>Lesquerella Fendleri</i> ^a				0.1		0.9	0.3			1.7	13.0		5.8	10.6		0.7		66.5							0.4
Linseed						4.4				3.8	20.7		15.9	54.6		0.2					0.3		0.1		
<i>Moringa Oleifera</i>						5.5	1.2			5.8	76.3		0.7			3.1	2.0				4.2		0.4		0.8
Mustard						2.6	0.2			1.2	20.6		20.6	13.3		0.9	10.7		1.0		0.5	25.6	0.2	1.5	1.1
Neem						14.9	0.1			20.6	43.9		17.9	0.4		1.6					0.3		0.3		
Palm			0.2	0.5		43.4	0.1			4.6	41.9		8.6	0.3		0.3					0.1				
Perilla Seed						5.3	0.1			2.2	16.6		13.7	62.1											
Poultry Fat			0.1	1.0		19.6	3.2	0.3	0.2	7.5	36.8		28.4	2.0		0.1			0.1		0.3	0.4			
Rice Bran				0.3		12.5				2.1	47.5		35.4	1.1		0.6					0.3		0.2		
Soybean						9.4				4.1	22.0		55.3	8.9							0.3				
Stillingia			0.4	0.1		7.5				2.3	16.7		31.5	41.5											
Sunflower						4.2				3.3	63.6		27.6	0.2							0.7		0.4		
Tung						1.8				2.1	5.3		6.8	0.7	72.2	0.2			0.1				10.4		0.4
Used Cooking Oil			0.1	0.1		11.8	0.4	0.1	0.1	4.4	25.3		49.5	7.1		0.3					0.4	0.3	0.1		
Yellow Grease			0.1	0.5		14.3	1.1	0.3	0.2	8.0	35.6		35.0	4.0		0.3					0.3	0.2		0.1	

^a In the GC/FID chromatogram the hydroxy ester peaks were missing. The quantity of the hydroxy ester peaks was estimated from the hydroxyl value with the assumption that all the hydroxy value was the primary hydroxy acid in the sample.

Figure I.1 – FAME profiles of a diverse set of biodiesel feedstocks possibilities [13]

Appendix J: Additional Data of MLA in TME/Diesel Blends

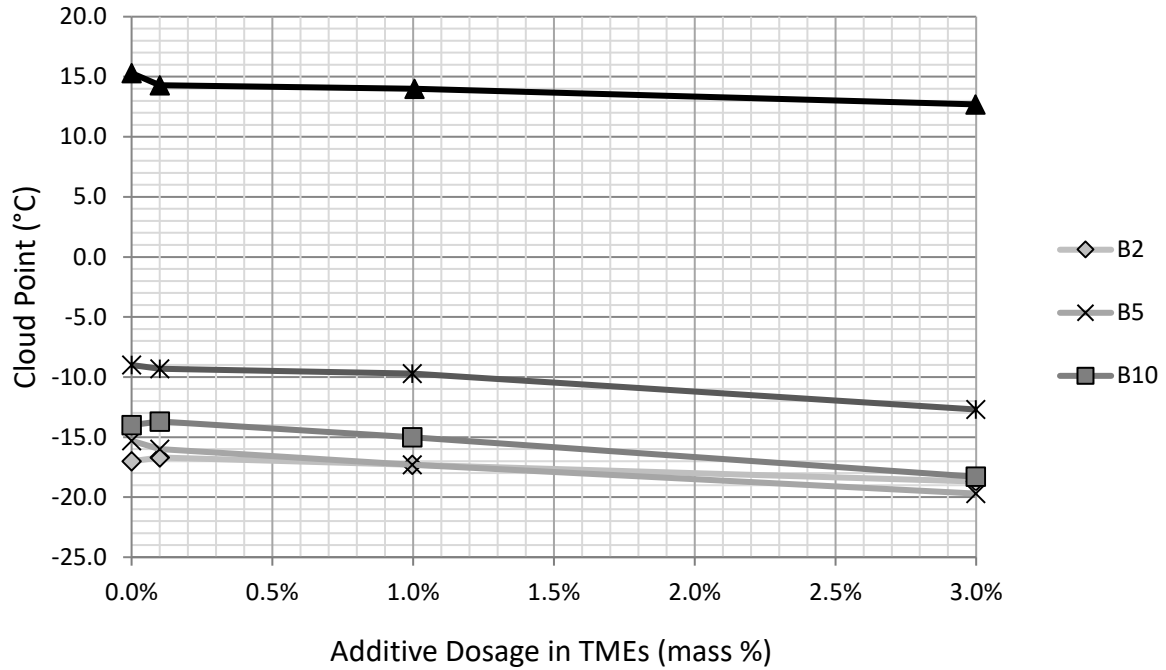


Figure J.1 - Effect of MLA additive on cloud point of TME/diesel blends

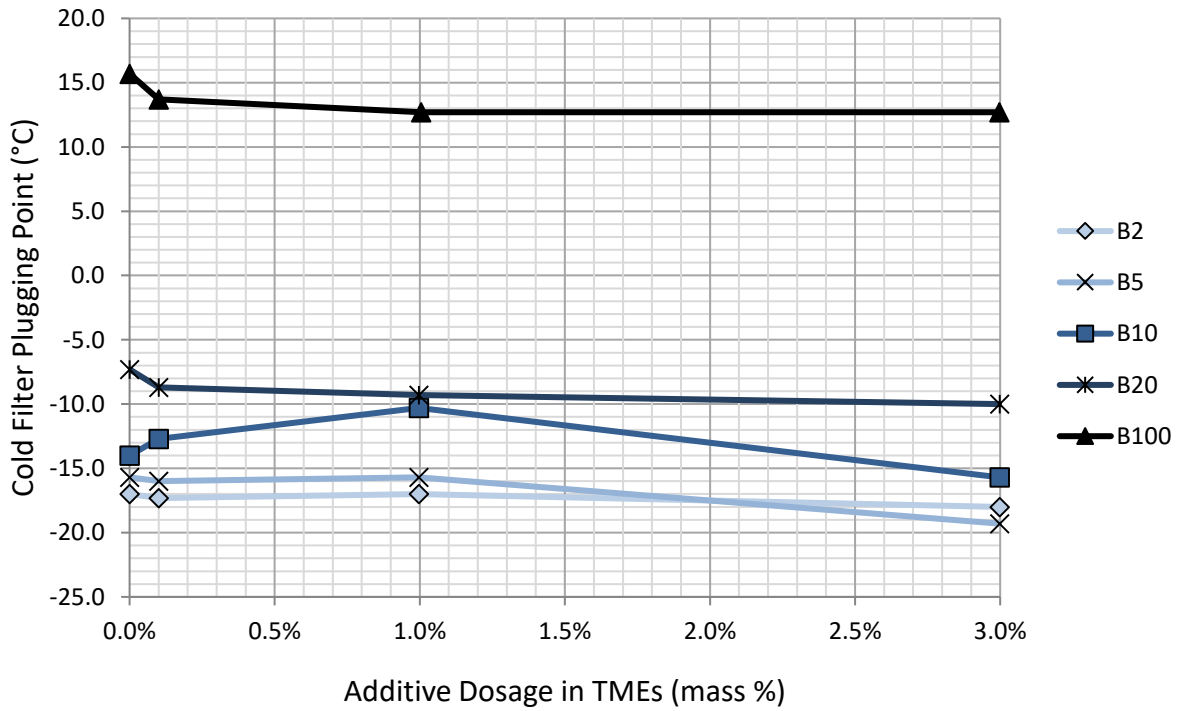


Figure J.2 - Effect of MLA additive on cold filter plugging point of TME/diesel blends

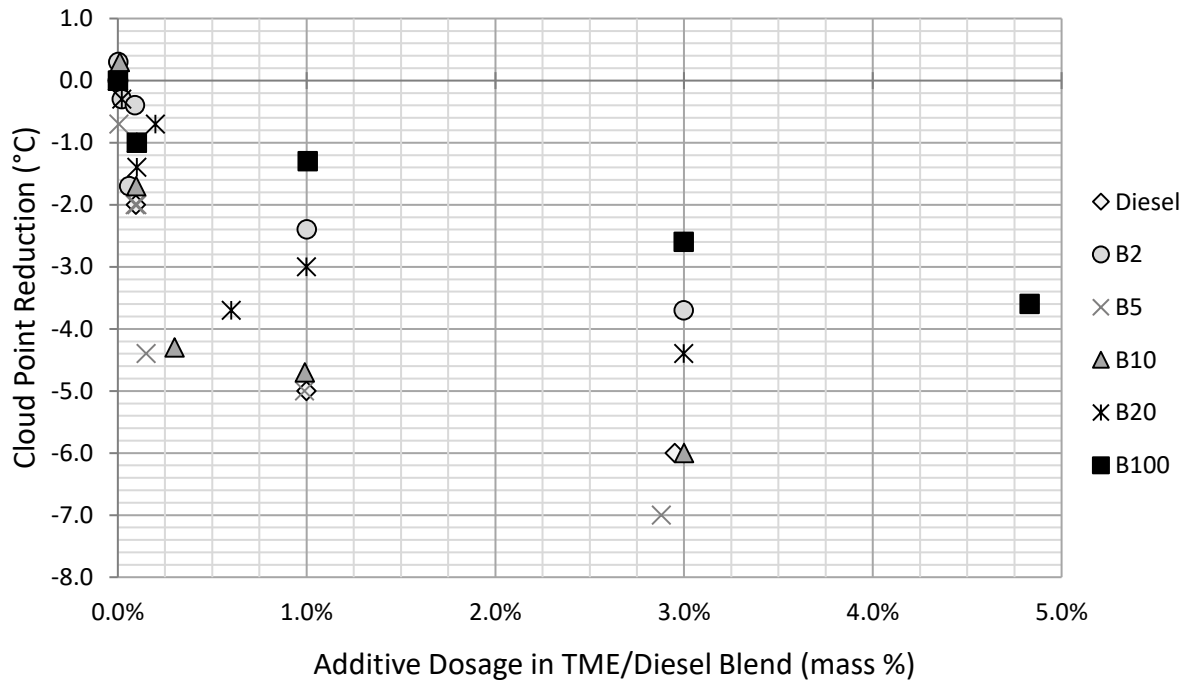


Figure J.3 – CP reduction with all MLA/TME/Diesel blend data at percent MLA of total

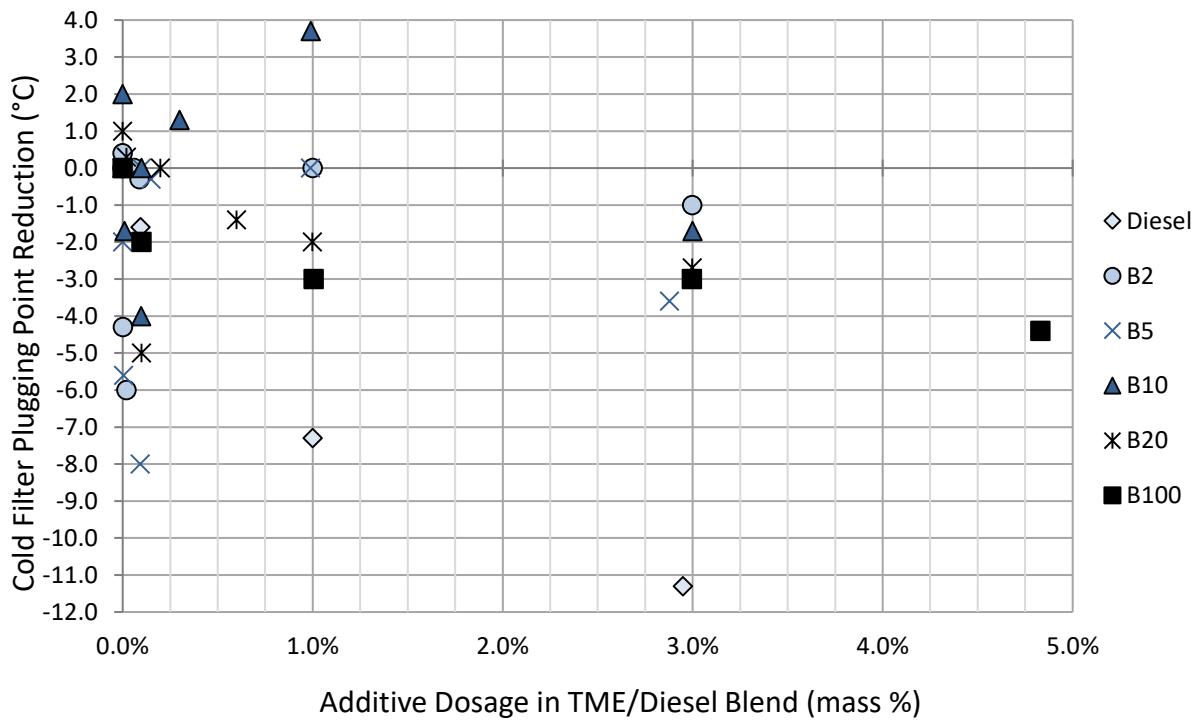


Figure J.4 – CFPP reduction with all MLA/TME/Diesel blend data at percent MLA of total

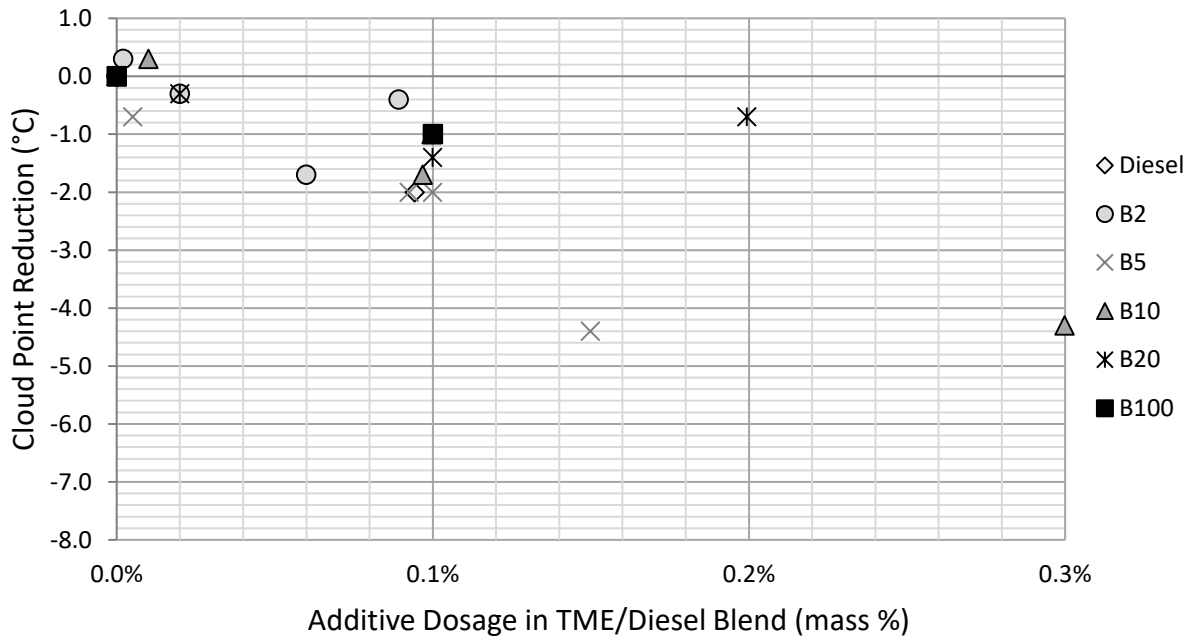


Figure J.5 - Detailed view of Figure J.3 at lower dosages

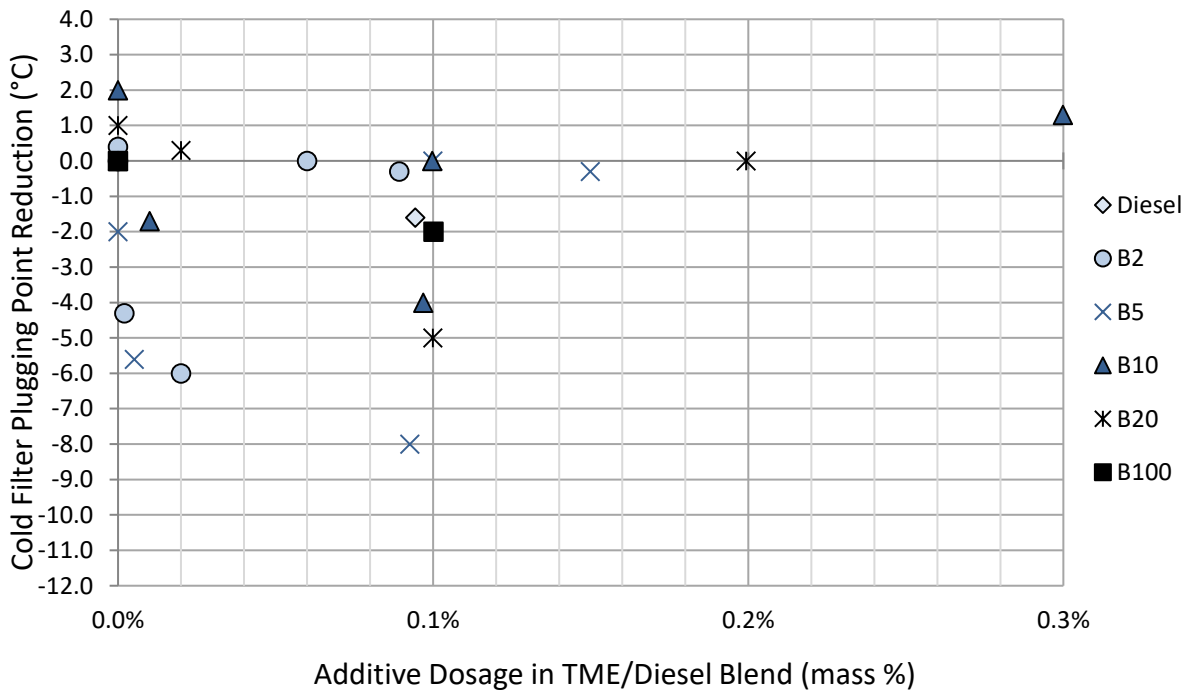


Figure J.6 - Detailed view of Figure J.4 at lower dosages

Appendix K: Comparison of Measured and Literature Cloud Points

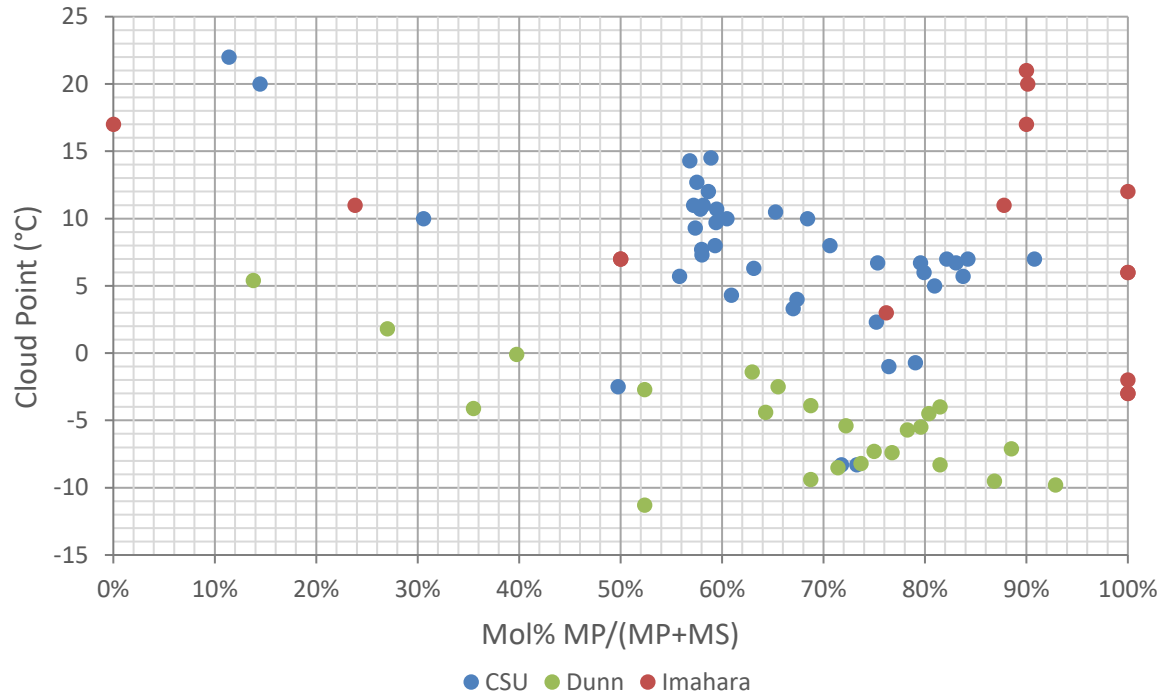


Figure K.1 – Plot of measured FAME CPs from CSU, Dunn and Imahara at MP/(MP+MS) ratio

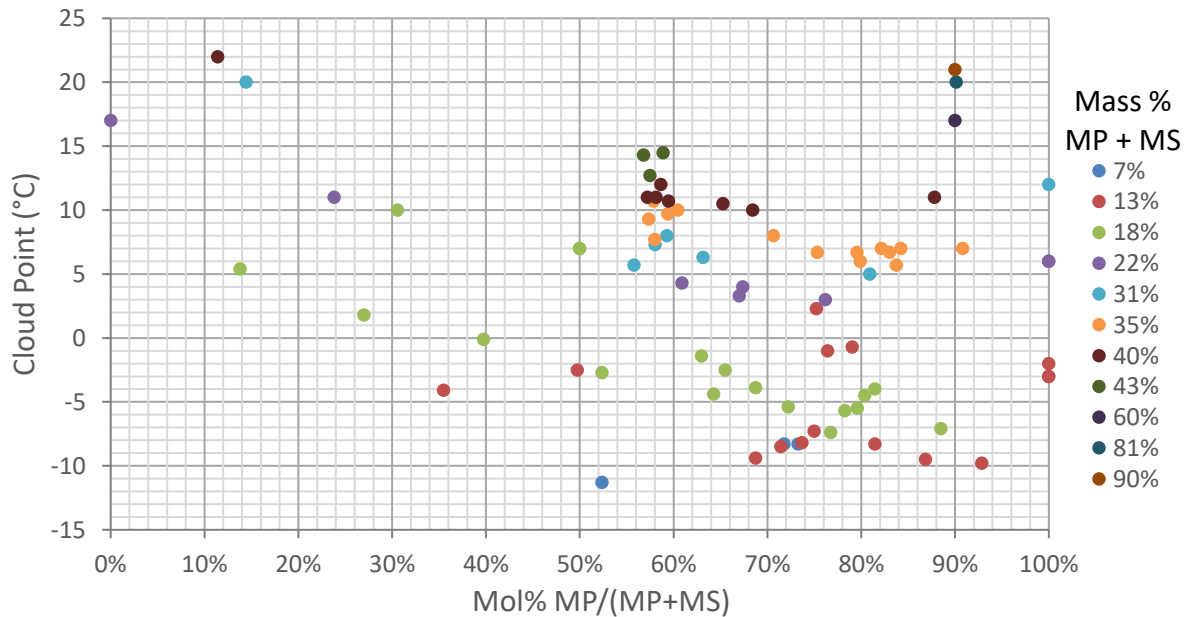


Figure K.2 – Plot of measured FAME CPs from CSU, Dunn and Imahara by MP+MS fraction

List of Abbreviations

ASTM	-	American Society of Testing and Materials
BXX	-	Percentage of biodiesel in petroleum diesel (i.e. B20 is 20% biodiesel/80% diesel)
Ca	-	Calcium
CCD	-	Charge coupled device
CFPP	-	Cold filter plugging point
CME	-	Canola methyl ester
CN	-	Cetane number
CO	-	Carbon monoxide
CO ₂	-	Carbon dioxide
CP	-	Cloud point
CSFT	-	Cold soak filtration test
CSU	-	Colorado State University
DE	-	Diatomaceous earth
DI	-	Deionized
DSC	-	Differential scanning calorimetry
EECL	-	Engines and Energy Conversion Lab
EMR	-	Electro-magnetic radiation
FA	-	Fatty acid
FAME	-	Fatty acid methyl ester
FFA	-	Free fatty acid
FPDT	-	Freezing point depression theory
GC	-	Gas chromatograph
GHG	-	Greenhouse gas
HC	-	Hydrocarbons
H ₂ O	-	Water
ICP	-	Inductively coupled plasma
IV	-	Iodine value
K	-	Potassium
Mg	-	Magnesium
MLA	-	Meat & Livestock Australia
MM	-	Methyl myristate
MO	-	Methyl oleate
MP	-	Melting point
MP	-	Methyl palmitate
MS	-	Methyl stearate
Na	-	Sodium
NO _x	-	Nitrogen oxides
OSI	-	Oxidative stability index

P	-	Phosphorus
PM	-	Particulate matter
PP	-	Pour point
S	-	Sulfur
Si	-	Silicon
SME	-	Soy methyl ester
SO _x	-	Sulfur oxides
SVO	-	Straight vegetable oil
TME	-	Tallow methyl ester
TG	-	Triglyceride